UNIVERSITY OF CALIFORNIA,
IRVINE

Reconstructing Hydrologic Variability in Southwestern North America Using Speleothem Proxies and Precipitation Isotopes from California

DISSERTATION

submitted in partial satisfaction of the requirements
for the degree of

DOCTOR OF PHILOSOPHY

in Earth System Science

by

Staryl McCabe-Glynn

Dissertation Committee:
Professor Kathleen Johnson, Chair
Professor Ellen Druffel
Professor Jin Yi Yu

2014

DEDICATION

To my husband Steven Glynn, and children, Danielle, Christopher, and Spencer Glynn
to my Mother, loving memory of my Father, my sister and brothers, aunts and uncles, nieces and nephews, and loving memory of my grandparents
for their love, support, and encouragement.

"To a large extent our lives are made by thoughts and ideas. We become finally what we think. Over the years the things we read and hear and hold in our thoughts condition our minds and ultimately our lives. If we put into our consciousness that which inspires and uplifts, it stands to reason that we shall tend to become inspired and uplifted persons. . . . We determine the type of thing we shall feed to our minds." -*Norman Vincent Peale*

"A grateful mind is a great mind which eventually attracts to itself great things". -*Plato*

"Education is not the filling of a pail, but the lighting of a fire." - *William Butler Yeats*

"It always seems impossible until it's done". -*Nelson Mandela*

TABLE OF CONTENTS

LIST OF FIGURES

LIST OF TABLES

ACKNOWLEDGMENTS

(Chronological order)

I thank Dr. Jerome Luine for expressing such enthusiasm and passion for education that initially inspired me to learn more about the universe and for providing me with continued motivation and encouragement toward pursuing higher education. I am so glad he is here with me today, not only as my mentor and continuous inspiration, but as my friend.

I thank Dr. Ashish Sinha for recognizing and cultivating my desire for education in Earth Science, providing me the opportunity to conduct research with him, taking time to teach me the knowledge and skills needed to excel in this field, encouraging me to apply for a pre-doctoral scholarship, and providing continued guidance, direction, and support. Lastly, for pushing me to my mental limits which has enabled me to seek and gain a better understanding of myself.

I thank Dr. John Southon for accepting me as a summer research intern and providing me with such a wonderful experience, measuring radiocarbon in stalagmite samples, that I decided to further develop my education and skills in this field. This prompted me to complete the required courses I needed for admission at UCI, and going from soccer Mom to scientist! I also thank him for his continued support and enjoyable, enlightening conversations.

I thank Sheila Griffin for her caring support and kind words during my summer internship and throughout the years I have known her at UCI and also for the love and kindness and encouragement she has shown me and my children.

I thank my advisor, Dr. Kathleen R. Johnson, for accepting me as her first graduate student and providing me with a top notch, high caliber role model to emulate. Her support and trust in my abilities and high expectations have led me to learn new skills which have enabled me to conduct research and to utilize and maintain mass spectrometers and other equipment in the laboratory independently. One of my favorite experiences was being part of the process witnessing Kathleen polish and tighten the manuscript that ultimately was accepted in a high profile journal and of course spelunking at various locations including Aldrich Park.

I thank my committee members, Dr. Ellen Druffel and Dr. Jin-Yi Yu for their support, encouragement, and enlightening conversations. I also thank Dr. Ellen Druffel for reviewing letters and for her kindness toward me and my children and for the inspirational, instrumental role and support she has provided to my daughter's research endeavors.

I thank Dr. Julie Ferguson for her guidance, support, and gentle, patient teaching style that helped me to gain a deeper understanding of conducting research and the laboratory methods and equipment. I also thank her for help assistance and guidance during the summer session class I

taught and for providing so generously her knowledge, PowerPoint slides, quizzes, exams, and her time to discuss anything.

I thank Steve Glynn for his support providing for the family and taking on many responsibilities that have enabled me to focus on completing my research, Danielle Glynn for providing support, encouragement, and constructive feedback during my practice presentations, editing papers and for being an inspiration, Christopher Glynn for providing support, encouragement, and humor, feedback and editing of letters and resumes, taking on additional responsibilities at home, and for being an inspiration, and Spencer Glynn for his support and encouragement, modifying graphs for poster figures and PPT slides, cleaning the Johnson Lab oven racks, listening to presentations, being an inspiration and my activity partner.

I thank Carol F., Saima D. Ram M. for personal development and support.

I thank Dr. Karli Anderson for her kindness and friendship, Dr. JT Reager for his help learning data analysis skills, Dr. Keith Moore for recommendation letters, Dr. Eric Saltzman for feedback on proposals and interesting enlightening conversations, Kristal Verhulst, Alysha Inez Coppola, Ann Bardin, and Francesca Hopkins for their friendship, honesty of experience, and uplifting conversations, Dachun Zhang for assistance with equipment and enjoyable conversations, Danielle Sison for assistance modifying chapters and adding references, and Hongying Yang for being an enjoyable person with which to discuss research.

CURRICULUM VITAE

Staryl McCabe-Glynn

Earth System Science Department
University of California, Irvine, Irvine, CA 92697-3100
Phone: (310) 462-5090 Email: mccabegs@uci.edu

Education:

2014 **Doctor of Philosophy in Earth System Science**
University of California, Irvine, (UCI)

2010 **Masters Degree in Earth System Science**
University of California, Irvine, (UCI)

2006 **Clear Multiple Subject Teaching Credential, K-12;**
California State University, Dominguez Hills, Carson, CA

2006 **Bachelor of Arts in Liberal Arts with a Natural Science**
California State University, Dominguez Hills, Carson, CA

Teaching Experience:

2013 **Adjunct Professor** taught course**: "The Atmosphere"**
University of California, Irvine

2009-2013 **Teaching Assistant**
University of California, Irvine
Courses:

- Ocean Biogeochemistry (2 quarters)
- The Atmosphere (2 quarters)
- On Thin Ice (2 quarters/2 sections each)
- Introduction to Earth System Science (1 quarter/3 sections)

Honors & Awards:

2014 UCI, Chancellor's Fund for Excellence Fellowship Award

2013 California State University Chancellor's Doctoral Incentive Program Award

2011 Brython Davis Fellowship

2010 National Science Foundation Graduate Research Fellowship Program honorable mention

2008 Eugene Cota-Robles Fellowship Award, ESS, UCI

2007 CSUDH Student Research Day, 1st Place Award

2006 Sally Casanova Pre Doctoral Scholarship

2005 Carson Companies Dominguez Brand Scholarship for outstanding scholastic achievement

2004 Aids in Training to be Teachers (ATT) Program Scholarship

Publications:

2013 **S. McCabe-Glynn**, K.R. Johnson, C. Strong, M. Berkelhammer, A. Sinha, H. Cheng, R.L. Edwards, 'Variable North Pacific influence on drought in southwestern North America since AD 854. **Nature Geoscience** 6, 617–621.

Abstracts/Presentations:

2014 Geological Society of America (GSA),Vancouver, British Columbia, 'Assessing the influence of extreme precipitation events on the isotopic values of drip water from a southern Sierra Nevada Cave', Oral presentation.

2014 GSA, Bozeman, MT, 'A Multi-proxy Reconstruction of Hydroclimate variability in the Southwestern North America over the Last Millennium', Oral presentation.

2013 S. McCabe-Glynn, K. R. Johnson, M. Berkelhammer, Pacific Climate Workshop (PacClim), Pacific Grove, CA, 'Assessing Modern Climatic Controls on Southern Sierra Nevada Precipitation and Speleothem $\delta^{18}O$', Poster.

2012 S. McCabe-Glynn, K. R. Johnson, M. Berkelhammer, American Geophysical Union (AGU) Fall Meeting, San Francisco, CA, 'Assessing Modern Climatic Controls on Southern Sierra Nevada Precipitation and Speleothem $\delta^{18}O$', PP21B-2021, Poster.

2012 University of California, Riverside, Invited, 'Paleoclimate Records From Speleothems', Earth Sciences Department, Oral presentation.

2011 S. McCabe -Glynn, K. R. Johnson, C. Strong, M. Berkelhammer; A. Sinha, H. Cheng, R. L. Edwards,AGU Fall Meeting, San Francisco, CA, 'A Multi-proxy Reconstruction of

Hydrologic Variability over the Last Millennium from a Sierra Nevada Mountain Stalagmite', PP51D-1908, Poster.

2011 S. McCabe-Glynn, K. Johnson, M. Berkelhammer, A.Sinha, H.Cheng, R. L. Edwards, 5th Graduate Climate Conference, MIT Program in Atmospheres, Oceans and Climate, Woods Hole Oceanographic Institution on Cape Cod, 'Pacific Sea Surface Temperature Influence on Southwestern United States Climate During the Past Millennium: New Evidence from a Well-calibrated, High-resolution Stalagmite $\delta^{18}O$ Record from the Sierra Nevada Mountains', Poster.

2011 6th Karst Record Conference (KR6)on Climate Change, Birmingham, UK, 'Pacific Sea Surface Temperature Influence on Southwestern United States Climate During the Past Millennium: New Evidence from a Well-calibrated, High-resolution Stalagmite $\delta^{18}O$ Record from the Sierra Nevada Mountains' Poster.

2011 PacClim, Pacific Grove, CA, 'Pacific Sea Surface Temperature Influence on Southwestern United States Climate During the Past Millennium: New Evidence from a Well-calibrated, High-resolution Stalagmite $\delta^{18}O$ Record from the Sierra Nevada Mountains', Poster.

2010 AGU Fall Meeting, San Francisco, CA, 'Pacific Sea Surface Temperature Influence on Southwestern United States Climate During the Past Millennium: New Evidence from a Well-calibrated, High-resolution Stalagmite $\delta^{18}O$ Record from the Sierra Nevada Mountains', PP43B-1701, Poster.

2010 S. McCabe-Glynn, K.R. Johnson, M. Berkelhammer, A. Sinha, GSA, Cordilleran Section, Anaheim CA, 'Assessing the Paleoclimate Potential of Speleothems from the Sierra Nevada Mountains: A Preliminary Study', Poster.

2008 22nd annual system-wide CSU Student Research Competition at CSU, East Bay, 'Reconstructing Past Climate and Hydrologic Variability of SW United States Using Speleothems from Sierra Nevada Mountains, California', Oral presentation.

2008 Dated Speleothems: Archives of the Paleoenvironment (DAPHNE) workshop, Heidelberg, Germany, 'Speleothems from Sierra Nevada Mountains California: A Possible Proxy for Reconstructing Climate and Hydrologic Variability',Oral Presentation.

2007 Student Research Day CSU, Dominguez Hills, 'Reconstructing Past Climate and Hydrologic Variability of SW United States Using Speleothems from Sierra Nevada Mountains, California', Oral presentation.

2006 S. McCabe-Glynn, J. Southon, A. Sinha, Summer Research Program Symposium, UCI, 'Stalagmite Based Reconstruction of Atmospheric Radiocarbon Levels during Deglaciation: Implications for Radiocarbon Calibration', Poster presentation.

2006 S. McCabe-Glynn, J. Southon, A. Sinha, AGU Fall Meeting, 'Stalagmite Based Reconstruction of Atmospheric Radiocarbon Levels during Deglaciation: Implications for Radiocarbon Calibration', PP41C-06, Poster presentation.

2006 CSU, Dominguez Hills Student Research Day (2006) 'Stalagmite Based Reconstruction of Atmospheric ^{14}C Levels: Implications for Radiocarbon Calibration', Oral presentation.

2006 S. McCabe-Glynn, J. Southon, A. Sinha, Dated Speleothems: Archives of the Paleoenvironment (DAPHNE) workshop Innsbruck, Austria, 'Stalagmite Based Reconstruction of Atmospheric ^{14}C Levels: Implications for Radiocarbon Calibration', Poster presentation.

Professional Affiliations:

American Geophysical Union (AGU)
Sigma Xi Scientific Research Society
Geological Society of America (GSA)
National Speleological Society (NSS)

Workshops:

2014 Smithsonian Environmental Research Center (SERC), Preparing for an Academic Career in the Geosciences, University of Pittsburgh, PA

Outreach Activities:

2011 - Present	CLEAN education, (Climate, Literacy, Empowerment And iNquiry), teaching students fundamental scientific background to help understand global climate change
2012 - 2013	AISESS (American Indian Summer Earth System Science) program volunteer
2012	Judge for the 31st Annual Irvine Unified School District Science Fair, Irvine, CA
2011 - Present	LASER (Leadership & Assistance Science Education Reform), volunteer research for "Science Night"
2008 - Present	Safety On Site (SOS) representative for the UCI Johnson Laboratory

2006 - Present Volunteer lectures on climate research at Madrona Marsh Community Center, Torrance, CA

2003 - Present Volunteer public astronomical viewings at UCI, Refugio and Joshua State Park, and Madrona Marsh Community Center, Torrance, CA, AISESS summer camp program

Volunteer for Torrance Unified School District GATE Program Science Camp:

2005 Los Angeles County Outdoor Science School (LACOSS) Colby Ranch San Gabriele Mountains

2004 Toyon Bay Science Camp at Catalina Island Marine Institute

2003 Astro Science Camp in Idyllwild

ABSTRACT OF THE DISSERTATION

Reconstructing Hydrologic Variability in the Southwestern United States Using Speleothem Proxies and Precipitation Isotopes from California

By

Staryl McCabe-Glynn

Doctor of Philosophy in Earth System Science

University of California, Irvine, 2014

Professor Kathleen Johnson, Chair

Precipitation in southwestern North America has exhibited significant natural variability over the past few thousand years. This variability has been attributed to sea surface temperature regimes in the Pacific and Atlantic oceans, and to the attendant shifts in atmospheric circulation patterns. In particular, decadal variability in the North Pacific has influenced precipitation in this region during the twentieth century, but links to earlier droughts and pluvials are unclear. Here I assess these links using $\delta^{18}O$ measurements from a speleothem from southern California that spans AD 854– 2007. I show that variations in the oxygen isotopes of the speleothem correlate to sea surface temperatures in the Kuroshio Extension region of the North Pacific, which affect the atmospheric trajectory and isotopic composition of moisture reaching the study site. Interpreting our speleothem data as a record of sea surface temperatures in the Kuroshio Extension, I find a strong 22-year periodicity, suggesting a persistent solar influence on North Pacific decadal variability. A comparison with tree-ring records of precipitation during the past millennium shows that some droughts occurred during periods of warmth in the Kuroshio Extension, similar to the instrumental record. However, other droughts did not and instead were likely influenced by other factors. The carbon isotope record indicates drier conditions are associated with higher

$\delta^{13}C$ values and may be a suitable proxy for reconstructing past drought variability. More research is needed to determine the controls on trace element concentrations. Finally, I find a significant increase in sea surface temperature variability over the past 150 years, which may reflect an influence of greenhouse gas concentrations on variability in the North Pacific. While drought is a common feature of climate in this region, most climate models also project extreme precipitation events to increase in frequency and severity because the climate changes largely due to increased water vapor content in a warmer atmosphere. I also utilize precipitation data and isotopic analysis from precipitation samples collected weekly from near the cave site at Giant Forest, Sequoia National Park, California, from 2001 to 2011, to analyze climate mode patterns during extreme precipitation events and to construct an isotopic data base of precipitation samples. Composite maps indicate extreme precipitation weeks consist of a weaker Aleutian Low, coupled with a deep low pressure cell located northwest of California and enhanced subtropical moisture. I find extreme precipitation weeks occur more often during the La Niña phase and less during the positive Eastern Pacific (EP) phase or during the Central Pacific (CP) neutral phase at our site. Analyses of climate mode patterns and precipitation amounts indicate that when the negative Arctic Oscillation (AO), negative and neutral Pacific North American pattern (PNA), and positive Southern Oscillation Index (SOI) (La Niña) are in sync, the maximum amount of precipitation anomalies are distributed along the Western US. Additionally, the central or eastern Pacific location of El Nino Southern Oscillation sea surface temperature anomalies can further enhance predictive capabilities of the landfall location of extreme precipitation.

CHAPTER 1

Introduction

1.1 Introduction and background

Severe and persistent droughts pose one of the greatest potential hazards to human welfare. Instrumental records of precipitation variability indicate that drought on interannual timescales is a recurrent feature of the Southwestern United States (SW) climate. Much of this region is currently experiencing a persistent drought since ~1999 (Seager et al., 2007), in which lake, reservoir, and snow pack levels have continued to decrease. In January 2014, a state of emergency was declared in California. More than 80% of the state experienced extreme drought conditions after receiving only half of the rainfall of the lowest rainfall year on record. A prolonged shortage in the water supply in this developing area will negatively impact the growing population. Furthermore, climate models project a continued drying trend in the SW in the 21st century (e.g. Seager et al., 2007).

While drought is a common feature of climate in this region, most climate models also project extreme precipitation events to increase in frequency and become more extreme (eg. Ralph and Dettinger, 2012) as the climate changes largely due to increased water vapor content in a warmer atmosphere (Trenberth, 1999). One of the most prevalent extreme precipitation events that occur along the west coast of North America are known as 'Atmospheric Rivers' (AR), whereby extensive fluxes of water vapor are transported from the subtropics to the western US, producing substantial orographic rains and flooding when they encounter mountains (Mass et al., 2011; Warner et al., 2012). These extreme precipitation events lead to floods, landslides, loss of life

and property damage, and are difficult to predict accurately beyond about a ten-day lead. Forecasts of landfall impact are even poorer.

Instrumental records and climate model simulations demonstrate that Pacific and Atlantic sea surface temperature (SST) patterns have exerted substantial control on North American hydroclimate over the 20th century related to coupled climate modes such as the El Niño/Southern Oscillation (ENSO), the Pacific Decadal Oscillation (PDO) (Cook et al., 2007; Dettinger et al., 1998; Mantua and Hare, 2002), and the Atlantic Multi-decadal Oscillation (AMO), (e.g. Enfield et al., 2001; McCabe et al., 2004). For example, the warm phase (positive ENSO and PDO) is correlated with wet conditions in the SWUS and dry conditions in the Northwestern United States (NWUS) (Cook et al., 2007; Dettinger et al., 1998; Mantua and Hare, 2002) while the cool phase (negative ENSO and PDO) is characterized by wet conditions in the NWUS and dry conditions in the SWUS (Gershunov and Barnett, 1998; Cayan et al., 1999). Furthermore, the warm, positive phase of the AMO is associated with drier conditions in northern US when in sync with the positive PDO and in southern US when in sync with the negative PDO and the cool phase with wetter conditions in the US (McCabe et al., 2004; Dettinger et al., 1998).

Instrumental records are too short to provide the full range of long-term climate variability. While the drought conditions in the SW are extensive, paleoclimate studies indicate the current 21st century drought pales in comparison to droughts of the past, such as a series of multi-decadal episodes that were of greater magnitude and of longer duration, between 900 and 1300 AD, often referred to as the Medieval Climate Anomaly (MCA) 'mega-droughts' (e.g. Cook et al., 2004;

2007). However, paleoclimate archives utilized to reconstruct SST patterns that coincided with the megadroughts from corals, marine sediments, lake sediments, tree rings and speleothems offer conflicting evidence about the cause of earlier droughts. For instance, the SWNA megadroughts of the MCA have been attributed to persistent La Niña-like conditions (Cook et al., 2007; Cobb et al., 2003; Mann et al., 2009), but interannual mechanisms such as ENSO may not be appropriate for explaining decadal- to centennial-scale precipitation variability. Although many reconstructed droughts of the past millennium do seem synchronous with cool eastern equatorial Pacific (EEP) SSTs, others do not (Cole et al., 2002; Conroy et al., 2009), thus highlighting the potential importance of other influences such as the North Pacific and the North Atlantic. The vast majority of paleoclimate records from the SWUS are either too short in duration, too poorly dated, and/or too low-resolution (centennial to millennial) to adequately verify the mechanisms controlling precipitation variability over longer time-scales (Seager et al., 2007). Therefore, high-resolution, well-dated paleoclimate records are needed. Proxy archives such as tree rings (e.g. Biondi et al., 2001; MacDonald and Case, 2005; Stahle et al., 2007; Cook et al., 2004) can be useful for inferring precipitation amount. However, speleothems (calcite cave deposits) provide additional climatic information about the mechanisms controlling precipitation variability at annual to interannual resolutions.

1.2 Speleothems as Paleoclimate Archives

Speleothems, such as stalagmites, stalactites, and flowstones, are archives of climatic change and can be used to generate high-resolution records of the paleoenvironment. Speleothems are formed as the infiltrating water above the cave reacts with the CO_2 in the soil, forming carbonic acid, a weak acid, which percolates through the limestone bedrock picking up Ca ions (Fig. 1.1).

Upon entering the ceiling of the cave, the relatively lower pCO_2 in the fissures and cave drives the degassing of $CO_2$from the solution, leaving behind a calcium carbonate ($CaCO_3$) precipitate (Fig. 1.1; Chapter 2.1).

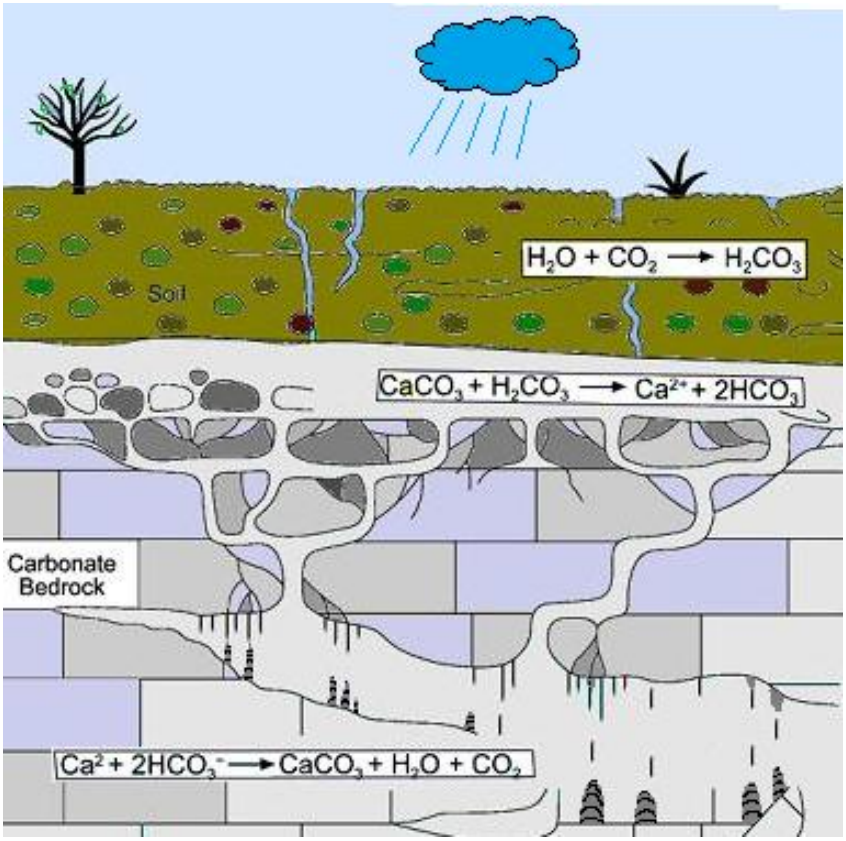

Figure 1.1. This schematic illustrates a model of the karst system and the water flow and CO_2 transport reactions that occur as water percolates through the carbonate bedrock leading to the formation of speleothems (adapted from Fairchild et al., 2006, modified by Spencer Glynn).

Speleothems offer significant advantages over other climate sensitive archives to extend the instrumental record as they can contain numerous types of paleoclimate proxy data (e.g. $\delta^{18}O$, $\delta^{13}C$, annual layer thickness, trace element concentrations, luminescence, etc.) (Fairchild et al., 2006), and can provide continuous high-resolution records extending back hundreds of thousands of years (Edwards et al., 1987; Wang et al., 2008). Stalagmites precipitate from water dripping

on cave floors, grow upward over time, and are generally favored for paleoclimate studies over other types of calcareous speleothems, such as stalactites and helictites (Fairchild et al., 2006). Columnar stalagmites are the most suitable because of their relatively simple, straightforward growth patterns (Fairchild et al., 2006) and generally high uniform growth rates (Baker et al., 1995). They tend to be very pure, well-preserved, and contain numerous types of physical and geochemical climate proxy data, often annual in nature (Fairchild et al., 2006). They can be very precisely dated using Uranium - Thorium (^{230}Th) dating methods due to a lack of detrital contamination (problematic with flowstones that can contain high impurities) (Richards and Dorale, 2003).

The geochemistry of speleothem calcite reflects the water chemistry and environmental conditions at the time of formation. For instance, isotopic equilibrium between the calcite and the drip water can be determined utilizing a theoretical equilibrium fractionation equation calculated from the calcite and drip water δ^{18}O values which is close to the measured average cave air temperature (Kim and O'Neil, 1997). Thus, variations in the δ^{18}O of speleothem calcite are a reflection of the δ^{18}O of precipitation above the cave and temperature (e.g. Fairchild et al., 2006). For a cave with relatively constant temperature, the calcite δ^{18}O primarily reflects the precipitation δ^{18}O above the cave which is linked to climate and can be a robust proxy for hydroclimate variability (e.g. Johnson and Ingram, 2004; Fairchild et al., 2001; Gat, 1996). However, the δ^{18}O of precipitation can be influenced by a variety of climatic factors, such as the temperature, amount of Rayleigh distillation, seasonality, and the source of precipitation (Dansgaard, 1964). For example, colder north Pacific sources lead to more depleted δ^{18}O versus warmer tropical Pacific sources which are more enriched and the amount of Rayleigh distillation,

in which increased rainout and decreased temperature leads to decreased $\delta^{18}O$ values (Lachniet, 2009). Previous research indicates that the isotopic composition of precipitation in Southern California is largely determined by the storm track delivering precipitation to this region, with the lowest $\delta^{18}O$ of precipitation arriving from the North Pacific and the highest from the tropical Pacific (Friedman et al., 1992; Berkelhammer et al., 2012). Thus, variations in the $\delta^{18}O$ of speleothems from this location can provide information of past atmospheric circulation patterns leading to increased understanding of the mechanisms and dynamics leading to both persistent drought and extreme precipitation events, thereby, improving predictability and mitigating negative outcomes.

Additional speleothem proxies such as carbon isotopes ($\delta^{13}C$) and trace element concentrations (eg. Mg/Ca, Sr/Ca, Ba/Ca) also provide information about past environmental and climatic conditions (e.g. Fairchild et al., 2001; Johnson et al., 2006). However, different factors can influence variations in the $\delta^{13}C$ and trace elements incorporated into cave speleothems, making it difficult to accurately interpret past environmental conditions (eg. Frisia et al., 2005). For example, variations in the $\delta^{13}C$ composition of soil CO_2 can vary according to the C_3:C_4 plant photosynthetic pathway ratio above the cave and varying soil respiration rates (Hendy. 1971). Differing flow rates of water infiltrating the cave and enhanced CO_2 degassing prior to the site of speleothem deposition can also affect variations in the calcite $\delta^{13}C$ and trace elements (e.g. Fairchild et al., 2006; Johnson et al., 2006). Therefore, in order to use these proxies to reconstruct past climatic and hydrologic changes, it is critical to understand how modern speleothems form in the individual study area and to calibrate speleothem proxies with local

instrumental climate data because various factors may affect the geochemistry of speleothem calcite differently.

1.3 Study Site Location and Speleothem Paleoclimate Proxies

Figure 1.2. Location map of Crystal Cave in Sequoia National Park, California (36.59 °N; 118.82 °W; 1,386 m).

In this dissertation, I utilize speleothem proxy variations incorporated into a stalagmite formed in Crystal Cave, Sequoia National Park, California (Fig. 1.2) to construct high resolution stable isotope ($\delta^{18}O$, $\delta^{13}C$) and trace element (Mg/Ca, Sr/Ca, Ba/Ca) records to provide a history of

hydroclimate variations and changes in atmospheric circulation patterns. I construct an age model based on ten U-Th dates, a top age of 2007 AD, and a StalAge algorithm that takes into account dating errors (see Chapter 3). I compare the geochemical time-series with numerous paleoclimate records from Western North America to investigate regional coherence in the paleoclimate record and shed light on dynamical processes that produce hydroclimate variability in the region. This study site, on the southwestern flank of the Sierra Nevada Mountains, is ideally located to capture precipitation signals related to shifts in the storm track that occur during events such as the ENSO, PDO, and the AMO. The combined influences of these climate modes modulate winter precipitation variability in the SWUS by altering storm trajectory, frequency, and magnitude on interannual to decadal timescales.

1.4 Main Research Objectives

My main research objectives are to use Sequoia National Park, CA speleothems and modern precipitation isotope data to address:

1. Are speleothems from Sequoia National Park, Crystal Cave, California well-suited for paleoclimate reconstruction?
2. What is the long-term history of hydroclimate patterns in the SWUS such as during climate events such as the Medieval Climate Anomaly (MCA; ~ 900 to 1300) and the Little Ice Age (LIA; ~ 1400 to 1850)?
3. What are the relationships between the hydrologic patterns in the SWUS and coupled ocean-atmosphere modes (eg. ENSO, PDO)?
4. What are the key climate modes and phases leading to extreme precipitation events and how are they characterized by isotopic values?

These research goals have been accomplished through:

1. Conducting continuous monitoring of Crystal Cave environmental variables, such as temperature, relative humidity, drip water, modern calcite, and modern precipitation samples.

2. Constructing an age model using high precision U-series methods and radiocarbon identification of the bomb peak.

3. Conducting measurements and analysis of 1054 micromilled calcite samples (~0.5 mm sampling width) for $\delta^{18}O$ and $\delta^{13}C$ using Isotope Ratio Mass Spectrometry (IRMS), and trace elements (Mg, Sr, and Ba) using Inductively Coupled Plasma Mass Spectrometry (ICPMS).

4. Investigating the modern stable isotope systematics in Crystal Cave through stable isotope ($\delta^{18}O$ and $\delta^{2}H$) analysis of precipitation samples from above Crystal Cave from 2001 to 2011, cave drip water samples from 2007 to 2013, and modern speleothem calcite samples ($\delta^{18}O$ and $\delta^{13}C$) from 2007 to 2011.

5. Conducting instrumental calibration of the proxy data for interpreting isotopic and trace element variations observed in the speleothems (eg. temperature, precipitation source, sea surface temperatures, and sea level pressures).

6. Comparing the isotopic time-series obtained from the Crystal Cave speleothem with other climate records.

7. Conducting analysis on precipitation data and isotopic ($\delta^{18}O$ and $\delta^{2}H$) measurements from precipitation samples from the National Atmospheric Deposition Program (NADP) archives collected from 2001 to 2011 from Giant Forest in Sequoia National Park, California (CA-75).

1.5 Chapter Outline

In Chapter 2 of the dissertation, I describe a cave monitoring project conducted to determine the suitability of speleothems from Crystal Cave for reconstructing past environmental change and to gain a proper understanding of site specific precipitation patterns, hydrological and geochemical behavior of cave drip water. I report the results of detailed continuous monitoring of cave environmental variables such as temperature, relative humidity, drip rate, drip water $\delta^{18}O$ values

and fresh calcite $\delta^{18}O$ values, which indicate that speleothems in Crystal Cave are suitable for paleoclimate reconstruction. I introduce the sample collected for this study, CRC-3, discuss the determination of isotopic equilibrium calcite precipitation, and present the results of the Hendy Test. Furthermore, I assess the drip logger data and investigate precipitation maxima and the influence of these events on drip rates and oxygen isotope ratios in Crystal Cave. I compare the drip rates with precipitation amounts recorded at Giant Forest CA-75, a station ~ 4 km from the cave, to infer the likely drip flow path scenario that could produce the maximum amplitudes observed for each of the three weeks. I present the results of isotopic variations in precipitation during the three drip logger rate maxima from four sites, two along the coast, and two further inland utilizing satellite images and Hysplit back trajectories.

In Chapter 3, I present the results of the calcite $\delta^{18}O$ time-series, instrumental calibration with modern environmental variables, and interpretation of the time-series variability. The results reveal an inverse correlation with the PDO Index (Mantua and Hare, 2002) between 1925 and 2008 ($r = -0.43$, $p < 0.0001$), indicating that speleothem $\delta^{18}O$ values at this site are sensitive to Pacific SST patterns. Further investigation indicates that CRC-3 $\delta^{18}O$ values are associated with anomalous SSTs in the Kuroshio Extension region east of Japan which affect the atmospheric trajectory and isotopic composition of moisture reaching the study site. I use this strong correlation to develop a high-resolution reconstruction of Kuroshio Extension SSTs extending back to 854 AD. The Kuroshio Extension SST reconstruction features strong decadal variability with strong 22-year periodicity, suggesting a persistent solar influence (Shindell et al., 1999). A comparison with tree-ring records of precipitation (Cook et al., 2007) during the past millennium shows that some droughts occurred during periods of warmth in the Kuroshio Extension, similar

to the instrumental record (Cook et al., 2011). However, other droughts did not and instead must have been influenced by other factors. Finally, I find a significant increase in sea surface temperature variability over the past 150 years, which may reflect an influence of greenhouse gas concentrations on variability in the North Pacific. Supplementary information is also presented.

In Chapter 4, I present the results of the calcite $\delta^{13}C$ and trace element, (Mg/Ca, Sr/Ca,Ba/Ca), time-series, instrumental calibrations, and interpretation of the time-series variability. The results show the $\delta^{13}C$ is moderately correlated with Mg/Ca suggesting a climatic influence, however, the lack of significant correlation between Mg/Ca and Sr/Ca suggests that prior calcite precipitation (PCP), where calcite deposition occurs before reaching the stalagmite, is not significant and/or that additional factors complicate this signal (Fairchild et al., 2000). Multiple regression analysis of $\delta^{13}C$ against instrumental temperature and precipitation data (Ash Mountain, previous 10-yrs mean) indicates that both factors are significant ($R^2 = 0.44$, <0.0001). The $\delta^{13}C$ record shows elevated values during the MCA megadroughts and agrees well with a tree ring based PDSI reconstruction from S. California, supporting the occurrence of MCA megadroughts. Surface air temperature and precipitation exert a strong control on local water balance, precipitation minus evaporation (P-ET). CRC-3 $\delta^{13}C$ appears to be sensitive to both factors and may be a suitable proxy for local water balance (P-ET), perhaps reflecting the sensitivity of soil respiration to local water balance and may hold great potential for reconstructing past drought variability.

In Chapter 5, I present the methods and results of isotope analyses conducted on 221 weekly precipitation NADP samples from Giant Forest, California from 2001 to 2011. Analysis reveals an average weekly precipitation amount of 44.8 mm with a large range in isotopic values. The

an average water year (WY) (Oct - Sept) precipitation amount is 977 mm with an average weighted δ^2H of -81.65 ‰ and $\delta^{18}O$ of -12.11 ‰. I also identify the top ten weeks of extreme precipitation events. Extreme precipitation events can result in major damage along the US west coast and are projected by most climate models to increase in frequency and become more extreme. Examination indicates that nine of the top ten weeks of extreme precipitation amounts delivered to this site contain 'Atmospheric River' events, narrow channels of enhanced meridional water vapor transport.

Investigation of the dominant environmental variables, such as sea surface temperatures, sea level pressure, and geopotential heights using reanalysis data composite maps shows a split Aleutian Low is the dominant pattern, characteristic of a weaker circulation, coupled with the presence of an offshore trough and the concurrent emplacement of subtropical moisture. Exploration of various climate mode combinations contributing to extreme precipitation is also explored. Remarkably, 90% of the top ten extreme precipitation events occurred during the daily negative phase of the Arctic Oscillation (AO), associated with a meridional atmospheric circulation pattern, similar to that observed due to Arctic Amplification, suggesting higher latitudinal warming is an important mechanism contributing to these events. Furthermore, analysis of the Southern Oscillation Index (SOI) indicates these extreme precipitation event weeks tend to occur more frequently during the La Niña and neutral El Niño Southern Oscillation phase. Analysis of the large-scale Pacific/North American (PNA) teleconnection pattern show they tend to occur more frequently during the neutral and positive phase at this site. However, a comparison of precipitation events over the Western US from 2001 to 2011 indicates

the greatest extent of anomalous precipitation occurs when the combination of the negative AO, negative PNA, and positive SOI (La Nina) are in sync.

In Chapter 6, I discuss areas where future research is needed using speleothem proxies and precipitation isotopes from California to enhance reconstructions of hydrologic variability in the Western US.

1.6 References

Baker, A., Smart, P. L., Edwards, R. L., 1995. Paleoclimate implications of mass spectrometric dating of a British flowstone. *Geology*. 23, 309-312.

Berkelhammer, M., Stott, L., Yoshimura, K., Johnson, K., Sinha, A., 2012. Synoptic and mesoscale controls on the isotopic composition of precipitation in the western United States. *Climate Dynamics.* 1-22.

Biondi, F., Gershunov, A., Cayan, D. R., 2001. North Pacific decadal climate variability since 1661. *Journal of Climate*. 14, 5-10.

Cayan, D. R., Redmond, K. T., Riddle, L. G., 1999. ENSO and Hydrologic Extremes in the Western United States. *Journal of Climate.* 12, 2881-2893.

Cobb, K. M., Charles, C. D., Cheng, H., Edwards, R. L., 2003. El Nino/Southern Oscillation and tropical Pacific climate during the last millennium. *Nature.* 424, 271-276.

Cole, J. E., Overpeck, J. T., Cook, E. R., 2002. Multiyear La Niña events and persistent drought in the contiguous United States. *Geophysical Research Letters.* 29, 1647.

Conroy, J. L., Restrepo, A., Overpeck, J. T., Steinitz-Kannan, M., Cole, J. E., Bush, M. B., Colinvaux, P. A., 2009. Unprecedented recent warming of surface temperatures in the eastern tropical Pacific Ocean. *Nature Geoscience.* 2, 46-50.

Cook, B. I., Cook, E. R., Anchukaitis, K. J., Seager, R., Miller, R. L., 2011. Forced and unforced variability of twentieth century North American droughts and pluvials. *Climate Dynamics.* 37, 1097-1110.

Cook, E. R., Seager, R., Cane, M. A., Stahle, D. W., 2007. North American drought: reconstructions, causes, and consequences. *Earth-Science Reviews*. 81, 93-134.

Cook, E. R., Woodhouse, C. A., Eakin, C. M., Meko, D. M., Stahle, D. W., 2004. Long-term aridity changes in the western United States. *Science*. 306, 1015-1018.

Coplen, T. B., Neiman, P. J., White, A. B., Landwehr, J. M., Ralph, F. M., Dettinger, M. D., 2008. Extreme changes in stable hydrogen isotopes and precipitation characteristics in a landfalling Pacific storm. *Geophysical Research Letters.* Vol. 35, L21808.

Dettinger, M. D., Cayan, D. R., Diaz, H. F., Meko, D. M., 1998. North-south precipitation patterns in western North America on interannual-to-decadal timescales. *Journal of Climate*. 11, 3095-3111.

Edwards, R. L., Chen, J. H., Ku, T. L., Wasserburg, G. J., 1987. Precise timing of the last interglacial period from mass spectrometric determination of thorium-230 in corals. *Science*. 236, 1547-1553.

Enfield, D. B., Mestas-Nunez, A. M., Trimble, P. J., 2001. The Atlantic multidecadal oscillation and its relation to rainfall and river flows in the continental U.S. *Geophysical Research Letters.* 28, 2077-2080.

Fairchild, I. J., Baker, A., Borsato, A., Frisia, S., Hinton, R. W., McDERMOTT, F., Tooth, A. F., 2001. Annual to sub-annual resolution of multiple trace-element trends in speleothems. *Journal of the Geological Society*. 158, 831-841.

Fairchild, I. J., Smith, C. L., Baker, A., Fuller, L., Spötl, C., Mattey, D., McDermott, F., 2006. Modification and preservation of environmental signals in speleothems. *Earth-Science Reviews*. 75, 105-153.

Friedman, I., Smith, G. I., Gleason, J. D., Warden, A., Harris, J. M., 1992. Stable isotope composition of waters in southeastern California. 1: Modern precipitation. *Journal of Geophysical Research*. 97, 5795-5812.

Friedman, I., Harris, J. M., Smith, G. I., Johnson, C. A., 2002. Stable isotope composition of waters in the Great Basin, United States 1. Air-mass trajectories. *Journal of Geophysical Research:* Atmospheres (1984–2012). 107, ACL 14-1-ACL 14-14.

Gat, J. R., 1996. Oxygen and Hydrogen isotopes in the hydrologic cycle. *Annual Reviews of Earth and Planetary Science.* 24, 225-262.

Gershunov, A. and Barnett, T. P., 1998. ENSO influence on intraseasonal extreme rainfall and temperature frequencies in the contiguous United States: Observations and model results. *Journal of Climate.* 11, 1575-1586.

Johnson, K. R. and Ingram, B. L., 2004. Spatial and temporal variability in the stable isotope systematics of modern precipitation in China: implications for paleoclimate reconstructions. *Earth and Planetary Science Letters*. 220, 365-377.

Lachniet, M. S., 2009. Climatic and environmental controls on speleothem oxygen-isotope values. *Quaternary Science Reviews*. 28, 412-432.

MacDonald, G. M. and Case, R. A., 2005. Variations in the Pacific Decadal Oscillation over the past millennium. *Geophysical Research Letters*. 32, L08703.

Mann, M. E., Zhang, Z., Rutherford, S., Bradley, R. S., Hughes, M. K., Shindell, D., Ammann, C., Faluvegi, G., Ni, F., 2009. Global signatures and dynamical origins of the Little Ice Age and Medieval Climate Anomaly. *Science*. 326, 1256-1260.

Mantua, N. J. and Hare, S. R., 2002. The Pacific decadal oscillation. *Journal of Oceanography*. 58, 35-44.

Mass, C., Skalenakis, A., Warner, M., 2011. Extreme precipitation over the West Coast of North America: Is there a trend? *Journal of Hydrometeorology*. 12, 310-318.

McCabe, G. J., Palecki, M. A., Betancourt, J. L., 2004. Pacific and Atlantic Ocean influences on multidecadal drought frequency in the United States. *Proceedings of the National Academy of Sciences of the United States of America*. 101, 4136.

Ralph, F. and Dettinger, M., 2012. Historical and national perspectives on extreme West Coast precipitation associated with atmospheric rivers during December 2010. *Bulletin of the American Meteorological Society*. 93, 783-790.

Richards, D.A., Dorale, J.A., 2003. Uranium-series chronology and environmental applications of speleothems, in: Bourdon, B., Henderson, G. M., Lundstrom, C. C., Turner, S. P. (Eds.), *Uranium-Series Geochemistry*. pp. 407-460.

Seager, R., Ting, M., Held, I., Kushnir, Y., Lu, J., Vecchi, G., Huang, H. P., Harnik, N., Leetmaa, A., Lau, N. C., 2007. Model projections of an imminent transition to a more arid climate in southwestern North America. *Science*. 316, 1181-1184.

Shindell, D., Rind, D., Balachandran, N., Lean, J., Lonergan, P., 1999. Solar cycle variability, ozone, and climate. *Science*. 284, 305-308.

Trenberth, K.E., 1999. Conceptual framework for changes of extremes of the hydrological cycle with climate change, in: *Anonymous Weather and Climate Extremes*. Springer, pp. 327-339.

Warner, M. D., Mass, C. F., Salathé Jr, E. P., 2012. Wintertime extreme precipitation events along the Pacific Northwest coast: Climatology and synoptic evolution. *Monthly Weather Review*. 140, 2021-2043.

CHAPTER 2

Assessing the Suitability of Utilizing Speleothems Proxies from the Sierra Nevada Mountains, California for Paleoclimate Reconstruction

2.1 Introduction

Speleothems are ideal for high-resolution paleoclimate reconstruction. In order to use speleothem proxies to derive information about past hydrographic variability, it is necessary to understand how modern speleothems form and to calibrate proxies, such as $\delta^{18}O$, $\delta^{13}C$, and trace elements, with local instrumental climate data to determine how they are recording environmental conditions. The most widely used proxies for paleoclimatic research are the stable isotopes of oxygen ($\delta^{18}O$) and carbon ($\delta^{13}C$). An important prerequisite in using the stable isotopes ($\delta^{18}O$ and $\delta^{13}C$) in speleothems as a proxy indicator of climate is that the carbonate deposition occurred at or close to isotopic equilibrium with the cave drip waters. The formation of speleothem calcite is driven by CO_2 degassing of cave drip water that has accumulated carbon from the soil and bedrock. Meteoric waters equilibrate with soil CO_2 to form carbonic acid:

$$CO_2 + H_2O \Rightarrow H_2CO_3$$

This weak acid causes dissolution of the cave host limestone bedrock as water moves through the epikarst:

$$H_2CO_3 + CaCO_3 \Rightarrow Ca^{2+} + 2HCO_3^-$$

Because of lower pCO_2 of cave air relative to the drip water, CO_2 degassing and calcite precipitation are initiated as drip water moves into the cave:

$$Ca^{2+} + 2HCO_3^- \Rightarrow CO_2 + H_2O + CaCO_3$$

Although high relative humidity and constant temperatures are optimal conditions for isotopic equilibrium, isotopic disequilibrium can still occur in response to varying rates of drip water or CO_2 degassing (see reviews in Fairchild, et al. 2006; McDermott et al., 2006) which may change the key climate signal preserved in speleothem calcite. During kinetic fractionation both oxygen and carbon isotopes behave in a similar way due to a faster degassing rate of CO_2, resulting in the enrichment of both isotopes (Hendy, 1971). For example, kinetic effects related to changes in the amount of CO_2 that can occur during decreased cave drip water flow rates or increasing temperatures leading to increased evaporation, can lead to ^{13}C and ^{18}O enrichment (Hendy, 1971; Mickler et al., 2004) and elevated trace element concentrations (Mg, Sr, and Ba) in the speleothem (Lorens, 1981). Thus, speleothems precipitated under kinetic fractionation conditions are not reliable for providing accurate palaeoclimate data (Hendy, 1971).

2.2 The $\delta^{18}O$ of cave drip water and speleothem calcite

The $\delta^{18}O$ value of cave drip water is a reflection of the precipitation above the cave site (e.g. see review in (Lachniet, 2009) and has been useful for reconstructing cave temperature and other aspects of hydroclimate such as precipitation amount, moisture source, and synoptic meteorology (McDermott, 2004). While the $\delta^{18}O$ values in speleothems can be affected by equilibrium and kinetic fractionation due to complex processes, the $\delta^{18}O$ value of speleothem calcite under equilibrium conditions is only affected by the $\delta^{18}O$ value of the drip water and the cave temperature (Kim and O'Neil, 1997). Therefore, assuming equilibrium deposition, the $\delta^{18}O_{calcite}$ depends only on the $\delta^{18}O$ of cave dripwater and cave temperature:

$$\delta^{18}O_{calcite} = f\,[\delta^{18}O_{water}, \text{Cave T} (\cong \text{MAT})]$$

where the measured $\delta^{18}O_{calcite}$ value is a function of the $\delta^{18}O_{water}$, value of the drip water, and cave T, which is ≅ the Mean Annual Temperature. The $d\delta^{18}O/dT$ = -0.23 ‰ /°C, meaning the $\delta^{18}O$ values would decrease about 1‰ with an increaseof 4°C. As variations in $\delta^{18}O$ values of the global water cycle are usually larger than the fractionation between the water and calcite, which is temperature-dependent, the hydrologic cycle is likely to be the main control of the speleothem $\delta^{18}O$ signal (Rozanski et al., 1993; Gat, 1996). Therefore, in caves with a relatively constant temperature, variations in the drip water $\delta^{18}O$ are primarily a reflection of the precipitation $\delta^{18}O$ above the cave.

2.3 Cave monitoring

To gain a proper understanding of site specific speleothem formation, a detailed and continuous monitoring regimen must be conducted to fully understand the hydrological and geochemical behavior of cave drip water and how they vary with changing precipitation patterns, and other environmental variables in the cave. In order to choose the right stalagmite and develop new, well-dated, high-resolution records of past precipitation in the SWUS, intensive studies need to be conducted. I utilized essentially three main criteria when selecting a sampling location: 1) an actively forming, columnar stalagmite, as evident by fresh calcite growth was present, 2) cave environment was stable (eg. constant temperature and high relative humidity), and 3) the cave was relatively easy to access for consistent continuous monitoring. After assessing and monitoring several caves in Sequoia National Park, in 2007, we chose an actively growing 10.4 cm columnar stalagmite, CRC-3, from Crystal Cave, (36.59°N, 118.82°W), a solution cave formed within a band of Paleozoic marble (see Fig. 2.1).

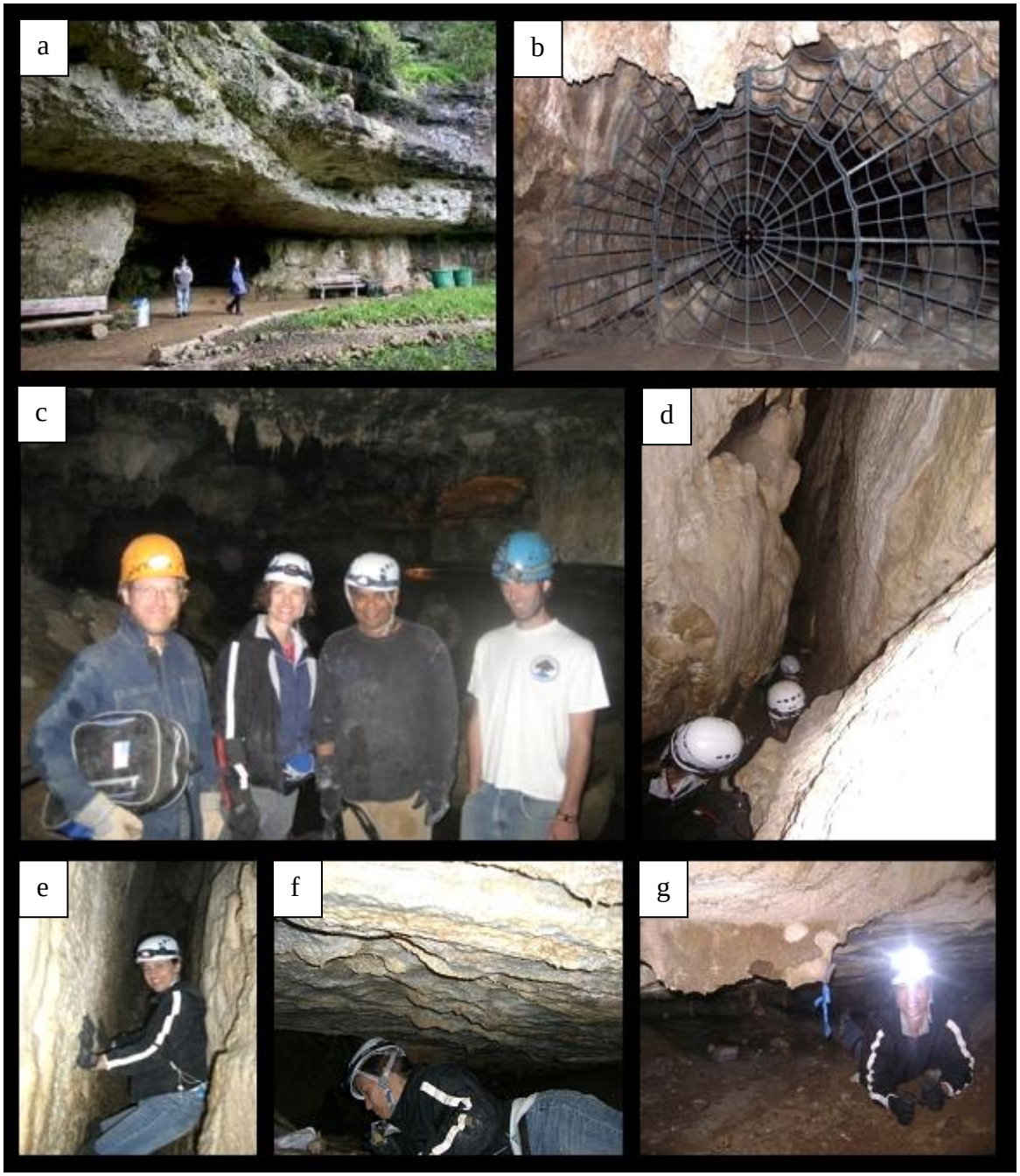

Figure 2.1 Assessing locations containing prospective stalagmite samples in Crystal Cave to monitor for paleoclimate reconstruction, a) the opening of Crystal Cave, b) the gated entranceway, c) exploration team (from left), Joel Despain, Staryl McCabe-Glynn, Ashish Sinha, and Ben Tobin (Despain and Tobin: Sequoia National Park cave specialists), d) the group descending under Marble Hall (Fig. 2.3), e) McCabe-Glynn traversing the narrow passage, f) crawling under the ledge, and g) the location of the chosen sample in the back left corner.

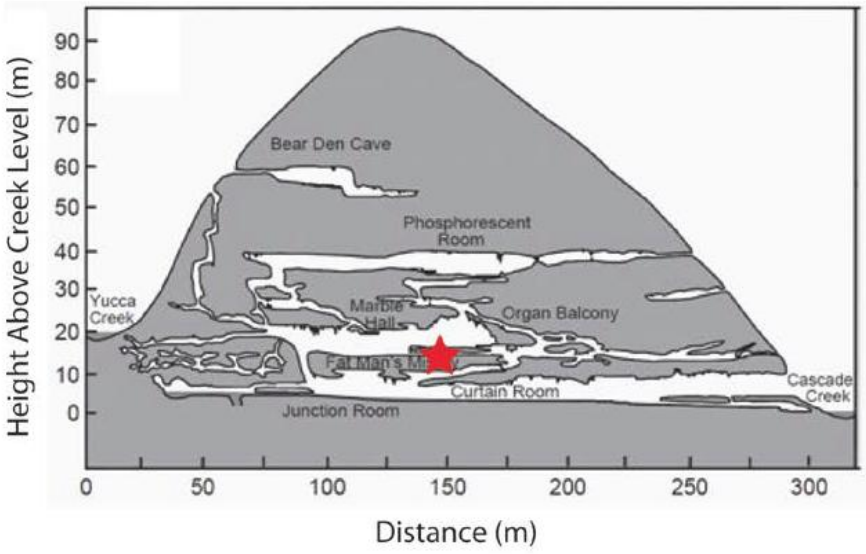

Figure 2.2 A profile view of Crystal Cave and surrounding caves. Red star marks the location where the CRC-3 stalagmite was collected in July 2008 from an isolated chamber beneath Marble Hall (Modified from Despain and Stock, 2005).

Crystal Cave, a tourist cave, is located at an elevation of 1386 m and occupies the lower 64 m of a marble ridge, approximately 160 m long and 40 m wide and contains 4.77 km of surveyed passages, set on six distinct levels (Fig. 2.2; Despain and Stock, 2005). CRC-3 was forming in a small isolated chamber located off the tourist trail underneath Marble Hall about 150 m from the cave entrance (Fig. 2.2).

2.4 Methods

2.4.1Cave monitoring and analytical methods

A detailed monitoring program was initiated consisting of logging cave temperature and relative humidity with a HOBO U23 Pro v2 Temperature/Relative Humidity Data Logger (Fig. 2.3b). Modern calcite was collected on frosted glass plates (Fig. 2.3c and d) and analyzed for $\delta^{18}O$ and $\delta^{13}C$ using a Kiel IV-carbonate device coupled with a Thermo-Finnigan Delta V Plus IRMS. A

total of 16 standards (NBS-19, NBS-18 and OX, an in-house quality control standard) were analyzed during each run of 30 unknown samples. The results of isotopic analysis are presented in conventional delta (δ) notation, defined as $\delta^{18}O = [(^{18}O/^{16}O)_{sample}/(^{18}O/^{16}O)_{VPDB} -1] *1{,}000‰$. The standard deviation of repeated NBS-19 measurements is ~0.06 ‰ for $\delta^{18}O$ presented in Table 2.3.

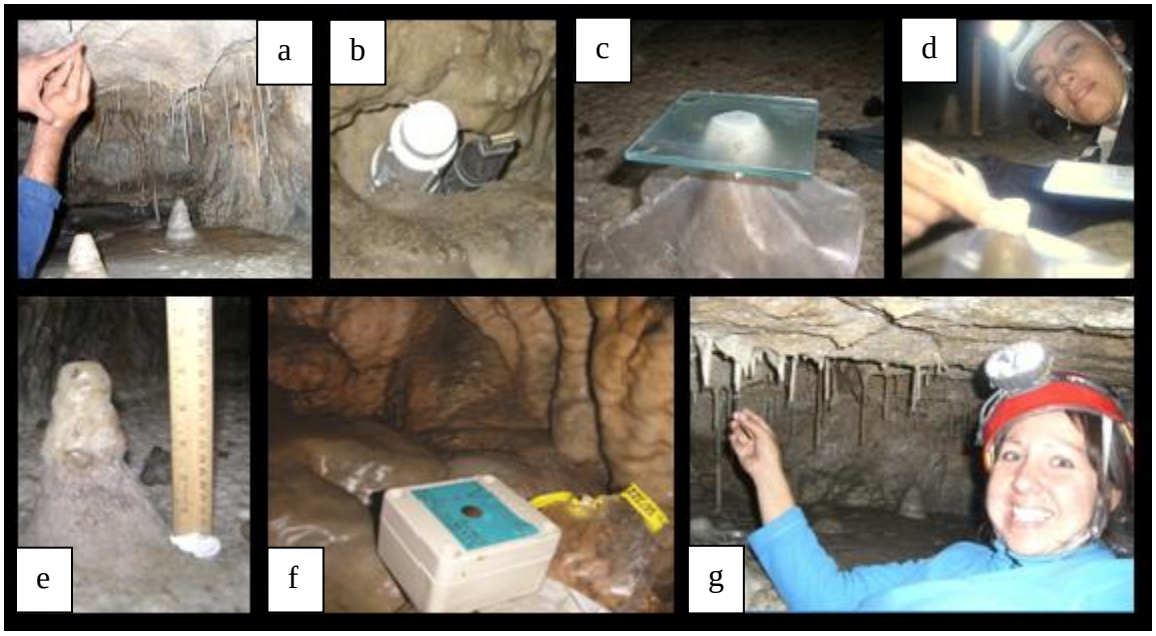

Figure 2.3 Crystal Cave monitoring activities a) collecting drip water over sample, b) temperature and relative humidity drip loggers, c) glass plate to collect fresh calcite, d) Staryl McCabe-Glynn setting glass plate, e) CRC-3 measures 10.4 cm, f) Stalagmate PLUS Mark 2 Driptych drip logger, and g) Kathleen R. Johnson collecting drip water.

Cave pCO_2 was measured with a Telaire 7001 portable pCO_2 monitor. Drip water samples were collected between May and November for stable isotope analysis (Fig. 2.3a and g) and analyzed for $\delta^{18}O$ and $\delta^{2}H$ on a Temperature Conversion Elemental Analyzer (TC/EA) coupled to a Thermofinnigan Delta Plus XP isotope ratio mass spectrometer (IRMS) instrument. Variations in drip rates in the cave can lead to isotopic variations in the drip water and eventually, speleothems. In order to better understand the controls on the isotopic composition

of speleothem calcite and the response to individual precipitation events, a Stalagmate PLUS Mark 2 Driptych drip logger (http://www.driptych.com/) was placed under the drip over the CRC-3 sample location on 7/29/2010, set to record number of drips per hour (Fig. 2.3f).

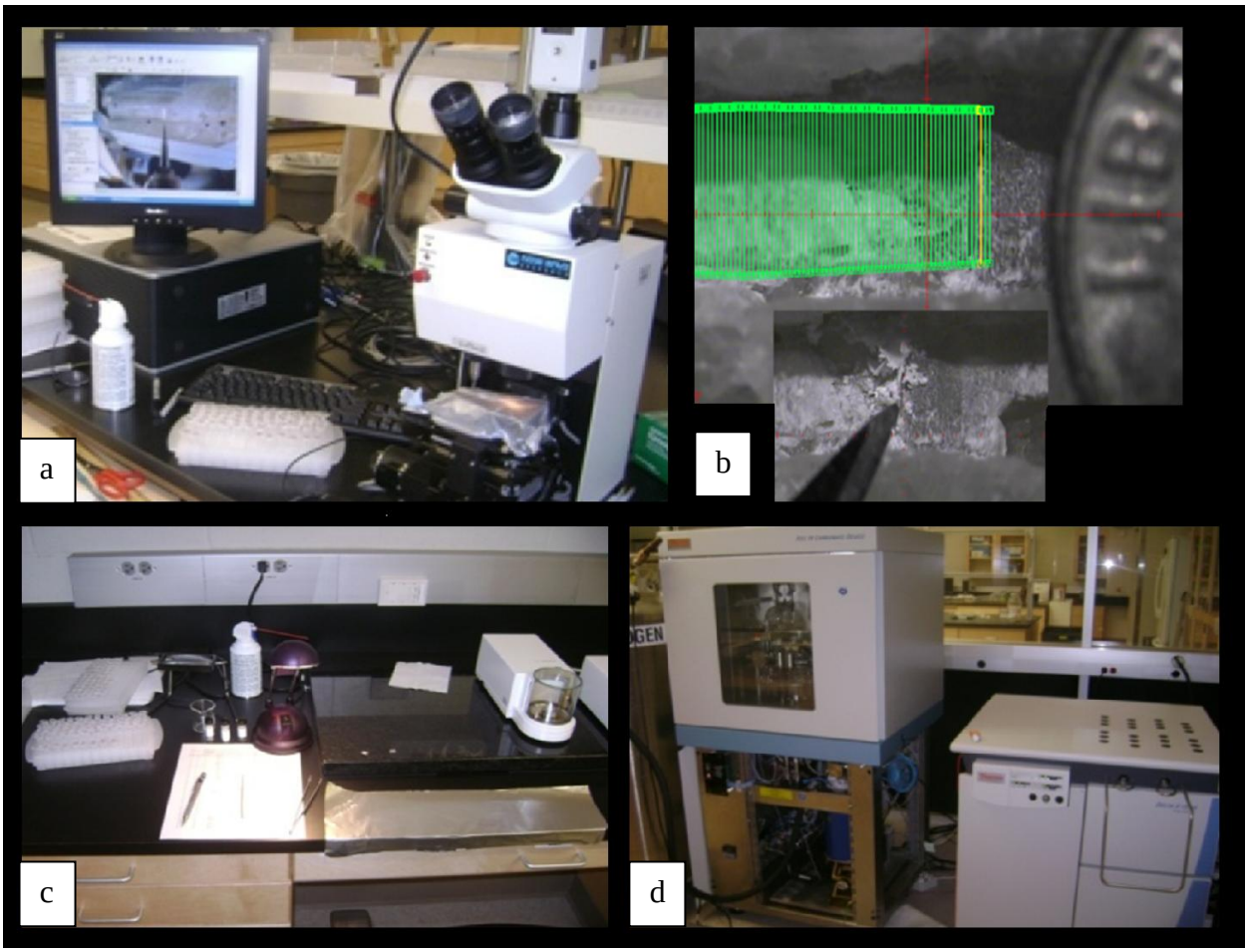

Figure 2.4 a) New Wave MicroMill drill set on the CRC-3 sample with accompanying vial tray for sample collection, b) shows the green computer generated interpolated scans ~0.05 mm apart with a dime (~1 cm diameter) to show size comparison and scalpel blade to collect calcite sample c) Sartorius scale and foil boats utilized to weigh calcite sample in, three vials containing standards, and vial holder trays, and d) the automated sampler Kiel IV-carbonate device coupled with a Thermofinnigan Delta V Plus isotope ratio mass spectrometer.

Fig. 2.4 shows the analytical methods utilized to collect the calcite samples and preparation techniques to analyze in IRMS (see caption for description). The stable isotope analysis results and interpretation are presented in Chapter 3. The stalagmite, CRC-3, was collected in July 2008

(Fig. 2.5a and b), cut in half parallel to the growth axis, and polished (Fig. 2.9 left). Petrographic analysis shows the stalagmite consists of clear, dense, columnar calcite with faintly visible growth lamina. Changes in crystal form and calcite fabrics may provide a record of changes in water availability (Frisia et al., 2000) (see A1.Thin sections).

Figure 2.5 Stalagmite collections a) Staryl McCabe-Glynn pouring water continuously over saw blade during stalagmite collection, and b) the stalagmite sample, CRC-3.

2.4.2 The Hendy Test method

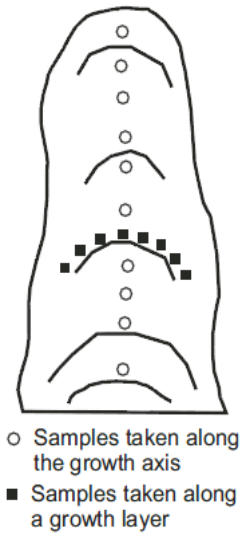

To determine whether isotopic equilibrium was consistent in the stalagmite in the past, I applied the Hendy Test. This test consists of measuring the $\delta^{18}O$ and $\delta^{13}C$ values from a single growth lamina of calcite along the growth axis and analyzing the $\delta^{18}O$ and $\delta^{13}C$ values from the center outward to evaluate the extent of isotopic equilibrium and kinetic fractionation (see Fig. 2.6) (Mickler et al., 2006). I utilized a Dremel Drill with a diamond dental drill bit to collect powdered calcite sub-samples (~ 50 μm) following two individual curved growth layers Fig. 2.8 left).

Figure 2.6 Shows a schematic of sample selection (squares) for the Hendy Test (adapted from Mickler et al., 2006).

2.4.3 Precipitation amount and associated isotopic value methods

To learn how moisture varies during modern precipitation events, I analyzed the isotopic composition and amount (mL) of precipitation collected weekly and stored in the National Atmospheric Deposition Program (NADP) archives from four sites, two along the coast, CA-42 Tanbark Flat and CA-66 Pinnacles National Monument-Bear Valley, and two inland, in the Sierra Nevada Mountains, CA-99 Yosemite National Park-Hodgdon Meadow and CA-75 Sequoia National Park-Giant Forest (Fig. 2.7, color coded). To determine how the precipitation isotopic composition varied spatially during the individual weeks, I focused on the three weeks of maxima precipitation noted by the Crystal Cave drip logger event 1) December 19, 2010 - sample from week date on 12/14/2010 date off 12/21/2010, 2) December 29, 2010 - sample week date on 12/28/2010 date off 1/4/2011, and 3) March 7, 2011 - sample week date on 3/2/2011 date off 3/9/2011 (Fig. 2.12). I also analyzed the week with the lowest $\delta^{18}O$ values, sample week on 12/21/2010 date off 12/28/2010 (Fig. 2.12b). Analysis for $\delta^{18}O$ and $\delta^{2}H$ was conducted on a TC/EA coupled to a Thermofinnigan Delta Plus XP IRMS.

2.4.4 Back trajectory analysis methods

Storm trajectories were investigated utilizing NOAA Hybrid Single Particle Lagrangian Integrated Trajectory Model (HYSPLIT) and reanalysis data (global, 1948-present) back-calculated particle trajectories (http://ready.arl.noaa.gov/HYSPLIT_traj.php) for the four storm weeks. These models are run at 36.59 °N; 118.82 °W, 1500 m above ground level, the approximate height of the 850 hPa level from where rain is expected to originate, at 24-hour time steps for 72-hours for each day of the week prior to landfall at Giant Forest site CA-75 (Fig. 2.14). Rainfall (mm/hr) is also plotted along each trajectory.

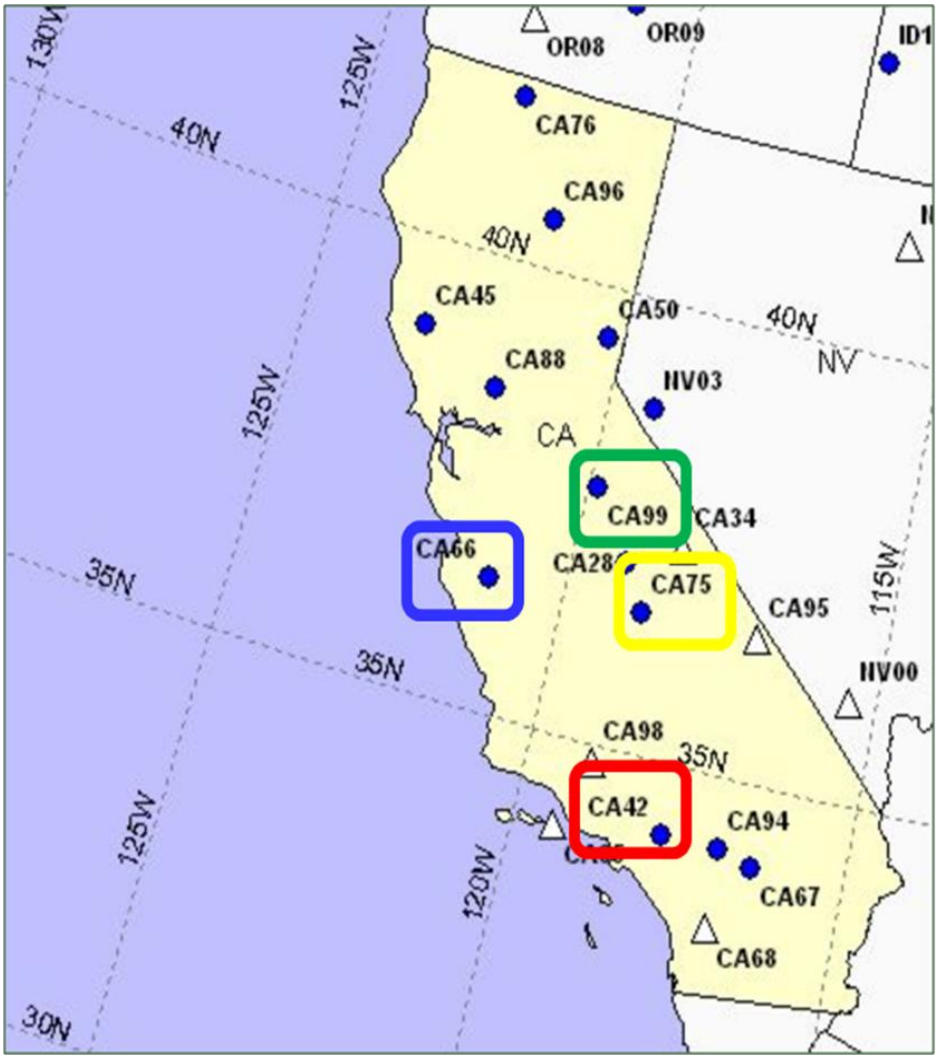

(CA42)	Tanbark Flat	34.21	-117.76	853 meters
(CA66)	Pinnacles National Monument-Bear Valley	36.48	-121.16	317 meters
(CA75)	Sequoia National Park-Giant Forest	36.57	-118.78	1921 meters
(CA99)	Yosemite National Park-Hodgdon Meadow	37.80	-119.86	1393 meters

Figure 2.7 Map showing NADP precipitation collection sites in California (color coded).

2.4.5 Daily temperature, precipitation, and satellite image methods

Daily temperature and precipitation data was obtained from the California Data Exchange Center (CDEC) for Giant Forest Sequoia National Park (http://cdec.water.ca.gov) (Table A2.1-2.3). All

data for precipitation were available and four missing temperature values were obtained by averaging the daily data one day above and one day below for the missing value. Satellite images were obtained from GOES West sea-level pressure analysis (GFS model) and surface observation infrared images from (http://virga.sfsu.edu/crws/archive/sathts_pac_arch.html) and San Francisco State University (SFSU)/ Meteorology infrared satellite image and 300 mb jet stream map (http://virga.sfsu.edu/crws/archive/sathts_pac_arch.html) (Fig. A3,4,6,7,9 and 10).

2.5 Results

2.5.1 Cave monitoring results

Monitoring results indicate that the microclimate inside the cave is characterized by fairly constant temperature of 8.0 ± 0.5 °C from 7/2007 to 6/2012 and the relative humidity remains close to 100% throughout the year, two critical pre-requisites for paleoclimate reconstruction since constant temperature and high humidity ensure that speleothem calcite is precipitated in isotopic equilibrium. The average pCO_2 concentrations were ~ 675 ppm ± 42 ppm. Continuous collecting and monitoring of the Crystal Cave drip water from 2007 to 2013, indicates the δ^2H and $\delta^{18}O$ average is -70.0 ‰ ± 8.73‰ and -10.2 ‰ ± 1.77 ‰, respectively (Table 2.1). The highest drip water isotopic value occurred 9/16/2009 (-5.69 ‰) and the lowest value occurred 10/30/2011 (-14.54 ‰) (Table 2.1). The highest average yearly drip water samples occurred in 2009 (-7.25 ‰) from September and October collections and the lowest average yearly values occurred in 2011 (-12.84 ‰) from July, September, and October collections (Table 2.2). Table 2.2).

Table 2.1. Crystal Cave drip water isotopic values from 6/29/2007 to 11/21/2013.

Date	δ^2H	$\delta^{18}O$	Date	δ^2H	$\delta^{18}O$
6/29/2007	-66.5	-10.27	9/20/2011	-78.8	-12.2
8/24/2007	-58.9	-9.2	10/30/2011	-84.73	-14.54
9/22/2007	-61.5	-9.63	6/16/2012	-73.82	-12.43
10/28/2007	-62	-9.45	7/25/2012	-80.1	-11.49
11/9/2007	-60.8	-9.35	9/6/2012	-77.88	-11.05
4/19/2008	-67.7	-10.43	9/25/2012	-77.19	-11.18
6/22/2008	-66.9	-10.2	10/28/2012	-77.76	-11
7/10/2008	-69.7	-9.42	5/28/2013	-75.8	-10.71
8/28/2008	-65.5	-9.89	5/28/2013	-74.9	-10.63
9/16/2009	-65.77	-5.69	7/16/2013	-75.4	-10.69
10/16/2009	-59.67	-8.81	7/16/2013	-75.3	-10.51
5/17/2010	-63.26	-7.44	8/28/2013	-76.1	-10.78
7/30/2010	-70.21	-10.61	8/28/2013	-76.5	-10.76
9/14/2010	-66.27	-10.04	9/27/2013	-77	-10.82
10/14/2010	-64.4	-9.89	9/27/2013	-76.6	-10.83
11/11/2010	-40.96	-7.37	11/21/2013	-54.2	-8.25
7/29/2011	-87.4	-11.78			

Table 2.2. Crystal Cave monitoring results of average drip water isotopic values (δ^2H and $\delta^{18}O$), glass plate calcite isotopic values ($\delta^{18}O$ and $\delta^{13}C$), and cave temperature (°C).

Drip water average			Winter glass plate			Temperature	Average
Year	δ^2H	$\delta^{18}O$	Year	$\delta^{18}O$	$\delta^{13}C$	Year	(°C)
2007	-61.94	-9.58	6/07 to 7/08	-8.15	-6.93	6/07 to 7/08	8.0
2008	-67.45	-9.99	7/08 to 5/09	-8.86	-7.19	4/08 to 9/09	7.9
2009	-62.72	-7.25	10/09 to 5/10	-8.57	-8.74	10/10 to 12/10	8.5
2010	-61.02	-9.07	6/10 to 7/11	-8.37	-8.35	7/11 to 6/12	8.2
2011	-83.64	-12.84					
2012	-77.35	-11.43					
2013	-73.55	-10.44					
Average	**-69.7**	**-10.1**	**Average**	**-8.5**	**-7.8**	**Average**	**8.1**
StDev	**8.7**	**1.8**	**StDev**	**0.3**	**0.9**	**StDev**	**0.3**

2.5.2 Speleothem calcite and Hendy Test results

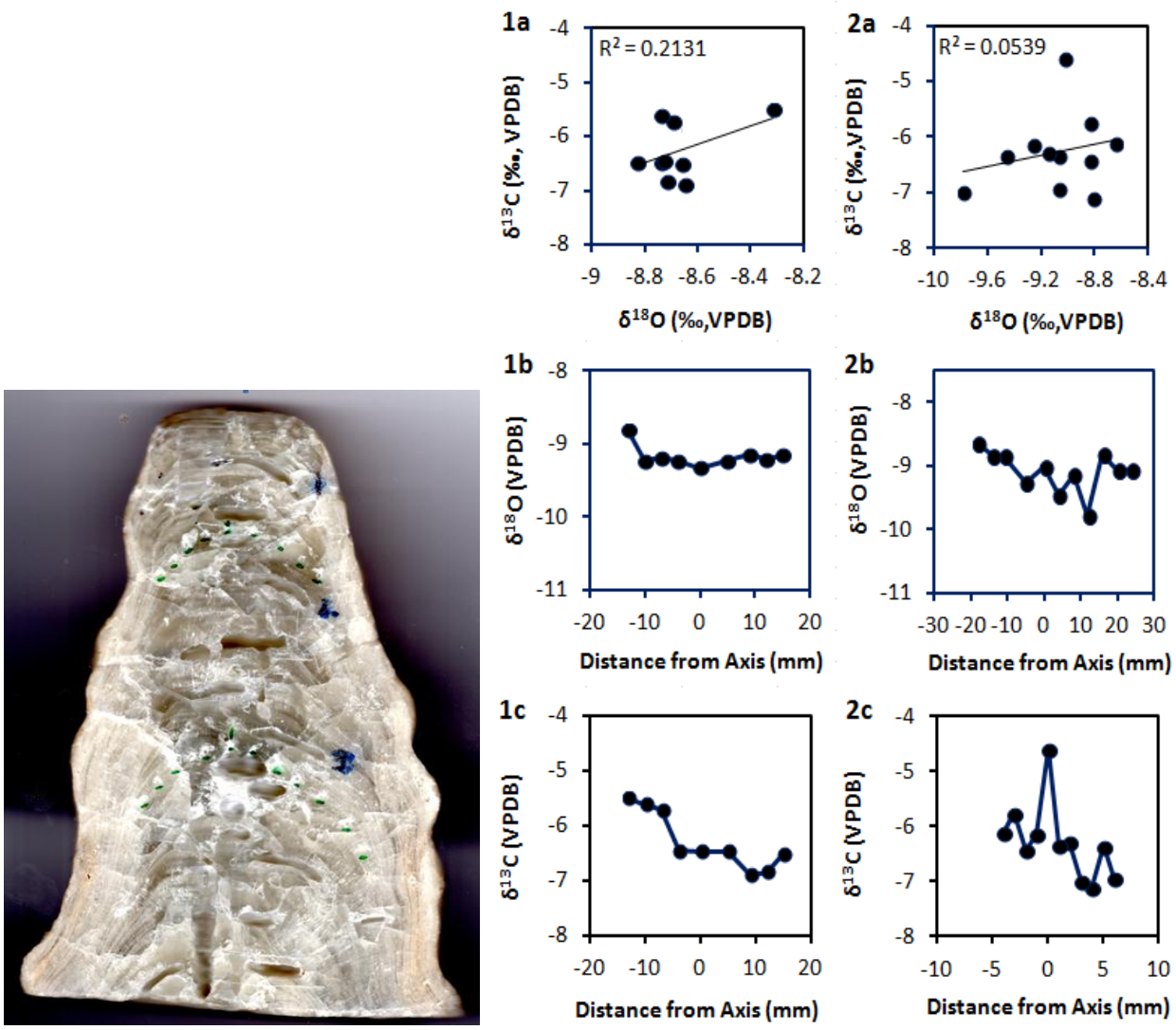

Figure 2.8 Scanned image of stalagmite CRC-3 showing the Hendy Test locations of samples collected from two growth bands (marked by green dots) (left) and results of two Hendy Tests conducted on CRC-3 (right). 1a and 2a) show the correlation between $\delta^{18}O$ and $\delta^{13}C$, and 1b, 2b) the $\delta^{18}O$ values, and 1c, 2c) the $\delta^{13}C$ values measured from the axis along two lamina.

Analysis of samples collected from two individual lamina of CRC-3 shows no correlation over $R^{2} = 0.21$ between the $\delta^{18}O$ and $\delta^{13}C$ along a single growth lamina (Hendy Test 1 $R^2 = 0.21$, $p = 0.54$; Hendy Test 2 $R^2 = 0.05$, $p = 0.87$) (Fig. 2.8;1a and 2a) and no significant change in $\delta^{18}O$

values along a growth layer, particularly in Hendy Test 1 (Fig. 2.8;1b and 2b) which supports that the $CaCO_3$ was precipitated in equilibrium with drip water and was not impacted by kinetic effects related to rapid degassing or evaporation. The distance from the axis to the left of Hendy Tests for the $\delta^{13}C$ shows more enriched values than the right, and the right side values appear to begin increasing further out (Fig. 2.8; 1c and 2c), likely reflecting the difficulties associated with identifying and drilling along a single continuous growth lamina.

2.5.3 Drip logger results

Analysis of the Stalagmate Driptych drip logger data from 7/29/2010 to 7/29/2011 reveals three maxima in drips/hour on 1) 12/19/2010 (2506 drips/hour), 2) 12/29/2010 (922 drips/hour), and 3) 3/7/2011 (382 drips/hour) (Fig. 2.9a; Fig. 2.11a, b, c). A close up view with a zoomed in scale indicates the average drip over that time period of 25.31drips/hour (Table 2.3; Fig. 2.9). The drip logger data results from 6/16/2012 to 11/21/2013 also show three maxima: 1) on 12/24/2012 (211 drips/hour), 2) 5/30/2013 (429 drips/hour), and 3) 10/4/2013 (403 drips/hour) (Fig. 2.10a). A close up view with a zoomed in scale indicates the average drip over that time period is 9.8 drips/hour (Table 2.3, Fig. 2.10b). Note, another Stalagmate Driptych drip logger was utilized from 7/29/2011 to 6/12/2012, however the results indicate the drip logger was defective and were not used.

Table 2.3. Crystal Cave drip logger data drips/hour average and seasonal values.

Date on - Date off	Average Drip/Hour	DJF Drip/Hour	MAM Drip/Hour	JJA Drip/Hour	SON Drip/Hour
7/29/2010-7/29/2011	25.3	61.2	23.7	11.3	6.2
6/15/2012-10/29/2012	9.6			11.2	7.3
10/29/2012 - 11/21/2013	10.0	17.1	11.0	7.9	6.0

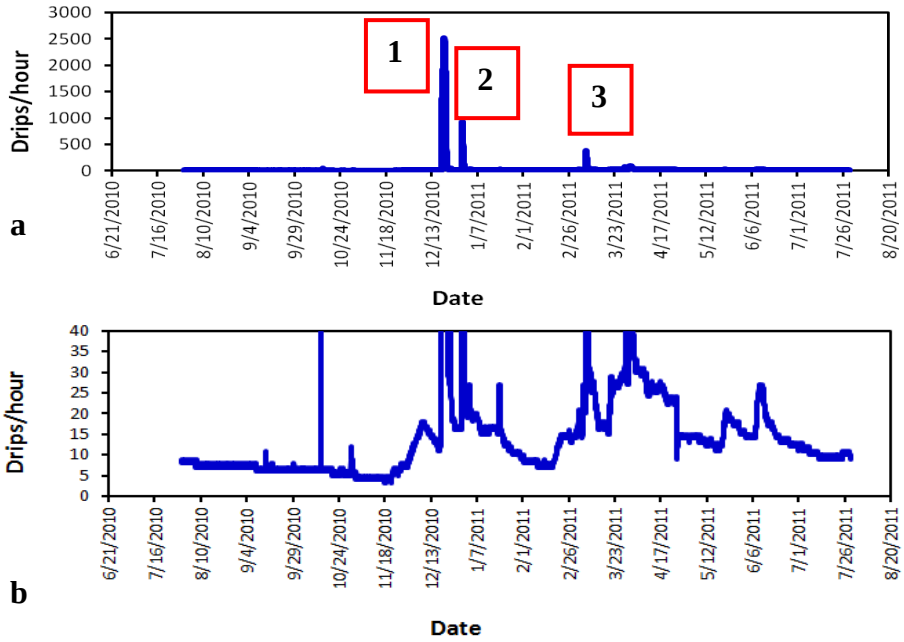

Figure 2.9. Driptych drip logger results from 7/29/2010 to 7/29/2011 show **a)** three extreme increases on 12/19/2010, 12/29/2010, and 3/7/2011, and **b)** a zoomed in scale indicating variability between ~5 and 30 drips/hour with an average of 25.3 drips/hour over the year.

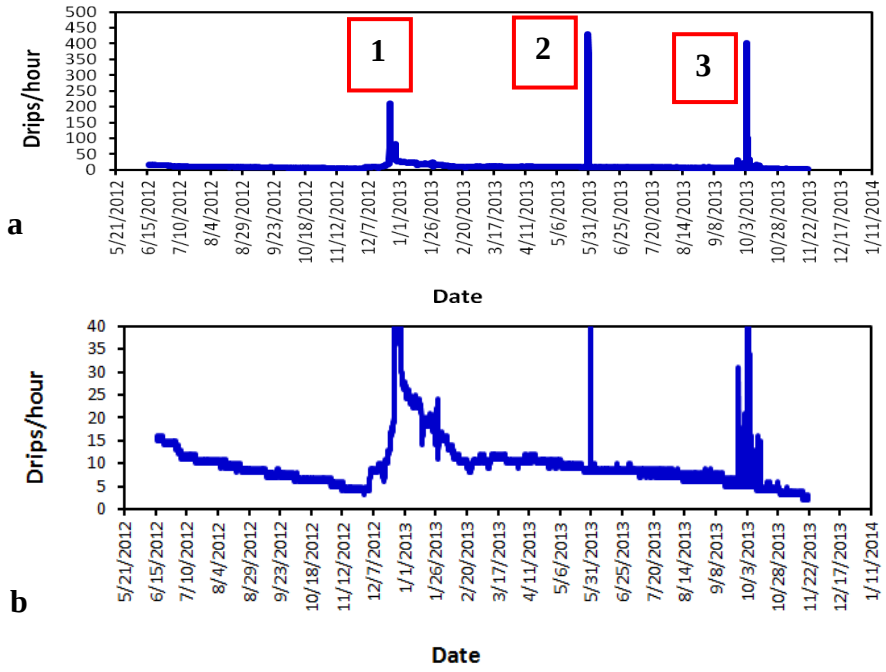

Figure 2.10. Driptych drip logger results from 6/16/2012 to 11/21/2013 show **a)** three extreme increases on 12/24/2012, 5/30/2013, and 10/4/2013), and **b)** a zoomed in scale indicating variability between ~3 and 25 drips/hour with an average of 9.8 drips/hour over the year.

The yearly drip rate is highest during the winter (DJF), when the majority of precipitation falls, and lowest during the fall (SON) (Table 2.3) (Fig. 2.9b and 2.10b). The drip rate slowed to 4 -5 drips/hour in November of 2012. Near the end of 2013, the driest year on historical record in California, when the drip logger was changed, we observed the slowest drip rate of 2-3 drips/hour (Fig. 2.10b).

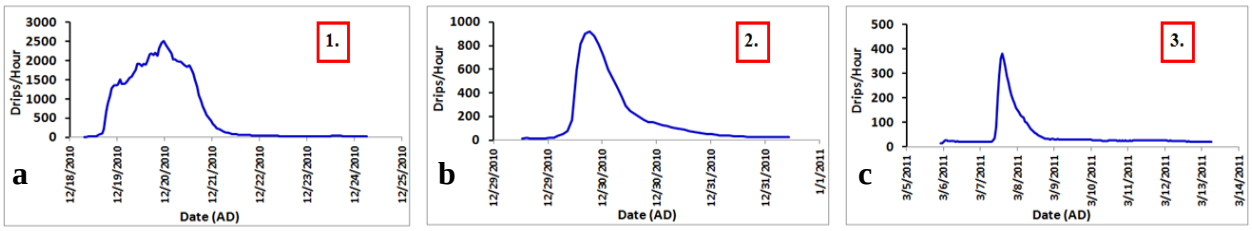

Figure 2.11. A close-up view of the three extreme drip logger events that peaked on a) 12/20/2010, b) 12/30/2010, and c) 3/8/2011 (see Fig. 2.10a).

A close view of the three extreme drip logger events that peaked on 1). 12/20/2010, 2). 12/30/2010, and 3). 3/8/2011 reveals a non linear response of drip rate to large precipitation events (Fig. 2.11). This pattern, widely seen in other caves, could reflect saturation of soil above the cave, a switch from primarily diffuse to fracture flow, or the passage of other pools beyond a threshold amount. The 12/19/2010 maxima (Fig. 2.11a) shows sustained high flow over several days. A comparison between the California Data Exchange Center (CDEC) Giant Forest Sequoia National Park precipitation amount data and the drip logger rates of the three maxima precipitation events indicates the peak cave drip/hour was recorded approximately one to two days after the precipitation peak (http://cdec.water.ca.gov; see A2 tables and figures).

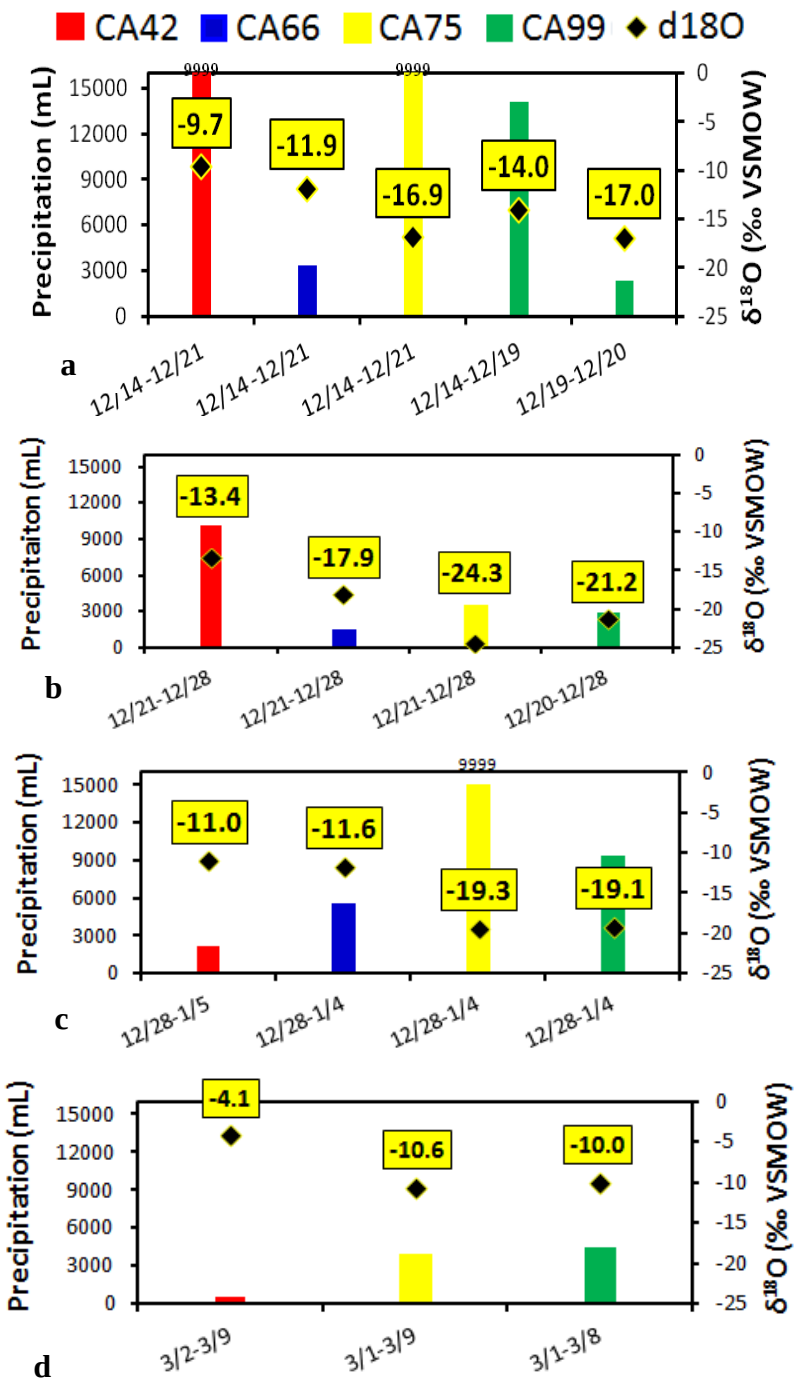

Figure 2.12. Plots of precipitation amounts and $\delta^{18}O$ at each of the four NADP sites (color coded) for extreme drip rate weeks, **a)** 12/14/2010 to 12/21/2010, **b)** 12/21/2010 to 12/28/2010, **c)** 12/28/2010 to 1/4/2011, and **d)** 3/2/2011 to 3/9/2011. (9999 signifies the collection bucket overflowed).

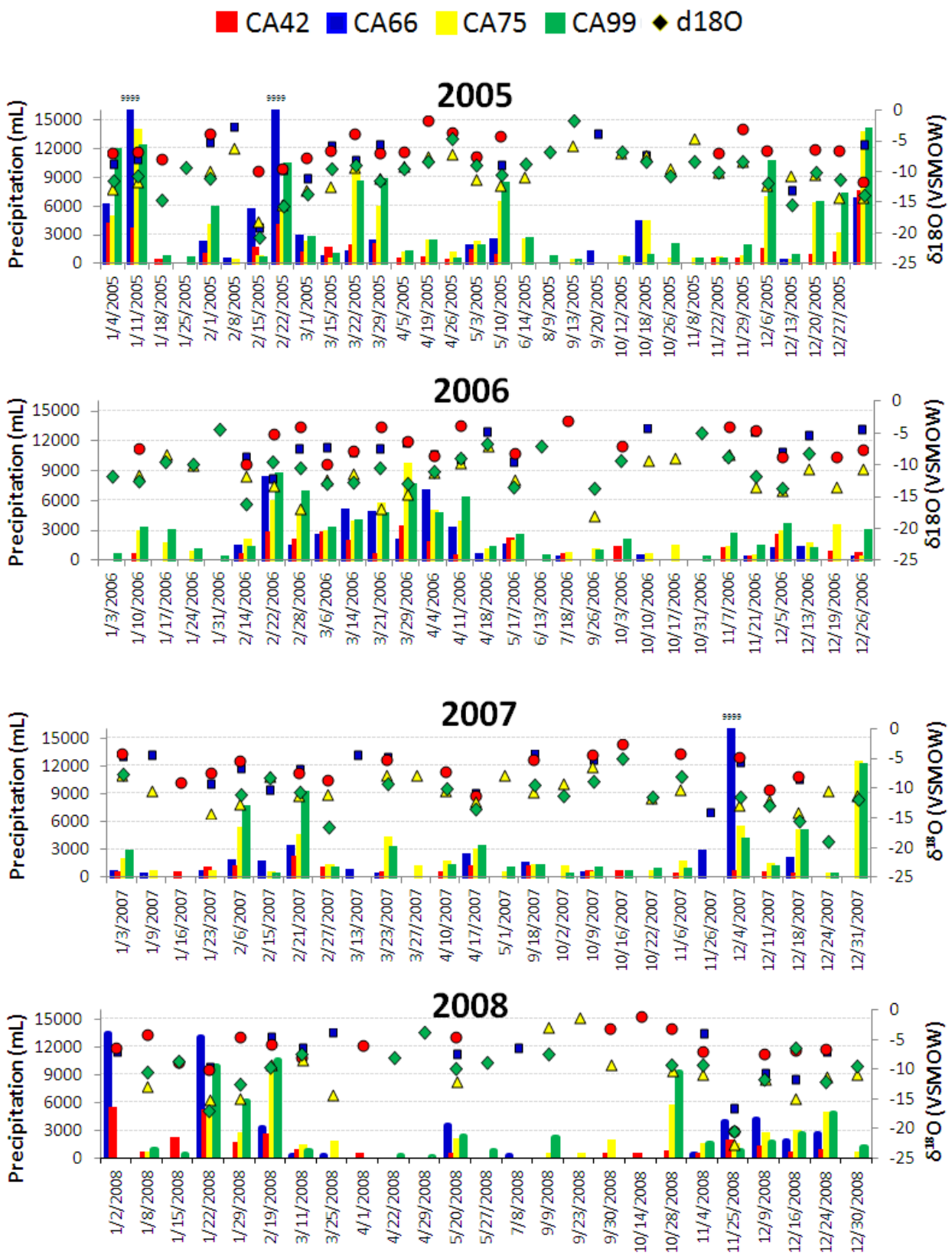
CA42
CA66
CA75
CA99
d18O
2005
2006
2007
2008
Precipitation (mL)
δ18O (VSMOW)
δ18O (VSMOW)

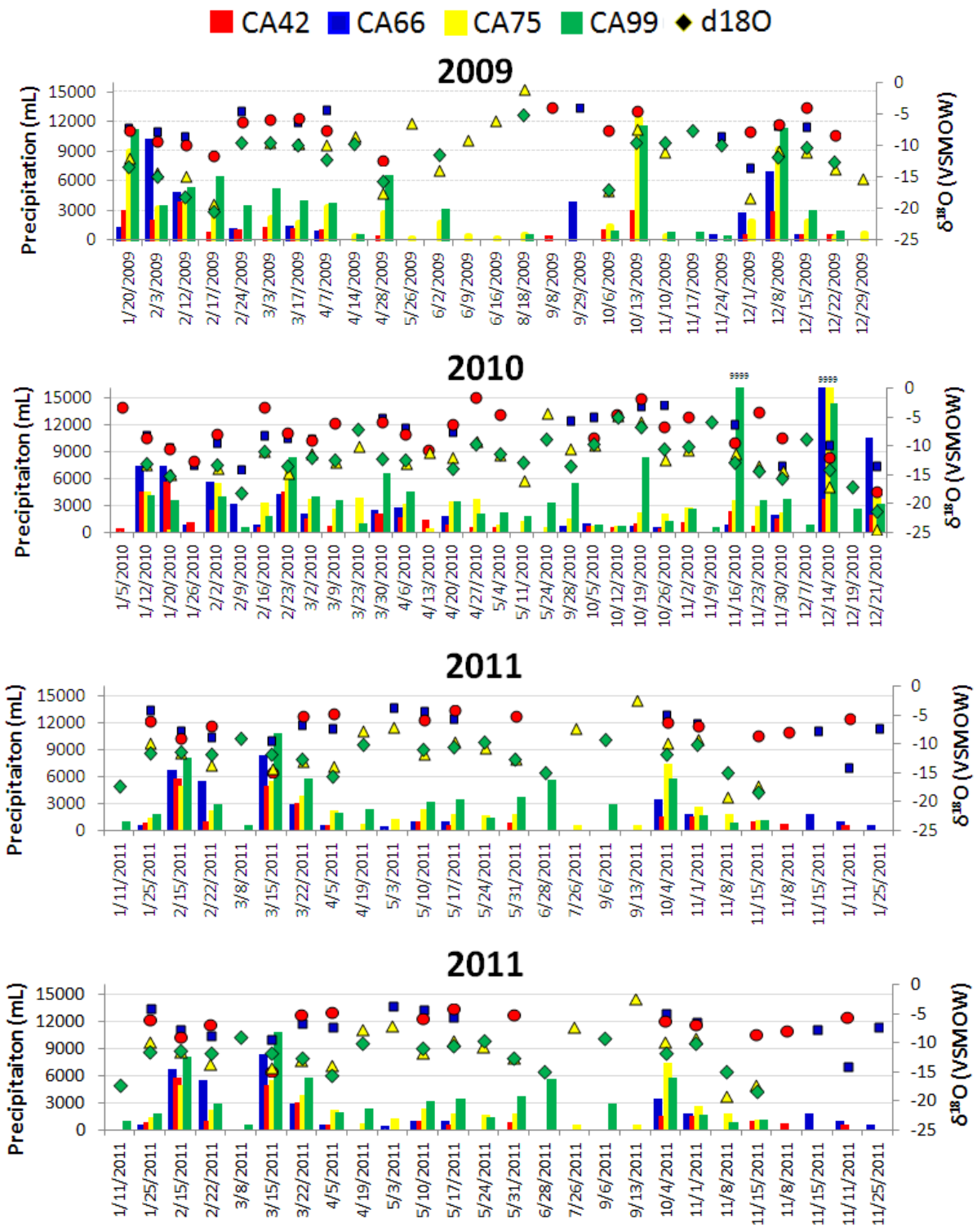

Figure 2.13. Plots show precipitation amount and coinciding $\delta^{18}O$ value from sites CA-42, CA-66, CA-75, and CA-99 between 2005 and 2011 (see color coding above plots and locations on map Fig. 2.7).

2.5.4 Precipitation amount and $\delta^{18}O$ results

Precipitation amounts and associated $\delta^{18}O$ values from each of the four NADP sites, CA-42, CA-66, CA-75, and CA-99, indicate that precipitation amounts at each site varied considerably, with some sites recording the collection bucket overflowed, and others, showing little or no record of precipittation and that isotopic values of individual storm event week also varied (Table A1) during the three extreme drip rate weeks, 12/14/2010 to 12/21/2010, 12/28/2010 to 1/4/2011, and 3/2/2011 to 3/9/2011. The coastal sites showed more positive isotopic values than the inland sites. The most negative isotopic values from all four sites over the 2005 to 2011 study period occurred the week of 12/21/2010 to 12/28/2010 (Table A1). Results of the analysis of NADP precipitation samples collected from all four sites between 2005 and 2011 show there is no correlation between the amount of precipitation and the $\delta^{18}O$ at site CA-75 and CA-99, and a low correlation of $r = 0.12$ at site CA-42 and $r = 0.13$ at site CA-66 (Fig. 2.13).

2.5.5 Back trajectory analysis results

Results of NOAA Hysplit model backward trajectories reaching the CA-75 Giant Forest site for the three extreme drip rate weeks and the week containing the lowest isotopic values show that different rainfall amounts were delivered on different days of the week transported via varying trajectories (Fig. 2.14; color-coded). While all weeks showed trajectories from various latitudes, the week ending 12/21/2010 show overall trajectories were delivered from the most southerly latitudes, whereas the week ending 1/4/2011 trajectories were overall directed from the highest latitudes (Fig. 2.14; color-coded). Hysplit rainfall amounts also varied indicating different precipitation amounts were transported via varying trajectories on different days of the week (Fig. 2.14; color-coded).

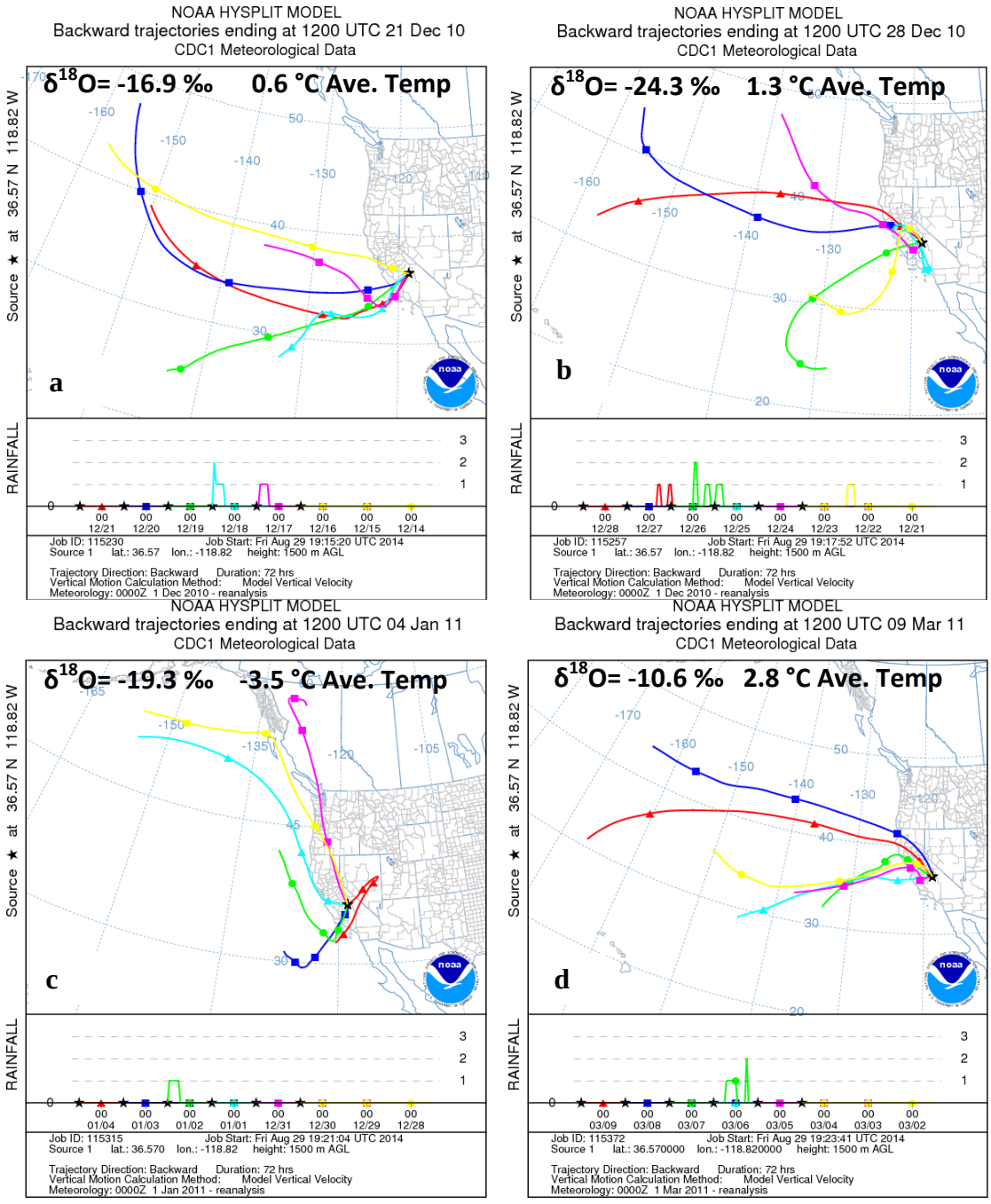

Figure 2.14. Plots show NOAA Hysplit model backward trajectories for the extreme drip rate weeks that occurred during the NADP collection weeks of **a)** 12/14/2010 to 12/21/2010, **c)** 12/28/2010 to 1/4/2011, and d) 3/4/2011 to 3/9/2011 and associated isotopic value. The week of **b)** 12/21/2010 to 12/28/2010 is also included to investigate trajectories that delivered the most negative precipitation isotopic values over the record. Individual trajectory days of the week are color coded with the corresponding rainfall amount (mm/hr) for NADP site CA-75 (Fig. 2.7).

2.5.6 Daily temperature, precipitation, and satellite image results

The California Data Exchange Center (CDEC) for Giant Forest Sequoia National Park (http://cdec.water.ca.gov; see appendix) daily temperature weekly average indicates each of the maxima precipitation events occurred during different temperatures ranging from -3.5°C the week ending 1/4/2011 to 2.8°C the week ending 3/9/2011. Satellite images reveal large amounts of moisture over the Pacific transported to the California coast during these weeks (Appendix Fig.A3,4,6,7,9,10).

2.6 Discussion

2.6.1 Cave monitoring and sample assessment

A year of continuous monitoring of a small isolated room in Crystal Cave showed pre-requisite criteria conditions were met for utilizing stalagmites for paleoclimate reconstruction such as a stable cave temperature and high relative humidity. This was further enhanced by the higher pCO_2 concentrations of ~675 ± 42 ppm that ensures slow degassing from drip waters and minimal kinetic fractionation during calcite precipitation. Furthermore, the average $\delta^{18}O$ of eight drip water samples collected between June 2007 and July 2008 at the CRC-3 drip site (-9.74 ± 0.48‰), the $\delta^{18}O$ value of modern glass plate calcite collected during the same period (-8.15‰), and the measured value of 7.87 °C, is very close to the calculated equilibrium temperature of 7.6 °C, indicating that CRC-3 calcite was likely precipitated under isotopic equilibrium conditions (Kim and O'Neil, 1997). The 10.4 cm columnar stalagmite, CRC-3, collected in 2008, consisted of clear calcite with slightly visible layers and no evident hiatuses. Although the application of the Hendy test is often problematic and unreliable because continuous sampling along a single

growth layer can be difficult to achieve and the visible layers are often thinner along the flanks of stalagmites than the central growth axis (Mickler et al., 2006; Dreybrodt, 2008), it is still standard practice amongst speleothem researchers. The Hendy test results in this study provide additional confidence that the CRC-3 stalagmite has been forming in equilibrium conditions over the past. Additionally, since Crystal Cave has a relatively constant temperature, the variations in the drip water $\delta^{18}O$ are thus a reflection of the precipitation $\delta^{18}O$ above the cave.

2.6.2 Drip logger data

A comparison of the drip logger maximum peak event on 12/19/2010 and the day of peak precipitation amount above the cave on 12/17/2010, (Appendix Table A2.1 and A2.1a), indicates that it took approximately two days for the precipitation to influence drip rates in the cave. Figure 2.9b shows an increased drip rate began earlier in December, suggesting the soil and karst region above the cave had some initial moisture storage before reaching a threshold that contributed to increased moisture delivered through the flow path to the drip logger. The second extreme drip rate week recorded by the cave drip logger indicates the peak day of precipitation matched the peak drip logger day, 12/29/2010 (Table 2.2 and 2.2a) suggesting the soil and karst region above the cave was likely at capacity with moisture storage and reached a threshold that contributed to increased moisture delivered through the flow path to the drip logger very quickly. The third drip maximum logger event registered, however, showed less than 25 mm of precipitation was delivered (Table A2.3 and A2.3a). Upon further investigation, the Giant Forest station site, (http://cdec.water.ca.gov) posted *"Station comments: 03/08/2011 Precipitation tube has failed and liquid appears to have discharged for unknown reasons. This seems to have started 3/2/2011. Repair date unknown"* which may cause some discrepancies

with the actual day registered that the precipitation fell above the cave. However, considering that the other two drip logger event weeks contained much greater amounts of precipitation delivered, 426.7 mm from 12/14/2010 to 12/20/2010 and 119.4 mm from 12/28/2010 to 1/3/2011, compared to the 25.4 mm delivered from 3/1/2011 to 3/8/2011 during the third extreme drip rate week, this suggests the storage region above the cave may have reached its threshold capacity and therefore responded rapidly to the small amount of precipitation delivered as shown in Fig. 2.9b with ~30 drips/hour prior to the third drip logger maxima.

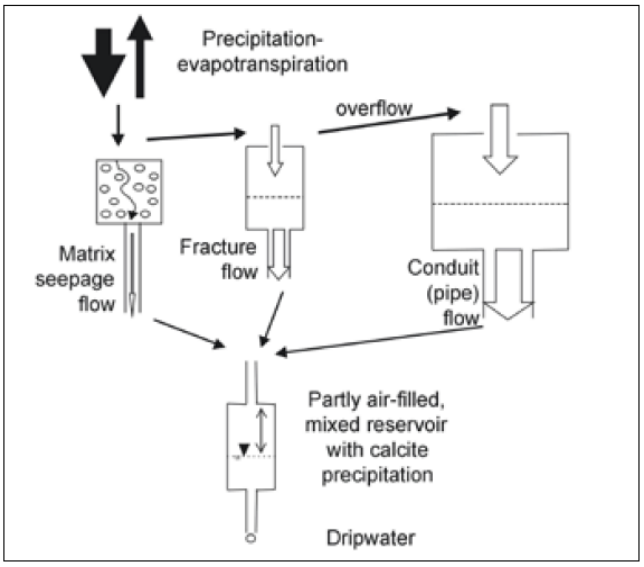

Figure 2.15. An example of a cave system model of controls on the composition in karstic drip waters show drips are fed by a mixture of water from different flow paths based on the modeling study by Fairchild et al., (2006a).

The three extreme drip rate weeks demonstrate a non-linear response of drip rate to large precipitation events and suggests the drip rate increases are due to a "piston flow" type behavior and likely do not represent water from that specific storm entering the cave (Tooth and Fairchild,

2003) which is also consistent with the small range in the cave drip water $\delta^{18}O$. This response could reflect saturation of soil above the cave, a switch from primarily diffuse to fracture flow, or the passage of other pools beyond a threshold amount as shown in the cave system model in Fig. 2.15.

2.6.3 Precipitation amount, $\delta^{18}O$ values, and moisture source regions

Analysis of the precipitation amount and $\delta^{18}O$ values for the four NADP sites during each of the three extreme drip rate weeks indicates various amounts of precipitation fell at each site with different isotopic compositions between the sites during individual events (Fig. 2.12). During the first drip logger event week, precipitation samples collected from 12/14/2010 to 12/21/2010 show the buckets at CA-42 and CA-75 overflowed (Fig. 2.12a). Meteorological evidence indicates this week, 12/14/2010 to 12/21/2010, contained a large atmospheric river, the 'Pineapple Express' type, transporting low-to-mid latitude moisture to California December 17 - 22, 2010 (Ralph and Dettinger, 2012; see Chapter 6). As studies have indicated the most negative $\delta^{18}O$ values are delivered via the North Pacific storm track and the most positive values from the Tropical Pacific, this would suggest moisture would consist of more positive $\delta^{18}O$ values (Berklehammer et al., 2012), however, the relatively more negative isotopic values are likely due to Rayleigh distillation occurring due to the long duration of this event. Personal communication with Christopher Lehmann from the NADP network, informed me that the bucket at CA-99 was collected and changed on 12/19/2010 and again on 12/20/2010 (Fig. 2.12a), so it did not overflow. Even though much less precipitation was collected in the bucket at the CA-99 site from 12/19 to 12/20/2010, the $\delta^{18}O$ values are 3‰ more negative than the precipitation collected from CA-99 12/14/2010 to 12/19/2010 (Fig. 2.12a), further supporting

Rayleigh distillation for the long lasting event (Ralph and Dettinger, 2012). While relatively more positive $\delta^{18}O$ values are observed at the coastal sites for the event weeks, more negative $\delta^{18}O$ values are observed for the inland sites, also consistent with Rayleigh distillation expected due to topographic and continentality effects. Hysplit analysis indicates the storms on 12/29/2010 and 3/7/2011 transport moisture from higher latitudes. However, more positive isotopic compositions from the 3/7/2011 event suggest the variability likely arises from local conditions, with decreased convective activity and/or decreased near surface relative humidity contributing to increased precipitation $\delta^{18}O$ (Berkelhammer et al., 2012).

The second largest drip logger event occurred during the week of 12/28/2010 to 1/4/2011 (Fig. 2.12c). Varying amounts of precipitation were delivered to each site, with more precipitation delivered to the inland sites, CA-75 and CA-99 with the greatest amount to the CA-75 mountainous site, in which the bucket overflowed (Fig. 2.12c). As the CA-99 site (Yosemite National Park) is about 160 km (100 miles) north of CA-75 (Sequoia National Park) and about 500 m lower in elevation, this precipitation amount difference is likely due to orographic effects. The isotopic compositions are similar for both coastal sites at about -11‰, and decrease greatly for both mountainous sites at about -19‰. Additionally, this week contained the lowest temperature of the three events at -3.5 °C. While the Hysplit trajectories show trajectories delivered from both higher and lower latitudes, the greater precipitation amounts for the CA-66 coastal site compared to the more southerly coastal site CA-42, suggests the bulk of precipitation was delivered from the mid to higher latitudes.

The third largest drip logger event occurred during the week of 3/2/2011 to 3/9/2011 and shows precipitation registered a very small amount at CA-42, the more southerly coastal site (34.21°N),

while no precipitation registered at CA-66 (36.48 °N) and relatively low amounts fell at the inland sites, compared to the two other December events (Fig. 2.12c). While the Hysplit trajectories show trajectories from both high and low latitudes, the relatively higher precipitation isotopic compositions suggest again that some isotopic variability likely arises from local conditions, with decreased convective activity and/or decreased near surface relative humidity contributing to increased precipitation $\delta^{18}O$ (Fig. 2.14) (Berkelhammer et al., 2012). This scenario is shown in the Hysplit rainfall amount which indicates the greatest precipitation fell on 3/6/2011 (green line mm/hr) in which the 3/6/2011 trajectory (green line) indicating the moisture was delivered from a lower latitude and more local source (Fig. 2.14d). The average temperature at CA-75 for this week was the highest of the three events at 2.2 °C (Fig. 2.14d). The similar isotopic values for the inland sites suggest the processes influencing condensation (percent convective precipitation) and post-condensation (relative humidity) were similar, implying an important role of local meteorological conditions (condensation height, droplet size and velocity) (Coplen et al., 2008; Friedman et al., 2002).

To further investigate how moisture varies during modern precipitation events, we compared the amount and the $\delta^{18}O$ of precipitation delivered to all four NADP sites from 2005 to 2011. The precipitation isotopic values indicate the most negative $\delta^{18}O$ precipitation values occurred the week of 12/21/2010 to 12/28/2010 (Table A2.4). While the CDEC daily precipitation data indicates the greatest amount of precipitation during that week, 27.9 mm, occurred on 12/22/2010 with a daily temperature of 0.0°C (Table A2.4) and the 12.7 mm of precipitation delivered on 12/26/2010 with a daily temperature of -2.8 °C, the Hysplit plot shows this trajectory is from a southerly location (yellow line; Fig. 2.14b), suggesting that the cool

temperatures contributed to more negative $\delta^{18}O$ precipitation values. Using the isotopic variability range of 0.5 to 0.7‰/°C for $\delta^{18}O$ in precipitation (Rozanski et al., 1993), we could expect 1.4 to 2‰ variability due to the difference in temperature. Furthermore, the CDEC daily precipitation data shows 0 mm for 12/27/2010 (Table A2.4), the Hysplit trajectory plot indicates high rainfall occurred on 12/27/2010 (Fig. 2.14; red line) with a long trajectory from a more northerly source location, likely influencing increased Rayleigh distillation and contributing to this low $\delta^{18}O$ value. Results of the analysis of NADP precipitation samples collected from all four sites between 2005 and 2011 show there is no correlation between the amount of precipitation and the $\delta^{18}O$ at site CA75 and CA99, and a low correlation of 0.12 at site CA42 and 0.13 at site CA-66 (Fig. 2.13; Table A1).

2.6.4 Crystal Cave drip water $\delta^{18}O$ and Giant Forest precipitation $\delta^{18}O$

The Crystal Cave drip water $\delta^{18}O$ values vary throughout the spring, summer, and fall collections, with an average $\delta^{18}O$ of -9.93‰. The Giant Forest CA-75 precipitation water year (Oct to Sept) weighted precipitation $\delta^{18}O$ values are lower due to the higher elevation of the cave. Interestingly, the Crystal Cave drip water isotopic analysis (Table 2.1) appears to reflect the isotopically depleted precipitation $\delta^{18}O$ from the weighted water year at CA75 (Table A4) which includes the large Pineapple Express storm, December 17 - 22, 2010, indicating that speleothems could be sensitive to years with large atmospheric rivers (see Chapter 5).

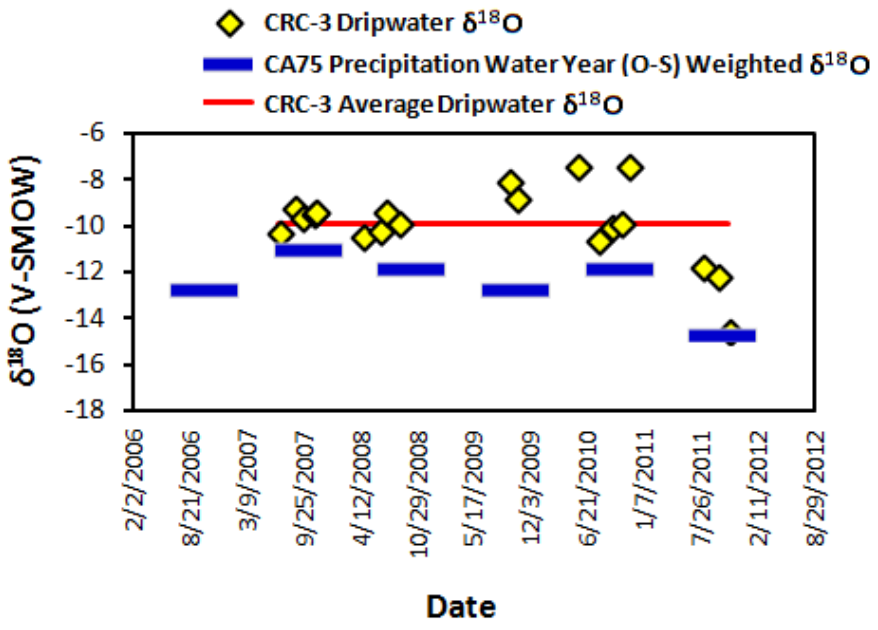

Figure 2.16 CRC-3 drip water $\delta^{18}O$ (yellow diamonds), Giant Forest weighted water year (Oct - Sept) precipitation $\delta^{18}O$ values (blue lines), and average drip water values (red line).

2.7 Conclusions

A detailed and continuous monitoring regimen in Crystal Cave in Sequoia National Park, California, indicates that speleothems from this location are suitable for paleoclimate reconstruction. A 10.4 cm columnar stalagmite, CRC-3, actively forming in a stable cave environment (eg. constant temperature and high relative humidity) was likely precipitated under isotopic equilibrium conditions (Kim and O'Neil, 1997). Additionally, the results of the Hendy Test supports that the $CaCO_3$ was precipitated in equilibrium with drip water in the past and was not impacted by kinetic effects related to rapid degassing or evaporation. Crystal Cave drip-water flow is fastest during the winter and spring, ~ 25 drips/hour and decreases late summer and fall to the lowest values of < 5 drips/hour with its lowest rates observed at removal in November

2013 (Fig. 2.9b and 2.10b), consistent with 2013 being the lowest precipitation year on record for California. The drip logger data reveals three extreme increases in drips/hour from 7/2010 to 7/2011that peaked on 1). 12/20/2010, 2). 12/30/2010, and 3). 3/8/2011 and reveals a non linear response of drip rate to large precipitation events (Fig. 2.11) with the 12/19/2010 event showing sustained high flow over several days (Fig. 2.11a). Comparison with precipitation data indicates the three extreme drip rate weeks took approximately one to two days for the cave drip flow to respond to precipitation delivered above the cave, suggesting the saturation of soil above the cave, a switch from primarily diffuse to fracture flow, or the passage of other pools beyond a threshold amount and demonstrating that Crystal Cave is hydrologically sensitive to the passing of storms above the cave. The drip logger data also reveals three extreme increases in drips/hour from 7/29/2010 to 7/29/2011 that peaked on 1) 12/19/2010, 2) 12/29/2010, and 3) 3/7/2011 (Figs. 2.9a).

Precipitation amounts and associated isotopic values from each of the four NADP sites, two coastal (CA-42 and CA-66), and two inland, (CA-75 and CA-99), varied considerably during the three extreme drip rate congruent weeks, with the coastal site isotopic values being more enriched than the inland sites. The lowest precipitation isotopic values from all four sites over the 2005 to 2011 study period occurred the week of 12/21/2010 to 12/28/2010, likely due to the more northerly Hysplit trajectories and low weekly temperature (Fig. 2.14c). The largest recorded precipitation event delivered between 12/14/2010 to 12/21/2010, also had relatively low isotopic values, however, Hysplit trajectories indicate more southerly trajectories, consistent with the 'Pineapple Express' type Atmospheric Rivers (see Chapter 5), indicating that Raleigh Distillation due to the duration and distance of each trajectory may have contributed to the

relatively lower values. The results of NADP archived precipitation samples from 2005 to 2011 reveal that there is no correlation between the amount of precipitation and the $\delta^{18}O$ at the Giant Forest site, CA-75, and lend support to the interpretation of speleothem $\delta^{18}O$ as a proxy for storm track and moisture source origin. This study can also be useful to validate isotope enabled climate models to determine the mechanisms contributing to isotopic variations both temporally and spatially at the four sites during individual storm events. Future research is warranted to decipher the other three extreme drip rate weeks noted by the drip logger data from 10/29/2012 to 11/21/2013.

2.8 References

Baker, A., Smith, C. L., Jex, C., Fairchild, I. J., Genty, D., Fuller, L., 2008. Annually Laminated Speleothems: a Review. *International Journal of Speleology*. 37, 193-206.

Baker, A., Genty, D., Smart, P. L., 1998. High-resolution records of soil humification and paleoclimate change from variations in speleothem luminescence excitation and emission wavelengths. *Geology*. 26, 903-906.

Berkelhammer, M., Stott, L., Yoshimura, K., Johnson, K., Sinha, A., 2012. Synoptic and mesoscale controls on the isotopic composition of precipitation in the western United States. *Climate Dynamics*. 38, 433-454.

Cayan, D. R., Dettinger, M. D., Diaz, H. F., Graham, N. E., 1998. Decadal variability of precipitation over western North America. *Journal of Climate*. 11, 3148-3166.

Coplen, T. B., Neiman, P. J., White, A. B., Landwehr, J. M., Ralph, F. M., Dettinger, M. D., 2008. Extreme changes in stable hydrogen isotopes and precipitation characteristics in a landfalling Pacific storm. *Geophysical Research Letters.* 35.

Dansgaard, W., 1964. Stable isotopes in precipitation. *Tellus.* 16, 436-468.

Despain, J. D. and Stock, G. M., 2005. Geomorphic history of Crystal Cave, Southern Sierra Nevada, California. *Journal of Cave and Karst Studies*. 67, 92-102.

Dreybrodt, W., 2008. Evolution of the isotopic composition of carbon and oxygen in a calcite precipitating H_2O–CO_2–$CaCO_3$ solution and the related isotopic composition of calcite in stalagmites. *Geochim. Cosmochim. Acta*. 72, 4712–4724.

Fairchild, I. J., Smith, C. L., Baker, A., Fuller, L., Spötl, C., Mattey, D., McDermott, F., 2006. Modification and preservation of environmental signals in speleothems. *Earth-Science Reviews.* 75, 105-153.

Francis, J. A. and Vavrus, S. J., 2012. Evidence linking Arctic amplification to extreme weather in mid-latitudes. *Geophysical Research Letters.* 39.

Friedman, I., Harris, J. M., Smith, G. I., Johnson, C. A., 2002. Stable isotope composition of waters in the Great Basin, United States 1. Air-mass trajectories. *Journal of Geophysical Research: Atmospheres* (1984–2012). 107, ACL 14-1-ACL 14-14.

Frisia, S., Borsato, A., Fairchild, I. J., McDermott, F., 2000. Calcite fabrics, growth mechanisms, and environments of formation in speleothems from the Italian Alps and southwestern Ireland. *Journal of Sedimentary Research.* 70, 1183-1196.

Gat, J. R., 1996. Oxygen and Hydrogen isotopes in the hydrologic cycle. *Annual Reviews of Earth and Planetary Science.* 24, 225-262.

Genty, D., Baker, A., Barnes, W., 1997. Comparison of annual luminescent and visible laminae in stalagmites. *Comptes Rendus De L Academie Des Sciences Serie Ii Fascicule a-Sciences De La Terre Et Des Planetes.* 325, 193-200.

Hendy, C. H., 1971. The isotopic geochemistry of speleothems. Part 1. The calculation of the effects of different modes of formation on the isotopic composition of speleothems and their applicability as paleoclimatic indicators. *Geochimica Et Cosmochimica Acta*. 35, 805-824.

Kim, S. T. and O'Neil, J. R., 1997. Equilibrium and nonequilibrium oxygen isotope effects in synthetic carbonates. *Geochimica Et Cosmochimica Acta*. 61, 3461-3475.

Lachniet, M. S., 2009. Climatic and environmental controls on speleothem oxygen-isotope values. *Quaternary Science Reviews*. 28, 412-432.

Lorens, R. B., 1981. Sr, Cd, Mn and Co distribution coefficients in calcite as a function of calcite precipitation rate. *Geochimica Et Cosmochimica Acta.* 45, 553-561.

McDermott, F., 2004. Palaeo-climate reconstruction from stable isotope variations in speleothems: a review. *Quaternary Science Reviews*. 23, 901-918.

McDermott, F., Schwarcz, H.P., Harmon, R.S., Thompson, P., Ford, D.C., 2006. Isotopes in speleothems, in: Leng, M. J. (Ed.), *Isotopes in Palaeoenvironmental Research.* Springer, Dordrecht, the Netherlands, pp. 185–225.

Mickler, P. J., Banner, J. L., Stern, L., Asmerom, Y., Edwards, R. L., Ito, E., 2004. Stable isotope variations in modern tropical speleothems: Evaluating equilibrium vs. kinetic isotope effects. *Geochimica Et Cosmochimica Acta.* 68, 4381-4393.

Mickler, P. J., Stern, L. A., Banner, J. L., 2006. Large kinetic isotope effects in modern speleothems. *Geological Society of America Bulletin.* 118, 65-81.

Nešić, M., Marković, M., Trajković, R., Pavlović, D., Ilić, M., Mitić, V., Stankov-Jovanović, V., 2010. Total content of organic acids in plants from fire affected forest. *Biol.Nyssana.* 1, 65-69.

Ralph, F. and Dettinger, M., 2012. Historical and national perspectives on extreme West Coast precipitation associated with atmospheric rivers during December 2010. *Bulletin of the American Meteorological Society*. 93, 783-790.

Rozanski, K., Araguas-Araguas, L., Gonfiantini, R., 1993. Isotopic patterns in modern global precipitation. *Geophysical Monograph*. 78, 1-36.

Swetnam, T. W., Baisan, C. H., Caprio, A. C., Brown, P. M., Touchan, R., Anderson, R. S., Hallett, D. J., 2009. Multi-millennial fire history of the giant forest, Sequoia National Park, California, USA. *Fire Ecology*. 5, 120-150.

Tooth, A. F. and Fairchild, I. J., 2003. Soil and karst aquifer hydrological controls on the geochemical evolution of speleothem-forming drip waters, Crag Cave, southwest Ireland. *Journal of Hydrology*. 273, 51-68.

CHAPTER 3

Variable North Pacific influence on drought in southwestern North America since AD 854

3.1 Introduction

Precipitation in southwestern North America (SWNA) is highly seasonal and exhibits interannual to multidecadal variability linked to naturally recurring large-scale atmospheric circulation patterns. Instrumental records and climate model simulations demonstrate that Pacific sea surface temperature (SST) patterns related to coupled climate modes such as the El Niño/Southern Oscillation (ENSO) and the Pacific Decadal Oscillation (PDO) exert substantial control on SWNA hydroclimate over the twentieth century, with typically drier conditions during the cool phases (negative PDO and La Niña) and wetter conditions during the warm phases (positive PDO and El Niño) (Cook et al., 2007; Dettinger et al., 1998; Mantua and Hare, 2002). Furthermore, North Atlantic SSTs also played a role in twentieth-century droughts, with warmer SSTs linked to drier conditions (McCabe, et al. 2004; Cook, et al. 2011). SST reconstructions, however, provide conflicting evidence about the cause of earlier droughts. For instance, the SWNA megadroughts of the Medieval Climate Anomaly (MCA) have been attributed to persistent La Niña-like conditions (Cook et al., 2007; Cobb et al., 2003; Mann et al., 2009), but interannual mechanisms such as ENSO may not be appropriate for explaining decadal- to centennial-scale precipitation variability. Although many reconstructed droughts of the past millennium do seem synchronous with cool eastern equatorial Pacific (EEP) SSTs, others do not (Cole et al., 2002; Conroy et al., 2009), thus highlighting the potential importance of other influences such as the North Pacific and the North Atlantic.

Most climate models project enhanced aridity in SWNA as a result of global warming (Seager and Vecchi, 2010). The projected drying trend is attributed to decreased winter precipitation as a result of a strengthening and poleward shift of the North Pacific storm track. However, given the strong influence of the Pacific Ocean on SWNA hydroclimate, the magnitude and extent of drought will be strongly dependent on the specific SST patterns that result from radiative forcing and natural decadal variability (Seager and Vecchi, 2010). Despite the fact that North Pacific decadal variability (NPDV) is a critical predictor of regional and global climate change, twentieth century simulations with Intergovernmental Panel on Climate Change Fourth Assessment Report models show little agreement with observations of the two leading North Pacific SST patterns, the PDO and the North Pacific Gyre Oscillation (Furtado et al., 2011). This reflects significant uncertainty about the mechanisms of NPDV, with several studies suggesting that NPDV is the low-frequency manifestation of tropical ENSO variability (Shakun and Shaman, 2009), whereas other studies suggest that mid-latitude ocean-atmosphere coupling dominates (Latif and Barnett, 1994).

Improved understanding of the dynamics of decadal-scale SST variability, tropical-North Pacific teleconnections, and the past response to changing boundary conditions is therefore critical for predicting future NPDV, yet progress is limited at present by the paucity of high-resolution palaeoclimate records. Existing records of North Pacific SSTs over the past millennium are primarily PDO reconstructions derived from tree rings that assume a consistent response of regional precipitation to NPDV (Biondi et al., 2001; MacDonald and Case, 2005; D'Arrigo and Wilson, 2006), and are influenced by multiple factors including temperature and evapotranspiration. These factors, variations in the spatial patterns of drought, and the potential

nonlinear response of tree growth to moisture availability may explain why there is only weak coherence among independent PDO reconstructions before the twentieth century (Kipfmueller et al., 2012). Here, we use a new speleothem-based approach to reconstruct North Pacific SSTs by taking advantage of the strong relationship between oxygen isotopes in precipitation in SWNA and North Pacific storm trajectories (Friedman et al., 1992; Berkelhammer et al., 2012).

3.2 Sample and methods

The CRC-3 stalagmite was collected from beneath an active drip in a small isolated chamber of Crystal Cave in Sequoia National Park in 2008. The sample was cut in half, parallel to the growth axis and polished. Subsamples (~100 mg) were drilled along the growth axis for ^{230}Th dating at the Minnesota Isotope Laboratory on a multiple-collector inductively coupled plasma mass spectrometer (Thermo-Finnigan Neptune). Corrected ^{230}Th ages assume an initial ^{230}Th/^{232}Th atomic ratio of $8 \pm 1 \times 10^{-5}$. A total of 10 ^{230}Th dates were obtained with typical uncertainties in age (2-sigma) less than 0.1 kyr, which include analytical errors and uncertainties in the initial ^{230}Th/^{232}Th ratios (Supplementary Table S2). Subsamples for stable isotope analysis were micromilled with a New Wave Research Micromill at 50μm resolution for the upper 2mm and 100 μm intervals for the remainder of the sample. The δ^{18}O values of 30-70 μg powdered calcite samples were determined using a Kiel IV-carbonate device coupled with a Thermofinnigan Delta V Plus isotope ratio mass spectrometer. A total of 16 standards (NBS-19, NBS-18 and OX, an in-house quality control standard) were analyzed during each run of 30 unknown samples. The results of isotopic analysis are presented in conventional delta (δ) notation, defined as: The ^{18}O/^{16}O ratios are expressed in ‰‘‘per mil’’ or parts per thousand

notation and expressed using ‘‘delta’’ (δ) notation. $\delta^{18}O = [(^{18}O/^{16}O)_{sample}/(^{18}O/^{16}O)_{VPDB} -1]$ *1,000‰. The standard deviation of repeated NBS-19 measurements is ~0.06 ‰ for $\delta^{18}O$.

The raw $\delta^{18}O$ and age data are presented in Supplementary Table S1. For wavelet analyses and all correlations, data were interpolated to an annual timescale using Matlab interp1 function. Statistical analyses were conducted using JMP software. All time series and residuals from linear or multiple regressions were checked for normal distributions using the Shapiro-Wilk W-test. All reported correlation coefficients are Pearson's *r* values. Spearman's ρ values were also calculated and were similar to r values in all cases. Significance testing was conducted using a combination of 1,000 Monte Carlo iterations and time-series modeling in the frequency domain to account for autocorrelation effects using the Matlab package of (Macias-Fauria et al., 2012).

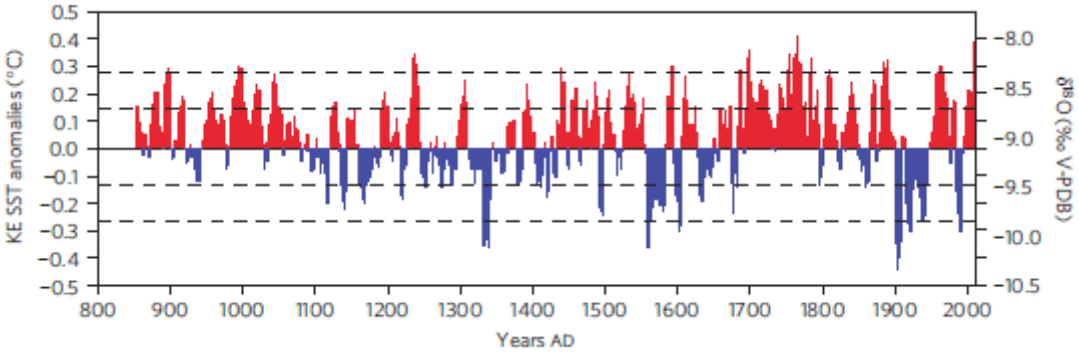

Figure 3.1. Extended Kuroshio Extension SST anomaly reconstruction and CRC-3 ^{18}O values. SST anomalies were calculated using a linear regression of low-pass-filtered SST anomalies within the Kuroshio Extension (KE) region and the CRC-3 $\delta^{18}O$ time series over the full period of overlap (1857–2007). Positive values (red) indicate warmer SSTs and negative values (blue) indicate cooler SSTs compared with the long-term mean. Dashed lines show 1 and 2 standard deviations (0.14 and 0.28°C), respectively.

We have developed an absolute-dated, high-resolution $\delta^{18}O$ record from a stalagmite, CRC-3, collected from Crystal Cave in Sequoia National Park, California (36.59°N; 118.82°W; 1,386 m;

Supplementary Fig. S1). The record is based on 1,054 $\delta^{18}O$ measurements (Supplementary Fig. S2) conducted on samples micromilled from the 10.4-cm-long stalagmite (Supplementary Table S1). The age model for CRC-3, which extends from AD 854 - 2007 (Supplementary Fig. S3), is based on ten ^{230}Th-^{234}U dates (Supplementary Table S2) and a top age of AD 2007, the time when a glass plate was placed over the stalagmite to confirm active calcite precipitation. The model was developed using the StalAge algorithm, which allows robust uncertainty estimation throughout the length of the record (Scholz and Hoffmann, 2011). To further constrain the age model over the twentieth century, we conducted 34 radiocarbon measurements on CRC-3 to locate the ^{14}C bomb peak. Results show that $\Delta^{14}C$ begins to rise at approximately AD 1955, synchronous with or slightly lagging the atmosphere. This is consistent with the rapid transmission of bomb ^{14}C observed at other sites (Genty and Massault, 1999) and thus provides support for the StalAge model (Supplementary Discussion and Fig. S4). Cave monitoring data suggest that the CRC-3 calcite formed under isotopic equilibrium conditions and that the $\delta^{18}O$ primarily reflects interannual changes in the $\delta^{18}O$ of precipitation above the cave (Supplementary Discussion).

Previous research indicates that the isotopic composition of precipitation in southern California is largely determined by the storm track delivering precipitation to this region (Friedman et al., 1992). To further investigate this, we conducted trajectory and clustering analysis and measured the isotopic composition of precipitation from storms reaching the study area between AD 2001 and 2005. Our analysis shows three primary clusters of storms entering the region, with the lowest $\delta^{18}O$ precipitation arriving from the North Pacific and the highest from the tropical Pacific (Supplementary Fig. S5). Although some isotopic variability may arise from local

conditions, these effects are most likely to enhance the proxy response. For instance, during the twentieth century, periods of warm Kuroshio Extension SSTs are associated with cool SSTs off the California coast (Qiu, 2000; Latif and Barnett, 1994) and increased aridity in SWNA (Cook et al., 2011); hence, the signal due to increased transport of isotopically enriched moisture during these periods may be amplified by decreased near-surface relative humidity and/or decreased rainfall, which also tend to increase precipitation $\delta^{18}O$ (Berkelhammer et al., 2012).

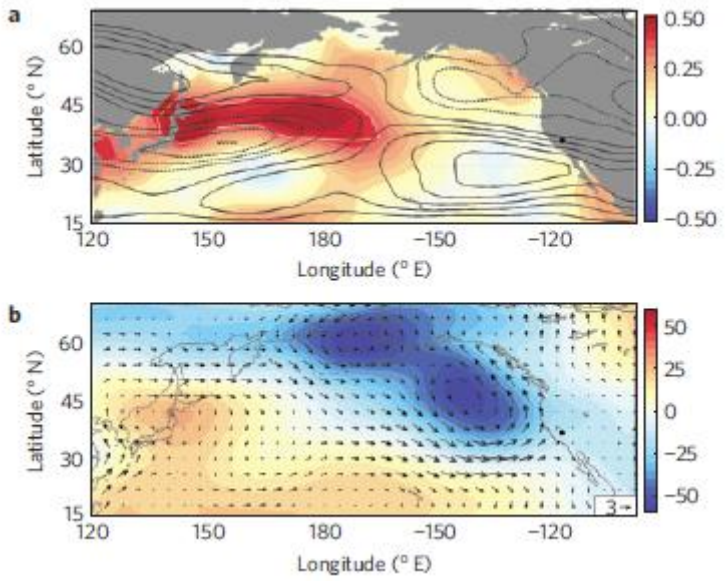

Figure 3.2 SST, wind and geopotential heights associated with CRC-3 $\delta^{18}O$ anomalies. All results show the mean from years in the upper quartile of $\delta^{18}O$ minus the mean of years in the lower quartile of $\delta^{18}O$. The black dot shows the Crystal Cave location. **a**, Shading is for low-pass-filtered annual mean (August–July) SST °C) for 1857–2007(Kaplan, et al. 1998). Contours are for November–April 250 hPa wind speed (contoured interval is 2 m s^{-1}; negative values dashed). **b**, For November–April data, shading is for 850-hPa geopotential height, and arrows are for 850-hPa wind velocity (scale arrow at lower right indicates a 3 m s^{-1} anomaly). Atmospheric fields in both panels are from the Twentieth-Century Reanalysis Project 1871–2007.

3.3 The influence of SSTs

The trajectory of storms arriving in SWNA is strongly dependent on Pacific SST patterns (Ren et al., 2008), which influence the position of the high- and low-pressure centres in the North Pacific and over the North American continent. An inverse correlation with the PDO Index (Mantua and Hare, 2002) between 1925 and 2008 ($r = -0.43$, $p = 0.04$) suggests that CRC-3 $\delta^{18}O$ values are sensitive to North Pacific SST patterns. To examine the underlying physical ocean-atmosphere mechanisms through which North Pacific SSTs may impact this record, we investigated SST anomalies (Kaplan et al., 1998) associated with the CRC-3 $\delta^{18}O$ values (Fig. 3.2a and Supplementary Fig. S6). High $\delta^{18}O$ values are strongly associated with anomalously warm SSTs in the Kuroshio Extension region east of Japan (white outline, Fig. 3.2a; essentially the PDO's western centre of action) whereas the corresponding anomalies in the eastern centre of action are relatively weak (off the west coast of North America, Fig. 3.2a). We thus compare the $\delta^{18}O$ record with standardized low-pass-filtered (30-year cutoff) SST anomalies from the Kuroshio Extension region (Kaplan et al., 1998) and observe a strong positive correlation ($r = 0.72$, $p < 0.001$) from AD 1857 to 2007 (Supplementary Fig. S7), accounting for more than half the variance in $\delta^{18}O$.

3.4 Interpreting CRC-3 $\delta^{18}O$ results

Anomalously high SSTs in the Kuroshio Extension provide heat fluxes that generate an atmospheric wave, shifting the jet stream north over the western Pacific and south over the eastern Pacific (Ren et al., 2008) (Fig. 3.2a). The same wave pattern is visible lower in the atmosphere where moisture is transported (~850 hPa) as a ridge over the western Pacific and a trough over the eastern Pacific (Fig. 3.2b). The troughing over the eastern Pacific is conducive to

mid-latitude cyclones travelling equatorward where they tap into ^{18}O-enriched moisture over the tropical Pacific. The overall tendency for a southwesterly fetch is indicated by the 850-hPa velocity anomalies directed towards the study site (Fig. 3.2b). Without the warm Kuroshio Extension anomalies, the jet stream lacks the amplified wave structure and the flow is more zonal, allowing the incoming systems to remain more poleward and transport ^{18}O-depleted moisture from higher latitudes. The strong correlation between speleothem $\delta^{18}O$ and Kuroshio Extension SSTs allows us to develop a calibrated and verified (Supplementary Methods and Table S3) high-resolution reconstruction of Kuroshio Extension SSTs from AD 854 to 2007 (Fig. 3.1). The Kuroshio Extension SST reconstruction features strong decadal variability with the highest SST anomaly (0.41 °C) occurring in AD 1765 and the lowest (-0.44 °C) in AD 1903, similar to the timing of extreme ENSO—PDO climate swings (AD 1750 and 1905) observed in some tree-ring records (Biondi et al., 2001). Taken as a whole, the mean SST anomalies are similar throughout the MCA (AD 900- 1,300 = 0.03 °C), Little Ice Age (LIA; 1,500- 1,850 = 0.07 °C) and the twentieth century (20th = 0.05 °C).

3.5 Kuroshio Extension SST record comparisons

A previous comparison with drought records from western North America showed that although most droughts occurred during periods of cool EEP SSTs, certain droughts were synchronous with warm EEP SSTs (El Niño-like) and thus required other explanations (Conroy et al., 2009). The Kuroshio Extension SST reconstruction further supports this interpretation. For instance, the record shows predominantly warm Kuroshio Extension SSTs during MCA droughts from AD~854-1080 (Fig. 3.3) when EEP SSTs were warm (Conroy et al., 2009), suggesting that some

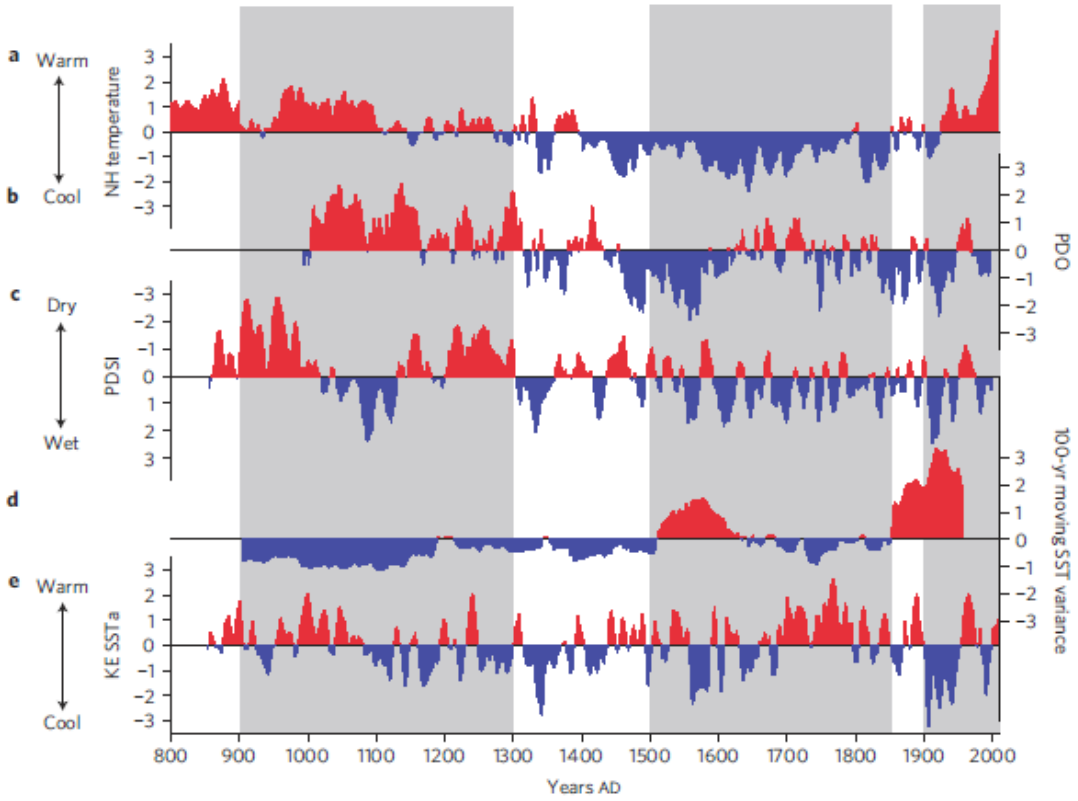

Figure 3.3 Comparison of the Kuroshio Extension SST anomaly *z*-scores with other key records. a, Northern Hemisphere (NH) temperatures (Mann et al., 2009). **b**, PDO Index AD 993–1996 (MacDonald and Case, 2005). **c**, Averaged PDSI for grid sites 48, 60, 61, 73 and 74 (Cook et al., 2007). **d**, 100-year moving variance for Kuroshio Extension SST Index. **e**, Reconstructed Kuroshio Extension SST anomalies. Northern Hemisphere temperature, PDO and PDSI data are 11-year moving averages. Shaded bars denote the MCA, the LIA and the twentieth century.

droughts could be driven more by NPDV than ENSO. Interestingly, the warmest Kuroshio Extension SSTs occurred during the LIA, from ~1,700 to 1,800, and the coolest occurred during the early twentieth century, a time in which SWNA was wetter than any other period of the past ~1,000 years (Cook et al., 2007; Woodhouse et al., 2010). The reconstructed Palmer Drought Severity Index (Cook et al., 2007) (PDSI) from grid points near the study site (Fig. 3.3c) indicates that Extension SSTs and perhaps during positive and negative PDO (Fig. 3b), although this is dependent on which PDO reconstruction is used (MacDonald and Case, 2005). Therefore,

this indicates that multiple factors are necessary to fully explain SWNA drought variability and highlights the need for further records to determine the mechanisms underlying North American droughts.

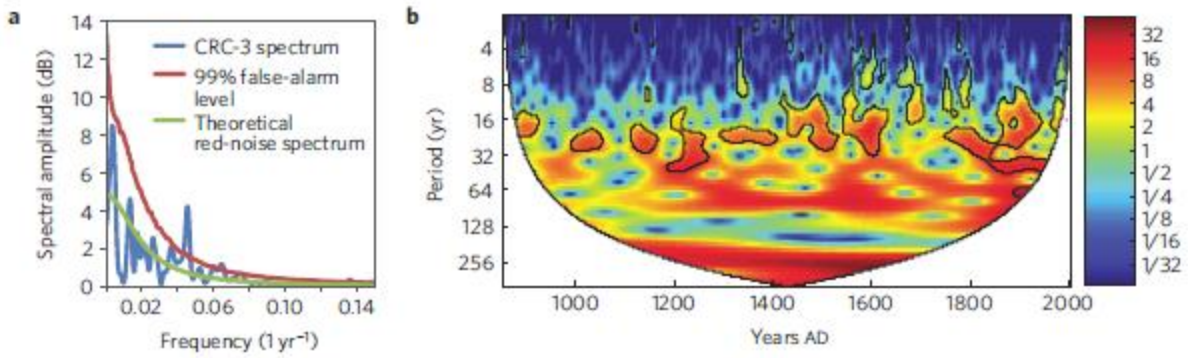

Figure 3.4 Spectral and wavelet analysis of the CRC-3 δ18O record. **a**, Spectrum of CRC-3 $\delta^{18}O$ time series estimated with a Lomb–Scargle Fourier Transform for unevenly spaced data (Schulz and Mudelsee, 2002). Three overlapping segments (50%) and a Hanning window were used. Results indicate a significant peak at 22 years (99% confidence level). **b**, Continuous wavelet power spectrum (Morlet wavelet) of the CRC-3 $\delta^{18}O$ record (Torrence and Compo, 1998). The black lines show the 5% significance level using the red noise model and the cone of influence. Results show significant periodicity in the 10–30-year band (centred at ~22). In addition, high multi-decadal power (~30–80 year band) is apparent between AD ~1300–1600 and AD 1800–2000.

3.6 Spectral and wavelet analyses

Spectral (Schulz and Mudelsee, 2002) and wavelet analyses (Torrence and Compo, 1998) of the reconstructed SST record indicate a strong and persistent 22-year periodicity (Fig. 3.4), similar to the twentieth-century PDO record (Mantua and Hare, 2002) and numerous tree-ring reconstructions (Biondi et al., 2001; MacDonald and Case, 2005), suggestive of the Hale solar cycle. Modeling studies suggest that the small solar irradiance signal may be amplified by changes in stratospheric heating or associated cloud feedbacks, both of which could influence the

position of the jet stream (Shindell et al., 1999; Meehl et al., 2003) and therefore, the source of moisture reaching the study site. An increase in low-frequency variance, which is also seen in other records (Mantua and Hare, 2002), becomes apparent from ~1,850 to the present (Fig. 3.4b). A plot of running variance shows the lowest values during the MCA (AD ~850-1100) and the highest values during the twentieth century (Fig. 3.3d), suggesting that NPDV may itself be affected by anthropogenic climate change rather than simply superimposed on the global-warming-related drying trend (Fig. 3.3a). The ensemble of 24 Intergovernmental Panel on Climate Change AR4 models is inconsistent with regard to variance change in either the PDO or North Pacific Gyre Oscillation, although the ensemble mean does suggest decreased twenty-first century variance in both modes (Furtado et al., 2011).

3.7 Conclusions

Precipitation in southwestern North America has exhibited significant natural variability over the past few thousand years (Cook et al., 2007). This variability has been attributed to sea surface temperature regimes in the Pacific and Atlantic oceans, and to the attendant shifts in atmospheric circulation patterns (Cook et al., 2007; McCabe et al., 2004). In particular, decadal variability in the North Pacific has influenced precipitation in this region during the twentieth century (Dettinger et al., 1998; Cook et al., 2011), but links to earlier droughts and pluvials are unclear. Here we assess these links using $\delta^{18}O$ data from a speleothem from southern California that spans AD 854– 2007. We show that variations in the oxygen isotopes of the speleothem correlate to sea surface temperatures in the Kuroshio Extension region (Qiu, 2000) of the North Pacific, which affect the atmospheric trajectory and isotopic composition of moisture reaching the study

site. Interpreting our speleothem data as a record of sea surface temperatures in the Kuroshio Extension, we find a strong 22-year periodicity, suggesting a persistent solar influence (Shindell et al., 1999) on North Pacific decadal variability. A comparison with tree-ring records of precipitation (Cook et al., 2007) during the past millennium shows that some droughts occurred during periods of warmth in the Kuroshio Extension, similar to the instrumental record (Cook et al., 2011). However, other droughts did not and instead must have been influenced by other factors. Finally, we find a significant increase in sea surface temperature variability over the past 150 years, which may reflect an influence of greenhouse gas concentrations on variability in the North Pacific.

The severity of future drought in the highly populated SWNA will undoubtedly reflect the combined influence of anthropogenic climate change and natural variability (Seager and Vecchi, 2010). Improved understanding of the mechanisms of natural NPDV is critical for accurate predictions of future hydroclimate. This new reconstruction is the first high-resolution record of Kuroshio Extension SSTs over the past millennium and provides evidence for variable North Pacific influence on past droughts in SWNA. In addition, the record contains evidence for recent changes in NPDV, perhaps in response to rising greenhouse gases, and highlights the importance of generating new and consistent SST reconstructions to determine how various climate modes contributed to past climate variability in SWNA. This record will provide valuable data for models to further investigate the ocean-atmosphere dynamics underlying NPDV, leading to improved predictions of future hydroclimate in SWNA.

3.8Acknowledgements

We would like to thank the Sequoia National Park staff, especially J. Despain, A. Esperanza, B. Tobin, H. Veercamp, E. Meyer and K. Nydick. All samples were collected with permission from the National Park Service (NPS Permits: SEKI-2007-SCI- 0024, SEKI-2008-SCI-0017, SEKI-2009-SCI-0004, SEKI-2010-SCI-0060, SEKI-2011-SCI-0053 and SEKI-2012-SCI-0440). We also thank J. Southon for assistance with radiocarbon dating. This work was partly supported by a faculty seed grant from the Newkirk Center for Science and Society at the University of California, Irvine, by the National Science Foundation grants to A.S. (ATM: 0823554 and AGS: 1103360) and by NSFC grant 41230524 to H.C.

3.9 References

Berkelhammer, M., Stott, L., Yoshimura, K., Johnson, K., Sinha, A., 2012. Synoptic and mesoscale controls on the isotopic composition of precipitation in the western United States. *Climate Dynamics.* 38, 433-454.

Biondi, F., Gershunov, A., Cayan, D. R., 2001. North Pacific decadal climate variability since 1661. *Journal of Climate.* 14, 5-10.

Cobb, K. M., Charles, C. D., Cheng, H., Edwards, R. L., 2003. El Nino/Southern Oscillation and tropical Pacific climate during the last millennium. *Nature.* 424, 271-276.

Cole, J. E., Overpeck, J. T., Cook, E. R., 2002. Multiyear La Niña events and persistent drought in the contiguous United States. *Geophysical Research Letters.* 29, 1647.

Conroy, J. L., Overpeck, J. T., Cole, J. E., Steinitz-Kannan, M., 2009. Variable oceanic influences on western North American drought over the last 1200 years. *Geophysical Research Letters.* 36, L17703.

Cook, B. I., Cook, E. R., Anchukaitis, K. J., Seager, R., Miller, R. L., 2011. Forced and unforced variability of twentieth century North American droughts and pluvials. *Climate Dynamics.* 37, 1097-1110.

Cook, E. R., Seager, R., Cane, M. A., Stahle, D. W., 2007. North American drought: reconstructions, causes, and consequences. *Earth-Science Reviews*. 81, 93-134.

D'Arrigo, R. and Wilson, R., 2006. On the Asian expression of the PDO. I*nternational Journal of Climatology.* 26, 1607-1617.

Dettinger, M. D., Cayan, D. R., Diaz, H. F., Meko, D. M., 1998. North-south precipitation patterns in western North America on interannual-to-decadal timescales. *Journal of Climate*. 11, 3095-3111.

Friedman, I., Smith, G. I., Gleason, J. D., Warden, A., Harris, J. M., 1992. Stable isotope composition of waters in southeastern California. 1: Modern precipitation. *Journal of Geophysical Research*. 97, 5795-5812.

Furtado, J. C., Di Lorenzo, E., Schneider, N., Bond, N. A., 2011. North Pacific decadal variability and climate change in the IPCC AR4 models. *Journal of Climate.* 24, 3049-3067.

Genty, D. and Massault, M., 1999. Carbon transfer dynamics from bomb ^{14}C and $\delta^{13}C$ time series of a laminated stalagmite from SW France; modelling and comparison with other stalagmite records. *Geochimica Et Cosmochimica Acta*. 63, 1537-1548.

Kaplan, A., Cane, M. A., Kushnir, Y., Clement, A. C., Blumenthal, M. B., Rajagopalan, B., 1998. Analyses of global sea surface temperature 1856-1991. J*ournal of Geophysical Research.* 103, 567-518.

Kipfmueller, K. F., Larson, E. R., George, S. S., 2012. Does proxy uncertainty affect the relations inferred between the Pacific Decadal Oscillation and wildfire activity in the western United States? *Geophysical Research Letters*. 39, L04703.

Latif, M. and Barnett, T. P., 1994. Causes of decadal climate variability over the North Pacific and North America. *Science.* 266, 634-637.

MacDonald, G. M. and Case, R. A., 2005. Variations in the Pacific Decadal Oscillation over the past millennium. *Geophysical Research Letters.* 32, L08703.

Macias-Fauria, M., Grinsted, A., Helama, S., Holopainen, J., 2012. Marc Macias-Fauria, Aslak Grinsted, Samuli Helama, Jari Holopainen. *Dendrochronologia*. 30, 179-187.

Mann, M. E., Zhang, Z., Rutherford, S., Bradley, R. S., Hughes, M. K., Shindell, D., Ammann, C., Faluvegi, G., Ni, F., 2009. Global signatures and dynamical origins of the Little Ice Age and Medieval Climate Anomaly. *Science*. 326, 1256-1260.

Mantua, N. J. and Hare, S. R., 2002. The Pacific decadal oscillation. J*ournal of Oceanography.* 58, 35-44.

McCabe, G. J., Palecki, M. A., Betancourt, J. L., 2004. Pacific and Atlantic Ocean influences on multidecadal drought frequency in the United States. *Proceedings of the National Academy of Sciences of the United States of America.* 101, 4136.

Meehl, G. A., Washington, W. M., Wigley, T. M. L., Arblaster, J. M., Dai, A., 2003. Solar and greenhouse gas forcing and climate response in the twentieth century. *Journal of Climate.* 16, 426-444.

Qiu, B., 2000. Interannual variability of the Kuroshio Extension system and its impact on the wintertime SST field. *Journal of Physical Oceanography*. 30, 1486-1502.

Ren, X., Zhang, Y., Xiang, Y., 2008. Connections between wintertime jet stream variability, oceanic surface heating, and transient eddy activity in the North Pacific. *Journal of Geophysical Research.* 113, D21119.

Scholz, D. and Hoffmann, D. L., 2011. StalAge-An algorithm designed for construction of speleothem age models. *Quaternary Geochronology*. 6, 369-382.

Schulz, M. and Mudelsee, M., 2002. REDFIT: estimating red-noise spectra directly from unevenly spaced paleoclimatic time series. *Computers & Geosciences*. 28, 421-426.

Seager, R. and Vecchi, G. A., 2010. Greenhouse warming and the 21st century hydroclimate of southwestern North America. *Proceedings of the National Academy of Sciences*. 107, 21277-21282.

Shakun, J. D. and Shaman, J., 2009. Tropical origins of North and South Pacific decadal variability. *Geophysical Research Letters*. 36, L19711.

Shindell, D., Rind, D., Balachandran, N., Lean, J., Lonergan, P., 1999. Solar cycle variability, ozone, and climate. *Science.* 284, 305-308.

Torrence, C. and Compo, G. P., 1998. A practical guide to wavelet analysis. *Bulletin of the American Meteorological Society.* 79, 61-78.

Woodhouse, C. A., Meko, D. M., MacDonald, G. M., Stahle, D. W., Cook, E. R., 2010. A 1,200-year perspective of 21st century drought in southwestern North America. *Proceedings of the National Academy of Sciences.* 107, 21283-21288.

Supplementary Information

Variable North Pacific influence on drought in southwestern North America since AD 854

Staryl McCabe-Glynn, Kathleen R. Johnson*, Courtenay Strong, Max Berkelhammer, Ashish Sinha, Hai Cheng, R. Lawrence Edwards

*Corresponding author: E-mail: kathleen.johnson@uci.edu, Phone: +1-949-824-6174

This file includes:

S3.1. Supplementary Figures

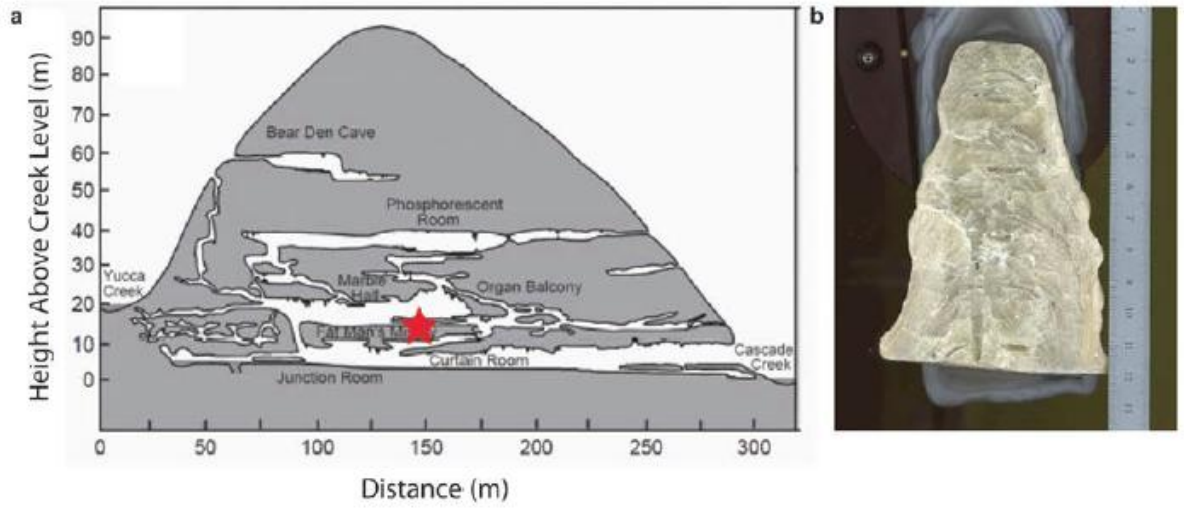

Supplementary Figure 1. Crystal Cave and CRC-3 stalagmite. a, Profile view of Crystal Cave and surrounding caves. Red star marks the location where the CRC-3 stalagmite was collected in July 2008 from an isolated chamber beneath Marble Hall. Modified from (Despain and Stock, 2005). **b,** Scanned image of stalagmite CRC-3.

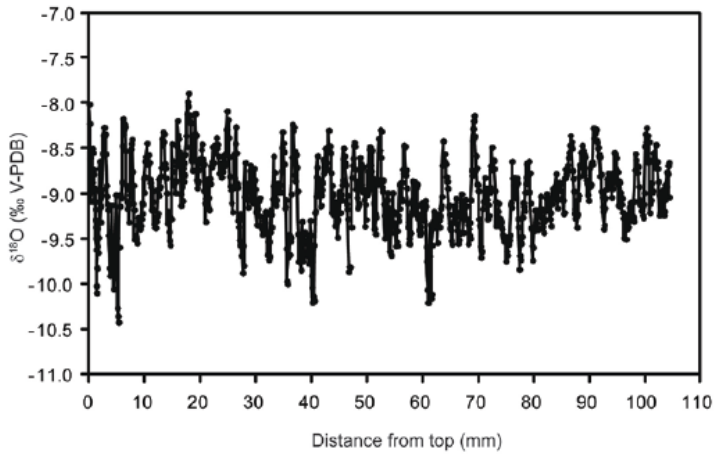

Supplementary Figure 2. CRC-3 $\delta^{18}O$ versus distance. Plot showing 1054 $\delta^{18}O$ measurements conducted along the growth axis of the CRC-3 stalagmite. (Scholz and Hoffmann, 2011)

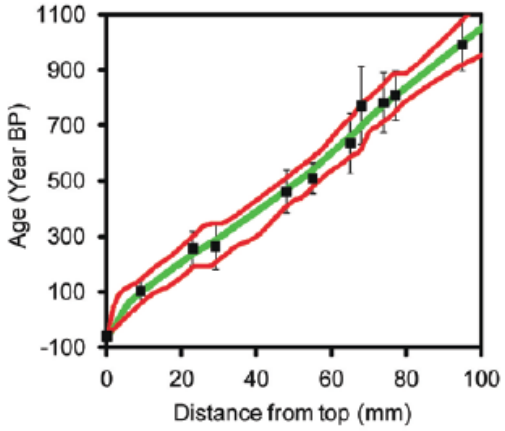

Supplementary Figure 3. Final CRC-3 age model. The CRC-3 age model (green line) is based on ten ^{230}Th dates (black squares) and an age of 2007 A.D. for the top of the sample. The model was developed utilizing the StalAge algorithm, which allows robust uncertainty estimation (red lines) throughout the length of the record (Scholz et al., 2009). The age model indicates that the sample grew at an average growth rate of 0.09 mm/year.

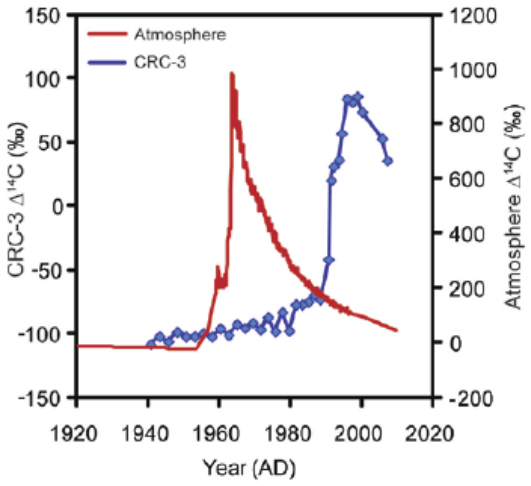

Supplementary Figure 4. ^{14}C bomb peak in CRC-3 stalagmite. 34 Δ^{14}C measurements plotted versus age according to the CRC-3 age-depth model (Supplementary fig. 3). Results show that speleothem ^{14}C begins to rise around 1955 A.D, synchronous with the atmosphere. (Kaplan et al., 1998)

Supplementary Figure 5. Backtracking and trajectory cluster analysis of storms reaching the southern Sierra Nevada mountains from 2001 - 2005 A.D. The North Pacific storm track is associated with the lowest $\delta^{18}O$ values (-14 to -22.0‰), while the Subtropical Pacific storms have intermediate values (-8 to -16.0‰), and the highest values are seen in the Tropical Pacific storms (-4 to -10.0‰).

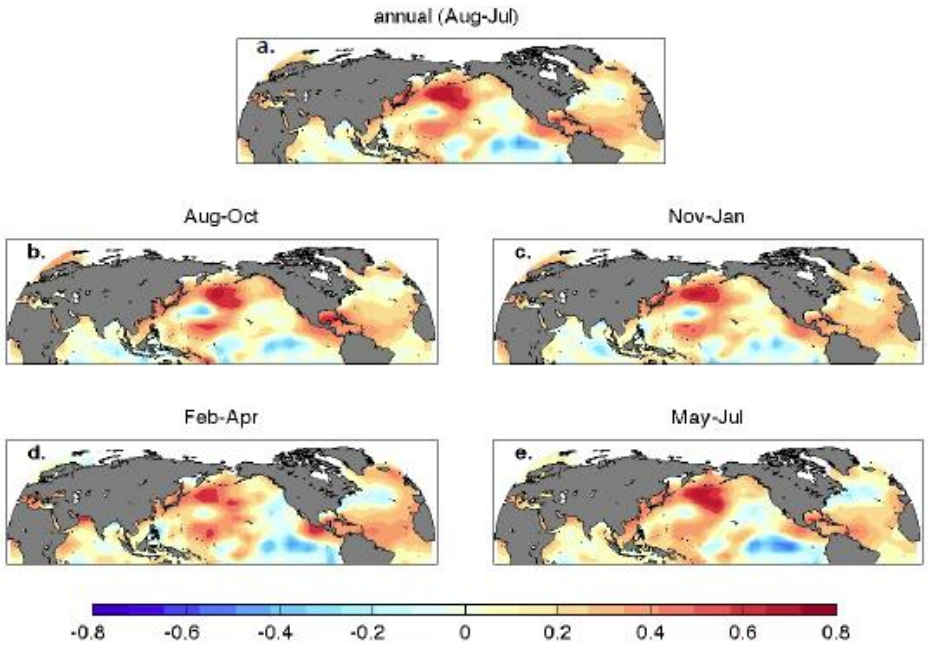

Supplementary Figure 6. Correlation maps of CRC-3 $\delta^{18}O$ versus Kaplan SST3. a, Correlation over full annual cycle (August – July). **b – e,** correlation with SST averaged over

four three- month blocks. This analysis illustrates that the relationship between SST and $\delta^{18}O$ is robustly focused in the KE region for all seasons.

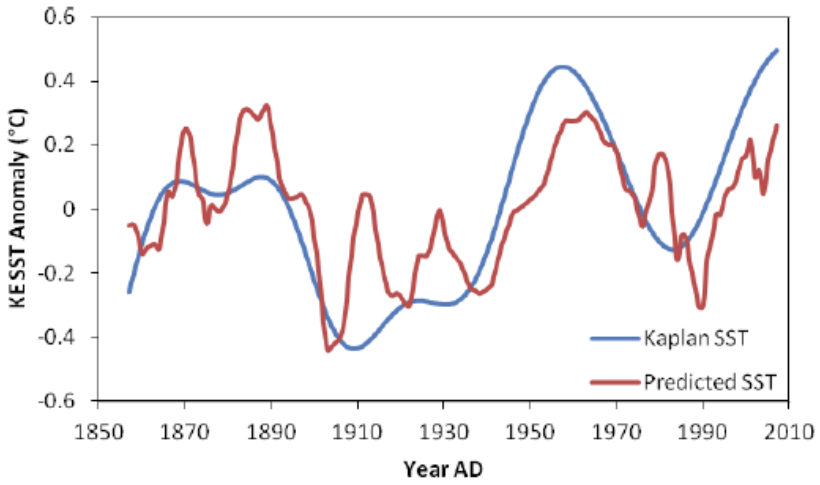

Supplementary Figure 7. Comparison of observed and reconstructed SST anomalies for the full calibration period (1857-2007 AD). Instrumental SST data (blue line) are 30-year low-pass filtered Kaplan SSTs3 for the Kuroshio Extension region outlined in Fig. 2. Predicted SST data (red line) are calculated from the CRC-3 $\delta^{18}O$ values using the "full" prediction equation shown in Supplementary Table 3.

S3.2. Supplementary methods trajectory and clustering analysis

Precipitation samples were provided from the National Atmospheric Deposition Program (NADP) archives (Harvey, 2005; National Atmospheric Deposition Program (NRSP-3), 2007). Samples from four sites in the Southwestern US (Pinnacles, Death Valley, Giant Forest (Sequoia), Joshua Tree) collected between 2001-2005 were analyzed for $\delta^{18}O$ via a Thermofinnigan TC/EA coupled to a Delta Plus XP IRMS instrument. Results were previously

compared with a nudged isotope-enabled GCM simulation to investigate the synoptic and mesoscale controls on precipitation isotopes in this region. We also conducted trajectory and clustering analysis for storms reaching the Giant Forest site (36.57°N, 118.78°W; 1921 m), (National Atmospheric Deposition Program (NRSP-3), 2007) located about 4 km from Crystal Cave, from 2001-2005 AD for comparison with the NADP sample results (Supplementary Figure 5). Trajectory analysis was conducted using the NOAA Hysplit model(Draxler and Rolph, 2003). Storms were sorted into three primary clusters. A) North Pacific, B) Subtropical Pacific and C) Tropical Pacific. The North Pacific storm track has the most negative $\delta^{18}O$ values (-14 to -22.0‰), the Subtropical Pacific has intermediate values (- 8 to -16.0‰), and the Tropical Pacific has the most positive values (- 4 to -10.0‰). Additional samples collected from 2006-2008 were analyzed via TC/EA-IRMS and included in calculation of the weighted mean precipitation $\delta^{18}O$ (2001-2008; -11.59‰) at the Giant Forest site. Analysis of the Giant Forest precipitation samples from 2001-2008 indicates no significant correlation between precipitation amount and precipitation $\delta^{18}O$ ($r = 0.17$, $n = 135$). This suggests that the so called "amount effect" (Dansgaard, 1964) is not a significant factor controlling precipitation $\delta^{18}O$ and that moisture source region/storm track are the dominant control.

S3.2.1 Calibration and verification

The CRC-3 $\delta^{18}O$ values range from -7.9 to -10.4‰ and exhibit prominent decadal scale variability (Fig. 1 and Supplementary Fig. 2). While CRC-3 $\delta^{18}O$ is not correlated with annual precipitation amount, it does exhibit a negative correlation with the average of the previous 10 years precipitation (1926-2007 AD, r=-0.39, p=0.04) from a nearby weather station (Ash

Mountain, CA; COOP Southwest station 040343). This is typical of cave drip waters and indicates that the rainfall signal is smoothed through mixing and storage in the epikarst prior to speleothem formation (Baker and Bradley, 2010; Oster et al., 2012) . The CRC-3 $\delta^{18}O$ data also exhibit a moderate correlation (1926 – 2003 AD, r=-0.44, p=0.09) with the reconstructed Palmer Drought Severity Index (Cook et al., 2004) from the 5 nearest grid points to our study site (average of sites 48, 60, 61, 73, 74). A multiple regression analysis indicates that Ash Mountain precipitation amount and PDSI could together explain up to 23% of the variance in CRC-3 $\delta^{18}O$. A linear regression between 30-year low pass filtered KE SST anomalies and $\delta^{18}O$, however, indicates that KE SST can explain 52% of the variance in CRC-3 $\delta^{18}O$ over the full calibration period (1857-2007 AD). The apparent correlation of speleothem $\delta^{18}O$ with the PDSI and precipitation amount may simply be a spurious relationship stemming from the correlation between North Pacific SST and precipitation in SWNA. In fact, a multiple regression analysis of CRC-3 $\delta^{18}O$ as a function of PDSI, precipitation amount, and Kuroshio Extension SSTs shows that KE SST is the only significant factor (1935-2003 AD; Precipitation $p = 0.0945$, PDSI $p = 0.9957$, KE SST $p < 0.0001$), demonstrating that the CRC-3 $\delta^{18}O$ record is primarily recording changes in moisture source region and storm track. To utilize CRC-3 $\delta^{18}O$ to develop a reconstruction of KE SSTs since 854 AD, we conducted verification tests routinely utilized in dendroclimatology (Cook and Kairiukstis, 1990) to assess the skill of our regression model (Supplementary Table 3). We applied a split-sample validation approach and tested four separate calibration/verification periods (Early, Early2, Late, and Late2). Calculated verification reduction of error (RE) values are all greater than 0, indicating that each calibration model has some skill compared with simply using the calibration period means. Verification coefficient of efficiency (CE) values are negative for the Early and Late calibration periods, perhaps reflecting

higher uncertainty in the Kaplan SST reconstruction during the early 20th century (Kaplan et al., 1998). When the Early2 and Late2 calibration periods are utilized, however, the model passes the CE test. In addition, all four models pass the sign test, which indicates that the reconstructed estimates successfully track the instrumental data. These results confirm that CRC-3 $\delta^{18}O$ record can be utilized to provide a useful reconstruction of KE SST anomalies. We therefore apply the full calibration model (1857-2007 AD) to reconstruct KE SST anomalies back to 854 AD. Supplementary Fig. 6 shows the actual versus reconstructed KE SST anomalies for the calibration period.

S3.3. Supplementary tables

Supplementary table S1. Raw $\delta^{18}O$ results for CRC-3 stalagmite from Crystal Cave in Sequoia National Park, CA. These data were interpolated to an annual timescale (see methods) for comparison with other time series. Interpolated data are archived online at the National Climatic Data Center for Paleoclimatology (http://www.ncdc.noaa.gov/paleo).

Supplementary Table S1. $\delta^{18}O$ results for CRC-3 stalagmite from Crystal Cave in Sequoia National Park, CA.

Distance from top (mm)	Age (Yr AD)	$\delta^{18}O$ (‰ V-PDB)
0.05	2007.7	-8.01
0.1	2007.0	-8.23
0.15	2006.3	-8.61
0.2	2005.6	-8.54
0.25	2004.9	-8.60
0.3	2004.2	-9.08
0.35	2003.5	-8.96
0.4	2002.8	-8.78
0.45	2002.1	-8.83
0.5	2001.4	-8.87
0.55	2000.7	-8.50
0.6	1999.9	-8.73
0.65	1999.2	-8.55
0.7	1998.5	-8.74
0.75	1997.8	-8.79
0.8	1997.1	-8.94
0.85	1996.4	-8.94
0.9	1995.7	-8.96
0.95	1995.0	-9.09
1	1994.2	-8.94
1.05	1993.5	-9.29
1.1	1992.8	-9.17
1.15	1992.0	-9.37
1.2	1991.2	-9.49
1.25	1990.5	-9.62
1.3	1989.7	-10.02
1.35	1988.9	-10.10

1.4	1988.1	-9.82
1.45	1987.3	-9.83
1.5	1986.5	-9.58
1.55	1985.7	-9.38
1.6	1984.8	-9.33
1.65	1984.0	-9.65
1.7	1983.1	-9.48
1.75	1982.2	-8.97
1.8	1981.3	-8.72
1.85	1980.4	-8.64
1.9	1979.5	-8.64
1.95	1978.5	-8.73
2	1977.6	-9.05
2.05	1976.6	-9.14
2.1	1975.6	-9.31
2.2	1973.5	-9.01
2.3	1971.4	-8.95
2.4	1969.3	-8.56
2.5	1967.1	-8.56
2.6	1964.8	-8.36
2.7	1962.5	-8.27
2.8	1960.1	-8.35
2.9	1957.8	-8.34
3	1955.4	-8.56
3.1	1952.9	-8.90
3.2	1950.5	-9.02
3.3	1948.0	-9.11
3.4	1945.6	-9.18
3.5	1943.1	-9.46
3.6	1940.6	-9.82
3.7	1938.2	-9.91
3.8	1935.7	-9.85
3.9	1933.3	-9.61
4	1930.8	-9.51
4.1	1928.4	-9.12
4.2	1926.1	-9.57
4.3	1923.7	-9.55
4.4	1921.4	-10.06
4.5	1919.2	-9.89
4.6	1916.9	-9.93
4.7	1914.7	-9.56
4.8	1912.5	-9.01
4.9	1910.4	-9.02
5	1908.3	-9.49
5.1	1906.2	-10.27
5.2	1904.2	-10.36
5.3	1902.3	-10.43
5.4	1900.3	-9.59
5.5	1898.5	-9.14
5.6	1896.7	-9.01
5.7	1894.9	-9.04
5.8	1893.2	-9.04
5.9	1891.5	-8.87
6	1889.9	-8.47
6.1	1888.4	-8.17
6.2	1886.9	-8.34
6.3	1885.5	-8.29
6.4	1884.1	-8.23
6.5	1882.8	-8.26
6.6	1881.5	-8.53
6.7	1880.2	-8.90
6.8	1879.0	-9.08
6.9	1877.8	-9.17
7	1876.6	-9.14
7.1	1875.5	-9.10
7.2	1874.4	-9.31
7.3	1873.3	-8.95
7.4	1872.2	-9.01
7.5	1871.2	-8.50
7.6	1870.1	-8.45
7.7	1869.1	-8.40
7.8	1868.0	-8.76
7.9	1867.0	-9.10
8	1865.9	-8.90
8.1	1864.9	-9.18
8.2	1863.8	-9.51
8.3	1862.8	-9.46
8.4	1861.7	-9.47
8.5	1860.6	-9.50
8.6	1859.5	-9.55
8.7	1858.4	-9.35
8.8	1857.4	-9.26
8.9	1856.3	-9.30
9	1855.2	-9.30
9.1	1854.1	-9.32
9.2	1853.0	-9.39
9.3	1851.8	-9.35
9.4	1850.7	-9.28
9.5	1849.6	-9.10
9.6	1848.5	-9.22
9.7	1847.4	-9.11
9.8	1846.3	-8.83
9.9	1845.2	-8.98
10	1844.1	-8.81
10.1	1842.9	-8.64
10.2	1841.8	-8.59
10.3	1840.7	-8.60
10.4	1839.6	-8.44
10.5	1838.5	-8.65
10.6	1837.4	-8.68
10.7	1836.3	-8.57
10.8	1835.2	-8.65
10.9	1834.1	-8.84
11	1833.0	-8.87
11.1	1831.9	-8.92
11.2	1830.8	-9.18
11.3	1829.7	-9.15
11.4	1828.6	-9.09
11.5	1827.5	-8.97
11.6	1826.5	-9.19
11.7	1825.4	-9.34
11.8	1824.3	-9.37
11.9	1823.2	-9.30
12	1822.2	-9.38
12.1	1821.1	-9.30
12.2	1820.0	-9.25
12.3	1819.0	-8.95
12.4	1817.9	-9.22
12.5	1816.9	-8.84
12.6	1815.9	-9.02
12.7	1814.8	-8.93
12.8	1813.8	-8.92
12.9	1812.8	-8.81
13	1811.7	-8.71
13.1	1810.7	-8.39
13.2	1809.7	-8.46
13.3	1808.7	-8.32
13.4	1807.7	-8.42
13.5	1806.7	-8.34
13.6	1805.7	-8.67
13.7	1804.7	-8.72
13.8	1803.7	-8.83
13.9	1802.7	-8.99
14	1801.7	-9.33
14.1	1800.8	-9.22
14.2	1799.8	-9.20
14.3	1798.8	-9.26
14.4	1797.8	-9.42
14.5	1796.9	-9.52
14.6	1795.9	-9.57
14.7	1795.0	-9.26
14.8	1794.0	-9.28
14.9	1793.0	-8.45
15	1792.1	-8.64
15.1	1791.1	-8.76
15.2	1790.2	-8.90
15.3	1789.2	-8.88
15.4	1788.3	-8.88
15.5	1787.3	-8.85
15.6	1786.4	-8.99

15.7	1785.4	-8.69
15.8	1784.4	-8.48
15.9	1783.5	-8.19
16	1782.5	-8.35
16.1	1781.6	-8.39
16.2	1780.6	-8.53
16.3	1779.6	-8.56
16.4	1778.7	-9.00
16.5	1777.7	-9.13
16.6	1776.7	-8.61
16.7	1775.8	-8.92
16.8	1774.8	-9.08
16.9	1773.8	-8.72
17	1772.8	-8.86
17.1	1771.9	-8.66
17.2	1770.9	-8.79
17.3	1769.9	-8.57
17.4	1768.9	-8.36
17.5	1768.0	-8.12
17.6	1767.0	-8.48
17.7	1766.0	-7.99
17.8	1765.0	-8.03
17.9	1764.1	-7.89
18	1763.1	-8.19
18.1	1762.1	-8.19
18.2	1761.1	-8.13
18.3	1760.1	-8.22
18.4	1759.2	-8.62
18.5	1758.2	-8.64
18.6	1757.2	-8.74
18.7	1756.2	-8.57
18.8	1755.3	-8.58
18.9	1754.3	-8.38
19	1753.3	-8.34
19.1	1752.3	-8.12
19.2	1751.4	-8.35
19.3	1750.4	-8.85
19.4	1749.4	-8.93
19.5	1748.4	-8.88
19.6	1747.5	-8.86
19.7	1746.5	-8.74
19.8	1745.5	-8.66
19.9	1744.5	-8.62
20	1743.6	-8.61
20.1	1742.6	
20.2	1741.6	-8.51
20.3	1740.6	-8.45
20.4	1739.7	-8.62
20.5	1738.7	-8.69
20.6	1737.7	-8.96

20.7	1736.7	-8.67
20.8	1735.8	-9.10
20.9	1734.8	-9.05
21	1733.8	-9.31
21.1	1732.8	-8.84
21.2	1731.9	-9.12
21.3	1730.9	-9.14
21.4	1729.9	-9.15
21.5	1728.9	-9.04
21.6	1727.9	-9.17
21.7	1727.0	-8.83
21.8	1726.0	-8.89
21.9	1725.0	-8.69
22	1724.0	-8.71
22.1	1723.0	-8.65
22.2	1722.0	-8.48
22.3	1721.1	
22.4	1720.1	-8.66
22.5	1719.1	-8.47
22.6	1718.1	
22.7	1717.1	-8.55
22.8	1716.2	-8.52
22.9	1715.2	-8.38
23	1714.2	-8.49
23.1	1713.3	-8.46
23.2	1712.3	
23.3	1711.4	-8.59
23.4	1710.4	-8.78
23.5	1709.5	-8.67
23.6	1708.6	-8.66
23.7	1707.6	-8.73
23.8	1706.7	-8.82
23.9	1705.8	-8.67
24	1704.9	-8.76
24.1	1704.1	-8.58
24.2	1703.2	-8.63
24.3	1702.3	-8.70
24.4	1701.5	-8.67
24.5	1700.6	-8.66
24.6	1699.8	-8.56
24.7	1699.0	-8.29
24.8	1698.2	-8.09
24.9	1697.4	
25	1696.5	-8.18
25.1	1695.7	-8.38
25.2	1695.0	-8.59
25.3	1694.2	-8.81
25.4	1693.4	-8.91
25.5	1692.6	-8.96
25.6	1691.8	-9.10

25.7	1691.0	
25.8	1690.3	-9.20
25.9	1689.5	-8.93
26	1688.7	-8.91
26.1	1688.0	-8.56
26.2	1687.2	-8.83
26.3	1686.4	-8.45
26.4	1685.7	-8.26
26.5	1684.9	-8.55
26.6	1684.1	-8.89
26.7	1683.4	-8.93
26.8	1682.6	-9.30
26.9	1681.8	-9.37
27	1681.0	-9.51
27.1	1680.3	-9.57
27.2	1679.5	-9.22
27.3	1678.7	-9.28
27.4	1677.9	-9.68
27.5	1677.1	-9.55
27.6	1676.4	-9.88
27.7	1675.6	-9.57
27.8	1674.8	-9.80
27.9	1674.0	-9.03
28	1673.2	-8.88
28.1	1672.4	-8.66
28.2	1671.5	-9.06
28.3	1670.7	-8.92
28.4	1669.9	-9.06
28.5	1669.1	-9.06
28.6	1668.2	-9.15
28.7	1667.4	-8.93
28.8	1666.5	-8.89
28.9	1665.7	-8.75
29	1664.8	-8.68
29.1	1664.0	-8.79
29.2	1663.1	-8.98
29.3	1662.2	-9.01
29.4	1661.3	-9.10
29.5	1660.4	-9.05
29.6	1659.5	-8.99
29.7	1658.6	-8.72
29.8	1657.7	-8.85
29.9	1656.8	-8.95
30	1655.8	-9.20
30.1	1654.9	-9.21
30.2	1654.0	-9.34
30.3	1653.0	-9.22
30.4	1652.1	-9.17
30.5	1651.1	-9.08
30.6	1650.1	-9.06

30.7	1649.2	-9.04
30.8	1648.2	-9.25
30.9	1647.2	-9.37
31	1646.2	-9.38
31.1	1645.3	-9.37
31.2	1644.3	-9.45
31.3	1643.3	-9.40
31.4	1642.3	-9.35
31.5	1641.3	-9.30
31.6	1640.3	-9.32
31.7	1639.4	-9.19
31.8	1638.4	-9.20
31.9	1637.4	-9.22
32	1636.4	-9.44
32.1	1635.5	-9.68
32.2	1634.5	-9.53
32.3	1633.6	-9.73
32.4	1632.6	-9.53
32.5	1631.7	-9.69
32.6	1630.7	-9.42
32.7	1629.8	-9.18
32.8	1628.8	-9.23
32.9	1627.9	-9.37
33	1626.9	-9.06
33.1	1626.0	-8.91
33.2	1625.0	-8.59
33.3	1624.1	-8.76
33.4	1623.2	-8.77
33.5	1622.2	-9.07
33.6	1621.3	-9.13
33.7	1620.3	-9.07
33.8	1619.4	-8.90
33.9	1618.5	-8.89
34	1617.5	-8.90
34.1	1616.6	-8.98
34.2	1615.6	-8.91
34.3	1614.7	-8.91
34.4	1613.7	-8.90
34.5	1612.8	-8.98
34.6	1611.8	-8.75
34.7	1610.9	-8.49
34.8	1609.9	-8.32
34.9	1609.0	-8.44
35	1608.0	-8.54
35.1	1607.1	-8.67
35.2	1606.1	-9.16
35.3	1605.2	-9.14
35.4	1604.3	-9.07
35.5	1603.3	-9.61
35.6	1602.4	-9.97

35.7	1601.4	-10.00
35.8	1600.5	-9.70
35.9	1599.5	-9.51
36	1598.6	-9.45
36.1	1597.7	-9.68
36.2	1596.7	-9.53
36.3	1595.8	-9.48
36.4	1594.9	-9.00
36.5	1593.9	-8.60
36.6	1593.0	-8.24
36.7	1592.1	-8.30
36.8	1591.2	-8.26
36.9	1590.2	-8.53
37	1589.3	-8.79
37.1	1588.4	-8.86
37.2	1587.5	-8.71
37.3	1586.5	-8.57
37.4	1585.6	-8.71
37.5	1584.7	-8.97
37.6	1583.8	-9.44
37.7	1582.8	-9.75
37.8	1581.9	-9.74
37.9	1581.0	-9.68
38	1580.1	-9.70
38.1	1579.1	-9.85
38.2	1578.2	-9.48
38.3	1577.3	-9.31
38.4	1576.3	-9.55
38.5	1575.4	-9.74
38.6	1574.5	-9.67
38.7	1573.6	-9.52
38.8	1572.6	-9.42
38.9	1571.7	
39	1570.8	-9.68
39.1	1569.8	-9.65
39.2	1568.9	-9.54
39.3	1567.9	-9.45
39.4	1567.0	-9.65
39.5	1566.1	-9.68
39.6	1565.1	-9.77
39.7	1564.2	-9.61
39.8	1563.3	-9.30
39.9	1562.3	-9.46
40	1561.4	-9.91
40.1	1560.5	-10.04
40.2	1559.5	-10.20
40.3	1558.6	-10.14
40.4	1557.7	-9.57
40.5	1556.7	-10.18
40.6	1555.8	-9.21

40.7	1554.8	-9.19
40.8	1553.9	-9.03
40.9	1553.0	-8.82
41	1552.0	-8.71
41.1	1551.1	-8.58
41.2	1550.2	-8.84
41.3	1549.2	-8.93
41.4	1548.3	-8.98
41.5	1547.3	-8.90
41.6	1546.4	-9.14
41.7	1545.4	-9.13
41.8	1544.5	-9.01
41.9	1543.5	-8.95
42	1542.6	-8.88
42.1	1541.6	-8.63
42.2	1540.7	-8.78
42.3	1539.7	-8.72
42.4	1538.7	-8.66
42.5	1537.8	-8.50
42.6	1536.8	-8.66
42.7	1535.8	-8.53
42.8	1534.9	-8.73
42.9	1533.9	-8.52
43	1532.9	-8.48
43.1	1531.9	-8.30
43.2	1531.0	-8.54
43.3	1530.0	-8.47
43.4	1529.0	-8.55
43.5	1528.0	-8.77
43.6	1527.0	-9.21
43.7	1526.0	-8.90
43.8	1525.0	-9.00
43.9	1524.0	-9.01
44	1523.0	-9.24
44.1	1522.0	-9.09
44.2	1521.0	-9.35
44.3	1520.0	-9.34
44.4	1519.0	-9.15
44.5	1518.0	-9.17
44.6	1517.0	-9.31
44.7	1516.0	-9.48
44.8	1515.0	-9.29
44.9	1513.9	-9.08
45	1512.9	-8.98
45.1	1511.9	-9.02
45.2	1510.9	-9.21
45.3	1509.9	-9.01
45.4	1508.9	-9.07
45.5	1507.8	-8.90
45.6	1506.8	-8.85

45.7	1505.8	-8.62
45.8	1504.8	-8.50
45.9	1503.8	-8.58
46	1502.7	-8.66
46.1	1501.7	-8.69
46.2	1500.7	-8.90
46.3	1499.7	-9.11
46.4	1498.7	-9.17
46.5	1497.6	-9.02
46.6	1496.6	-9.28
46.7	1495.6	-9.86
46.8	1494.6	-9.81
46.9	1493.6	-9.82
47	1492.6	-9.81
47.1	1491.6	
47.2	1490.5	-9.37
47.3	1489.5	-8.82
47.4	1488.5	-8.69
47.5	1487.5	-8.61
47.6	1486.5	-8.47
47.7	1485.4	-8.43
47.8	1484.4	-8.47
47.9	1483.4	-8.73
48	1482.4	-8.95
48.1	1481.4	-8.86
48.2	1480.3	-9.04
48.3	1479.3	-9.16
48.4	1478.3	-9.13
48.5	1477.3	-9.10
48.6	1476.2	-8.92
48.7	1475.2	-8.60
48.8	1474.2	-8.73
48.9	1473.2	-8.67
49	1472.2	-8.89
49.1	1471.2	-8.71
49.2	1470.2	-8.97
49.3	1469.1	-8.71
49.4	1468.1	-8.95
49.5	1467.1	-9.06
49.6	1466.2	-9.36
49.7	1465.2	-9.12
49.8	1464.2	-9.28
49.9	1463.2	-9.01
50	1462.2	-9.01
50.1	1461.3	-8.75
50.2	1460.3	-8.98
50.3	1459.3	-8.68
50.4	1458.4	-8.51
50.5	1457.4	-8.48
50.6	1456.5	-8.68
50.7	1455.5	-8.75
50.8	1454.6	-8.93
50.9	1453.6	-8.52
51	1452.7	-8.83
51.1	1451.8	-8.89
51.2	1450.8	-9.10
51.3	1449.9	-9.39
51.4	1448.9	-9.22
51.5	1448.0	-9.44
51.6	1447.0	-9.26
51.7	1446.1	-8.90
51.8	1445.1	-8.90
51.9	1444.2	-8.87
52	1443.2	-8.84
52.1	1442.2	-8.39
52.2	1441.2	-8.55
52.3	1440.2	-8.52
52.4	1439.3	-8.29
52.5	1438.3	-8.60
52.6	1437.2	-8.31
52.7	1436.2	-8.92
52.8	1435.2	-8.97
52.9	1434.2	-8.85
53	1433.2	-9.11
53.1	1432.1	-9.24
53.2	1431.1	-9.49
53.3	1430.0	-9.16
53.4	1429.0	-9.30
53.5	1427.9	-9.44
53.6	1426.9	-9.06
53.7	1425.8	-8.99
53.8	1424.7	-9.15
53.9	1423.6	-9.19
54	1422.5	-9.21
54.1	1421.4	-9.64
54.2	1420.3	-9.36
54.3	1419.2	-9.68
54.4	1418.1	-9.20
54.5	1417.0	-9.23
54.6	1415.8	-8.99
54.7	1414.7	-9.32
54.8	1413.6	-9.20
54.9	1412.4	-9.43
55	1411.3	-9.36
55.1	1410.1	-9.58
55.2	1409.0	-9.42
55.3	1407.8	-9.53
55.4	1406.7	-9.41
55.5	1405.5	-9.57
55.6	1404.3	-9.24
55.7	1403.2	-9.30
55.8	1402.0	-8.89
55.9	1400.8	-9.16
56	1399.7	-8.93
56.1	1398.5	-9.05
56.2	1397.3	-8.87
56.3	1396.2	-9.08
56.4	1395.0	-8.73
56.5	1393.8	-8.78
56.6	1392.6	-8.47
56.7	1391.4	-8.49
56.8	1390.3	-8.47
56.9	1389.1	-8.79
57	1387.9	-8.74
57.1	1386.7	-8.94
57.2	1385.5	-9.10
57.3	1384.3	-9.37
57.4	1383.1	-9.31
57.5	1381.9	-9.55
57.6	1380.7	-9.49
57.7	1379.4	-9.55
57.8	1378.2	-9.23
57.9	1377.0	-9.43
58	1375.8	-9.19
58.1	1374.5	-9.07
58.2	1373.3	-8.86
58.3	1372.0	-9.12
58.4	1370.8	-8.91
58.5	1369.5	-9.13
58.6	1368.2	-8.87
58.7	1367.0	-9.10
58.8	1365.7	-8.93
58.9	1364.5	-9.23
59	1363.2	-8.89
59.1	1361.9	-9.27
59.2	1360.7	-9.13
59.3	1359.4	-9.40
59.4	1358.1	-9.23
59.5	1356.9	-9.45
59.6	1355.6	-9.37
59.7	1354.3	-9.43
59.8	1353.1	-9.10
59.9	1351.8	-9.24
60	1350.6	-9.27
60.1	1349.4	-9.13
60.2	1348.1	-9.29
60.3	1346.9	-9.10
60.4	1345.7	-9.17
60.5	1344.4	-9.08
60.6	1343.2	-9.14

60.7	1342.0	-9.59
60.8	1340.8	-9.74
60.9	1339.6	-10.06
61	1338.4	-10.21
61.1	1337.2	-10.09
61.2	1336.0	-9.87
61.3	1334.7	-9.69
61.4	1333.6	-9.34
61.5	1332.4	-10.16
61.6	1331.2	-10.11
61.7	1330.0	-9.57
61.8	1328.8	-9.38
61.9	1327.6	-9.30
62	1326.4	-9.19
62.1	1325.2	-9.28
62.2	1324.0	-9.29
62.3	1322.8	-9.37
62.4	1321.6	-9.22
62.5	1320.4	-9.33
62.6	1319.2	-9.28
62.7	1318.0	-9.54
62.8	1316.9	-9.27
62.9	1315.7	-9.24
63	1314.5	-9.29
63.1	1313.3	-9.37
63.2	1312.1	-9.25
63.3	1310.9	-9.16
63.4	1309.7	-9.13
63.5	1308.6	-9.03
63.6	1307.4	-8.69
63.7	1306.2	-8.42
63.8	1305.0	-8.66
63.9	1303.8	-8.64
64	1302.6	-8.56
64.1	1301.5	-8.68
64.2	1300.3	-8.67
64.3	1299.1	-8.81
64.4	1297.9	-8.86
64.5	1296.7	-8.94
64.6	1295.6	-9.14
64.7	1294.4	-9.12
64.8	1293.2	-9.23
64.9	1292.0	-9.38
65	1290.9	-9.33
65.1	1289.7	-9.40
65.2	1288.5	-9.52
65.3	1287.3	-9.56
65.4	1286.1	-9.32
65.5	1284.9	-9.30
65.6	1283.8	-9.32

65.7	1282.6	-9.13
65.8	1281.4	-9.20
65.9	1280.2	-9.25
66	1279.0	-9.05
66.1	1277.8	-9.25
66.2	1276.6	-9.33
66.3	1275.4	-9.40
66.4	1274.2	-9.55
66.5	1273.0	-9.51
66.6	1271.8	-9.44
66.7	1270.5	-9.20
66.8	1269.3	-9.24
66.9	1268.1	-9.09
67	1266.8	-9.00
67.1	1265.6	-9.26
67.2	1264.3	-9.09
67.3	1263.0	-9.43
67.4	1261.8	-9.18
67.5	1260.5	-9.16
67.6	1259.2	-9.15
67.7	1257.9	-9.06
67.8	1256.5	-9.13
67.9	1255.2	-9.28
68	1253.9	-9.29
68.1	1252.5	-9.34
68.2	1251.1	-9.55
68.3	1249.7	-9.38
68.4	1248.3	-9.46
68.5	1246.9	-9.32
68.6	1245.5	-9.49
68.7	1244.1	-9.07
68.8	1242.7	-8.74
68.9	1241.3	-8.80
69	1239.8	-8.42
69.1	1238.4	-8.28
69.2	1237.0	-8.19
69.3	1235.6	-8.14
69.4	1234.2	-8.37
69.5	1232.8	-8.75
69.6	1231.4	-8.58
69.7	1230.0	-8.72
69.8	1228.7	-8.89
69.9	1227.3	-8.90
70	1226.0	-8.97
70.1	1224.7	-9.28
70.2	1223.4	-9.35
70.3	1222.1	-9.37
70.4	1220.8	-9.58
70.5	1219.6	-9.71
70.6	1218.3	-9.64

70.7	1217.1	-9.64
70.8	1215.9	-9.17
70.9	1214.6	-9.08
71	1213.4	-8.97
71.1	1212.2	-8.96
71.2	1211.1	-8.82
71.3	1209.9	-9.03
71.4	1208.7	-8.94
71.5	1207.5	-9.11
71.6	1206.3	-9.06
71.7	1205.2	-9.28
71.8	1204.0	-9.12
71.9	1202.8	-9.24
72	1201.7	-8.98
72.1	1200.5	-8.93
72.2	1199.3	-8.69
72.3	1198.2	-8.74
72.4	1197.0	-8.72
72.5	1195.8	-8.49
72.6	1194.6	-8.74
72.7	1193.5	-8.64
72.8	1192.3	-8.63
72.9	1191.1	-8.73
73	1190.0	-8.97
73.1	1188.8	-9.09
73.2	1187.6	-9.35
73.3	1186.4	-9.31
73.4	1185.3	-9.24
73.5	1184.1	-9.28
73.6	1183.0	-9.19
73.7	1181.8	-9.10
73.8	1180.6	-9.30
73.9	1179.5	-9.27
74	1178.3	-9.35
74.1	1177.2	-9.37
74.2	1176.1	-9.31
74.3	1174.9	-9.39
74.4	1173.8	-9.45
74.5	1172.6	-9.47
74.6	1171.5	-9.50
74.7	1170.4	-9.53
74.8	1169.3	-9.53
74.9	1168.1	-9.47
75	1167.0	-9.75
75.1	1165.9	-9.64
75.2	1164.8	-9.68
75.3	1163.7	-9.55
75.4	1162.6	-9.56
75.5	1161.4	-9.51
75.6	1160.3	-9.51

75.7	1159.2	-9.46
75.8	1158.1	-9.12
75.9	1157.0	-9.10
76	1155.9	-9.15
76.1	1154.8	-8.64
76.2	1153.7	-8.83
76.3	1152.6	-8.90
76.4	1151.4	-9.00
76.5	1150.3	-8.82
76.6	1149.2	-8.97
76.7	1148.1	-9.04
76.8	1147.0	-8.91
76.9	1145.9	-8.85
77	1144.8	-8.83
77.1	1143.8	-8.88
77.2	1142.7	-9.27
77.3	1141.6	-9.37
77.4	1140.5	-9.84
77.5	1139.5	-9.68
77.6	1138.4	-9.73
77.7	1137.3	-9.48
77.8	1136.3	-9.55
77.9	1135.3	-9.47
78	1134.2	-9.26
78.1	1133.2	-9.10
78.2	1132.2	-9.14
78.3	1131.2	-9.19
78.4	1130.2	-8.98
78.5	1129.2	-8.89
78.6	1128.2	-8.82
78.7	1127.2	-8.67
78.8	1126.2	-8.66
78.9	1125.2	-8.76
79	1124.2	-8.80
79.1	1123.2	-8.64
79.2	1122.2	-8.98
79.3	1121.2	-8.77
79.4	1120.2	-9.10
79.5	1119.2	-9.38
79.6	1118.2	-9.39
79.7	1117.2	-9.57
79.8	1116.2	-9.74
79.9	1115.2	-9.59
80	1114.1	-9.41
80.1	1113.1	-9.39
80.2	1112.0	-9.18
80.3	1111.0	-9.34
80.4	1109.9	-9.18
80.5	1108.8	-9.32
80.6	1107.8	-9.38
80.7	1106.7	-9.40
80.8	1105.6	-9.22
80.9	1104.5	-9.18
81	1103.4	-9.23
81.1	1102.3	-9.22
81.2	1101.2	-9.03
81.3	1100.1	-9.16
81.4	1099.0	-9.26
81.5	1097.9	-9.38
81.6	1096.8	-9.36
81.7	1095.7	-9.29
81.8	1094.6	-9.43
81.9	1093.4	-9.30
82	1092.3	-9.28
82.1	1091.2	-9.19
82.2	1090.1	-9.05
82.3	1089.1	-9.00
82.4	1088.0	-9.06
82.5	1086.9	-9.18
82.6	1085.8	-9.10
82.7	1084.7	-9.18
82.8	1083.6	-9.04
82.9	1082.5	-9.28
83	1081.5	-9.21
83.1	1080.4	-9.36
83.2	1079.3	-9.10
83.3	1078.2	-9.11
83.4	1077.2	-8.94
83.5	1076.1	-9.04
83.6	1075.0	-8.95
83.7	1074.0	-8.98
83.8	1072.9	-8.91
83.9	1071.8	-8.90
84	1070.8	-8.78
84.1	1069.7	-8.96
84.2	1068.6	-9.07
84.3	1067.6	-9.16
84.4	1066.5	-8.96
84.5	1065.4	-8.87
84.6	1064.4	-8.88
84.7	1063.3	-8.88
84.8	1062.2	-8.96
84.9	1061.2	-8.88
85	1060.1	-8.88
85.1	1059.0	-9.04
85.2	1058.0	-9.07
85.3	1056.9	-9.07
85.4	1055.8	-9.22
85.5	1054.7	-9.21
85.6	1053.7	-8.83
85.7	1052.6	-8.73
85.8	1051.5	-8.78
85.9	1050.5	-8.79
86	1049.4	-8.75
86.1	1048.3	-8.68
86.2	1047.2	-8.74
86.3	1046.1	-8.60
86.4	1045.0	-8.55
86.5	1044.0	-8.46
86.6	1042.9	-8.36
86.7	1041.8	-8.46
86.8	1040.7	-8.42
86.9	1039.6	-8.50
87	1038.5	-8.75
87.1	1037.4	-8.83
87.2	1036.4	-8.97
87.3	1035.3	-9.21
87.4	1034.2	-9.17
87.5	1033.1	-9.27
87.6	1032.0	-9.07
87.7	1030.9	-9.25
87.8	1029.8	-9.37
87.9	1028.7	-9.23
88	1027.7	-9.05
88.1	1026.6	-9.02
88.2	1025.5	-8.81
88.3	1024.4	-8.68
88.4	1023.3	-8.70
88.5	1022.3	-8.54
88.6	1021.2	-8.54
88.7	1020.1	-8.47
88.8	1019.0	-8.55
88.9	1018.0	-8.53
89	1016.9	-8.79
89.1	1015.8	-8.57
89.2	1014.7	-8.58
89.3	1013.7	-8.59
89.4	1012.6	-8.85
89.5	1011.5	-8.88
89.6	1010.5	-8.89
89.7	1009.4	-9.01
89.8	1008.4	-8.92
89.9	1007.3	-9.07
90	1006.2	-8.89
90.1	1005.2	-8.71
90.2	1004.1	-8.92
90.3	1003.1	-8.89
90.4	1002.0	-8.67
90.5	1000.9	-8.65
90.6	999.9	-8.68

90.7	998.8	-8.28
90.8	997.8	-8.39
90.9	996.7	-8.28
91	995.7	-8.33
91.1	994.6	-8.29
91.2	993.5	-8.29
91.3	992.5	-8.41
91.4	991.4	-8.43
91.5	990.4	-8.50
91.6	989.3	-8.49
91.7	988.2	-8.58
91.8	987.2	-8.57
91.9	986.1	-8.81
92	985.1	-8.59
92.1	984.0	-8.97
92.2	982.9	-8.79
92.3	981.9	-9.03
92.4	980.8	-9.14
92.5	979.7	-9.19
92.6	978.6	-9.39
92.7	977.6	-9.35
92.8	976.5	-9.16
92.9	975.4	-9.05
93	974.4	-8.95
93.1	973.3	-8.95
93.2	972.2	-8.84
93.3	971.1	-8.86
93.4	970.1	-8.78
93.5	969.0	-8.89
93.6	967.9	
93.7	966.9	-8.87
93.8	965.8	-8.91
93.9	964.7	
94	963.7	-9.04
94.1	962.6	-8.79
94.2	961.6	-8.94
94.3	960.5	-8.77
94.4	959.5	-8.86
94.5	958.4	-8.55
94.6	957.4	-8.56
94.7	956.3	-8.57
94.8	955.3	-8.73
94.9	954.2	-8.61
95	953.1	-8.89
95.1	952.1	-8.76
95.2	951.0	-9.13
95.3	950.0	-8.86
95.4	948.9	-9.13
95.5	947.9	-8.87
95.6	946.8	-8.98
95.7	945.7	-9.03
95.8	944.7	-9.11
95.9	943.6	-9.05
96	942.5	-9.20
96.1	941.4	-9.27
96.2	940.4	-9.49
96.3	939.3	
96.4	938.2	-9.50
96.5	937.1	-9.39
96.6	936.0	-9.50
96.7	934.9	-9.23
96.8	933.8	-9.38
96.9	932.7	-9.27
97	931.6	-9.37
97.1	930.5	-9.30
97.2	929.4	-9.15
97.3	928.3	-9.20
97.4	927.2	-9.10
97.5	926.1	-9.17
97.6	925.1	-9.23
97.7	924.0	-9.27
97.8	922.9	-9.25
97.9	921.8	-9.26
98	920.7	-9.30
98.1	919.7	-9.08
98.2	918.6	-8.74
98.3	917.5	-8.56
98.4	916.5	-8.63
98.5	915.4	-8.68
98.6	914.3	-8.77
98.7	913.3	-8.70
98.8	912.2	-8.70
98.9	911.2	-8.92
99	910.1	-9.10
99.1	909.1	-9.12
99.2	908.0	-9.07
99.3	906.9	-9.07
99.4	905.9	-9.18
99.5	904.8	-9.14
99.6	903.8	-9.24
99.7	902.7	-9.26
99.8	901.6	-9.11
99.9	900.5	-8.99
100	899.5	-8.47
100.1	898.4	-8.34
100.2	897.3	-8.43
100.3	896.2	-8.27
100.4	895.1	-8.38
100.5	894.0	-8.36
100.6	892.9	-8.65
100.7	891.8	-8.63
100.8	890.7	-8.43
100.9	889.6	-9.21
101	888.5	-9.10
101.1	887.4	-9.07
101.2	886.3	-8.88
101.3	885.2	-8.98
101.4	884.1	-8.97
101.5	883.0	-8.55
101.6	881.9	-8.61
101.7	880.8	-8.61
101.8	879.7	-8.62
101.9	878.6	-8.69
102	877.5	-8.46
102.1	876.4	-8.72
102.2	875.3	-8.65
102.3	874.2	-8.72
102.4	873.2	-8.86
102.5	872.1	-9.01
102.6	871.0	-9.24
102.7	870.0	-9.20
102.8	868.9	-9.12
102.9	867.8	-9.21
103	866.8	-8.97
103.1	865.7	-9.17
103.2	864.7	-8.95
103.3	863.6	-9.08
103.4	862.5	-9.24
103.5	861.5	-9.19
103.6	860.4	-8.90
103.7	859.4	-9.06
103.8	858.3	-9.02
103.9	857.2	-8.92
104	856.2	-8.76
104.1	855.1	-8.78
104.2	854.1	-8.69
104.3	853.0	-8.66
104.4	851.9	-9.04

Supplementary Table S2. ^{230}Th dating results for stalagmite CRC-3.

Sample ID	Depth (mm)	^{238}U (ppb)	^{232}Th (ppt)	^{230}Th / ^{232}Th (atomic x10^{-6})	δ^{234}U* (measured)	^{230}Th / ^{238}U (activity)	^{230}Th Age (yr) (uncorrected)	^{230}Th Age (yr) (corrected)	$\delta^{234}U_{Initial}$** (corrected)	^{230}Th Age (yr BP) (corrected)
CRC-3-1	**9**	220.0 ±0.4	933 ±19	14 ±1	-8.8 ±2.0	0.0035 ±0.0002	391 ±21	**164 ±45**	-9 ±2	**105 ±45**
CRC-3-1A	**23**	187.7 ±0.2	546 ±11	24 ±3	-6.6 ±1.9	0.0043 ±0.0005	474 ±57	**319 ±63**	-7 ±2	**259 ±63**
CRC-3-2	**29**	193.6 ±0.3	1563 ±31	14 ±1	-10.8 ±1.9	0.0068 ±0.0003	757 ±30	**324 ±82**	-11 ±2	**265 ±82**
CRC-3-2B	**48**	190.8 ±0.2	1204 ±24	20 ±1	-11.8 ±1.8	0.0078 ±0.0004	862 ±49	**523 ±78**	-12 ±2	**463 ±78**
CRC-3-3	**55**	166.8 ±0.3	732 ±15	27 ±1	-11.0 ±2.0	0.0073 ±0.0003	805 ±38	**570 ±56**	-11 ±2	**511 ±56**
CRC-3-3C	**65**	169.6 ±0.2	1377 ±28	21 ±1	-13.6 ±2.2	0.0102 ±0.0007	1134 ±75	**698 ±108**	-14 ±2	**638 ±108**
CRC-3-8	**68**	191.0 ±0.3	2706 ±54	17 ±1	-10.7 ±2.1	0.0143 ±0.0003	1592 ±39	**832 ±141**	-11 ±2	**773 ±141**
CRC-3-4D	**74**	159.3 ±0.2	1250 ±25	24 ±2	-14.3 ±2.0	0.0114 ±0.0007	1266 ±79	**844 ±109**	-14 ±2	**784 ±109**
CRC-3-4	**77**	153.5 ±0.3	1158 ±23	25 ±1	-6.0 ±2.2	0.0115 ±0.0005	1272 ±52	**869 ±89**	-6 ±2	**810 ±89**
CRC-3-5	**95**	207.1 ±0.3	1826 ±37	26 ±1	-11.0 ±1.8	0.0137 ±0.0004	1525 ±42	**1052 ±94**	-11 ±2	**993 ±94**

*$\delta^{234}U = ([^{234}U/^{238}U]_{activity} - 1)x1000$. ** $\delta^{234}U_{initial}$ was calculated based on ^{230}Th age (T), i.e., $\delta^{234}U_{initial} = \delta^{234}U_{measured} \times e^{\lambda 234 \times T}$.
Corrected ^{230}Th ages assume the initial $^{230}Th/^{232}Th$ atomic ratio of 8 ±1 x10^{-6}. Those are the values for a material at secular equilibrium, with the bulk earth $^{232}Th/^{238}U$ value of 3.8. The errors are arbitrarily assumed to be 50%. All reported errors are 2σ.

Supplementary Table S3. Calibration and verification statistics for Kuroshio Extension SST reconstruction model

Model	Calibration period	R_c	R^2_c	Verification period	R^2_v	RE	CE	Sign test	Prediction Formula
Full	1857-2007	0.72	0.52						SST=3.1603437+0.3457807*δ^{18}O
Early	1900-1950	0.67	0.45	1951-2000	0.49	0.71	-0.45	30/50 (P=0.1013)	SST=2.1934392+0.2493286*δ^{18}O
Late	1951-2000	0.70	0.49	1901-1950	0.15	0.67	-0.74	41/50 (P<0.0001)	SST=2.9358691+0.3110572*δ^{18}O
Early2	1928-1967	0.86	0.73	1968-2007	-0.34	0.22	0.22	30/40 (P=0.0011)	SST=4.1640373+0.4463372*d18O
Late2	1968-2007	0.58	0.34	1928-1967	0.73	0.63	0.63	37/40 (P<0.0001)	SST=2.6768289+0.2833088*d18O

S3.4. Supplementary discussion

S3.4.1 Radiocarbon bomb peak

To further constrain the age model during the late 20th century, we conducted 34 radiocarbon analyses on the upper 3.6 mm of the CRC-3 stalagmite. Powdered samples were micromilled in approximately 100 μm increments from the same section utilized for stable isotope and U-Th analyses. Powdered calcite samples were converted to graphite and analyzed on the UC Irvine Keck Carbon Cycle AMS following standard procedures as described in (Southon et al., 2011). $\Delta^{14}C$ results are plotted versus age based on the depth-age model developed utilizing StalAge

(Supplementary Fig. 3). The radiocarbon bomb peak in speleothems has been previously used as a chronological tool (Mattey et al., 2008), and for studies of soil organic matter turnover times in karst soils (Genty and Massault, 1999). Atmospheric ^{14}C is thought to become incorporated in speleothem calcite through a combination of fast and slow processes. The fast component may stem from root respiration, quickly decomposing soil organic matter, or direct exchange between dripwater dissolved inorganic carbon and cave air (Genty and Massault, 1999; Frisia et al., 2011). In a range of climatic settings and vegetation types, it has been shown that speleothem ^{14}C begins to rise synchronously with the atmosphere (1954) or with a very short lag (<2 years) due to this fast component. Thus, the start of the speleothem ^{14}C rise should correspond to 1954-1956 AD and can be utilized as an independent test of speleothem age models. The slow component of speleothem C reflects the slow turnover of soil organic matter, which can occur over a range of timescales (years to centuries) (Genty and Massault, 1999; Trumbore, 2000). Contribution from soil organic matter with slow turnover times leads to speleothem ^{14}C records that are damped and lagged relative to the atmosphere.

The CRC-3 bomb peak (Supplementary Fig. 4) shows that speleothem $\Delta^{14}C$ begins to slowly rise between 1955 and 1960, providing strong support for the 20th century portion of the U-Th age model. The peak speleothem $\Delta^{14}C$ value lags the atmosphere by approximately 34 years indicating a relatively slow turnover of soil organic matter. Crystal Cave lies within the Sierra Nevada lower montane forest where a large proportion of soil organic matter is likely to have a slow turnover time (Genty and Massault, 1999; Koarashi et al., 2012). The timing of the bomb peak is thus also consistent with the U-Th age model. While detailed modeling of soil organic matter turnover and speleothem ^{14}C is beyond the scope of this paper, the CRC-3 ^{14}C record

provides a valuable independent validation of the U-Th age model since 1954. While age uncertainty during the early part of our calibration period could confound the KE SST – $\delta^{18}O$ regression, the age model since ~1950 is very robust. Since the prediction formula using only the data from 1951-2000 AD is very similar to that using the full calibration period (1857-2007 AD), we are confident that age model uncertainties are unlikely to significantly change the calibration. In addition, the dynamical mechanisms used to explain the observed KE SST – $\delta^{18}O$ relationship are robust and further support the validity of the calibration.

S3.4.2 Study site, modern calibration, and CRC-3 stalagmite

Crystal Cave (36.59°N, 118.82°W), a tourist cave located within Sequoia National Park at an elevation of 1386 m, occupies the lower 64 m of a marble ridge approximately 160 m long and 40 m wide (Despain and Stock, 2005). Crystal Cave contains 4.77 km of surveyed passages, set on six distinct levels (Supplementary Fig. 1a). CRC-3 is a 10.4 cm long stalagmite (Supplementary Fig. 1b) that was actively growing at the time of collection in July 2008. The stalagmite consists of clear, dense, columnar calcite with faintly visible growth lamina. CRC-3 was collected from a small isolated chamber, located off the tourist trail underneath Marble Hall about 150 m from the cave entrance. The climate above the cave consists of cool, wet winters and hot, dry summers. The mean annual temperature and precipitation at the nearest weather station (COOP Southwest Station 043397: Giant Forest) are 8.1 °C and 106 cm, respectively, with approximately 90% of the precipitation falling between November and April. The majority of precipitation falls as rain, though up to 20% of annual precipitation may fall as snow (National Operational Hydrologic Remote Sensing Center. 2004). A modern calibration study, initiated in 2007 and continuing to the present, consists of logging cave temperature and relative humidity

(HOBO U23 Pro v2 Temperature/Relative Humidity Data Logger), measuring drip rate (manual counts and Driptych logger), collecting modern calcite on frosted glass plates, measuring pCO2 (Telaire 7001 portable pCO2 monitor), and collecting drip water samples for stable isotope and trace element analysis. Results indicate that the microclimate inside the cave is characterized by fairly constant temperature of 8.0 ± 0.5 °C and the relative humidity remains close to 100% throughout the year. We confirmed that stalagmite CRC-3 was actively forming prior to collecting the sample in July 2008 by collecting modern calcite growth on a frosted glass plate placed on top of the stalagmite in 2007. The average $\delta^{18}O$ of eight drip water samples collected between June 2007 and July 2008 at the CRC-3 drip site is -9.74 ± 0.48‰. The $\delta^{18}O$ value of modern glass plate calcite collected during the same period is -8.15‰ and the calculated equilibrium temperature is 7.6 °C (Kim and ONeil, 1997), very close to the measured value of 7.87 °C, indicating that CRC-3 calcite was likely precipitated under isotopic equilibrium conditions. The weighted mean $\delta^{18}O$ of biweekly precipitation samples collected from July 2001 to June 2008 from the CA75 Giant Forest, located about 4 km 18 away from and 535 m higher than Crystal Cave is -11.59‰. The mean drip water $\delta^{18}O$ from 2007-2011 is -9.93‰. To estimate the mean precipitation $\delta^{18}O$ over the cave site, for which no samples are available, we applied an isotopic lapse rate of -3‰/km (Cayan et al., 1998) and obtain a predicted mean value of -9.99‰, very close to the observed drip water value. The cave temperature reflects the mean annual temperature at the surface which is unlikely to have varied by more than ~1 °C over the last millennium (Mann et al., 2009). Since the $\delta^{18}O$ of speleothem calcite deposited under isotopic equilibrium conditions is dependent only on cave temperature, which is constant, and the $\delta^{18}O$ of cave drip water, which closely reflects precipitation, the CRC-3 speleothem $\delta^{18}O$ record should primarily reflect variability in the isotopic composition of precipitation.

Crystal Cave drip water is likely composed of a mixture of precipitation that fell over the previous year or more. Recharge in karst aquifers generally follows a complex mixture of fast and slow pathways and some isotopic variability may therefore stem from fractionation and mixing in the overlying soil and epikarst (Baker and Bradley, 2010; Tooth and Fairchild, 2003). Essentially, the karst aquifer behaves as a low-pass filter, removing the high-frequency signal of precipitation $\delta^{18}O$ and introducing a time lag. Dripwater $\delta^{18}O$, therefore, is unlikely to be correlated with precipitation $\delta^{18}O$ from the concurrent time period, but is much more likely to reflect the integrated signal over the preceding year or more (Baker and Bradley, 2010; Oster, et al., 2012). While preferential infiltration or removal of isotopically light snow melt water could introduce a seasonal bias to the stable isotope signal of cave drip water (Lachniet, 2009), the Crystal Cave data suggests that drip water isotope composition reflects a weighted average of precipitation, including rain and snow that fell over the cave. Similarly, changes in the seasonality of precipitation could also influence the isotopic composition of cave drip water over decadal timescales. However, a study of precipitation variability in the Western US indicates that decadal variability in California precipitation is driven largely by changes in wet season precipitation (December to April) and that the seasonal contributions to decadal variability were quite stable from 1880 to 1994 (Cayan et al., 1998). Therefore, we argue that the CRC-3 $\delta^{18}O$ variability is driven by interannual to decadal scale variations in the isotopic composition of precipitation, which in turn are primarily reflecting changes in moisture source region and storm track.

S3.5. Supplementary References

Baker, A. and Bradley, C., 2010. Modern stalagmite $\delta^{18}O$: Instrumental calibration and forward modelling. *Global and Planetary Change.* 71, 201-206.

Cayan, D. R., Dettinger, M. D., Diaz, H. F., Graham, N. E., 1998. Decadal variability of precipitation over western North America. *Journal of Climate*. 11, 3148-3166.

Cook, E.R., Kairiukstis, L.A., 1990. Methods of dendrochronology: applications in the environmental sciences. *Springer* .

Cook, E. R., Woodhouse, C. A., Eakin, C. M., Meko, D. M., Stahle, D. W., 2004. Long-term aridity changes in the western United States. *Science*. 306, 1015-1018.

Dansgaard, W., 1964. Stable isotopes in precipitation. *Tellus*. 16, 436-468.

Despain, J. D. and Stock, G. M., 2005. Geomorphic history of Crystal Cave, Southern Sierra Nevada, California. *Journal of Cave and Karst Studies*. 67, 92-102.

Draxler, R. and Rolph, G., 2003. HYSPLIT (HYbrid Single-Particle Lagrangian Integrated Trajectory) model access via NOAA ARL READY website (http://www. arl. noaa. gov/ready/hysplit4. html). *NOAA Air Resources Laboratory,* Silver Spring.

Frisia, S., Fairchild, I. J., Fohlmeister, J., Miorandi, R., Spötl, C., Borsato, A., 2011. Carbon mass-balance modelling and carbon isotope exchange processes in dynamic caves. *Geochimica Et Cosmochimica Acta.* 75, 380-400.

Genty, D. and Massault, M., 1999. Carbon transfer dynamics from bomb ^{14}C and $\delta^{13}C$ time series of a laminated stalagmite from SW France; modelling and comparison with other stalagmite records. *Geochimica Et Cosmochimica Acta.* 63, 1537-1548.

Harvey, F. E., 2005. Use of NADP archive samples to determine the isotope composition of precipitation: characterizing the meteoric input function for use in ground water studies. *Ground Water.* 39, 380-390.

Kaplan, A., Cane, M. A., Kushnir, Y., Clement, A. C., Blumenthal, M. B., Rajagopalan, B., 1998. Analyses of global sea surface temperature 1856-1991. *Journal of Geophysical Research.* 103, 567-518.

Kim, S. T. and ONeil, J. R., 1997. Equilibrium and nonequilibrium oxygen isotope effects in synthetic carbonates. *Geochimica Et Cosmochimica Acta*. 61, 3461-3475.

Koarashi, J., Hockaday, W. C., Masiello, C. A., Trumbore, S. E., 2012. Dynamics of decadally cycling carbon in subsurface soils. *Journal of Geophysical Research*. 117, G03033.

Lachniet, M. S., 2009. Climatic and environmental controls on speleothem oxygen-isotope values. *Quaternary Science Reviews*. 28, 412-432.

Mann, M. E., Zhang, Z. H., Rutherford, S., Bradley, R. S., Hughes, M. K., Shindell, D., Ammann, C., Faluvegi, G., Ni, F. B., 2009. Global Signatures and Dynamical Origins of the Little Ice Age and Medieval Climate Anomaly. *Science.* 326, 1256-1260.

Mattey, D., Lowry, D., Duffet, J., Fisher, R., Hodge, E., Frisia, S., 2008. A 53 year seasonally resolved oxygen and carbon isotope record from a modern Gibraltar speleothem: reconstructed drip water and relationship to local precipitation. *Earth and Planetary Science Letters*. 269, 80-95.

National Atmospheric Deposition Program (NRSP-3), 2007. NADP Program Office, Illinois State Water Survey, 2204 Griffith Dr., Champaign, IL 61820.

National Operational Hydrologic Remote Sensing Center, 2004. *Snow Data Assimilation System (SNODAS) Data Products at NSIDC,* Boulder, Colorado USA: National Snow and Ice Data Center. Digital media.

Oster, J. L., Montañez, I. P., Kelley, N. P., 2012. Response of a modern cave system to large seasonal precipitation variability. *Geochimica Et Cosmochimica Acta*. 91, 92-108.

Scholz, D. and Hoffmann, D. L., 2011. StalAge-An algorithm designed for construction of speleothem age models. *Quaternary Geochronology.* 6, 369-382.

Scholz, D., Mühlinghaus, C., Mangini, A., 2009. Modelling $\delta^{13}C$ and $\delta^{18}O$ in the solution layer on stalagmite surfaces. *Geochimica Et Cosmochimica Acta*. 73, 2592-2602.

Southon, J., Noronha, A. L., Cheng, H., Edwards, R. L., Wang, Y., 2011. A high-resolution record of atmospheric ^{14}C based on Hulu Cave speleothem H82. *Quaternary Science Reviews.* 33, 32-41.

Tooth, A. F. and Fairchild, I. J., 2003. Soil and karst aquifer hydrological controls on the geochemical evolution of speleothem-forming drip waters, Crag Cave, southwest Ireland. *Journal of Hydrology*. 273, 51-68.

Trumbore, S. E., 2000. Constraints on below ground carbon cycling from radiocarbon: the age of soil organic matter and respired CO_2. *Ecological Applications.* 10, 399-411.

CHAPTER 4:

Investigation and interpretation of Crystal Cave speleothem $\delta^{13}C$ and trace element variations since AD 854

4.1 Introduction

Complex geochemical processes and interactions that occur in the cave environment can be directly and indirectly related to changes in climate. Therefore, utilizing multiple proxies in speleothems can provide a better understanding of the controlling mechanisms to facilitate more accurate interpretations of past climate conditions. The $\delta^{13}C$ and trace-element composition of speleothem calcite may be used to provide additional information to enhance the interpretation of the oxygen isotope records as they are sensitive to local environmental factors (eg. Tooth and Fairchild. 2003; Treble et al. 2003; Johnson et al., 2006). The $\delta^{13}C$ depends on the carbon isotopic composition of the dissolved inorganic carbon (DIC) in the drip water which can be derived from the CO_2 of the atmosphere (~ -7 ‰), the soil (~ -26 ‰ for C3 vegetation) and from the dissolution of the karstic host rock (~ 0 ‰). The trace elements (Mg, Sr and Ba) can substitute for Ca in the carbonate ($CaCO_3$) crystal lattice (Fig. 4.1) (Fairchild et al. 2006) and provide information about recharge, seasonal cycles, temperature, soil conditions, and other environmental conditions (Fairchild and Treble. 2009) as they are related to water-rock residence times and vegetation changes above the cave (Richards and Dorale. 2003). Because the chemistry of speleothem calcite may be affected by environmental and climatic factors, it is necessary that the variations in the $\delta^{13}C$ and trace element composition are thoroughly understood, well calibrated, and tested for each individual cave study area.

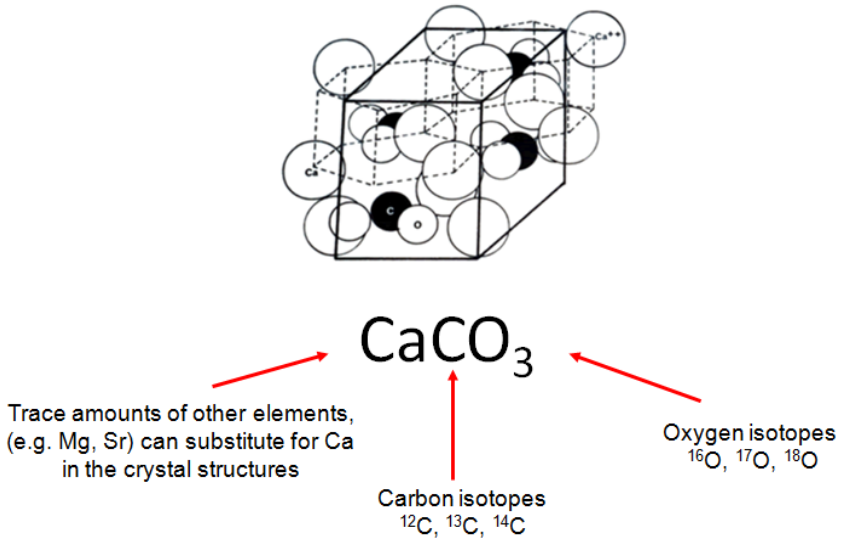

Figure 4.1. Schematic of calcite, CaCO3, molecule structure and the possible elemental variations. (http://www.pengellytrust.org/museum/aragonite.htm)

4.2 Factors influencing speleothem $\delta^{13}C$ composition

Different factors can influence variations in $\delta^{13}C$ incorporated into cave speleothems and make it difficult to make accurate interpretations of past environmental conditions (eg. Frisia et al., 2005). For example, variations in the $\delta^{13}C$ composition of soil CO_2 can vary according to the C_3:C_4 plant photosynthetic pathway ratio above the cave, with C_3 plants contributing to lower $\delta^{13}C$ values (Cerling et al., 1993). Varying soil respiration rates can also influence soil CO_2 and speleothem $\delta^{13}C$, as drier periods lead to decreased soil CO_2 and more positive, atmospheric like $\delta^{13}C$ values, while wetter periods lead to increased soil respiration and decreased $\delta^{13}C$ values (Oster et al., 2010). Differing flow rates of water infiltrating the cave can also affect variations in the $\delta^{13}C$, in which drier conditions contribute to decreased drip rates, longer water residence times in the epikarst, and enhanced CO_2 degassing prior to the site of speleothem deposition, such as in the epikarst above the cave or on the cave ceiling (e.g. Fairchild et al., 2006). This process, known as prior calcite precipitation (PCP), causes calcite deposition to occur before

reaching the stalagmite. Here, the lighter $^{12}CO_2$ molecule is preferentially released during degassing leading to enriched ^{13}C values in the drip water (Fairchild et al., 2000). Another factor that can influence the $\delta^{13}C$ composition can be due the variations of carbon derived from the soil vs the bedrock. In an 'open system' the carbonic acid solution is continuously in contact with soil CO_2 gas in which the $\delta^{13}C$ in the soil CO_2 is isotopically identical to the plant material from which it is derived (Fig. 4.2) and the DIC pool maintains equilibrium with this soil CO_2 during dissolution leading to low DIC and speleothem $\delta^{13}C$ values in equilibrium soil CO_2. In a purely 'closed system', the carbonic acid solution is isolated from soil CO_2 during dissolution, hence the DIC and speleothem $\delta^{13}C$ pools evolve to higher $\delta^{13}C$ values, reflecting a 50:50 mixture of soil and bedrock sources (Hendy, 1971). Cave formations are likely to reflect a mixture of these two end-member scenarios (Genty et al., 1999) (Fig. 4.2).

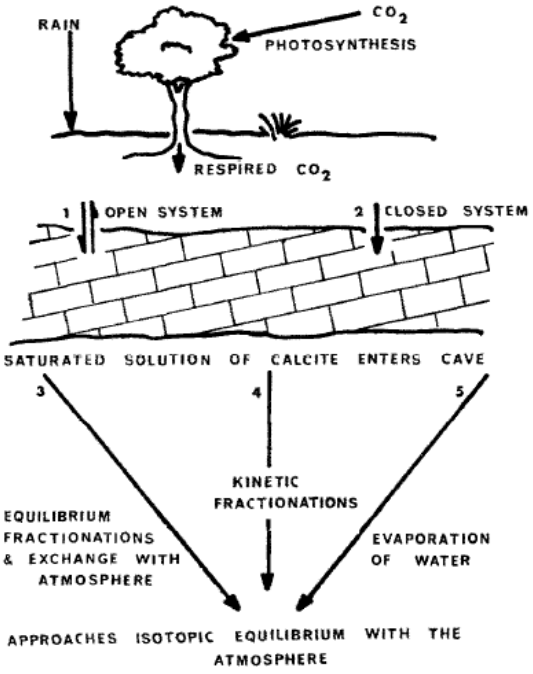

Figure 4.2 A schematic diagram of the dissolution of limestone and the formation of speleothems in an open and closed system and conditions leading to equilibrium and kinetic fractionation and evaporation (Hendy, 1971).

Speleothem $\delta^{13}C$ may also be affected by non-climatic influences such as kinetic fractionation, when the rate of CO_2 loss from solution is too rapid to prevent equilibrium from being maintained between aqueous carbon dioxide and bicarbonate ions (Fig. 4.2) (Hendy, 1971). The Hendy Test results indicate that the Crystal Cave, CRC-3, speleothem formed in equilibrium (Chapter 2). Combining $\delta^{13}C$ with other proxies and calibrating with instrumental records can help us more confidently interpret this proxy.

4.3 Factors influencing speleothem trace element composition

Numerous factors and complex processes can also influence variations in trace element concentrations incorporated into speleothem calcite. The principal source of calcium and most trace elements incorporated into speleothems is derived from the bedrock (including fragments in the soil) and the overlying materials (Fairchild et al., 2000), however, the trace element concentrations can also be influenced by atmospheric input, vegetation/soil, karstic aquifer, crystal growth, and secondary alteration (Fairchild et al., 2006). While the incorporation of Sr into calcite is not affected by temperature variations (Fairchild and Treble, 2009), the incorporation of Mg is a function of both the temperature and the Mg concentration of the solution it is precipitated from (Gascoyne, 1983). Because the temperature in most deep caves is constant and equal to the mean annual surface temperature throughout the year (Wigley and Brown, 1976), the Mg/Ca variations are usually controlled by variations in the Mg/Ca ratio of cave drip water (e.g. Johnson et al., 2006) and by the differential rates of dissolution in the dolomite and calcite bedrock in the karst structure (Fairchild et al., 2000). However, a positive correlation between Mg, Sr, and Ba suggest that dolomite dissolution is not the dominant control

on Mg since dolomite typically has lower Sr and Ba concentrations than calcite (Hellstrom and McCulloch, 2000). During periods with increased PCP, where calcite is precipitated before reaching the stalagmite leading to the preferential removal of Ca (discrimination against Mg and Sr), the remaining water contains higher trace element (TE) concentrations as the distribution coefficient, D, where:

$$D_{TE} = (TE/Ca)_{calcite}/(TE/Ca)_{water} \quad \text{(Eq. 1)}$$

is much less than 1 and lead to increased TE ratios (e.g. Mg/Ca, Sr/Ca, Ba/Ca) in dripwaters and speleothems (Fairchild et al. 2000; Lorens. 1981; Johnson et al., 2006), which typically occurs during drier conditions. Alternatively, wetter conditions contribute to reduced PCP and lower TE ratios (Fairchild et al., 2000; Treble et al., 2003; Johnson et al., 2006; Cruz et al., 2007). Thus, the co-variation of Mg, Sr, Ba, and $\delta^{13}C$ in speleothems is an indicator that PCP is the dominant mechanism (e.g. Fairchild and Treble, 2009; Johnson et al., 2006; Tremaine and Froelich, 2013).

4.4. Stable carbon isotope analytical methods

To analyze the carbon stable isotope variations, I utilized the 1054 micromilled subsamples (see Chapter 3) measured using a Kiel IV-carbonate device coupled with a Thermofinnigan Delta V Plus isotope ratio mass spectrometer. A total of 16 standards, (NBS-19, NBS-18, and OX, an in-house quality control standard), were analyzed during each run of 30 unknown samples. The results of isotopic analysis are presented in conventional delta (δ) notation, defined as:

$\delta^{13}C = [(^{13}C/^{12}C)_{sample}/(^{13}C/^{12}C)_{VPDB} -1] * 1{,}000‰$.

4.5 Trace element analytical methods

Trace element analysis was carried out on 1054 micromilled subsamples from the Crystal Cave stalagmite, CRC-3, (see Chapter 3). Variations in Mg/Ca, Sr/Ca, and Ba/Ca ratios were measured using a high resolution, single-collector, Nu Instruments AttoM ICPMS (Inductively Coupled Plasma Mass Spectrometer) (Fig. 4.3a). The samples were dissolved in double distilled 2% HNO_3 and introduced into the ICP-MS via "dry plasma" introduction, in which liquid samples are introduced using a “desolvating nebulizer” (DSN-100), which reduces oxides by 10x, removes water, and converts the sample to a dry aerosol (Fig. 4.3b). This method has low memory and rapid washout of sample, improved sensitivity (by a factor of 5-10), and improved beam stability obtained due to the reduced solvent loading on the plasma and 100% sample vaporization.

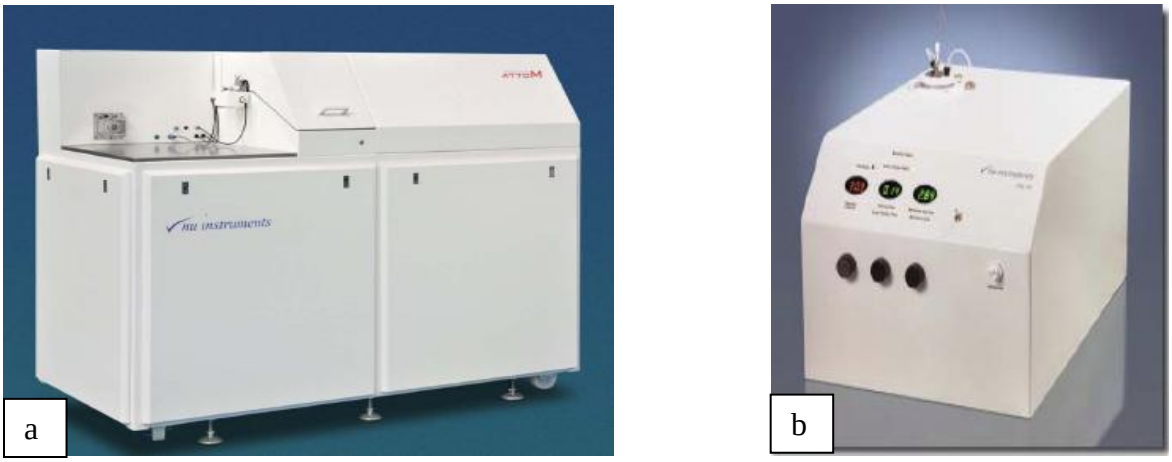

Figure 4.3. Instruments used to measure trace elements, a) Nu Instruments attoM™ICPMS (Inductively Coupled Plasma Mass Spectrometer) and b) desolvating nebulizer (DSN 100) which converts the sample into a dry aerosol.

The samples were measured based on the 'Ratio method' developed by Rosenthal et al., (1999) and modified by Marchitto (Marchitto, 2006), which consists of simultaneous determination of

X/Ca (eg. Mg/Ca, Sr/Ca) directly from intensity ratios made by the single-collector ICP-MS. This method is used to determine the ratio of elements relative to one other element such as the Mg/Ca, Sr/Ca or other elements/Ca. In this method, sample bracketing is used (standard–sample–standard), with the standard composition matrix matched to the dissolved concentrations in the speleothem samples. The X/Ca ratios are calculated from intensity ratios using the standard sample bracketing to correct for instrumental mass discrimination and drift. Simultaneous determination of several elemental ratios reduces the overall sample size requirement and analysis time and also eliminates the uncertainty associated with correlating between different samples (as when each ratio is determined individually). Precision of <0.5% for Mg/Ca and Sr/Ca, <1% for Ba/Ca can be obtained when measured simultaneously (Marchitto. 2006).

One drawback of this method noted in Rosenthal et al., (1999) is that it only allows determination of elemental ratios and not concentrations. The outliers were removed by using the Ca/Ca ratio calculated from both Ca-43 and Ca-46, in which the result of the "Ca/Ca" ratio is unity (1), and then any data (for all elements) for samples where this ratio was more than 5% off from 1 was removed. The relative standard deviation (RSD) is useful for comparing the uncertainty between different measurements of varying absolute magnitude. The uncertainty for each element is calculated for all data by treating every other standard as a sample.

4.6 Carbon stable isotope results

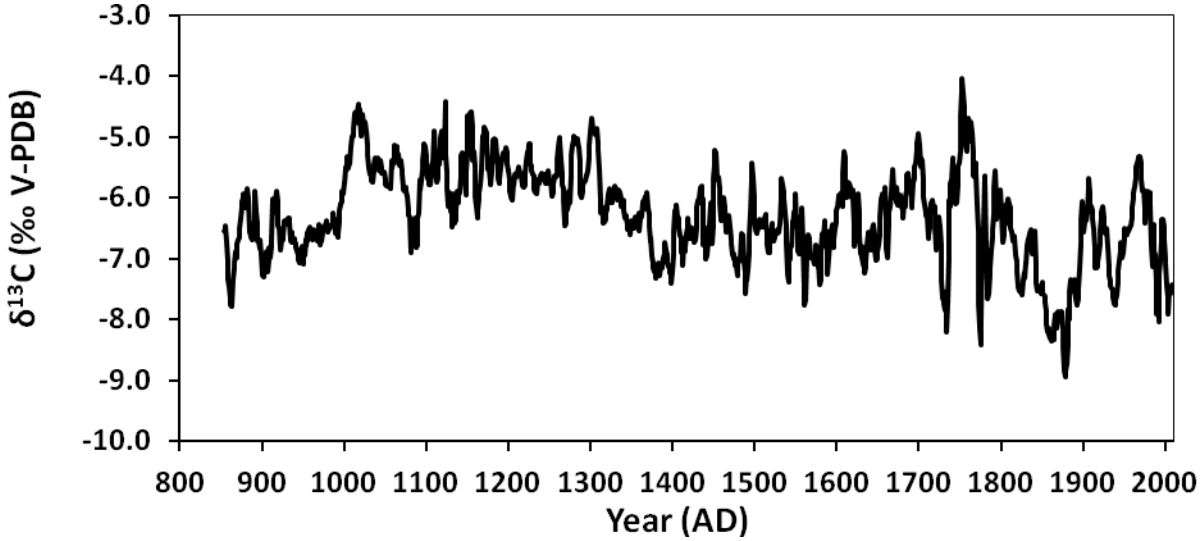

Figure 4.4. Results of 1054 $\delta^{13}C$ measurements conducted along the growth axis of the CRC-3 stalagmite.

Based on the age model developed in Chapter 3, the results show the CRC-3 $\delta^{13}C$ values exhibits prominent decadal scale variability with a range of 4.99 ‰, from -3.98 ‰ in 1752.3 to -8.97 ‰ in 1877.8 (Fig. 4.4; Table A3). The mean $\delta^{13}C$ values (-6.29 ‰) are more positive throughout the Medieval Climate Anomaly (MCA) (~900-1300 AD; -5.81‰), than the Little Ice Age (LIA) (1500-1850 AD; -6.40‰), and the 20th century (-6.64 ‰) (Table A3). There is no correlation between the $\delta^{18}O$ and $\delta^{13}C$ ($R^2 = 0.029$).

4.7 Trace element results

Table 4.1. Average $\delta^{13}C$ and trace element values.

	$\delta^{13}C$ (‰)	Mg/Ca (mmol/mol)	Sr/Ca (µmol/mol)	Ba/Ca (µmol/mol)
20th Century	-6.77	1.76	78.22	10.22
LIA 1500-1850	-6.40	1.75	78.35	10.56
MCA 900-1300	-5.81	1.76	79.35	10.60

Table 4.2. Isotope and trace element correlation coefficients (r)

	Correlations (r)	5 yr smooth
$\delta^{18}O$-$\delta^{13}C$	0.17	0.16
$\delta^{18}O$-Mg/Ca	0.19	0.25
$\delta^{18}O$-Sr/Ca	0.11	0.15
$\delta^{18}O$-Ba/Ca	-0.01	-0.04
$\delta^{13}C$-Mg/Ca	0.36	0.49
$\delta^{13}C$-Sr/Ca	0.12	0.13
$\delta^{13}C$-Ba/Ca	-0.04	-0.09
Mg/Ca-Sr/Ca	0.05	0.05
Mg/Ca-Ba/Ca	0.18	0.09
Sr/Ca-Ba/Ca	0.29	0.40

The Mg/Ca values show a range of 1.27 mmol/mol, with a maximum of 2.37 in 1973 and a minimum of 1.10 mmol/mol in 1877, and an average of 1.76 mmol/mol and (Table A3). This average remains about the same during the MCA, the LIA, and the 20th Century (Table 4.1). The Sr/Ca values range 35.41 µmol/mol, with a maximum of 95.31 µmol/mol in 1731 and a minimum of 59.90 µmol/mol in 1679, and an average of 78.57 µmol/mol and (Table A3). The average values are higher for the MCA than the LIA and 20th Century (Table 4.1). The Ba/Ca values range 10.45 µmol/mol, with a maximum of 16.37 µmol/mol in 1546 and a minimum of 5.92 µmol/mol in 1272, and an average 10.54 µmol/mol. The average values are higher for the

MCA and LIA than the 20th Century (Table 4.1). All trace element results show low calculated relative standard deviations. A moderate correlation is observed between the δ^{13}C-Mg/Ca and the Sr/Ca-Ba/Ca (Table 4.2).

4.8 Discussion

In order to reconstruct drought and hydrological changes in the SWUS, we investigated the potential of additional proxies (δ^{13}C, Mg/Ca, Sr/Ca, Ba/Ca) known to be sensitive to local water balance. The CRC-3 δ^{13}C variations may reflect a number of complex factors, for example changes in the photosynthetic pathways (C_4:C_3) of vegetation above the cave. However, studies finding a lack of pollen or packrat midden evidence for C_4 flora over the last ~20,000 years in the Sierra Nevada Mountains (see Oster et al., 2009) suggests that C_3:C_4 plant ratios have remained the same and have not contributed to changes in soil derived δ^{13}C above Crystal Cave. Likewise, whereas large variations in the cave pCO_2 can also affect the δ^{13}C values, our monitoring measurements indicate relatively similar pCO2 between winter and summer, suggesting this is also not a factor influencing δ^{13}C variations. However, records from ASH Mountain station (36.48°N; 118.83°W; 521 m), located near the cave in Sequoia National Park, indicate the amount of yearly precipitation can vary greatly. From 1926 to 2011, yearly precipitation amounts ranged from 1005 mm, with the greatest amount of 1297 mm occurring in 1982 and the least of 292 mm occurring in 1959 (http://cdec.water.ca.gov). Over the 85 year long record, 8 years had greater than 1000 mm precipitation delivered and ten years had less than 400 mm. This large range would likely lead to changes in rechargerates that could promote δ^{13}C variations due to prior calcite precipitation (PCP). PCP increases with increased evaporation, degassing, or slower seepage rates by contributing to calcite precipitation in the epikarst before

reaching the stalagmite formation (Fairchild et al., 2000). Therefore, drier conditions contribute to decreased drip rates thereby enhancing CO_2 degassing and leading to higher $\delta^{13}C$ values, whereas wetter conditions lead to slower CO_2 degassing and lower $\delta^{13}C$ values (Fairchild et al., 2000).

Multiple regression analysis of $\delta^{13}C$ against annual mean instrumental temperature (T) and precipitation (P) data (Ash Mountain site, previous 10 years mean, 1935 - 2007 AD) indicates that both factors are significant ($R^2 = 0.44$, $p < 0.0001$; $\delta^{13}C$ versus P is $R^2 = 0.14$, $p = 0.2375$ and versus T is $R^2 = 0.23$, $p = 0.0503$). Increased soil respiration, which in arid and semi-arid environments is controlled by both temperature and soil moisture, is associated with more negative $\delta^{13}C$ values (e.g. Oster et al., 2012). As surface air temperature and precipitation exert a strong control on local water balance (P-ET), CRC-3 $\delta^{13}C$, which appears to be sensitive to both factors, may, therefore, be a suitable proxy for P-ET.

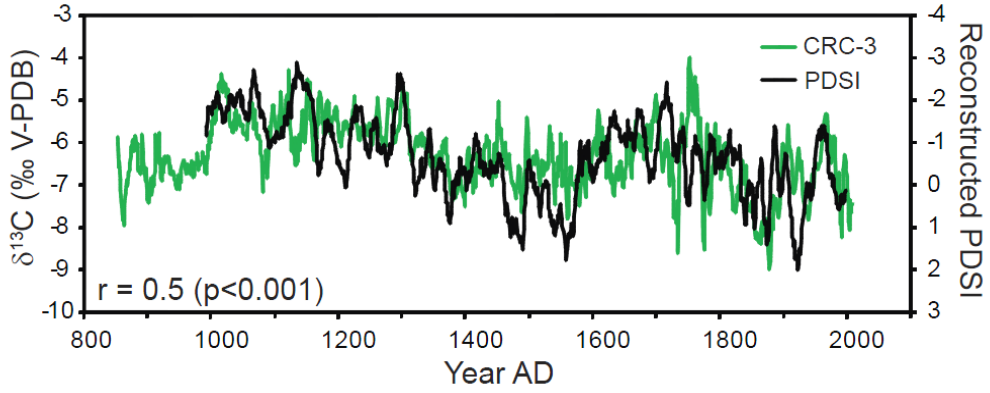

Figure 4.5. Comparison of CRC-3 $\delta^{13}C$ record with the reconstructed PDSI (Macdonald et al., 2007).

A comparison of the CRC-3 $\delta^{13}C$ time series with several tree ring records indicates correlations vary depending upon which record is used. Low correlations were found between the Biondi et

al., (2001) record (1661-1991) which utilized trees from Southern and Baja California ($r = -0.15$, $p = 0.0063$) and the D'Arrigo et al., (2001) record (1716-1995) based on trees from coastal Alaska and the Pacific Northwest ($r = 0.23$, $p = 0.0001$). However, we observe a moderate negative correlation ($r = -0.5$, $p < 0.001$) with the Palmer Drought Severity Index (PDSI) reconstruction based on trees from San Gorgonio Mountains in Southern California (MacDonald, 2007) (982-1998), likely due to proximity (Fig. 4.5). This inverse relationship indicates drier conditions are prevalent when $\delta^{13}C$ values are high and furthermore, reveals relatively elevated $\delta^{13}C$ values during the Medieval Climate Anomaly (MCA) megadroughts compared to the Little Ice Age (LIA) and 20th century (Table 4.1; Fig. 4.7).

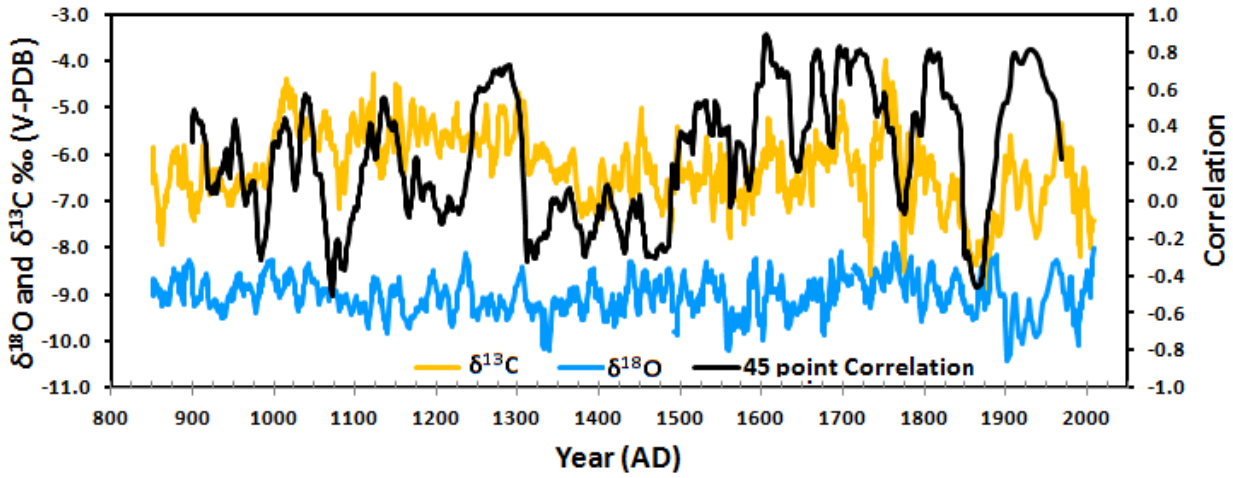

Figure 4.6. 45 yr running mean correlation (black line) between an CRC-3 $\delta^{18}O$ (blue line) and $\delta^{13}C$ (gold line) time series since 854 AD.

While there is no correlation between the CRC-3 $\delta^{18}O$ and $\delta^{13}C$ over the entire record ($R^2 = 0.029$, $p = 0.3348$), a 45 point running mean correlation between the CRC-3 $\delta^{18}O$ and $\delta^{13}C$ time series indicates there were episodes during the record that showed significant correlations, particularly notable during the Little Ice Age (LIA 1500-1800) (Fig.4.6). As higher $\delta^{13}C$ values represent drier conditions, high correlations suggest less moisture from lower latitudinal sources,

whereas lower $\delta^{13}C$ values represent wetter conditions, suggesting more moisture was delivered during these periods originating from higher latitudinal sources (Berkelhammer et al., 2012, Friedman et al., 2002). However, this relationship is not consistent throughout the record, suggesting other factors contributed to these variations.

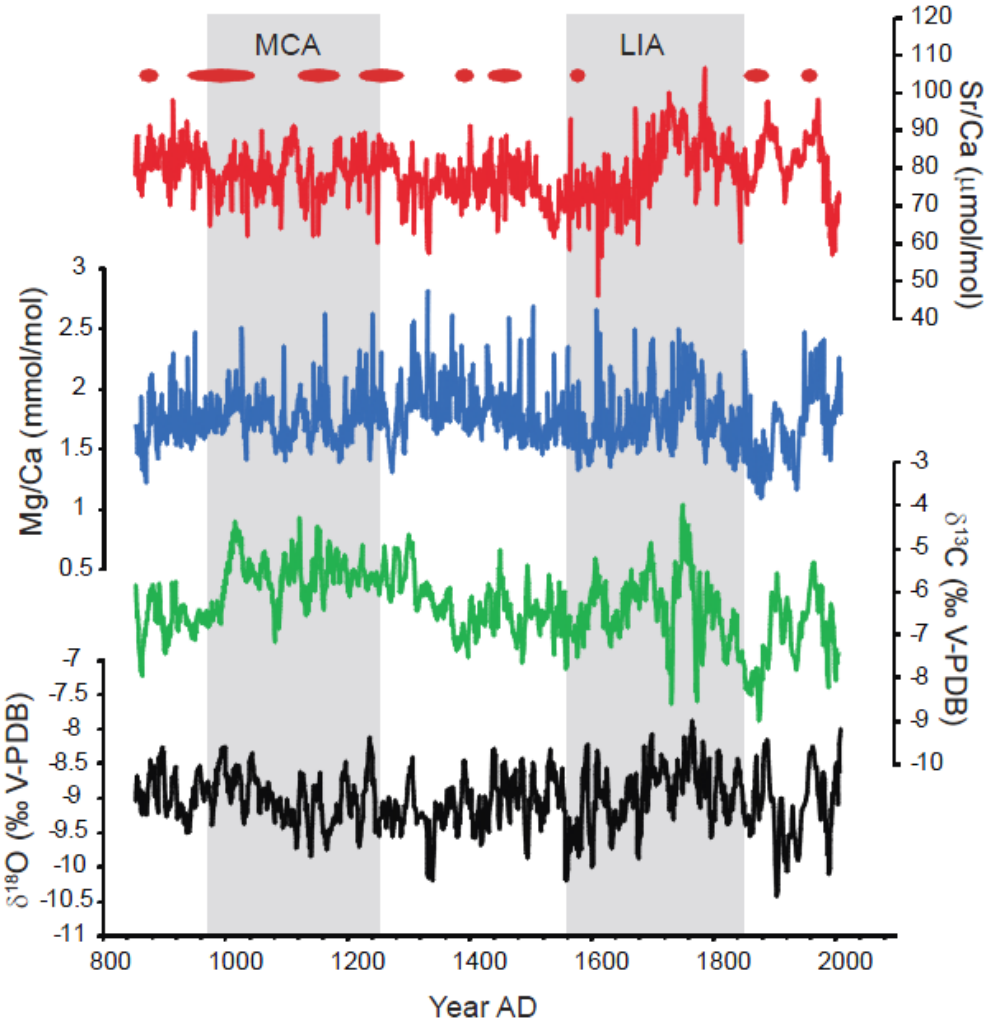

Figure 4.7. $\delta^{18}O$ (black), $\delta^{13}C$ (green), Mg/Ca (blue), and Sr/Ca (red) results from CRC-3. The MCA (950-1250 AD) and LIA (1550 - 1850 AD) are highlighted in gray. The red ellipses show the approximate duration of reconstructed multidecadal droughts in Western North America (Conroy et al., 2009).

Speleothem trace element variations can also reflect numerous factors, including changing temperature (Mg/Ca) (Gascoyne, 1983), growth rate (Sr/Ca) (Morse and Bender, 1990; Lea and Spero, 1994), and cave air pCO_2 (Mattey et al., 2010), due to increased PCP in the epikarst or on the cave ceiling, and/or a greater degree of CO_2 degassing and calcite precipitation on stalagmite surfaces when drip-rates are lower (e.g. Fairchild et al., 2006). Both mechanisms would have the effect of enriching Mg/Ca, Sr/Ca, Ba/Ca, and $\delta^{13}C$ values during drier periods (Fairchild et al., 2006). In the absence of cave dripwater and other monitoring data, it has been suggested that a positive correlation between speleothem $\delta^{13}C$, Mg/Ca, and Sr/Ca is strong evidence for PCP, which is thought to be driven by variations in local water balance (e.g. Johnson et al., 2006). The average Mg/Ca values remain about the same during the MCA, the LIA, and the 20th Century, and the Sr/Ca and somewhat Ba/Ca values are higher for the MCA than the LIA and 20th Century (Table 4.1). This study reveals moderate correlations between the $\delta^{13}C$ and Mg/Ca ($r = 0.36$, $p < 0.0001$ and 5 point smooth $r = 0.49$, $p < 0.0001$), low correlations between the $\delta^{13}C$ and Sr/Ca ($r = 0.12$, $p = 0.0001$ and 5 point smooth 0.13, $p < 0.0001$), and no correlation with Ba/Ca (Table 4.1), suggesting that PCP is not a significant influencing factor at this site.

A study of a speleothem record from McLean's Cave in the central Sierra Nevada Mountains suggests that elevated $\delta^{18}O$, $\delta^{13}C$ and trace element concentrations indicate warmer and drier conditions during Greenland interstadials (Oster et al., 2014). Since the Mg/Ca of calcite is a function of both temperature and the Mg concentration of the solution from which the calcite precipitates (Gascoyne, 1983), the variations in the $\delta^{13}C$ and Mg/Ca correlations during the MCA indicate that the Mg concentrations may have been influenced by both. As the Sr and Ba calcite concentrations are not affected by changes in temperature but are dependent on the chemistry of

the drip water and to some extent on crystal growth rate (Morse and Bender, 1990; Lea and Spero, 1994), the differences between Mg/Ca and Sr/Ca and Ba/Ca may also be due to incongruent dissolution of carbonate in the host rock above the cave. A recent study of trace element incorporation in farmed calcite found that while the relationship between rainfall and Mg/Ca and Sr/Ca ratios is unique at each site, in order to interpret these proxies as 'wet vs. dry', the calcite Sr/Ca and Mg/Ca variations must be coherent and in-phase over all time periods (Tremaine and Froelich, 2013). While the Mg/Ca, Sr/Ca, Ba/Ca, and $\delta^{13}C$ records show strong positive correlations during certain periods (Fig. 4.6 and 4.8), which indicate possible PCP, given the lack of correlation during some time periods, other mechanisms likely play a role. More research is needed to determine the controls of trace element concentrations (Mg, Sr, and Ba) in the overlying bedrock, the cave drip water, and modern of climate factors at this site.

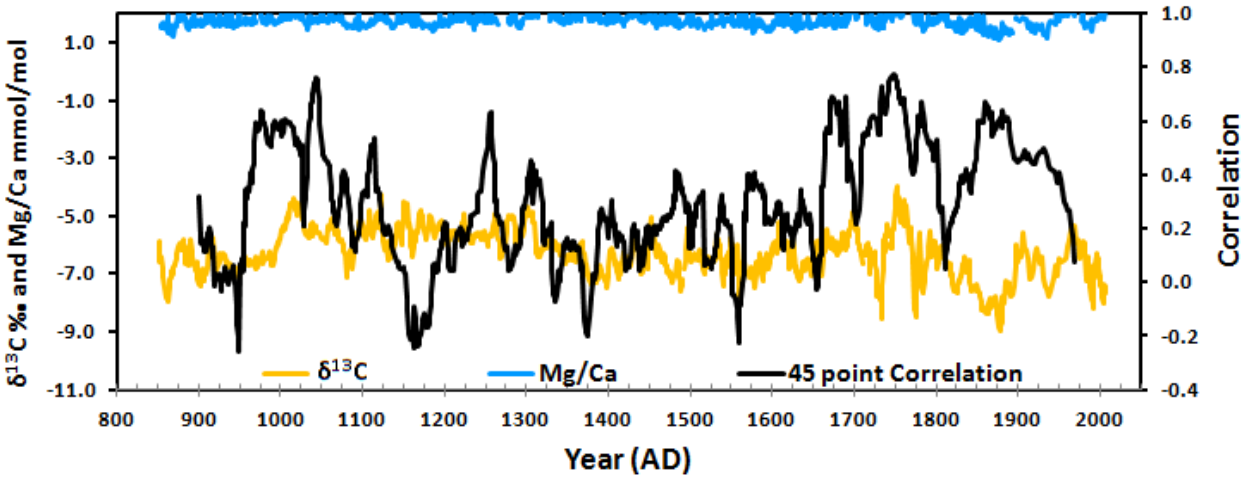

Figure 4.8. 45 point running mean correlation between CRC-3 $\delta^{13}C$ and Mg/Ca time series. Plot shows correlation (black line) between Mg/Ca (blue line) and $\delta^{13}C$ (gold line) since 854 AD.

4.9 Conclusions

Multiple proxies in speleothems such as $\delta^{13}C$ and trace elements (Mg/Ca, Sr/Ca, Ba/Ca) can provide additional information to reconstruct hydroclimate (eg. Tooth and Fairchild, 2003; Treble et al., 2003; Johnson et al., 2006), however accurate interpretation can be complicated by other factors. The Crystal Cave stalagmite, CRC-3, $\delta^{13}C$ values exhibit prominent decadal scale variability and show a wide range of ~ 5 ‰ (Fig.4.4, Table A3). While these variations may reflect a number of complex processes, research indicates that it is unlikely variations in C_3:C_4 type vegetation or cave pCO_2 are a significant influence and more likely that change in drip rate is the dominant factor influencing $\delta^{13}C$ values. Since the yearly amount of precipitation at ASH Mountain station, a location near the cave, can vary greatly, ranging from 1297 mm delivered in 1982, to 292 mm in 1959, this large range would likely lead to changes in precipitation drip rates in the cave with wetter conditions leading to slower CO_2 degassing and lower $\delta^{13}C$ values and drier conditions contributing to decreased drip rates, thereby enhancing CO_2 degassing, and leading to higher $\delta^{13}C$ values.

A 45 year running mean correlation between CRC-3 $\delta^{18}O$ and $\delta^{13}C$ time series showed the highest correlations during the Little Ice Age (LIA) from ~1500 to 1850 AD and early 20th Century (Fig.4.5). A comparison between the CRC-3 $\delta^{13}C$ record and the Southern California PDSI reconstruction (MacDonald, 2007) indicates the negative PDSI (drier conditions) is associated with higher $\delta^{13}C$ values. This relationship occurs throughout the $\delta^{13}C$ record showing elevated values during the MCA megadroughts and increased variability during the Little Ice Age (LIA) and 20th century (Fig. 4.5). Multiple regression analysis of $\delta^{13}C$ data indicates that

both temperature and precipitation factors are significant and therefore, the CRC-3 $\delta^{13}C$ record may be a suitable proxy for reconstructing past drought variability.

The CRC-3 trace element record indicates that Mg/Ca is moderately correlated with $\delta^{13}C$, suggesting some climatic influence on both proxies. However, the lower correlation observed during the MCA indicates that increased PCP in the epikarst or on the cave ceiling, and/or a greater degree of CO_2 degassing and calcite precipitation on stalagmite surfaces when drip-rates are lower is not a major influence during the drier periods. The correlation between Mg/$\delta^{13}C$ could also reflect water balance but perhaps requires another source for Mg but given the lack of correlation during some time periods indicate further investigation is required. The lack of significant correlation between Mg/Ca, Sr/Ca, and Ba/Ca further suggests that PCP is not significant here and that additional factors such as bedrock mixing may complicate this signal. Since the Mg/Ca ratios are more dependent on temperature, the varying correlations between the Mg/Ca, Sr/Ca, and Ba/Ca may be due to the incongruent dissolution of carbonate in the host rock above the cave. More research is needed to determine the controls of trace element concentrations (Mg, Sr, and Ba) in the overlying bedrock, the cave drip water, and modern of climate factors at this site.

4.10 References

Baker, A., Genty, D., Fairchild, I. J., 2000. Hydrological characterisation of stalagmite dripwaters at Grotte de Villars, Dordogne, by the analysis of inorganic species and luminescent organic matter. *Hydrology and Earth System Sciences.* 4, 439-449.

Berkelhammer, M., Stott, L., Yoshimura, K., Johnson, K., Sinha, A., 2012. Synoptic and mesoscale controls on the isotopic composition of precipitation in the western United States. *Climate Dynamics.* 38, 433-454.

Cerling, T.E., Wang, Y., and Quade, J., 1993. Expansion of C4 ecosystems as an indicator of global ecological change in the late Miocene. *Nature* 361, 344 - 345.

Conroy, J. L., Overpeck, J. T., Cole, J. E., Steinitz-Kannan, M., 2009. Variable oceanic influences on western North American drought over the last 1200 years. *Geophysical Research Letters.* 36, L17703.

Cook, E. R., Seager, R., Cane, M. A., Stahle, D. W., 2007. North American drought: reconstructions, causes, and consequences. *Earth-Science Reviews.* 81, 93-134.

Cruz, F. W., Burns, S. J., Jercinovic, M., Karmann, I., Sharp, W. D., Vuille, M., 2007. Evidence of rainfall variations in Southern Brazil from trace element ratios (Mg/Ca and Sr/Ca) in a Late Pleistocene stalagmite. *Geochimica Et Cosmochimica Acta*. 71, 2250-2263.

D'Arrigo, R., R. Villalba, and G. Wiles. 2001. Tree-ring estimates of Pacific decadal climate variability. *Climate Dynamics*, Volume 18, Numbers 3-4, pp. 219-224.

Fairchild, I. J., Borsato, A., Tooth, A. F., Frisia, S., Hawkesworth, C. J., Huang, Y. M., McDermott, F., Spiro, B., 2000. Controls on trace element (Sr-Mg) compositions of carbonate cave waters: implications for speleothem climatic records. *Chemical Geology*. 166, 255-269.

Fairchild, I. J., Smith, C. L., Baker, A., Fuller, L., Spötl, C., Mattey, D., McDermott, F., 2006. Modification and preservation of environmental signals in speleothems. *Earth-Science Reviews*. 75, 105-153.

Fairchild, I. J. and Treble, P. C., 2009. Trace elements in speleothems as recorders of environmental change. *Quaternary Science Reviews*. 28, 449-468.

Frisia, S., Borsato, A., Fairchild, I. J., Susini, J., 2005. Variations in atmospheric sulphate recorded in stalagmites by synchrotron micro-XU and XANES analyses. *Earth and Planetary Science Letters.* 235, 729-740.

Gascoyne, M., 1983. Trace element partition coefficients in the calcite-water system and their palaeoclimatic significance in cave studies. *Journal of Hydrology*. 61, 231.

Hellstrom, J.C., McCulloch, M.T., 2000. Multi-proxy constraints on the climatic significance of trace element records from a New Zealand speleothem. *Earth and Planetary Science Letters.* 179, 287 - 297.

Hendy, C. H., 1971. The isotopic geochemistry of speleothems. Part 1. The calculation of the effects of different modes of formation on the isotopic composition of speleothems and their applicability as paleoclimatic indicators. *Geochimica Et Cosmochimica Acta.* 35, 805-824.

Johnson, K. R., Hu, C. Y., Belshaw, N. S., Henderson, G. M., 2006. Seasonal trace-element and stable-isotope variations in a Chinese speleothem: The potential for high-resolution paleomonsoon reconstruction. *Earth and Planetary Science Letters*. 244, 394-407.

Lea, D.W., and Spero H.J., 1994. Assessing the reliability of paleochemical tracers – barium uptake in the shells of planktonic foraminifera, *Paleoceanography* 9 (3) 445–452.

Lorens, R. B., 1981. Sr, Cd, Mn and Co distribution coefficients in calcite as a function of calcite precipitation rate. *Geochimica Et Cosmochimica Acta.* 45, 553-561.

MacDonald, G. M., 2007. Severe and sustained drought in southern California and the West: Present conditions and insights from the past on causes and impacts. *Quaternary International*. 173, 87-100.

Marchitto, T. M., 2006. Precise multi-elemental ratios in small foraminiferal samples determined by sector field ICP-MS. *Geochemistry Geophysics Geosystems*. 7, Q05P13.

Mattey, D. P., Fairchild, I. J., Atkinson, T. C., Latin, J-P., Ainsworth, M., and Durell, R., 2010. Seasonal microclimate control of calcite fabrics, stable isotopes and trace elements in modern speleothem from St Michaels Cave, Gibraltar. *Geological Society, London, Special Publications*. v. 336, p. 323-344.

Morse, J.W., and Bender, M.L., 1990. Partition coefficients in calcite: examination of factors influencing the validity of experimental results and their application to natural systems, *Chem. Geol.* 82, 265–277.

Oster, J.L., Montañez, I.P., Guilderson, T.P., Sharp, W.D., Banner, J.L., 2010. Modeling speleothem $\delta^{13}C$ variability in a central Sierra Nevada cave using ^{14}C and $^{87}Sr/^{86}Sr$. *Geochimica et Cosmochimica Acta*. Volume 74, Issue 18, Pages 5228–5242.

Oster, J.L., Montañez, I.P., Mertz-Kraus,R., Sharp, W.D., Stock, G. M., Spero, H.J., Tinsley, J., Zachos, J.C., 2014. Millennial-scale variations in western Sierra Nevada precipitation during the last glacial cycle MIS 4/3 transition. *Quaternary Research*, Volume 82, Issue 1, July, Pages 236-248.

Richards, D.A., Dorale, J.A., 2003. Uranium-series chronology and environmental applications of speleothems, in: Bourdon, B., Henderson, G. M., Lundstrom, C. C., Turner, S. P. (Eds.), *Uranium-Series Geochemistry*.pp. 407-460.

Rosenthal, Y., Fiedl, M.P., Sherrell, R.M., 1999. Precise determination of element/calcium ratios in calcareous samples using sector field inductively coupled plasma mass spectrometry, *Anal. Chem*., 71, 3248–3253.

Thompson, R.S., Whitlock, C., Bartlein, P.J., Harrison, S.P., Spaulding, W.G., 1993. Climatic changes in the western United States since 18,000 yr B.P. In: *Wright H.E.Jr.*

Tooth, A. F. and Fairchild, I. J., 2003. Soil and karst aquifer hydrological controls on the geochemical evolution of speleothem-forming drip waters, Crag Cave, southwest Ireland. *Journal of Hydrology*. 273, 51-68.

Treble, P., Shelley, J. M. G., Chappell, J., 2003. Comparison of high resolution sub-annual records of trace elements in a modern (1911-1992) speleothem with instrumental climate data from southwest Australia. *Earth and Planetary Science Letters.* 216, 141-153.

Tremaine, D. M., and Froelich, P.N., 2013. Speleothem trace element signatures: A hydrologic geochemical study of modern cave dripwaters and farmed calcite. *Geochimica et Cosmochimica Acta*.121, 522–545.

Wigley, T.M.L., Brown, M.C., 1976. The physics of caves, in: Ford, T. D., Cullingford, C. H. D. (Eds.), The science of speleology. *Academic Press,* London, pp. 329-358.

Woodhouse, C. A., Meko, D. M., MacDonald, G. M., Stahle, D. W., Cook, E. R., 2010. A 1,200-year perspective of 21st century drought in southwestern North America. *Proceedings of the National Academy of Sciences.* 107, 21283-21288.

Wright, H.E. Jr., Kutzbach, J.E., Webb, T. Iii, Ruddiman, W.F., Street-Perrott, F.A., Bartlein, P.J. (Eds.), Global Climates since the Last Glacial Maximum. *University of Minnesota Press, Minneapolis.* 569 pp.

CHAPTER 5:

Assessing climatic influence on extreme precipitation and isotopic values in the Western US

5.1 Introduction

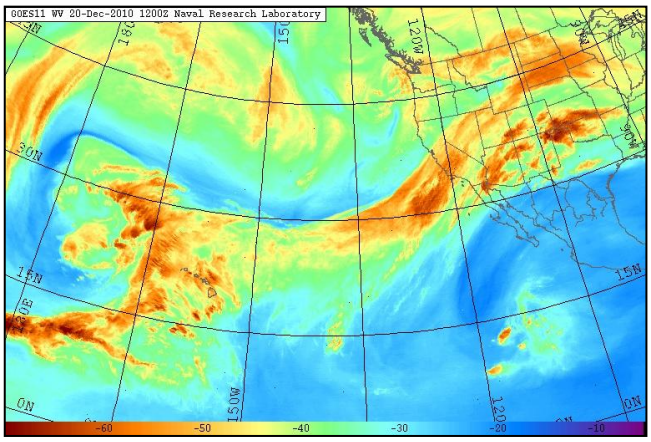

Figure 5.1. GOES 11 satellite imagery of vertically integrated water vapor showing atmospheric river conditions associated with extreme precipitation events across California from December 17-22, 2010. http://www.nrlmry.navy.mil/archdat/pacific/eastern/pacus/vapor/20101220.1200.

Extreme precipitation events can contribute extensively to replenishing reservoirs and groundwater supplies, however, they can also result in harmful consequences along the west coast of North America, including excessive flooding, landslides, loss of life, and extensive property damage (Mass et al., 2011; Warner et al., 2012; Ralph and Dettinger, 2012). One of the most prevalent extreme precipitation events that occur are known as 'Atmospheric Rivers' (ARs), whereby extensive fluxes of water vapor are transported from the subtropics, delivering substantial precipitation and contributing to flooding when they encounter mountains (Ralph and Dettinger, 2012). California's largest and most severe storms (Neiman et al., 2002) and essentially all major historical floods have been associated with landfalling ARs (Dettinger, 2011) linked to winter-spring atmospheric circulation patterns (Cayan and Riddle, 1992). Fig. 5.1 shows an example of a strong AR that occurred December 17 to 22, 2010, producing up to 670 mm (26.4 in.) of precipitation in Southern California (Ralph

and Dettinger, 2012) and exceptional snow fall in California's Sierra Nevada Mountains (Guan et al., 2010; 2013). Another AR in early January 2005 produced more than 1016 mm (40 in.) of rainfall in the mountains of southern California in only four days, causing widespread flooding and a massive mudslide that took ten lives. Extreme precipitation events are projected by almost all global climate models to become more extreme as the climate changes (Trenberth, 1999; Cayan et al., 2009; Das et al., 2011; Jain et al., 2005; Ralph and Dettinger, 2012), largely due to increased water vapor content in a warmer atmosphere (Trenberth, 1999). Multiple climate models forecast increases in years with many AR episodes and higher-than-historical water-vapor transport rates (Ralph and Dettinger, 2012), indicating that California flood risks may increase beyond those we have known historically (Ralph and Dettinger, 2012). However, great uncertainties exist about future changes in long-term average precipitation rates in California (Dettinger, 2005; Cayan et al., 2009). Despite the fact that California has begun implementation of key land-based sensors and modern satellite advances have led to enhanced awareness and improved understanding of extreme precipitation events, they are still difficult to predict accurately beyond about a ten-day lead and forecasts of landfall impact are even poorer (Wick et al., 2013). Understanding the characteristics and dynamics of extreme precipitation events and ARs is therefore critical for improved predictability of future ARs and extreme precipitation events to thereby mitigate negative consequences.

Instrumental records and climate model simulations demonstrate that Pacific sea surface temperature (SST) patterns have exerted substantial control on the hydroclimate of North America over the 20th century related to coupled climate modes such as the El Niño/Southern Oscillation (ENSO) and the Pacific Decadal Oscillation (PDO) (Cook et al., 2007; Dettinger et

al., 1998; Mantua and Hare, 2002). For example, the warm phase (positive ENSO and PDO) is typically associated with wetter conditions in the Southwestern United States (SWUS) and drier conditions in the Northwestern US (NWUS) (Cook et al., 2007; Dettinger et al., 1998; Mantua and Hare, 2002) and vice versa during the cool phase (negative ENSO and PDO). Additionally, my recent study reconstructing past atmospheric circulation patterns utilizing the oxygen ($\delta^{18}O$) isotopic variations in a stalagmite collected from Crystal Cave, California, found a strong positive correlation between the SSTs in the Kuroshio extension region of the northwest Pacific and the $\delta^{18}O$ (McCabe-Glynn et al., 2013). This was interpreted as reflecting the moisture source delivering precipitation to this region, with the lowest $\delta^{18}O$ values originating from the North Pacific storm track and the highest $\delta^{18}O$ values from the tropical Pacific (Friedman et al., 2002; Berkelhammer et al., 2012). Stable isotopes in precipitation have been found to be useful in tracking hydrological processes in modern climate (Coplen et al., 2008; Yoshimura et al., 2010) and because of the subtropical origin of ARs, these events can carry unique water isotope properties (Friedman et al., 2002; Berkelhammer et al., 2012). A paleo - $\delta^{18}O$ record of ARs could provide a temporal baseline of these events thereby enhancing predictive capabilities.

Here I analyze the isotopic composition of precipitation samples and precipitation amount data collected from 2001 to 2011, near the Crystal Cave site, at Giant Forest in Sequoia National Park, to test whether extreme events, in particular ARs, are characterized by unique stable isotope ($\delta^{2}H$, $\delta^{18}O$) values that may be recorded in paleoclimate archives such as speleothems and tree rings. This site receives the majority of precipitation during the 'wet season' (November to April) and is ideally located to investigate the physical dynamics and mechanisms contributing to these events. I also analyze climatic features utilizing mean and anomalous composite maps

and Hysplit back trajectories from all days included in the top ten weeks of precipitation (> 150 mm). Lastly, I compare several indices including the Pacific North American (PNA) pattern, the Arctic Oscillation (AO), and the Southern Oscillation Index (SOI), including the eastern Pacific (EP) and the central Pacific (CP) SSTs to determine the dominant controls of these events and how they affect precipitation patterns of the Western US during the positive, negative, and neutral phase.

5.2. Methods

5.2.1 Precipitation isotope analysis

The National Atmospheric Deposition Program (NADP) collected a total of 240 weekly precipitation samples over the ten year period, 2001 to 2011, from site CA-75, Giant Forest in Sequoia National Park, California (36.57 °N; 118.78 °W; 1921 m). Samples were collected in a wet deposition collector in which the collector opens automatically during wet weather, allowing the precipitation to fall into a collection bucket, and then closes as soon as the precipitation stops. Samples are collected continuously at approximately 9:00 a.m. every Tuesday morning. Each site is also equipped with a weighing-bucket rain gauge that provides a continuous record of rainfall amounts. Rainfall is recorded to the nearest 0.01 in. The rain gauge also monitors the wet deposition collector, recording whether the collector was properly open during wet periods and closed during dry periods. At the site, the operator replaces the collection bucket with one specially cleaned for the next sample. The operator then takes the sample to a field laboratory, where it is weighed. Next, the sample is transferred to a shipping bottle and sent to the CAL in Champaign, Illinois. All NADP National Trends Network (NADP/NTN) samples are sent for analysis to the Central Analytical Laboratory (CAL) where they are stored in 1 liter polyethylene

bottles in a cooler at ~ 4 ºC and retained for five years. For this study we utilized precipitation collected weekly, utilizing the Tuesday 'date on' as the first day of the collection week. Daily precipitation amounts and temperature values were obtained from the Climate Data Exchange Center (CDEC) Giant Forest (GNF) station (36.56 °N; 118.77 °W; 2027 m) site (http://cdec.water.ca.gov/index.html).

I conducted isotope ($\delta^{18}O$) measurements on 220 weekly precipitation samples (20 samples were missing). The water samples were analyzed by continuous flow IRMS using a Thermofinnigan TC/EA and Delta Plus XP mass spectrometer. The 0.5 µl water samples were injected into He carrier gas and carried in vapor form to the TC/EA reduction furnace where the water undergoes a pyrolysis reaction at 1400°C ($H_2O + C \Rightarrow H_2 + CO$). The reaction products are separated by a GC column and analyzed directly. Data are corrected using five in-house and certified standards (ICI D.I., SHASTA, GAL5, TAP, ARHD, AND AIUCI). The precision is ± 0.2 ‰ for $\delta^{18}O$ and ± 2‰ for $\delta^{2}H$.

5.2.2 Climate Indices Analysis

Table 5.1. Climate indices abbreviations.

Index	Name
SOI	Southern Oscillation Index
MEI	Multivariate ENSO Index
ONI	Ocean Niño Index
PDO	Pacific Decadal Oscillation
EP	Eastern Pacific
CP	Central Pacific
AO	Arctic Oscillation
PNA	Pacific North American

Precipitation in the SWUS is highly seasonal, with the bulk of precipitation delivered during the winter months. In order to compare the $\delta^{18}O$ and precipitation amounts with the ENSO, we utilized the Multivariate ENSO Index (MEI) {SEP-OCT OCT-NOV NOV-DEC DEC-JAN JAN-FEB FEB-MAR} values (http://www.esrl.noaa.gov/psd/data/correlation/mei.data). The Multivariate ENSO Index (MEI) is based on six main observed variables over the tropical Pacific:sea-level pressure, zonal and meridional components of the surface wind, sea surface temperature, surface air temperature, and total cloudiness fraction of the sky. We also analyzed the monthly Southern Oscillation Index (SOI) values and other ENSO climate indices (e.g. Nino3.4 Hadley and Kalnay, Ocean Nino Index (ONI)) from the National Oceanic and Atmospheric Administration (NOAA) Earth System Research Laboratory (ERSL) monthly climate indices site (http://www.esrl.noaa.gov/psd/data/climateindices/list/).

To further investigate the precipitation response to various climate modes, I chose to analyze climate indices from the Arctic region, the mid-latitudes, and the tropical Pacific, regions known to influence atmospheric circulation patterns delivering precipitation to the Western US utilizing the daily index for the Arctic Oscillation (AO), the Pacific North American pattern (PNA),and the Southern Oscillation Index (SOI). I chose the SOI, which measures the atmospheric component of the ENSO system, over other indices of tropical Pacific conditions because of its strong lag relationship with winter precipitation in the West (Cayan et al., 1999; Brown and Comrie, 2004). I used the daily PNA and AO index (www.cpc.ncep.noaa.gov/) and the daily SOI z-score data derived from the Science Delivery Division of the Department of Science, Information Technology, Innovation and the Arts (http://www.longpaddock.qld.gov.au/seasonalclimateoutlook/southernoscillationindex/soidatafile

s/index.php). I also used the monthly indices for the two types of ENSO, the Eastern Pacific (EP), and Central Pacific (CP). The EP and CP indices data are calculated using a regression-empirical orthogonal function (EOF) analysis (Yu et al., 2012; Zou et al., 2014). The SST data used in this calculation are from the Extended Reconstructed Sea Surface Temperature v3b data set with a resolution of 89 x 180 (2° × 2°) from the National Oceanic and Atmospheric Administration (NOAA). Niño 3.4 is the area averaged SST anomaly from 5°S-5°N and 170°W - 120°W. I performed a one-sample t-test between proportions to determine whether there was a significant relationship between the extreme precipitation weeks and specific climate mode phases.

To investigate the precipitation response to various combinations of climate indices phases in the Western US, we utilized the daily precipitation data from NCEP North American Regional Reanalysis (NARR) for daily precipitation amounts >150 mm from: http://www.esrl.noaa.gov/psd/data/gridded/data.narr.monolevel.html with a resolution of 349 x 277 in North America, approximately 0.3 degrees (32 km) at the lowest latitude. The precipitation data are in a polygon. Corners of the grid are 12.2°N; 133.5°W, 54.5°N; 152.9°W, 57.3°N; 49.4°W, 14.3°N; 65.1°W (essentially, North America) with combined daily AO, PNA, and SOI, and monthly average EP and CP indices data. We also analyzed the monthly PDO and North Pacific indices (NPI) data average for individual days (http://www.esrl.noaa.gov/psd/data/climateindices/list/). The North Pacific Index (NP index or NPI) is the area-weighted sea level pressure over the region 30°N-65°N, 160°E-140°W defined to measure interannual to decadal variations in the atmospheric circulation.

5.2.3 NCEP/NCAR Reanalysis Composite Analysis

We compare composite mean and anomaly maps of Sea Level Pressure (SLP) (mb), Geopotential Height (500 mb), 1000 mb Air Temperature (K), Columnar Precipitable Water (kg/m^2), and 700 mb Vector Winds (Anomaly: 1981 - 2010 Climatology) utilizing data from the National Centers for Environmental Prediction (NCEP)/National Center for Atmospheric Research (NCAR) reanalysis (Kalnay et al., 1996) (http://www.esrl.noaa.gov/psd/data/composites/day/) for all days in the top ten weeks that delivered the greatest amount of precipitation (> 150 mm) (Table 5.3).

5.2.4 Back Trajectory Analysis

In order to identify the causes of differing precipitation $\delta^{18}O$ values for each storm week, I investigate storm track trajectories utilizing NOAA Hybrid Single Particle Lagrangian Integrated Trajectory Model (HYSPLIT) and reanalysis data (global, 1948-present) back-calculated particle trajectories (http://ready.arl.noaa.gov/HYSPLIT_traj.php) for all days in the top ten precipitation weeks (>150 mm) (Table 5.3) to show the storm trajectories throughout the week (Draxler and Rolph, 2003). These models are run at 36.57 °N; 118.78 °W; 1500 m above ground level, the approximate height of the 850 hPa level from where rain is expected to originate, and most (~75%) of the water vapor transport within ARs occurs within the lowest 2.5 km of the atmosphere (Ralph, et al. 2005), at 24-h time steps for 72-h for each day of the week prior to landfall at CA-75 Giant Forest. Along each of the trajectories, the NOAA Hysplit Model also includes a color coded amount of rainfall for each daily trajectory delivered during the collection week.

5.2.5 200 hPa Wind Speed Analysis

I also analyze composites of 200 hPa winds of the peak date for each storm week using the Modern-Era Retrospective Analysis for Research and Applications (MERRA) reanalysis dataset, available starting from 1979 from NASA (Rienecker et al., 2011). Horizontal winds, temperature and specific humidity were retrieved from pressure levels at reduced spatial resolution ($1.25^{\circ} \times 1.25^{\circ}$) at 3-hour intervals. Moisture transport in the lower troposphere is calculated as the magnitude of the vertically integrated vapor transport (IVT):

IVT(\lambda,\phi,t) = 1/g*integral(q*|*v*|*dp)_1000hPa^700hPa

where |*v*| is the horizontal wind speed on isobaric surfaces measured in units of m/s, q is specific humidity measured in units of kg/kg, and g is the gravitational acceleration (9.81 m/s).

5.3. Results

5.3.1 Precipitation Isotopes

Results of 240 weeks of precipitation samples collected at CA-75 Giant Forest Sequoia National Park reveals an average weekly amount of precipitation of 44.8 ± 54 mm. Isotopic measurements of 220 weekly precipitation events indicate $\delta^{2}H$ values ranged from -175.61 to 3.02 ‰ and $\delta^{18}O$ values ranged from -24.31 to 0.88 ‰ (Table A4). The average 'water year' (WY), defined as the 12-month period starting October 1, for any given year, through September 30 of the following year, precipitation amount is 977 mm with an average weighted $\delta^{18}O$ of -12.11‰ (Table 5.2). There is a low inverse correlation between the $\delta^{18}O$ values and precipitation amount ($r = -0.22$, $p = 0.0072$), a moderate correlation between the $\delta^{18}O$ values and temperature ($r = 0.48$, $p = < 0.0001$), and an inverse correlation between precipitation amounts and temperature ($r = -0.35$, p

= < 0.0001) from 2001 to 2011. The three highest total annual precipitation amounts occurred in the WY 2011 (1558 mm; -14.59‰), 2010 (1437 mm; -11.73‰), and 2006 (1232 mm; -12.62‰) and the three lowest in 2009 (825 mm; -12.63‰), 2007 (548 mm; -10.87‰), and 2004 (302 mm; -13.11‰) (excluding 2001) (Table 5.2).

Table 5.2 Water year (Oct - Sept) precipitation amount and weighted isotopic value.

Oct-Sept	Ppt (mm)	δ^2H ‰	δ^{18}O ‰
2001-2002	846.3	-91.59	-11.92
2002-2003	1104.1	-70.26	-10.58
2003-2004	302.5	-72.26	-13.11
2004-2005	1095.1	-75.80	-11.30
2005-2006	1231.5	-86.24	-12.62
2006-2007	548.0	-76.39	-10.87
2007-2008	824.9	-82.55	-11.74
2008-2009	824.6	-84.50	-12.63
2009-2010	1436.9	-78.12	-11.73
2010-2011	1557.9	-98.83	-14.59
Average	977.2	-81.65	-12.11
StDev	386.8	8.92	1.18

Of the 220 weekly precipitation samples, I focused on the top ten precipitation weeks (> 150 mm) (Table 5.3). Results reveal a large range in both isotopic values and daily temperatures associated with each event. The δ^2H ranged from -150.03 to -49.52 ‰ with an average of -84.05 ‰ and the δ^{18}O ranged from -19.27 to -7.20 ‰ with an average of -12.39 ‰. The weekly temperature averages ranged 12.76 °C, from 9.29 to -3.47 °C, with an average of 2 °C. Nine of the top ten precipitation amount weeks contain noted AR events according to Neiman et al. (2008) criteria using Special Sensor Microwave Imager (SSM/I) observations showing Integrated Water Vapor (IWV) with core values $\geq$ ~2 cm that impacted the California coast (32.5 °N–41.0

°N), with the exception being week 8, 12/08/2009 and 16 of the top 22 weeks contained ARs (see Table 5.3).

Table 5.3. Giant Forest CA-75 Top 10% (22) precipitation amount weeks from 2001 to 2011.

Atmospheric River Dates	Week	Date on	Date off	Prec mm	δ^2H	$\delta^{18}O$	Temp °C
12/17/10, 12/18/10, 12/19/10, 12/20/10, 12/21/10	1	12/14/2010	12/21/2010	498.9	-109.30	-16.89	0.6
11/7/02, 11/8/02, 11/9/02	2	11/5/2002	11/12/2002	270.8	-59.56	-9.06	7.7
1/9/05, 1/10/05	3	1/4/2005	1/11/2005	217.7	-78.43	-11.57	-2.1
12/28/05, 12/30/05, 12/31/05	4	12/27/2005	1/3/2006	199.4	-98.21	-14.06	4.6
10/13/09, 10/17/09	5	10/13/2009	10/20/2009	196.9	-49.52	-7.20	9.3
1/5/2008	6	12/31/2007	1/8/2007	188.0	-74.63	-11.24	1.8
1/19/2010	7	1/19/2010	1/26/2010	162.8	-99.89	-14.70	-2.6
X	8	12/8/2009	12/15/2009	156.7	-62.94	-10.61	-1.7
12/28/10, 12/29/10	9	12/28/2010	1/4/2011	154.7	-150.03	-19.27	-3.5
3/22/2005	10	3/15/2005	3/22/2005	151.6	-60.34	-9.26	1.3
X	11	2/19/2008	2/26/2008	147.8	-61.71	-9.09	0.6
3/28/06, 4/3/06, 4/4/06	12	3/28/2006	4/4/2006	144.3	-105.23	-14.54	0.5
X	13	2/22/2011	3/1/2011	141.0	-90.63	-13.56	-3.8
3/29/2010	14	3/23/2010	4/6/2010	131.1	-64.96	-9.86	0.9
1/22/2009	15	1/20/2009	1/27/2009	127.8	-83.86	-11.87	2.2
12/27/2002	16	12/23/2002	12/31/2002	127.3	-82.45	-12.44	-2.4
11/29/01, 12/2/01	17	11/27/2001	12/4/2001	121.7	-72.52	-11.10	-2.2
X	18	2/6/2001	2/13/2001	115.3	-72.78	-11.56	-4.0
X	19	2/15/2011	2/22/2011	115.3	-66.82	-11.33	-3.3
12/29/01, 1/2/02	20	12/26/2001	1/2/2001	114.3	-113.55	-15.18	4.4
10/5/11, 10/10/11, 10/11/11	21	10/4/2011	10/11/2011	113.0	-66.87	-9.78	4.7
X	22	2/24/2004	3/2/2004	109.2	-80.01	-11.84	-2.4
			Average	**168.0**	**-82.01**	**-12.09**	**0.0**
			Max	**499.0**	**-49.52**	**-7.20**	**9.0**
			Min	**109.0**	**-150.03**	**-19.27**	**-4.0**
			Range	**390.0**	**100.50**	**12.06**	**13.0**
			Total	**3705.0**			

*AR events according to Neiman et al., (2008) criteria (ARs; long, narrow plumes of IWV with core values >~2 cm) during water years 1998-2011 that impacted the California coast (32.5N – 41.0N).The bold dates denote IWV >3cm.

Table 5.4 shows the NADP CA-75 Giant Forest top ten weekly precipitation amounts and associated isotopic values (gray shading) with the average daily GNF CDEC temperature and the GNF CDEC daily precipitation amounts and temperatures listed for each day. While the weekly NADP and daily CDEC precipitation data amounts are similar, they do not add up to the same

amount, which may be due to collection measuring techniques and/or the slightly different station site location and elevation. No GNF precipitation data is available for week 6, 10/14/2009 to 10/20/2009, therefore I utilized precipitation dataset from ASM, Ash Mountain, a nearby station (36.48 °N; 118.83 °W; 521m), to determine the day of greatest precipitation amount (Table 5.4). The CDEC data shows the lowest daily temperature of -9.4 °C occurs during the week of 12/28/2010 and the highest daily temperature of 16.7 °C occurs during the week of 10/13/2009.

Table 5.4. NADP CA-75 Giant Forest top ten precipitation weekly amounts and isotopic values with daily CDEC precipitation and temperature data.

Week	Date on	Date off	Prec. Amount	δ^2H	$\delta^{18}O$	Temp (ave)
1	**11/5/2002**	**11/12/2002**	**270.76**	**-59.56**	**-9.06**	**6.94**
	Day		***Prec.(mm)**			***Temp (°C)**
	11/5/2002		0			8.89
	11/6/2002		0			9.44
	11/7/2002		50.8			--
	11/8/2002		251.46			--
	11/9/2002		40.64			3.33
	11/10/2002		0			--
	11/11/2002		0			6.11
2	**1/4/2005**	**1/11/2005**	**217.68**	**-78.43**	**-11.57**	**-2.11**
	1/4/2005		12.7			-4.44
	1/5/2005		0			-4.44
	1/6/2005		0			-5
	1/7/2005		38.1			--
	1/8/2005		96.52			--
	1/9/2005		66.04			2.22
	1/10/2005		10.16			1.11
3	**3/15/2005**	**3/22/2005**	**151.64**	**-60.34**	**-9.26**	**1.35**
	3/15/2005		0			2.22
	3/16/2005		0			3.33
	3/17/2005		0			2.78

	3/18/2005		0			1.11
	3/19/2005		43.18			0.56
	3/20/2005		40.64			-1.11
	3/21/2005		20.32			0.56
4	**12/27/2005**	**1/3/2006**	**199.39**	**-98.21**	**-14.06**	**6.67**
	12/27/2005		20.32			7.22
	12/28/2005		2.54			--
	12/29/2005		5.08			--
	12/30/2005		0			6.11
	12/31/2005		0			--
	1/1/2006		129.54			--
	1/2/2006		50.8			--
5	**12/31/2007**	**1/8/2007**	**187.96**	**-74.63**	**-11.24**	**1.3**
	12/31/2007		2.54			6.67
	1/1/2008		0			9.44
	1/2/2008		0			7.78
	1/3/2008		0			--
	1/4/2008		170.18			1.67
	1/5/2008		40.64			-2.22
	1/6/2008		38.1			-4.44
	1/7/2008		5.08			-4.44
6	**10/13/2009**	**10/20/2009**	**196.85**	**-49.52**	**-7.2**	**10.19**
	10/13/2009	--	0 (****ASM prec.)**			3.89
	10/14/2009	--	95			8.89
	10/15/2009	--	0.25			11.11
	10/16/2009	--	0			--
	10/17/2009	--	0			16.67
	10/18/2009	--	0			13.89
	10/19/2009	--	0			6.67
7	**12/8/2009**	**12/15/2009**	**156.72**	**-62.94**	**-10.61**	**-2.3**
	12/8/2009		2.54			-8.33
	12/9/2009		2.54			-3.33
	12/10/2009		0			0
	12/11/2009		33.02			0
	12/12/2009		88.9			0
	12/13/2009		38.1			-2.22
	12/14/2009		2.54			-2.22

8	**1/19/2010**	**1/26/2010**	**162.81**	**-99.89**	**-14.7**	**-3.24**
	1/19/2010		0			-3.33
	1/20/2010		0			-3.33
	1/21/2010		0			--
	1/22/2010		68.58			-5
	1/23/2010		10.16			-5.56
	1/24/2010		5.08			-3.33
	1/25/2010		0			1.11
9	**12/14/2010**	**12/21/2010**	**498.86**	**-109.3**	**-16.89**	**0.87**
	12/14/2010		0			6.67
	12/15/2010		2.54			0
	12/16/2010		0			-1.67
	12/17/2010		68.58			0.56
	12/18/2010		177.8			1.11
	12/19/2010		144.78			1.11
	12/20/2010		33.02			-1.67
10	**12/28/2010**	**1/4/2011**	**154.69**	**-150.03**	**-19.27**	**-3.47**
	12/28/2010		20.32			2.78
	12/29/2010		68.58			-2.78
	12/30/2010		5.08			-9.44
	12/31/2010		7.62			-8.33
	1/1/2011		2.54			-2.78
	1/2/2011		0			-1.67
	1/3/2011		7.62			-3.89
	1/4/2011		7.62			-1.67

*Daily data from http://cdec.water.ca.gov/cdec

****Week 6*** -10/14/2009 is noted by nearby site, ASM, to be the day with the most precipitation.

5.3.2 Climate indices analysis results

In order to gain a better understanding of how various climate indice phases influence precipitation delivered to Giant Forest CA-75, I analyzed the top 10, 22 and 40 weeks with climate indices known to influence precipitation patterns in the Western US. Investigation

shows variations between ENSO indices (Table 5.5) and also between daily (Table 5.6) and monthly (Table 5.7) indices results for the dates of the extreme precipitation weeks.

Table 5.5 Monthly climate indices values for the top ten % (22 weeks) precipitation amount days at Giant Forest CA-75 from 2001 to 2011.

Week	Date on	Date off	Prec. mm	δ^2H	$\delta^{18}O$	Indice month	ONI	MEI	Nino3.4 Kaplan	Nino3.4 Hadley	SOI	EP	CP	PDO
1	12/14/2010	12/21/2010	498.9	-109.30	-16.89	12/1/2010	-1.40	-1.58	-1.62	-1.61	4.80	-0.91	-2.41	-1.21
2	11/5/2002	11/12/2002	270.8	-59.56	-9.06	11/1/2002	1.39	1.06	1.62	1.47	-0.70	1.17	1.24	1.51
3	1/4/2005	1/11/2005	217.7	-76.82	-11.58	1/1/2005	0.64	0.30	0.53	0.60	0.60	-0.44	1.19	0.44
4	12/27/2005	1/3/2006	199.4	-98.21	-14.06	12/1/2005	-0.88	-0.59	-0.68	-0.74	0.00	-1.23	-1.04	0.20
5	10/13/2009	10/20/2009	196.9	-49.52	-7.20	10/1/2009	0.99	1.02	0.94	1.00	-2.00	0.40	1.61	0.27
6	12/31/2007	1/8/2007	188.0	-74.63	-11.24	12/1/2007	-1.30	-1.17	-1.60	-1.60	2.70	-1.41	-1.57	-0.58
7	1/19/2010	1/26/2010	162.8	-99.89	-14.70	1/1/2010	1.57	1.15	1.50	1.47	-1.80	-0.09	2.06	0.83
8	12/8/2009	12/15/2009	156.7	-62.94	-10.61	12/1/2009	1.78	1.01	1.72	1.83	-1.20	0.43	2.35	0.08
9	12/28/2010	1/4/2011	154.7	-150.03	-19.27	12/1/2010	-1.40	-1.58	-1.62	-1.61	4.80	-0.91	-2.41	-1.21
10	3/15/2005	3/22/2005	151.6	-59.59	-9.30	3/1/2005	0.31	1.02	0.33	0.33	0.50	-0.87	0.82	1.36
11	2/19/2008	2/26/2008	147.8	-61.71	-9.09	2/1/2008	-1.64	-1.40	-1.89	-1.68	4.40	0.25	-2.74	-0.77
12	3/28/2006	4/4/2006	144.3	-105.23	-14.54	3/1/2006	-0.52	-0.59	-0.65	-0.68	2.90	-0.08	-0.79	0.05
13	2/15/2011	2/22/2011	141.0	-66.82	-11.33	2/1/2011	-1.15	-1.56	-1.27	-1.25	4.50	-0.38	-2.15	-0.83
14	3/23/2010	4/6/2010	131.1	-64.96	-9.86	3/1/2010	0.99	1.39	1.08	1.12	-1.10	0.01	1.19	0.44
15	1/20/2009	1/27/2009	127.8	-83.86	-11.87	1/1/2009	-0.94	-0.75	-1.03	-0.95	1.80	0.30	-1.31	-1.40
16	12/23/2002	12/31/2002	127.3	-82.45	-12.44	12/1/2002	1.39	1.11	1.52	1.43	-1.80	0.94	1.47	2.10
17	11/27/2001	12/4/2001	121.7	-72.52	-11.10	11/1/2001	-0.26	-0.18	-0.20	-0.23	1.10	-1.23	0.19	-1.26
18	2/6/2001	2/13/2001	115.3	-72.78	-11.56	2/1/2001	-0.58	-0.72	-0.61	-0.61	2.80	0.72	-1.04	0.29
19	2/22/2011	3/1/2011	115.3	-90.63	-13.56	2/1/2011	-1.15	-1.56	-1.27	-1.25	4.50	-0.38	-2.15	-0.83
20	12/26/2001	1/2/2002	114.3	-113.55	-15.18	12/1/2001	-0.36	0.00	-0.40	-0.45	-1.40	-1.18	-0.07	-0.93
21	10/4/2011	10/11/2011	113.0	-66.87	-9.78	10/1/2011	-0.81	-0.97	-0.97	-0.88	1.20	-0.91	-1.38	-1.34
22	2/24/2004	3/2/2004	109.2	-80.01	-11.84	2/1/2004	0.23	0.33	0.14	0.18	2.00	0.20	0.36	0.48

*Color coded: pink for positive values > 0.5, blue for negative values < 0.5 and white for neutral < 0.5 and > - 0.5.

Results of the comparison of the top ten extreme precipitation weeks with associated monthly climate indices indicate extreme weeks of precipitation events occurred similarly during both phases of the El Niño Southern Oscillation (ENSO) from 2001 to 2011, as seen in the Ocean Niño Index (ONI), Multivariate ENSO Index (MEI), and NIÑO 3.4 (Table 5.5). While the aforementioned indices indicate the top ten extreme precipitation weeks occurred slightly more during El Nino conditions, the Southern Oscillation Index (SOI) shows extreme weeks occurred slightly more during La Nina conditions, highlighting the importance of considering the index utilized (Table 5.5). *Note the positive pink values for the SOI signify La Niña conditions. Further investigation of the location of the tropical Pacific SST anomalies shows that extreme

precipitation events occur similarly during the negative and neutral Eastern Pacific (EP) phase, however, are least likely to occur during the positive EP type ENSO phase than during the negative or neutral EP phases ($t = 4.216$, $p = 0.0023$) and while they occur similarly during the positive and negative Central Pacific (CP) phase, none of top ten occurred during the neutral CP phase (Table 5.5).

However, examination of the top 10% (22) extreme weeks of precipitation shows a greater tendency to occur during the negative ENSO phase, (La Niña) as seen in the ONI, MEI, and the NIÑO 3.4 (Kaplan and Hadley), and SOI (SOI: $t = 1.368$, $p = 0.1858$) (Table 5.5) with more than 50% of top 40 weeks occurring during the positive SOI phase (La Niña) (SOI: $t = 0.636$, $p = 0.5287$) (Table 5.8), but these results are not statistically significant. An interesting feature is that the extreme precipitation weeks at this site very rarely occurred during the ENSO neutral phase (SOI Top 10: $t = 4.216$, $p = 0.0023$; top 22: $t = 9.684$, $p = 0.0000$; top 40: $t = 7.171$, $p = 0.0000$) (Table 5.5 and 5.8). Focus on the EP indicates that the extreme precipitation weeks rarely occur during the positive phase (EP top 22: $t = 4.981$, $p = 0.0001$; top 40: $t = 7.171$, $p = 0.0000$) and focus on the CP indicate extreme precipitation weeks rarely occur during the neutral phase (CP top 22: $t = 4.981$, $p = 0.0001$; top 40: $t = 7.171$, $p = 0.0000$) (Table 5.5).

While extreme precipitation events occurred similarly during all phases of the Pacific Decadal Oscillation (PDO), for the top 10 weeks they occurred least frequently during the positive PDO phase over the top 22 weeks ($t = 3.907$, $p = 0.0008$ (Table 5.5).

Table 5.6. Daily climate indices, precipitation amount, and isotopic values for the top ten precipitation amount weeks (> 150 mm) at CA-75.

Week	Date on	Date off	$\delta^{18}O$	AO	PNA	SOI
1	11/5/2002	11/12/2002	-11.92	-1.56	0.37	0.35
2	1/4/2005	1/11/2005	-10.58	3.48	-1.02	0.22
3	3/15/2005	3/22/2005	-13.11	-1.81	0.19	0.83
4	12/27/2005	1/3/2006	-11.30	-1.89	0.64	0.10
5	12/31/2007	1/8/2008	-12.62	-1.15	-0.24	1.55
6	10/13/2009	10/20/2009	-10.87	-0.70	0.60	-1.12
7	12/8/2009	12/15/2009	-11.74	-2.71	-0.43	-0.31
8	1/19/2010	1/26/2010	-12.63	-1.84	0.08	-0.75
9	12/14/2010	12/21/2010	-11.73	-3.47	-1.36	0.91
10	12/28/2010	1/4/2011	-14.59	-3.14	-0.11	1.13

*Pink for positive values > 0.5, blue for negative < 0.5 and white for neutral < 0.5 and > - 0.5).

Table 5.7. Monthly climate indices, precipitation amount, and isotopic values for the top ten precipitation amount (> 150 mm) at CA-75.

Week	Date on	Date off	$\delta^{18}O$	AO	PNA	SOI
1	11/5/2002	11/12/2002	-11.92	-1.43	1.46	-0.70
2	1/4/2005	1/11/2005	-10.58	0.36	-0.62	0.60
3	3/15/2005	3/22/2005	-13.11	-1.35	0.56	0.50
4	12/27/2005	1/3/2006	-11.30	-2.10	1.07	0.00
5	12/31/2007	1/8/2008	-12.62	0.82	-0.16	2.70
6	10/13/2009	10/20/2009	-10.87	-1.54	0.64	-2.00
7	12/8/2009	12/15/2009	-11.74	-3.41	0.04	-1.20
8	1/19/2010	1/26/2010	-12.63	-2.59	0.96	-1.80
9	12/14/2010	12/21/2010	-11.73	-2.63	-2.08	4.80
10	12/28/2010	1/4/2011	-14.59	-2.63	-2.08	4.80

*Pink for positive values > 0.5, blue for negative < 0.5 and white for neutral < 0.5 and > - 0.5).

A comparison between the occurrence of the top ten extreme precipitation weeks and climate indices shows the daily Arctic Oscillation (AO) index indicate that 9 out of 10 extreme precipitation weeks occurred during the negative phase of AO ($t = 4.216$, $p = 0.0023$) (Table 5.6) and 8 out of 10 using the monthly AO index ($t = 2.372$, $p = 0.0418$) (Table 5.7). This pattern is associated with higher pressure in the Arctic and lower pressure in the surrounding lower

latitudes which leads to weaker westerlies in the upper atmosphere. The PNA and SOI daily and monthly indices also differ slightly with the daily PNA showing extreme precipitation events occurred the same for the positive and negative phase and more frequently during the neutral phase and the monthly showing they occurred the least during the neutral phase and most during the positive phase (Table 5.6). The daily SOI shows extreme events occurred the least during the negative phase ($t = 2.372$, $p = 0.0418$) (Table 5.6) vs the monthly indices with the least occurring during the neutral phase ($t = 2.372$, $p = 0.0418$) (Table 5.7).

Table 5.8. Monthly climate indices phases and associated average $\delta^{18}O$ value for the top 10, 22, and 40 Giant Forest CA-75 NADP precipitation event weeks.

TOP 10 Weeks			TOP 22 Weeks			TOP 40 Weeks		
Index	$\delta^{18}O$	# events	Index	$\delta^{18}O$	# events	Index	$\delta^{18}O$	# events
AO+	-11.24	1	AO+	-11.14	7	AO+	-10.48	8
AO-	-12.64	8	AO-	-12.82	13	AO-	-12.88	25
AO N	-11.58	1	AO N	-10.72	2	AO N	-11.41	7
PNA+	-10.82	5	PNA+	-10.93	10	PNA+	-11.41	19
PNA -	-15.91	3	PNA -	-14.1	7	PNA -	-13.49	11
PNA N	-11.24	2	PNA N	-11.6	5	PNA N	-11.9	10
SOI+	-13.66	5	SOI+	-12.35	14	SOI+	-12.24	22
SOI-	-10.39	4	SOI-	-11.29	7	SOI-	-12.12	13
SOI N	-14.06	1	SOI N	-14.06	1	SOI N	-11.78	5
EP+	-9.06	1	EP+	-11.02	3	EP+	-10.6	5
EP-	-14.15	5	EP-	-13.35	8	EP-	-12.52	14
EP N	-11.02	4	EP N	-11.47	11	EP N	-12.26	21
CP+	-10.41	6	CP+	-10.59	8	CP+	-11.28	17
CP-	-15.36	4	CP-	-13.02	11	CP-	-13.12	18
CP N	NA	0	CP N	-12.71	3	CP N	-11.56	5

*Color coded pink for positive values, blue for negative values, and white for neutral.

A comparison of monthly climate indices phases and associated average $\delta^{18}O$ value for the top 10, 22, and 40 Giant Forest CA-75 NADP greatest precipitation event weeks shows these events

tend to occur overall more often during the negative AO consisting of more negative average $\delta^{18}O$ values, the positive PNA consisting of more positive average $\delta^{18}O$ values, and the positive SOI (La Nina conditions) consisting of more negative average $\delta^{18}O$ values (Table 5.8). They also tend to occur most often during the EP neutral phase consisting of the most negative average $\delta^{18}O$ values during the EP positive phase and the CP negative phase with extreme events occurring very similarly between both the positive and negative phase but rarely during the CP neutral phase (Table 5.8).

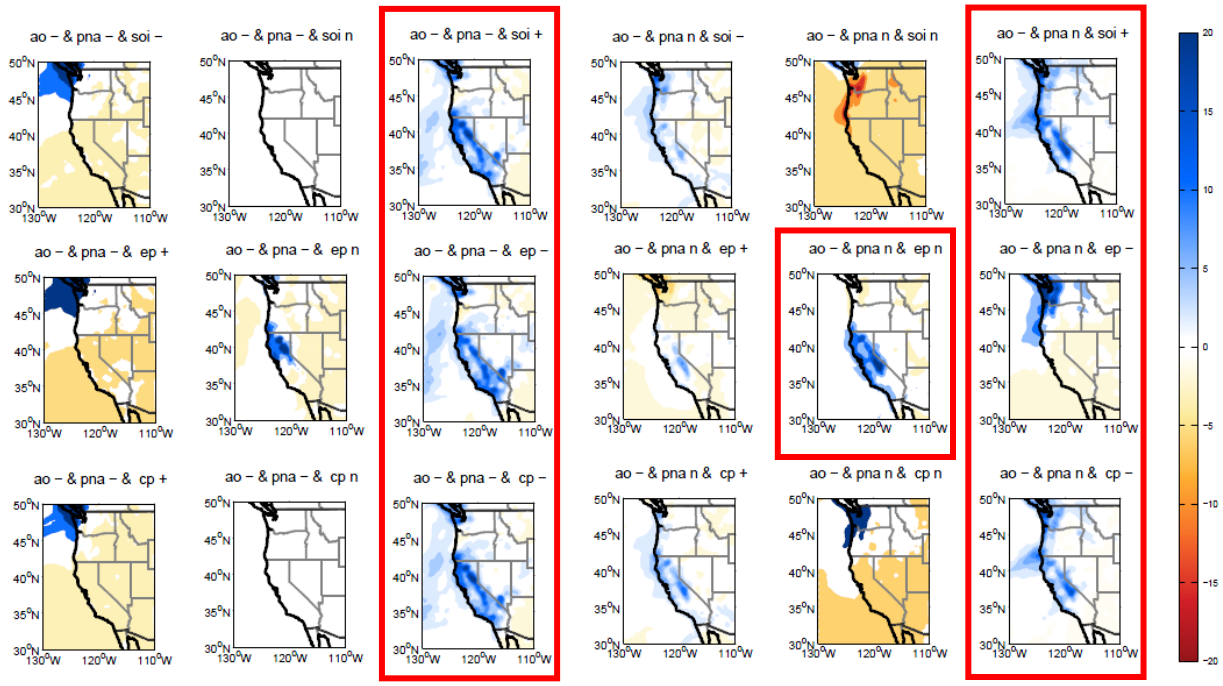

Figure 5.2. North American Regional Reanalysis daily anomalous precipitation events (> 100 mm) in the western US and accompanying combinations of various indices phases of daily AO, PNA, SOI, EP and CP values from 2001 to 2011. Red outlines show the phase combinations producing the most anomalous precipitation.

5.3.3 Climate Indices influence on Daily Precipitation Amount (> 100 mm/day) in the Western US

In order to learn how various combinations of climate indice phases influence anomalous

precipitation (> 100 mm/day) in the Western US, I conducted analysis of several climate indices combinations known to influence precipitation patterns such as the AO, PNA, SOI, (Fig. A5a and b), the AO, PNA, EP (Fig. A5c), the AO, PNA, CP (Fig. A5d), the AO, PNA, PDO (Fig. A5e), and the AO, PNA, NPI (Fig. A5f). The dark blue shading represents areas that received anomalous precipitation amounts, greater than 100 mm/day, delivered during various phase combinations (Fig. 5.2). Certain combinations are more conducive to contributing to extreme precipitation events (Fig. A5a-f). (See fig. 5.2 red highlights, discussion and conclusion section.

5.3.4 NCEP/NCAR Reanalysis Composite Results

NCEP/NCAR composite maps were constructed with all days in the top ten extreme precipitation weeks (Table 5.3). The Sea Level Pressure (SLP) composite mean map reveals two relatively low pressure centers, with one in the Northwest Pacific (~ 50 °N; 170 °E) and the other in the Gulf of Alaska (~ 50 °N; 140 °W) (Fig. 5.3a). The distribution of SLP anomalies features a deep low anomaly (~ -12 mb) centered more south-eastward over the Northeastern Pacific/Northwestern America (~ 45 °N; 130 °W) (Fig. 5.3b). The 500 mb geopotential height composite mean map indicates the lowest heights are over the Siberia region and also seen in a large dip in the Gulf of Alaska (~ 5200 m) (Fig. 5.3c). The anomalous geopotential height features a deep low over the northeast Pacific and Northwest America and a high over the Aleutian Low region (~ -120 m; Fig. 5.3d). The mean 1000 mb Air Temperature (K) composite map indicates the dominant features of extreme precipitation weeks include the lowest temperatures over central Siberia (~ 250 K) and warmer temperatures penetrating the Gulf of Alaska (~ 275to 280 K) (Fig. 5.3e).

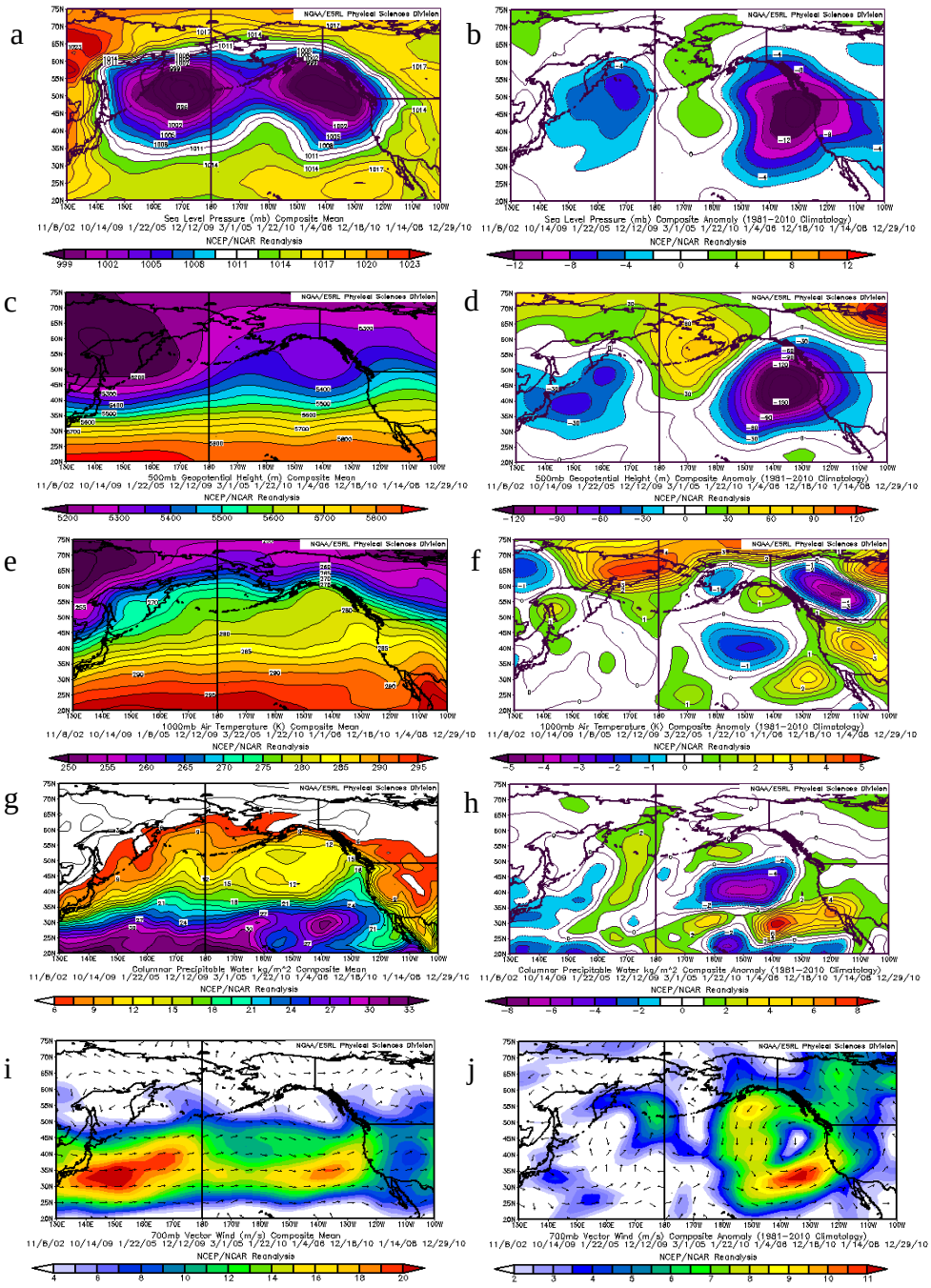

Figure 5.3. Composite analysis derived from the NCEP-NCAR daily reanalysis dataset for the top ten greatest weekly precipitation amounts each totaling over 150 mm (Table 5.1) mean and anomaly, respectively, a) and b) Sea Level Pressure (mb); c) and d) Geopotential Height (500 mb); e) and f) 1000 mb Air Temperature (K); g) and h) Columnar Precipitable Water (kg/m^2); i) and j) and the vectors in show the direction of 700 mb winds (m/s) (anomaly: 1981-2010 Climatology).

Anomalously cool temperatures are seen over central Siberia, western Canada (Brittish Columbia/Yukon Territory), and the central northeastern Pacific (~ -2 to -5 K) while anomalously warm temperatures over eastern Siberia (~ 5 K) and western North America and offshore of southern North America (~ 3 to 4 K) (Fig. 5.3f). The Columar Precipitable Water (kg/m^2) composite mean shows high values in the tropics with ~ 25 to 30 kg/m^2 extending northwest toward California and lower values at higher latudtudes above ~ 40°N (Fig. 5.3g). The Columnar Precipitable Water (kg/m^2) composite anomaly shows ~ 4 to 6 kg/m^2 penetrating into California with ~ 8 kg/m^2 just off the coast and lower values of ~ -5 to -8 kg/m^2 in the North East Pacific just outside Northern California (Fig. 5.3h). The 700 mb Vector Wind (m/s) composite mean shows increased wind speeds in the western Pacific mid-latitudes near Japan and on the eastern Pacific, just outside the US west coast (~ 20 m/s) (Fig. 5.3i). The distribution of 700 mb Vector Wind (m/s) anomalies features a circular motion of winds from the Gulf of Alaska traveling south at ~ 9 m/s where they turn and head eastward at ~ 25 to 35 °N; 145 to 150 °W, slightly increasing in speed, to ~ 11 m/s before proceeding northeast into the southwestern US (Fig. 5.3j).

5.3.5 Back Trajectory Analysis Results

Hysplit trajectory analysis shows the top ten extreme precipitation week events received moisture from a variety of trajectories from both higher and lower latitudes within each week, all of which contributed to the weekly precipitation sample collected and isotopic composition (Fig. 5.4). The week of 12/28/2010 indicates trajectories were delivered from higher latitudes (above 60°N), consisted of the coldest weekly average temperatures (-3.47 °C) of the top ten extreme

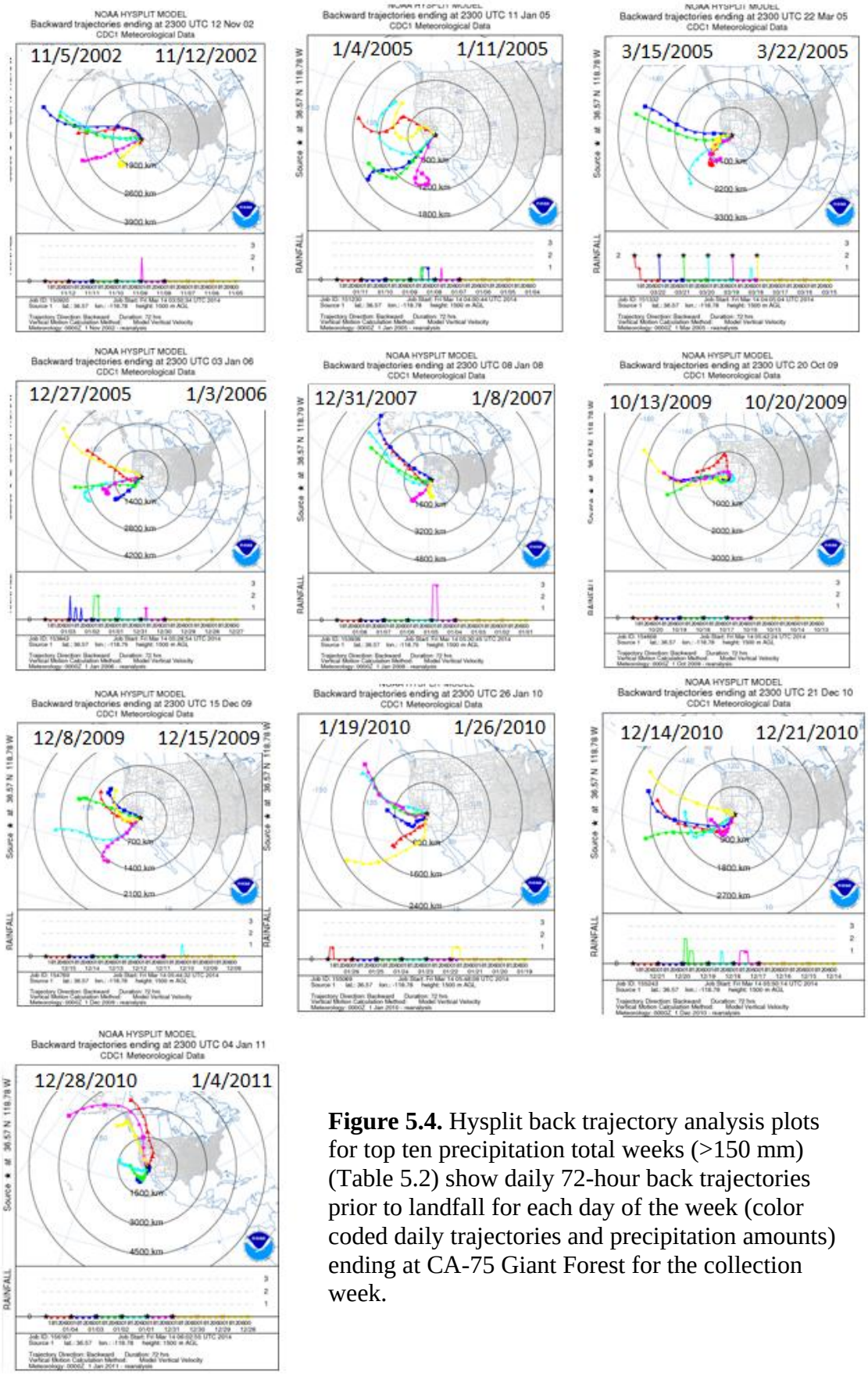

Figure 5.4. Hysplit back trajectory analysis plots for top ten precipitation total weeks (>150 mm) (Table 5.2) show daily 72-hour back trajectories prior to landfall for each day of the week (color coded daily trajectories and precipitation amounts) ending at CA-75 Giant Forest for the collection week.

precipitation event weeks, and had the most negative isotopic values (δ^2H = -150.03 ‰, $\delta^{18}O$ = -19.27 ‰) (Fig. 5.4) (Daily Indices: AO = -3.14, PNA = -0.11, SOI = 1.13; Monthly: AO = -2.63, PNA = -2.08, SOI = 4.80). The week of 12/14/2010, the greatest precipitation week from 2001 to 2011, had trajectories delivering precipitation from lower latitudes, however, this week consisted of the second most negative isotopic values (δ^2H = -109.03 ‰, $\delta^{18}O$ = -16.89 ‰), possibly due to a combination of low weekly average temperatures (0.63 °C) and/or the long duration of this known AR event (Fig. 5.4) (Daily Indices: AO = -3.47, PNA = -1.36, SOI = 0.91; Monthly: AO = -2.63, PNA = -2.08, SOI = 4.80). The warmest temperature for all ten weeks, 10/13/2009 of 9.29 °C, is concurrent with the most positive $\delta^{18}O$ value (-7.20 ‰) and second warmest weekly temperatures, 11/5/2005 of 7.67 °C, with the second most positive $\delta^{18}O$ value of -9.06 ‰ (Fig. 5.4; Table 5.4).

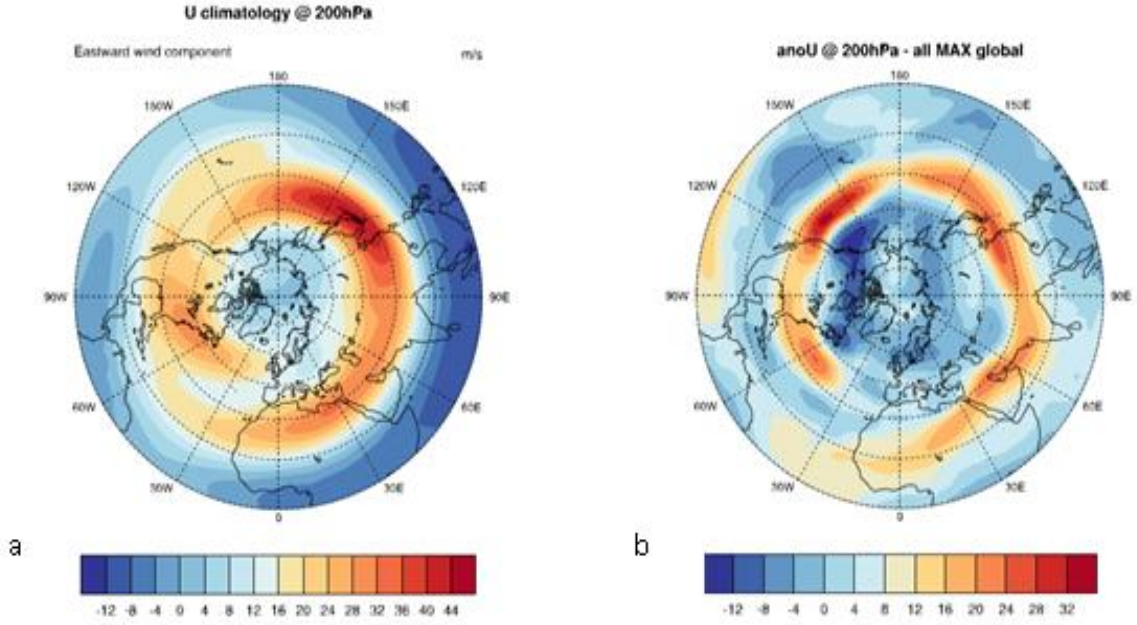

Figure 5.5. Composite maps of 200 hPa winds from 2001 to 2011 with **a)** the climatological mean and **b)** the Giant Forest CA-75 maximum precipitation days that occurred during the top ten weeks (Table 5.4).

5.3.6 Results of 200 hPa Wind Speed Analysis

The results of a comparison between the 200 hPa wind speeds MERRA reanalysis dataset composites from 2001 to 2011 of the climatological mean and the maximum precipitation days that occurred during the top ten weeks (Table 5.4) show slower wind speeds for the days with maximum precipitation delivered, consistent with a weaker, more meridional jetstream (~ 32 m/s) (Figure 5.4b) compared to the faster overall speeds in the climatological mean composite (~ 44 m/s) (Figure 5.4a).

5.4 Discussion

5.4.1 Precipitation Samples and Isotopes

In order to assess the modern precipitation patterns and associated isotopic values to provide additional information for paleoclimate interpretation, we analyzed every precipitation sample collected from CA-75 Giant Forest, Sequoia National Park over 240 weeks between 2001 and 2011. Results show an average of 44.8 mm/week and average water year (WY) (October to September) of 977 mm (Table 5.2). Isotopic analysis of 220 precipitation samples show a large range of isotopic values (δ^2H from -175.61 to 3.02 ‰ and $\delta^{18}O$ from -24.31 to 0.88 ‰) with an average WY $\delta^{18}O$ value of -12.11‰ (Table A4), demonstrating the influence of multiple processes and complex interactions. While there is a low inverse correlation between the $\delta^{18}O$ values and precipitation amount ($r = -0.18$, $p = 0.0072$), we observe a moderate correlation between the $\delta^{18}O$ values and temperature ($r = 0.48$, $p = < 0.0001$) and an inverse correlation between precipitation amounts and temperature ($r = -0.35$, $p = < 0.0001$) from 2001 to 2011.

Of the 220 precipitation events analyzed, the top ten greatest weekly precipitation amounts (> 150 mm), indicate that nine of these weeks contain known AR events (Neiman et al., 2008) (Table 5.3). Because the subtropical origin of ARs can lead to the delivery of precipitation with unique isotopic properties (Friedman et al., 2002; Berkelhammer et al., 2012), I expected to observe higher $\delta^{18}O$ values for at least nine of the ten sample weeks, however, measurements reveal a large range in isotopic values ($\delta^{2}H$ from -150.03 to -49.52 ‰, average of -84.05 ‰ and the $\delta^{18}O$ from19.27 to -7.20 ‰ with an average of -12.39 ‰, slightly more negative than the average weighted WY (-12.11‰; Table 5.2). The weekly temperature averages also had a wide range from 9.29 to -3.47 °C, with an average of 2 °C (Table 5.4). This may be due to the variety of trajectories which contributed to the weekly precipitation sample collected and accompanying isotopic composition as shown in the Hysplit back trajectory analysis (Fig. 5.4) and the varying precipitation amounts delivered during different daily temperatures. However, other processes that can influence contributions of moisture from different source locations, rainout occurring along the storm trajectory, duration of each event, associated air temperature, and conditions that prevail during and after condensation can also lead to isotopic variability (e.g. Dansgaard, 1964).

For example, a recent study of isotopic measurements from storm events at four sites in southern California, from 2001 to 2005, found ~ 40% of the isotopic variability of storms was due to the convective percentage of precipitation and near surface relative humidity within days before landfall (Berkelhammer et al., 2012). Another study showed that high vertical wind shear during storms contributes to more isotopically depleted rainfall (Friedman et al., 2002). Furthermore, a study based on isotopic measurements of precipitation collected over a 60-minute period during an AR struck the coast of California on 21 March 2005, suggested that a change in isotopic

composition reflect changes in condensation temperature due to altitude (Coplen et al., 2008). An isotope enabled climate model (IsoGSM) simulation of the same storm analyzed in the Coplen et al., (2008) study, indicates the source of isotopic variations was likely from changes in the isotopic composition of moisture and not the temperature (Yoshimura et al., 2010). More research is needed to determine the processes influencing the isotopic variations in ARs and extreme precipitation events.

5.4.2 C**omposite Mean and Anomaly Maps**

The NCAR/NCEP composite mean and anomaly maps for the top ten weekly precipitation amounts (> 150 mm) provide additional insight into these events. The composite mean sea level pressure (SLP) reveals a split Aleutian Low type is the dominant pattern, which usually occurs during a weaker Aleutian Low, and is characteristic of La Niña like conditions (Figure 5.3a) (Rodionov et al., 2007). The Aleutian low has also been shown to co-vary with the Pacific–North American (PNA) pattern and the Arctic Oscillation (AO) (Overland et al., 1999). A deep low pressure cell located northwest of California in the Gulf of Alaska is observed in the SLP and geopotential height composite anomalies (Figure 5.3b and d) and the 500 mb geopotential height (m) composite mean (Figure 5.3c), suggestive of a deep offshore trough. This low, coupled with increased 700 mb vector winds (m/s) (Figure 5.3i and j) and enhanced subtropical columnar precipitable water, (~ 6 to 8 kg/m^2) (Figure 5.3g and h) are conducive to heavy rainfall events in the Western US, consistent with the Feldl and Roe (2010) study which showed similar findings.

5.4.3 Climate Indices and 200 hPa Wind Speed

To further investigate these events, I compared the top ten precipitation weeks with numerous climate indices in which I found minor differences between the monthly ENSO indices and the daily and monthly indices of the Arctic Oscillation (AO), Pacific North America pattern (PNA), and the Southern Oscillation Index (SOI) (Table 5.6 and 5.7). Remarkably, 9 of 10 events occurred during the negative phase of the daily AO, (8 of 10 using the monthly AO index), a large scale climate mode associated with higher pressure in the Arctic and lower pressure in the surrounding lower latitudes, leading to weaker and southward displaced westerlies in the upper atmosphere. While the AO can vary considerably on short timescales and the causes of variability aren't entirely known, recent studies link shifts in the jet stream to changes in the AO due to reduced summer Arctic sea ice (Cohen et al., 2012; Francis and Vavrus, 2012). The reduction of summer Arctic sea ice leads to increased absorption of solar radiation causing increased Arctic warming, known as Arctic Amplification, which causes a decrease in the equator-to-pole temperature gradient, thereby weakening the jet stream, and resulting in more persistent weather patterns in the mid-latitudes (Francis and Vavrus, 2012). The 200 hPa wind composite maps show the wind speeds for the top ten individual days of maximum precipitation (Table 5.4) for each week are consistent with a weaker, more meridional jetstream (Fig. 5.5b) compared to the overall composite mean from 2005 to 2011 (Fig. 5.5a), consistent with the Arctic Amplification study. This warming also leads to increased evaporation and an increase of precipitation over high latitudes causing a rapid advance of Siberian snow cover, linked with the negative AO phase (Cohen, et al. 2012), thereby moving the temperature gradient further south and causing the jet stream to shift southward. While these studies demonstrate a physical connection between reduced Arctic sea ice in the summer and weather in North America

(Overland and Wang, 2010), the results are controversial (Barnes, 2013) and highlight that observed trends in mid-latitude weather patterns are complex and likely not simply understood in terms of Arctic Amplification alone.

A recent study by Guan et al., (2013) of all winter atmospheric rivers (ARs) in California from 1998-2011 also found AR frequency increased during the daily negative AO phase as well as the negative phase of the PNA teleconnection pattern, another large scale weather pattern, as they both provide favorable dynamical conditions for ARs by creating a persistent atmospheric low-pressure system just northwest of California that directs the AR toward the Sierra Nevada's over/near the southern two thirds of California (Guan et al., 2013). However, this study indicates the top ten greatest weekly precipitation amounts (> 150 mm) from CA-75, occurred similarly between the daily positive and negative phase of the PNA and most frequently during the neutral phase (Table 5.6), whereas the monthly index indicates these events occur more frequently during the positive phase and least likely during the neutral phase (Table 5.7). Another study by Moore et al., (2012) found that ARs manifest along the US West Coast as a decrease in the AO and a transition to a negative PNA. As all extreme precipitation weeks at this site do not include ARs, this highlights the importance of understanding the relationship between different large-scale climate mode phases and the latitudinal location of landfall.

The PNA pattern is a natural internal atmospheric variation that may be strongly influenced by SST variability associated with the ENSO and PDO. The results of the ENSO indices indicate these events occurred similarly between the El Niño and La Niña phase for the top ten events and occurred more frequently during the La Niña phase for the top 22 weeks, similarly for the PDO,

occurring more during the cooler phase during the top 22 weeks (Table 5.5). While numerous studies have shown seasonal precipitation in the Southwest is enhanced during El Niño events and vice versa during La Niña, based on the daily Southern Oscillation Index (SOI), our results indicate that extreme weeks of precipitation occurred more frequently during the La Niña (4 weeks) and neutral (4 weeks) phase than the El Niño phase (2 weeks) of ENSO (Table 5.6) while the monthly SOI shows the La Niña phase (5 weeks) is more frequent but similar to the El Niño phase (4 weeks) and less for the neutral phase (1 week) (Table 5.7). However, analysis of the top 10% of extreme precipitation, (22 weeks) (>109 mm), shows a clear bias toward the La Niña phase (14 weeks) over the El Niño (7 weeks) and rarely for the neutral phase (1 week) (Table 5.5). Dettinger et al., (2004) found AR features along the west coast of North America are most pronounced during neutral/near neutral ENSO conditions, possibly due to a weakened subtropical Pacific high during the neutral phase of ENSO which enhances conditions for the entrainment of tropical water vapor (Bao et al., 2006). Conversely, Guan et al., (2013) that found ARs were stronger during El Niño conditions. Another study by Feldl and Roe (2011) characterizing the relationship between large-scale atmospheric circulation patterns and daily precipitation distribution found that ENSO variability has different impacts on the mean and extreme precipitation in southwestern US, with more mean precipitation delivered during El Nino but more extreme precipitation delivered during La Nina.

Deeper examination of the ENSO characteristics reveals the top ten precipitation total weeks occurred most frequently when the eastern Pacific (EP) type, in which SST anomalies are located off the South American coast (Kao and Yu, 2009), was in the negative phase and neutral phase, and it is noteworthy to mention, the EP was positive during only one extreme precipitation week

(Table 5.5). Analysis of the top 22 and top 40 weeks indicate extreme precipitation events at this site also occurred most frequently during the neutral and negative EP phase and were least likely to occur during the positive EP phase (Table 5.8). The central Pacific (CP) type, in which anomalies are confined around the International Date Line (Kao and Yu, 2009), occurred similarly during both the negative and positive phase and did not occur at all during the neutral phase for the top ten events (Table 5.5, 5.8). Over the top 22 and top 40 weeks, we find a similar occurrence of large precipitation weeks during the positive and negative phase but these events rarely occurred during the neutral phase (Table 5.5, 5.8).

5.4.4 Anomalous Precipitation and Climate Modes

To further investigate the dynamics of how temporally varying large scale climate modes, SSTs, and tropical-North Pacific teleconnections intermingle to influence atmospheric circulation patterns, I combined daily climate indices phases representing the polar latitudes, the mid-latitudes, and the tropics with daily extreme precipitation events (>100 mm/day) from western US stations from 2001 to 2011 (Fig. A11a-e). The combination of the negative AO, negative PNA, and positive SOI (La Niña) displayed the maximum amount of anomalous precipitation extent along the western US (Fig. 5.2 and A11a). Furthermore, the negative AO, neutral PNA, and positive SOI (La Niña) phase combination is shown to deliver more anomalous precipitation, however, the extent is largely north of ~ 35 °N, extending over northern California up the US coast to Washington (Fig. 5.2 and A11a), whereas the negative PNA phase combination is more conducive to delivering extensive anomalous precipitation particularly below ~ 42 °N, essentially covering much of the state of California. The most anomalous precipitation extents were similar for the negative AO, negative PDO, neutral SOI, the negative AO, neutral PDO,

neutral SOI, and the positive AO, neutral PDO, neutral SOI, all above ~ 40 °N (Fig. Ae). The positive AO, positive NPI, and negative SOI shows anomalous precipitation delivered to the lower southwestern states where as the negative AO, neutral NPI, and positive SOI show the greatest extent of anomalous precipitation over the state of California (Fig. A11f).

The EP and CP indices combination with the negative AO and negative PNA are congruent with the positive SOI, however, in combination with the neutral PNA phase, while the negative CP phase is similar to the positive SOI precipitation extent, the negative EP phase combination is shown to resemble a dipole affect, with extreme precipitation anomalies above ~ 40 °N and a maximum over the Washington coast (Fig. 5.2, A11c and d). Of all the combinations examined, the negative AO, neutral PNA, and neutral EP combination, showed the most anomalous precipitation delivered between ~ 35 °N and ~ 42 °N (Fig. 5.2, A11d).

While the study of anomalous precipitation (> 100 mm/day) showed the greatest extent of events occurred during the daily AO, negative PNA, and positive SOI (La Niña), the CA-75 Giant Forest site precipitation analysis indicates the top weeks of precipitation events (> 150 mm/week) tended to occur during the daily negative AO, neutral PNA, and positive/neutral SOI (Table 5.6) and during the monthly negative AO, positive PNA, and positive SOI (Table 5.7). As the negative PNA phase is associated with a weaker, more southward displaced jet, and more rainfall in Southern California, the difference between the phase combinations seen at our site may be due to the higher latitudinal location of 36.57 °N which is near the western United States north–south precipitation dipole transition zone, (e.g. ~ 40 °N; Dettinger et al., 1998), which has varied over time and space (Brown and Comrie, 2004) and may also be influenced by the fact

that only 5 of the top 10 weeks had precipitation days delivering greater than 100 mm of precipitation.

Analysis of the isotopic values associated with the monthly climate indices for the top ten extreme precipitation weeks, the top 10%, 22 weeks, and the top 40 weeks shows preferred climate modes to be more conducive to delivering isotopically enhanced or depleted precipitation (Table 5.8). Both the negative AO and PNA phase reveal more negative average precipitation $\delta^{18}O$ values, with a difference of 5.09 ‰ between the positive and negative PNA phases for the top ten events (Table 5.6 and 5.7; average -12.11 ‰ ± 1.18). For the top 10% (22 weeks), the negative phase PNA values were > 3.15 ‰ more negative than during the positive phase (average -12.09‰ ± 2.83), and for the top 40 weeks were > 2 ‰ more negative than during the positive PNA phase (average -12.09 ‰ ± 2.93) (Table 5.8). This correlation is consistent with a study of precipitation isotope ratios across the contiguous US, which found a positive correlation between precipitation isotopes and the PNA in the Western USA (Lui et al., 2011, 2012). This is likely because both the negative AO and negative PNA influence the polar jet to shift southward thereby transporting precipitation from higher latitudes.

The most positive $\delta^{18}O$ values occurred during the negative SOI phase (El Niño) for the top ten and top 22 weeks and the SOI neutral phase for the top 40 weeks. These results are not consistent with other studies that found more negative precipitation $\delta^{18}O$ values during El Niño events. For example, a recent study conducted on weekly precipitation samples collected by the NADP from 77 sites across the US between 1989 and 1995 (Welker, 2012), showed seasonal precipitation $\delta^{18}O$ anomalies during El Niño years with negative $\delta^{18}O$ anomalies as compared to neutral years

occurring primarily in the Southwest and Great Plains in the fall months (OND) were more negative (by −4‰ to −3‰). Anomalies over the west coast and around the Great Lakes in the winter months (JFM) were also more negative (by − 3 ‰ to − 2 ‰) (Winnick et al., 2012). While this study did find positive anomalies (3 – 6 ‰) in the Southwest in the spring months (AMJ), the majority of precipitation at the Giant Forest CA-75 site is delivered during November to April. However, this study did not analyze isotopic values during La Niña years. A study of oxygen stable isotope ratios of cactus from the American Southwest showed that annual decreases in the maximum cactus $\delta^{18}O$ were positively correlated with the SOI attributing the decreases to enhanced winter rainfall associated with the El Niño phase (English et al., 2010), consistent with another study in which lower isotopic values in cactus grown in 1983 and 1993 were associated with winter rains enhanced by the El Niño phase (Gutzler et al., 2002).

The ENSO and the PDO influence precipitation amounts in the western United States by modifying the strength and position of the Aleutian Low and North Pacific high-pressure systems. During El Niño a deeper Aleutian low shifts the subtropical jet and westerly storm track equator-ward (Bjerknes, 1969; Trenberth et al., 1998) contributing to more zonal circulation patterns (Rodionov et al., 2007) that are conducive to transporting precipitation with more negative $\delta^{18}O$ values to this location site, whereas the La Niña phase shifts the subtropical jet northward, transporting moisture from lower latitudes consisting of more positive $\delta^{18}O$ values. This relationship is also observed in long-term records such as the ~ 1000 year Crystal Cave speleothem oxygen isotope record which found $\delta^{18}O$ values were more negative during zonal wind circulation patterns and more positive during meridional circulation patterns (McCabe-Glynn et al., 2013). Additionally, a 3000 year California lake leaf wax $\delta^{18}O$ record that showed

centennial-duration negative isotopic excursions were associated with North Pacific sources and wetter conditions and positive $\delta^{18}O$ excursions were associated with more sub-tropical moisture sources and drier conditions (Feakins et al., 2013).

Considering that similar amounts of precipitation were delivered during both El Niño and La Niño over the last decade (Table 5.3) with more negative $\delta^{18}O$ values occurring during La Niña events (Table 5.8), this seems to suggest that precipitation patterns may be different or changing perhaps due to the influence of a slower circulation pattern on the amount of precipitation being delivered and the accompanying isotopic values or may reflect spatial and/or temporal variability associated with the different timescales involved. This recent change may be seen in the climate indices combination plots in which the greatest extent of precipitation anomalies (negative AO, negative PNA, and negative SOI phase), have shown an increase in anomalous precipitation over the last decade, 2001 to 2011 (Fig. A11a), as compared to the longer term mean, 1979 to 2011 (Fig. A11b). More research is needed to determine whether or not the isotopic values have a dominant signature during ENSO phases.

5.5 Conclusions

The results of 240 weeks of Giant Forest CA-75 station precipitation samples collected from 2001 to 2011 reveals an average weekly precipitation amount of 44.8 mm (Table A4). The isotopic measurements of 220 weekly precipitation samples show a large range in values (Table A4) with an average water year (WY) (Oct - Sept) precipitation amount of 977 mm and an average weighted $\delta^{2}H$ of -81.65 ‰ ± 8.92‰ and $\delta^{18}O$ of -12.11 ‰ ± 1.18‰ (Table 5.2). There is a low inverse correlation between the $\delta^{18}O$ values and precipitation amount (-0.22, p =

0.0010), a moderate correlation between the $\delta^{18}O$ values and temperature (0.48, p = < 0.0001), and an inverse correlation between precipitation amount and temperature (-0.35, p = < 0.0001) from 2001 to 2011. The three highest total annual precipitation occurred in the WY (Oct- Sept) 2011, 2010, and 2006 and the three lowest in 2009, 2007, and 2004 (Table 5.2). The top ten weeks with precipitation amounts totaling >150 mm from 2001 to 2011 indicate these extreme precipitation weeks contribute about 10% of the total WY precipitation at this site. We also observe a large range in both isotopic values and daily temperatures associated with each of the top ten weeks ($\delta^{2}H$ -150.03 to -49.52 ‰, average of -84.05‰ and $\delta^{18}O$ -19.27 to -7.20 ‰, average of -12.39 ‰) (Table 5.3), and the lowest daily temperature of -9.4 °C and the highest daily temperature of 16.7 °C with an average weekly temperature of 1.53°C (Table 5.4). Nine of the top ten weeks contain noted atmospheric rivers events (Table 5.3). While these events tend to have a sub-tropical origin, the Hysplit back trajectory analysis shows that a variety of trajectories contributed to the weekly precipitation sample collected and accompanying isotopic composition (Fig. 5.4).

The NCAR-NCEP composite maps for the top ten weeks of precipitation amounts (>150 mm) indicate that the SLP composite mean shows a split Aleutian Low type pattern, characteristic of La Nina conditions (Fig. 5.3a) with anomalous SLP composite map features a deep low pressure cell located northwest of California in the Gulf of Alaska (Fig. 5.3b), characteristic of the negative PNA phase. This, coupled with winds ideally located (Fig. 5.3i and j) to transport enhanced subtropical columnar precipitable water (Fig. 5.3g and h), provide conditions conducive for heavy rainfall events along the western US.

Comparison of climate indices known to influence precipitation on the Western US shows, remarkably, 9 of 10 events occurred during the negative phase of the daily AO (Table 5.6) and 8 of 10 during the monthly AO index (Table 5.7). The daily PNA index indicates they occur most frequently during the neutral PNA phase (Table 5.6) and monthly index indicating they occur most frequently during the positive PNA phase (Table 5.7) for the top 22 and top 40 weeks. The daily SOI shows these high precipitation weeks occur more frequently during the La Niña and neutral phase and less for the El Niño phase (Table 5.6) while the monthly ENSO indices indicate they occurred similarly during both El Niño and La Niña and rarely during the neutral phase. The tendency for occurrence increases in frequency for the SOI monthly negative (La Niña) phase for the top 22 and top 40 weeks (Table 5.5, 5.8). Further examination of the ENSO type suggests that extreme precipitation events at this site are most likely to occur during the neutral and negative EP phase and least likely to occur during the positive EP phase and most likely to occur during both the negative and positive CP phase and least likely to occur during the neutral phase (Table 5.5, 5.8). The average precipitation isotopic values for the AO, PNA, and SOI climate indices for the top 10, 22, and 40 weeks are overall more negative during the monthly negative AO and PNA phase than the positive and neutral phase and most positive isotopic values during the negative SOI (El Niño) phase than the negative and neutral phase (Table 5.8).

The combination of temporally varying large scale climate modes with daily extreme precipitation events (>100 mm/day) at western US stations from 2001 to 2011 demonstrates when the negative AO, negative PNA, and positive SOI (La Niña) are in sync, the maximum amount of anomalous precipitation extent along the Western US, essentially covering much of

the state of California (Fig. 5.3 and A11a). When this combination (negative AO, positive SOI) is in sync with the neutral PNA phase, more anomalous precipitation is delivered north of ~ 35 °N, extending over northern California up the US coast to Washington (Fig.5.3 and A11a). Additionally, when in this phase combination, the type of ENSO (EP vs CP) can provide more information as to where these extreme precipitation anomalies will occur. While the extent of anomalous precipitation during the negative CP phase combination is similar to the positive SOI (La Nina) (Fig. 5.3 and A11c), the negative EP phase combination resembles more of a dipole relationship showing extreme precipitation anomalies (> 100 mm/day) occur above ~ 40 °N with a maximum over the Washington coast (Fig.5.3, A11d). The climate indices study also shows that the negative AO, neutral PNA, and neutral EP combination, showed the most anomalous precipitation delivered between ~ 35 °N and ~ 42 °N (Fig. 5.3 and A11a). However, the CA-75 Giant Forest site precipitation analysis indicates the top ten weeks of precipitation events tended to occur during the daily negative AO, neutral PNA, and positive/neutral SOI phase (Table 5.6) and during the monthly negative AO, positive PNA, and positive SOI phase (Table 5.7), suggesting the negative PNA phase is more conducive to increased rainfall transported to locations in the Western US lower than 36.57 °N (Fig. 5.3 and A11a).

This study suggests that extreme precipitation weeks in Sequoia National Park, CA, are associated with a meridional atmospheric circulation pattern. While the Arctic Amplification study leading to more persistent precipitation patterns is controversial, as the Arctic continues to warm more than in mid-latitudes, positive feedback responses to sea ice-temperature effects will likely contribute to increased Arctic warming and sea ice decline (Serreze and Barry, 2011) and are sure to affect atmospheric circulation patterns. This study only covers a 10 year span,

however, it emphasizes the importance of understanding the dynamic controls on the hydroclimate in the Western US to prepare for and mitigate large precipitation events. Additionally, this study provides a basis for how atmospheric circulation patterns may respond both spatially and temporally when climate mode phases combine to direct enhanced moisture toward the Western US.

5.6 References

Bao, J., Michelson, S., Neiman, P., Ralph, F., Wilczak, J., 2006. Interpretation of enhanced integrated water vapor bands associated with extratropical cyclones: Their formation and connection to tropical moisture. *Monthly Weather Review*. 134, 1063-1080.

Barnes, E. A., 2013. Revisiting the evidence linking Arctic amplification to extreme weather in midlatitudes. *Geophysical Research Letters.* 40, 4734-4739.

Berkelhammer, M., Stott, L., Yoshimura, K., Johnson, K., Sinha, A., 2012. Synoptic and mesoscale controls on the isotopic composition of precipitation in the western United States. *Climate Dynamics.* 1-22.

Brown, D. P. and Comrie, A. C., 2004. A winter precipitation 'dipole'in the western United States associated with multidecadal ENSO variability. *Geophysical Research Letters*. 31.

Cayan, D., Tyree, M., Dettinger, M., Hidalgo, H., Das, T., Maurer, E., Bromirski, P., Graham, N., Flick, R., 2009. Climate change scenarios and sea level rise estimates for the California 2008 Climate Change Scenarios Assessment. *California Climate Change Center CEC*-500-2009-014-D.

Cayan, D. R., Redmond, K. T., Riddle, L. G., 1999. ENSO and Hydrologic Extremes in the Western United States*. *Journal of Climate*. 12, 2881-2893.

Cayan, D. and Riddle, L., 1992. Atmospheric circulation and precipitation in the Sierra Nevada. *Managing Water Resources during Global Change*. 711-720.

Cohen, J. L., Furtado, J. C., Barlow, M. A., Alexeev, V. A., Cherry, J. E., 2012. Arctic warming, increasing snow cover and widespread boreal winter cooling. *Environmental Research Letters*. 7, 014007.

Cook, E. R., Seager, R., Cane, M. A., Stahle, D. W., 2007. North American drought: reconstructions, causes, and consequences. *Earth-Science Reviews.* 81, 93-134.

Coplen, T. B., Neiman, P. J., White, A. B., Landwehr, J. M., Ralph, F. M., Dettinger, M. D., 2008. Extreme changes in stable hydrogen isotopes and precipitation characteristics in a landfalling Pacific storm. *Geophysical Research Letters.* 35.

Dansgaard, W., 1964. Stable isotopes in precipitation. Tellus. 16, 436-468.

Das, T., Dettinger, M. D., Cayan, D. R., Hidalgo, H. G., 2011. Potential increase in floods in California's Sierra Nevada under future climate projections. *Climatic Change*. 109, 71-94.

Dettinger, M. D., Cayan, D. R., Diaz, H. F., Meko, D. M., 1998. North-south precipitation patterns in western North America on interannual-to-decadal timescales. *Journal of Climate*. 11, 3095-3111.

Dettinger, M., 2011. Climate Change, Atmospheric Rivers, and Floods in California–a Multimodel Analysis of Storm Frequency and Magnitude Changes. *Journal of the American Water Resouces Association*. Vol. 47, No. 3.

Dettinger, M. D., 2005. From climate-change spaghetti to climate-change distributions for 21st Century California. *San Francisco Estuary and Watershed Science*. 3.

Draxler, R. and Rolph, G., 2003. HYSPLIT (HYbrid Single-Particle Lagrangian Integrated Trajectory) model access via NOAA ARL READY website (http://www. arl. noaa. gov/ready/hysplit4. html). *NOAA Air Resources Laboratory, Silver Spring.*

English, N. B., Dettman, D. L., Williams, D. G., 2010. A 26-year stable isotope record of humidity and El Niño-enhanced precipitation in the spines of saguaro cactus, Carnegiea gigantea. *Palaeogeography, Palaeoclimatology, Palaeoecology*. 293, 108-119.

Feakins, S.J., Kirby, M. E., Cheetham, M. I., Ibarra, Y., Zimmerman, S., R.H., 2014. Fluctuation in leaf wax D/H ratio from a southern California lake records significant variability in isotopes in precipitation during the late Holocene. *Organic Geochemistry.* 66, 48–5.

Feldl, N. and Roe, G. H., 2011. Climate variability and the shape of daily precipitation: A case study of ENSO and the American West. *Journal of Climate*. 24, 2483-2499.

Francis, J. A. and Vavrus, S. J., 2012. Evidence linking Arctic amplification to extreme weather in mid-latitudes. *Geophysical Research Letters.* 39.

Friedman, I., Harris, J. M., Smith, G. I., Johnson, C. A., 2002. Stable isotope composition of waters in the Great Basin, United States 1. Air-mass trajectories. *Journal of Geophysical Research: Atmospheres* (1984–2012). 107, ACL 14-1-ACL 14-14.

Guan, B., Molotch, N. P., Waliser, D. E., Fetzer, E. J., Neiman, P. J., 2013. The 2010/2011 snow season in California's Sierra Nevada: Role of atmospheric rivers and modes of large-scale variability. *Water Resources Research*. 49, 6731-6743.

Guan, B., Molotch, N. P., Waliser, D. E., Fetzer, E. J., Neiman, P. J., 2010. Extreme snowfall events linked to atmospheric rivers and surface air temperature via satellite measurements. *Geophysical Research Letters.* Vol. 37. Issue 20.

Gutzler, D. S., Kann, D. M., Thornbrugh, C., 2002. Modulation of ENSO-based long-lead outlooks of southwestern US winter precipitation by the Pacific decadal oscillation. *Weather and Forecasting.* 17, 1163-1172.

Jain, S., Hoerling, M., Eischeid, J., 2005. Decreasing reliability and increasing synchroneity of western North American streamflow. *Journal of Climate.* 18, 613-618.

Kalnay, E., Kanamitsu, M., Kistler, R., Collins, W., Deaven, D., Gandin, L., Iredell, M., Saha, S., White, G., Woollen, J., 1996. The NCEP/NCAR 40-year reanalysis project. *Bulletin of the American Meteorological Society.* 77, 437-471.

Kanamitsu, M., Ebisuzaki, W., Woollen, J., Yang, S., Hnilo, J., Fiorino, M., Potter, G., 2002. Ncep-doe amip-ii reanalysis (r-2). *Bulletin of the American Meteorological Society*. 83, 1631-1643.

Kao, H.-Y., and Yu, J.-Y., 2009: Contrasting Eastern-Pacific and Central-Pacific Types of ENSO. *J. Climate*, **22**, 615–632. doi: http://dx.doi.org/10.1175/2008JCLI2309.1

Mantua, N. J. and Hare, S. R., 2002. The Pacific decadal oscillation. *Journal of Oceanography*. 58, 35-44.

Mass, C., Skalenakis, A., Warner, M., 2011. Extreme precipitation over the West Coast of North America: Is there a trend? J*ournal of Hydrometeorology.* 12, 310-318.

McCabe-Glynn, S., Johnson, K. R., Strong, C., Berkelhammer, M., Sinha, A., Cheng, H., Edwards, R. L., 2013. Variable North Pacific influence on drought in southwestern North America since AD 854. *Nature Geoscience*. 6, 617-621.

Neiman, P. J., Ralph, F. M., White, A., Kingsmill, D., Persson, P., 2002. The statistical relationship between upslope flow and rainfall in California's coastal mountains: Observations during CALJET. *Monthly Weather Review*. 130, 1468-1492.

Neiman, P. J., Ralph, F. M., Wick, G. A., Kuo, Y., Wee, T., Ma, Z., Taylor, G. H., Dettinger, M. D., 2008. Diagnosis of an intense atmospheric river impacting the Pacific Northwest: Storm summary and offshore vertical structure observed with COSMIC satellite retrievals. *Monthly Weather Review*. 136, 4398-4420.

Overland, J. E. and Wang, M., 2010. Large-scale atmospheric circulation changes are associated with the recent loss of Arctic sea ice. *Tellus A.* 62, 1-9.

Ralph, F. M., Neiman, P. J., Rotunno, R., 2005. Dropsonde observations in low-level jets over the northeastern Pacific Ocean from CALJET-1998 and PACJET-2001: Mean vertical-profile and atmospheric-river characteristics. *Monthly Weather Review.* 133, 889-910.

Ralph, F. and Dettinger, M., 2012. Historical and national perspectives on extreme West Coast precipitation associated with atmospheric rivers during December 2010. *Bulletin of the American Meteorological Society*. 93, 783-790.

Reynolds, R. W., Smith, T. M., Liu, C., Chelton, D. B., Casey, K. S., Schlax, M. G., 2007. Daily high-resolution-blended analyses for sea surface temperature. *Journal of Climate.* 20, 5473-5496.

Rienecker, M. M., Suarez, M. J., Gelaro, R., Todling, R., Bacmeister, J., Liu, E., Bosilovich, M. G., Schubert, S. D., Takacs, L., Kim, G., 2011. MERRA: NASA's modern-era retrospective analysis for research and applications. *Journal of Climate*. 24, 3624-3648.

Rodionov, S., Bond, N., Overland, J., 2007. The Aleutian Low, storm tracks, and winter climate variability in the Bering Sea. *Deep Sea Research Part II: Topical Studies in Oceanography*. 54, 2560-2577.

Sellars, S., Nguyen, P., Chu, W., Gao, X., Hsu, K., Sorooshian, S., 2013. Computational Earth Science: Big Data Transformed Into Insight. *Eos, Transactions American Geophysical Union.* 94, 277-278.

Serreze, M. C. and Barry, R. G., 2011. Processes and impacts of Arctic amplification: A research synthesis. *Global and Planetary Change.* 77, 85-96.

Trenberth, K.E., 1999. Conceptual framework for changes of extremes of the hydrological cycle with climate change, in: A*nonymous Weather and Climate Extremes.* Springer, pp. 327-339.

Warner, M. D., Mass, C. F., Salathé Jr, E. P., 2012. Wintertime extreme precipitation events along the Pacific Northwest coast: Climatology and synoptic evolution. *Monthly Weather Review*. 140, 2021-2043.

Welker, J., 2012. ENSO effects on $\delta^{18}O$, $\delta^{2}H$ and d-excess values in precipitation across the U.S. using a high-density, long-term network (USNIP). *Rapid Commun. Mass Spectrom.* 26, 1893–1898.

Wick, G. A., Neiman, P. J., Ralph, F. M., 2013. Description and validation of an automated objective technique for identification and characterization of the integrated water vapor signature of atmospheric rivers. *Geoscience and Remote Sensing, IEEE Transactions On*. 51, 2166-2176.

Yoshimura, K. and Kanamitsu, M., 2008. Dynamical global downscaling of global reanalysis. *Monthly Weather Review*. 136, 2983-2998.

Yoshimura, K., Kanamitsu, M., Dettinger, M., 2010. Regional downscaling for stable water isotopes: A case study of an atmospheric river event. *Journal of Geophysical Research: Atmospheres* (1984–2012). 115.

Yu, J., Zou, Y., Kim, S. T., Lee, T., 2012. The changing impact of El Niño on US winter temperatures. *Geophysical Research Letters*. Vol. 39, Issue 15.

Zou, Y., J.-Y. Yu, T. Lee, M.-M. Lu, and S. T. Kim. 2014.CMIP5 Model Simulations of the Impacts of the Two Types of El Niño on US Winter Temperature, *Journal of Geophysical Research: Atmospheres,* Vol. 119, Issue 6, pages 3076–3092, 27.

CHAPTER 6

6.1 Future Work

6.1 Cave Monitoring and Additional Analysis

Precipitation in the Western US exhibits interannual to multidecadal variability linked to naturally recurring large-scale atmospheric circulation patterns. The findings in this dissertation demonstrate that speleothems from Crystal Cave, Sequoia National Park, California, located on the south western flank of the Sierra Nevada Mountains (36:59 °N; 118:82 °W; 1,386 m) (Fig. 1.2), are well-suited for reconstructing past hydrologic variability. The application of oxygen isotope measurements and interpretations from the Crystal Cave stalagmite, CRC-3, indicate that speleothem $\delta^{18}O$ values at this site are sensitive to Pacific SST patterns, particularly the Kuroshio Extension region. This strong correlation was utilized to develop a high-resolution reconstruction of Kuroshio Extension region SSTs extending the record back to 854 AD. Future research includes utilizing this correlation on older stalagmites found in the cave to extend this record even further back in time.

There are many caves in Sequoia National Park that contain stalagmites which could be useful for replication of our results, enhancing the robustness of our interpretations, and extending the current Kuroshio Extension region SST record beyond 854 AD. For example, the newly found Ursa Minor Cave, not a tourist cave, contains hundreds of tall, columnar stalagmites forming in high relative humidity (~100%) and a constant temperature. Our group has located an ideal stalagmite for extending this record in an isolated room located high in the back of Ursa Minor Cave, in the Skyline Room and has been monitoring key environmental variables (drip rate,

dripwater isotope values, relative humidity, and temperature) for the last ~ 5 years. The stalagmites in this room consist of clear dense calcite suggesting few impurities and low detrital inclusions, making it ideal for high-precision uranium-series dating. Results of this study depict the importance of these records and the need for acquiring sampling permits to continue this research.

For future analyses and to better understand the hydrologic variability of the karst region, the monitoring of Crystal Cave environmental variables (e.g., drip rate and drip water isotopic values, relative humidity, temperature, etc.) also needs to be continued. Currently, this study indicates that it takes approximately two days for the maximum precipitation events above the cave to percolate through the bedrock and fractures within the karst system before reaching the drip logger. However, not all extreme precipitation events above the cave over the last 4 years were registered by the cave drip logger as maximum events and likewise, not all of the extreme drip logger maximum events registered were due to extreme amounts of precipitation delivered above the cave. The maxima drip logger rate responses suggests that the epikarst region above the cave was hydrologically saturated contributing to a 'piston flow' through the karst cracks and fissures, and after they were emptied, the piston flow ceased and a became more porous flow type again (e.g.,Tremaine et al., 2014). To gain a better understanding of the thresholds involved within the karst system, modeling studies are needed which combine the drip logger flow rates with the amount of precipitation registered above the cave to provide additional information about the cave hydrology and flow paths (e.g. Fairchild et al., 2006; Baker and Fairchild, 2012). The analysis of the 2011 to 2013 drip logger maxima data is also needed.

The greatest precipitation above Crystal Cave occurs from November to April (Dettinger et al., 1998), thereby influencing the three major factors known to affect the stalagmite growth rate: the calcium ion concentration, the temperature of the dripwater, and the drip water flow rate (e.g., Genty et al., 2001; Baker et al., 1998; Dreybrodt, 1988). Since Crystal Cave is inaccessible during the winter, the time of greatest growth rate is unknown. This study indicates winter and spring drip rates are higher than summer and fall. If the drip time is significantly longer than what is needed for complete degassing to occur, then the growth rate will be slow (Genty et al., 2001). Therefore, future research includes utilizing glass plates to measure fresh calcite growth during the winter (November when the cave closes to April or May when the cave becomes accessible) versus the summer/fall (~May to November). Since high soil CO_2 leads to increased dissolved Ca^{2+}, future research would also include seasonal soil *p*CO2 measurements above the stalagmite collection site. Additionally, to enhance the trace element interpretations, measurements of trace element concentrations in the bedrock and soil material above the cave, as well as in fresh calcite collected on glass plates and the cave drip water, could also provide information about processes influencing calcite trace element variations (e.g. Johnson et al., 2006; Tremaine et al., 2014; Oster et al., 2009). Glass plate analysis of the calcite color and/or increased organic acids (humic and fulvic) as seen under ultraviolet light could also provide information as to the darkened and fluorescent lamina (Baker et al., 2008) seen every ~6 years on the CRC-3 thin sections (Fig. A1).

Speleothem calcite $^{87}Sr/^{86}Sr$ ratios have also been used to provide additional climatic information (Oster et al., 2009; 2014; Banner, et al. 1996). For example, wetter conditions contribute to decreased karst water residence times leading to drip water containing less radiogenic Sr,

suggestive of more soil derived Sr and drier periods contributing to increased water residence times leading to more radiogenic Sr, are suggestive of more bedrock derived Sr (e.g. Banner et al., 1996). Future research of the CRC-3 calcite $^{87}Sr/^{86}Sr$ ratios can provide additional support for the $\delta^{13}C$ and trace element record interpretations because studies indicate drier conditions lead to increased radiogenic $^{87}Sr/^{86}Sr$ and elevated $\delta^{13}C$ trace elements (e.g. Oster et al., 2009; 2014). Speleothem sulphur concentrations may also be useful for recording aspects of atmospheric variability. In non-seasalt sulfate, one of the sources is the oxidation of marine dimethylsulfide (DMS) which reacts in the atmosphere to form a sulfate and methane sulphonate (MSA) aerosol. While there are complex interactions, the sulfur isotopes in speleothems can be useful for determining periods of high primary productivity (e.g. Wynn et al., 2008; Tremaine et al., 2014) for the DMS producing marine phytoplankton Phaeocystis species (Stefels and van Boekel, 1993). The DMS in the atmosphere can influence the amount of cloud-condensation nuclei (CCN) and ultimately the climate. Since variations associated with changes in ocean and atmospheric circulation patterns can affect the transport of non-seasalt sulfate, speleothem calcite sulfur isotope variations may provide additional information of past atmospheric circulation patterns.

6.2 Extreme Precipitation and AR Modeling Studies of Isotopes and d-excess

Analysis of 240 weekly precipitation samples collected from CA-75, Giant Forest in Sequoia National Park, California over the ten year period, 2001 to 2011, show the top ten precipitation amount weeks (>150 mm/week) contain nine noted atmospheric rivers (ARs), which play a critical role in driving wintertime precipitation extremes. While ARs contribute extensively to replenishing reservoirs and groundwater supplies, they can also result in harmful consequences

for the US West Coast, including flooding, landslides, loss of life and extensive property damage (Mass et al., 2011; Warner et al., 2012; Ralph and Dettinger, 2012). Despite the fact that California has begun implementation of key land-based sensors and modern satellite advances have led to enhanced awareness and improved understanding of extreme precipitation events, they are still difficult to predict accurately beyond about a ten-day lead and forecasts of landfall impact are even poorer (Wick et al., 2013). Understanding the characteristics and dynamics of extreme precipitation events and ARs is therefore critical to lead to improved predictability of future AR and extreme precipitation events to thereby mitigate negative consequences. Because of the subtropical origin of ARs, they can deliver precipitation with unique isotopic properties (Friedman et al., 2002; Berkelhammer et al., 2012). However, this study shows a large range of isotopic variability (δ^2H = -150.03 to -49.52 ‰ and $\delta^{18}O$ = -19.27 to -7.20 ‰) coupled with a high range in temperature (-9.4 ^{0}C to 16.7 ^{0}C; Table 5.2) and trajectories from both higher and lower latitudes during each of the top ten precipitation amount weeks (Fig. 5.3). Future research includes utilizing isotope enabled climate models such as IsoGSM, which may be able to provide more information regarding the processes leading to this isotopic variability (Yoshimura et al., 2010). Furthermore, the US Network for Isotopes in Precipitation (USNIP) has isotopic information available from several sites along the US West Coast going back about 30 years, and more sites with archived precipitation samples (Welker, 2012). The isotopic data from this study can be compared with other sites during AR and extreme precipitation events and utilized by the climate models to better understand the modern spatial and temporal water isotope manifestations of ARs and extreme events along the Pacific west coast states as they progress inland, as well as to provide an isotopic catalog to benchmark and validate the performance of isotopes in general circulation models. This can provide additional insight as to the climate

mechanisms governing ARs and extreme events (Guan et al., 2013) and their possible isotopic signature in climate archives such as tree rings, leaf waxes, and speleothems.

Variations in the deuterium excess (d-excess) values of precipitation have been shown to be a useful diagnostic tool for measuring the contribution of evaporated moisture to the downwind atmosphere and enhancing identification of the vapor source region (Gat et al., 1994). The d-excess values, where (d) is defined as $d= \delta^{2}H-8* \delta^{18}O$ (Dansgaard, 1964), results from kinetic fractionation during evaporation due to the different diffusivity factors of water molecules, with the $^{2}H^{1}H^{16}O$ having a higher diffusivity compared to the $^{1}H^{1}H^{18}O$, causing a greater separation and higher deuterium excess. The major controlling factors of the d-excess are the relative humidity of the air masses at their oceanic origin and the wind speed. Future research includes analyzing the d-excess of precipitation samples utilizing Global Network of Isotopes in Precipitation (GNIP) archived precipitation samples dating back about the last 25 years, and even further in some cases, and combining this information with the modeling studies to provide additional information regarding ARs and extreme precipitation events in the Western US (Welker, 2012).

6.3 Precipitation Relationship with Arctic Amplification

My analysis of extreme precipitation events suggests they are associated with a meridional atmospheric circulation pattern influenced by the Arctic Oscillation, similar to that observed with Arctic Amplification, a warming trend in the Arctic, indicating higher latitudinal warming could be an important mechanism contributing to these events. As the Arctic continues to warm more than in mid-latitudes, positive feedback responses to sea ice-temperature effects will likely

contribute to increased Arctic warming and sea ice decline (Serreze and Barry, 2011), which is certain to affect atmospheric circulation patterns. While this study of CA-75 Giant Forest precipitation data only covers a 10 year span, it emphasizes the importance of understanding the dynamic controls on the hydroclimate in the western US to prepare for and mitigate large precipitation events. As Arctic air temperatures have continued to increase, this study provides a basis for how atmospheric circulation patterns respond both spatially and temporally when climate mode phases combine. Future research would include analysis of the relationship between the Arctic sea ice and extreme precipitation amounts and AR events in the Western US.

6.4 References:

Baker, A., Genty, D., Dreybrodt, W., Barnes, W.L., Mockler, N.J., and Grapes,J., 1998. Testing theoretically predicted stalagmite growth rate with Recent annualy laminated samples: Implications for past stalagmite deposition. *Geochim. Cosmochim. Acta.* 62, 393-404.

Baker, A. and Fairchild, I., 2012. Drip Water Hydrology and Speleothems. *Nature Education Knowledge.* 3, 16.

Baker, A., Smith, C. L., Jex, C., Fairchild, I. J., Genty, D., Fuller, L., 2008. Annually laminated speleothems: a review. I*nternational Journal of Speleology*. 37, 4.

Baker, A., Genty, D., Smart, P. L., 1998. High-resolution records of soil humification and paleoclimate change from variations in speleothem luminescence excitation and emission wavelengths. *Geology.* 26, 903-906.

Banner, J. L., Musgrove, M., Asmerom, Y., Edwards, R. L., Hoff, J. A., 1996. High-resolution temporal record of Holocene ground-water chemistry; tracing links between climate and hydrology. *Geology.* 24, 1049-1053.

Berkelhammer, M., Stott, L., Yoshimura, K., Johnson, K., Sinha, A., 2012. Synoptic and mesoscale controls on the isotopic composition of precipitation in the western United States. *Climate Dynamics.* 1-22.

Dansgaard W. 1964. Stable isotopes in precipitation. *Tellus* 16:436–68

Dreybrodt, W., 1988. Processes in Karst Systems: Berlin, *Springer-Verlag*, 287 p.

Fairchild, I. J., Smith, C. L., Baker, A., Fuller, L., Spötl, C., Mattey, D., McDermott, F., 2006. Modification and preservation of environmental signals in speleothems. *Earth-Science Reviews.* 75, 105-153.

Friedman, I., Harris, J. M., Smith, G. I., Johnson, C. A., 2002. Stable isotope composition of waters in the Great Basin, United States 1. Air-mass trajectories. *Journal of Geophysical Research: Atmospheres* (1984–2012). 107, ACL 14-1-ACL 14-14.

Fairchild, I. J., Smith, C. L., Baker, A., Fuller, L., Spötl, C., Mattey, D., McDermott, F., 2006. Modification and preservation of environmental signals in speleothems. *Earth-Science Reviews.* 75, 105-153.

Friedman, I., Harris, J. M., Smith, G. I., Johnson, C. A., 2002. Stable isotope composition of waters in the Great Basin, United States 1. Air- mass trajectories. *Journal of Geophysical Research: Atmospheres* (1984–2012). 107, ACL 14-1-ACL 14-14.

Gat, J.R., Bowser, C., Kendall, C., 1994. The contribution of evaporation from the Great Lakes to the continental atmosphere: estimate based on stable isotope data. *Geophys. Res. Lett.*,21:557–60

Genty, D., Baker, A., Vokal, B., 2001. Intra- and inter-annual growth rate of modern stalagmites. *Chemical Geology*. Volume 176, Issues 1–4, 1 July 2001, Pages 191–212

Guan, B., Molotch, N. P., Waliser, D. E., Fetzer, E. J., Neiman, P. J., 2013. The 2010/2011 snow season in California's Sierra Nevada: Role of atmospheric rivers and modes of large-scale variability. *Water Resources Research*. 49, 6731-6743.

Johnson, K. R., Hu, C. Y., Belshaw, N. S., Henderson, G. M., 2006. Seasonal trace-element and stable-isotope variations in a Chinese speleothem: The potential for high-resolution paleomonsoon reconstruction. *Earth and Planetary Science Letters.* 244, 394-407.

Mass, C., Skalenakis, A., Warner, M., 2011. Extreme precipitation over the West Coast of North America: Is there a trend? *Journal of Hydrometeorology.* 12, 310-318.

Oster, J.L., Montañez, I.P., Mertz-Kraus,R., Sharp, W.D., Cooper, K. M., 2009. Late Pleistocene California droughts during deglaciation and Arctic warming. *Earth and Planetary Science Letters*. 288 (2009) 434–443

Oster, J.L., Montañez, I.P., Mertz-Kraus,R., Sharp, W.D., Stock, G. M., Spero, H.J., Tinsley, J., Zachos, J.C., 2014. Millennial-scale variations in western Sierra Nevada precipitation during the last glacial cycle MIS 4/3 transition. *Quaternary Research,* Volume 82, Issue 1, July, Pages 236-248

Ralph, F. and Dettinger, M., 2012. Historical and national perspectives on extreme West Coast precipitation associated with atmospheric rivers during December 2010. *Bulletin of the American Meteorological Society*. 93, 783-790.

Serreze, M. C. and Barry, R. G., 2011. Processes and impacts of Arctic amplification: A research synthesis. *Global and Planetary Change*. 77, 85-96.

Stefels, J. and van Boekel, W. H. M., 1993. Production of DMS from dissolved DMSP in axenic cultures of the marine phytoplankton species Phaeocystis. *Marine Ecology Progress Series*.Vol. 97: 11-18,1993.

Tremaine, D. M., Froelich, P. N., 2013. Speleothem trace element signatures: A hydrologic geochemical study of modern cave dripwaters and farmed calcite. *Geochimica et Cosmochimica Acta*, 121 (2013) 522–545.

Warner, M. D., Mass, C. F., Salathé Jr, E. P., 2012. Wintertime extreme precipitation events along the Pacific Northwest coast: Climatology and synoptic evolution. *Monthly Weather Review*. 140, 2021-2043.

Welker, J. M., 2000. Isotopic ($\delta^{18}O$) characteristics of weekly precipitation collected across the United States: An initial analysis with application to water source studies. *Hydrological Processes*. 14: 1449-1464.

Wick, G. A., Neiman, P. J., Ralph, F. M., 2013. Description and validation of an automated objective technique for identification and characterization of the integrated water vapor signature of atmospheric rivers. *Geoscience and Remote Sensing, IEEE Transactions On.* 51, 2166-2176.

Wynn, P. M., Fairchild, I. J., Baker, A., Frisia, S., Borsato, A., Baldini, J. U.L., McDermott, F., 2008. Isotopic archives of sulphate in speleothems. *Geochimica et Cosmochimica Acta,* 72, 2465–2477

Yoshimura, K., Kanamitsu, M., Dettinger, M., 2010. Regional downscaling for stable water isotopes: A case study of an atmospheric river event. *Journal of Geophysical Research: Atmospheres* (1984–2012). 115.

APPENDEX

A1. Thin Sections

Precise chronologies of speleothem records for the calibration period are most critical as it directly determines the interpretation and quality of the calibration statistics. Obtaining precise chronologies for stalagmites younger than ~2000 years is difficult as concentration of ^{230}Th is low and close to the detection limit. As a result, age uncertainties for young speleothems with low U can be in the range of 5 to 10% of the absolute age, which limits the ability of correlating speleothem-based time series with other records, such as instrumental time series and annually-precise tree ring records. By counting annually laminated bands, radiometric chronologies can be significantly improved. In caves, such as Crystal Cave, where there is strong seasonality in the overlying climate, annually laminated stalagmites should be expected and offer a tool for resolving annual chronological markers. Fluorescence imaging allows molecules beyond the resolution limit of the light microscope to be visualized. Applying and analyzing transmitted and fluorescent light to thin sections obtained from a stalagmite can be beneficial toward the identification of variations in the lamina. Variations in the crystalline structure, including organic compounds, mineralogy, shape, size, clarity, and orientation of crystals can reveal annual/countable laminations to be used to improve the absolute U/Th dated age model chronological uncertainties and provide information of the environmental conditions at the time the speleothem was formed.

To conduct petrographic analysis on CRC-3, I cut a layer of calcite off one half of the stalagmite approximately 4 mm wide and had 4 thin sections prepared. Utilizing a Nikon polarizing

microscope, I examined the top thin section (30 mm) representing ~ 350 years and observed dark lamina to appear approximately every ~ 6 to 7 years (Fig. A1). Further examination under ultra-violet light (~253.7 and 365 nm), showed a blue-green fluorescence was also emitted with similar spacing.

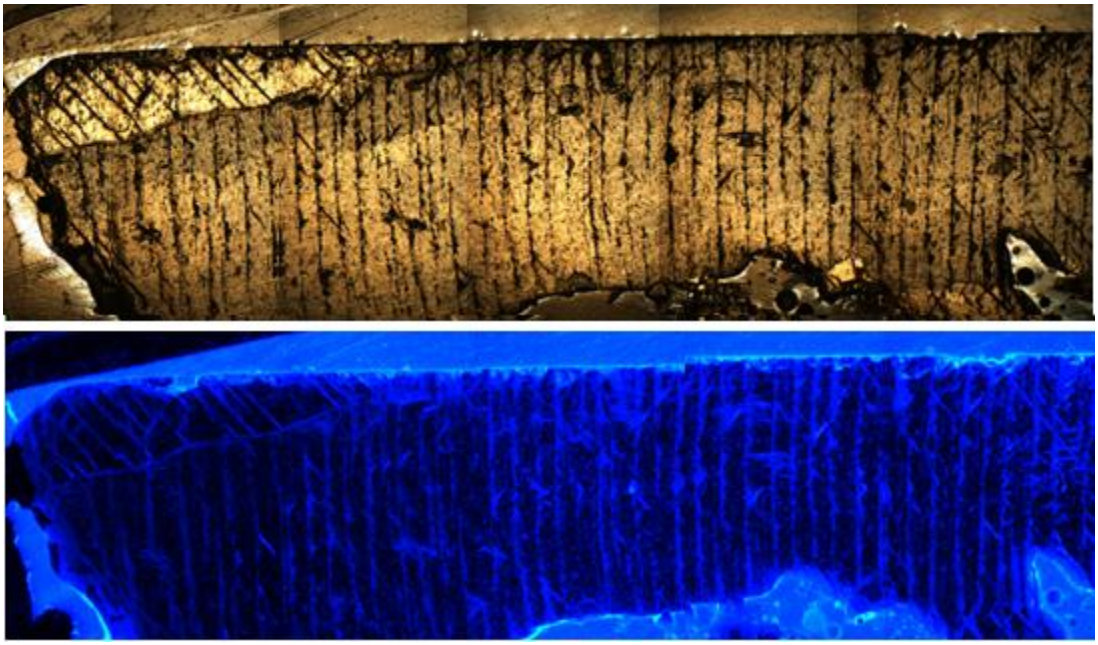

Figure A1. CRC-3 top thin section (30 mm) showing transmitted light (top) and fluorescent light emitted (bottom).

Baker et al., (2008) showed that luminescence demonstrates a strong relationship between the excitation and emission wavelengths and both the extent of soil humification and mean annual rainfall. Humification describes topsoil that contains organic matter, such as humic and fulvic acids, organic acids transported by groundwater, that become incorporated into speleothem calcite and produce luminescence in the blue (list wavelength range) spectral region (Baker, et al. 2008). A study of fluorescence intensity variations in speleothems suggests that variations in

groundwater discharge, in which the first groundwater to infiltrate the soil during the season is comprised of 'old' stored groundwater, versus water that infiltrates the soil later, has a higher organic acid concentration (Baker, et al. 2008). This suggests that florescent organic acids may provide a proxy for past moisture variations, with the exception of rapid periods of high rainfall intensity or quantity (Baker, et al. 2008; Genty, et al. 1997). Therefore, one possible explanation for the darkened lamina in CRC-3 is that organic acids were introduced from the overlying soil and vegetation by percolation of waters after high rainfall events ~ every 6 years, suggestive of El Nino (~2 to 7 years). Annual precipitation recorded near the cave at ASH Mountain (36.48 °N; 118.83 °W; 1708 m) from 1926 to 2011, showed a great range with the highest (1297 mm) occurring in 1982 and the lowest (292 mm) occurring in 1959 (http://cdec.water.ca.gov). Over the 85 year long record, eight years had greater than 1000 mm precipitation delivered, with an average of eleven year intervals, and fourteen years had greater than 900 mm precipitation delivered, with an average of ~ six years, suggesting these large precipitation events may have contributed to produce the organic signal.

Another possible cause for the darkened and luminescent organic acid lamina can be due to a major defense mechanism in some plant reactions to stress conditions. Forest fires create the conditions for many unfavorable ecological factors such as high temperature, low moisture, increased evaporation and significant changes in soil composition. A recent study shows the total organic acid content was higher for all plants in forests affected by fire (Nešić, et al. 2010). However, another study that developed a 3000 year chronology of fire events in Giant Forest, found the mean fire-free intervals occurred about every 16 years and based on fire scars only, about every 22 years, over the analyzed 1500 yr period (Swetnam, et al. 2009). More research is

needed to determine the cause of the CRC-3 darkened and fluorescent lamina, though it appears that the humic acids in the overlying soil and vegetation transported by the percolation of waters after high rainfall events is the likely cause.

A2. NADP sites precipitation amounts and corresponding $\delta^{18}O$ values

Table A1. NADP sites precipitation amounts and corresponding $\delta^{18}O$ values.

	CA42	CA66	CA75	CA99		CA42	CA66	CA75	CA99
DATE ON	**mL**	**mL**	**mL**	**mL**		**$\delta^{18}O$**	**$\delta^{18}O$**	**$\delta^{18}O$**	**$\delta^{18}O$**
12/28/2004	5969	3897	4669	11754		-8.62	-6.87	-13.19	-11.34
1/4/2005	16000	3501	13708	12158		-7.79	-6.68	-11.58	-10.66
1/11/2005		158		546			-7.85		-14.5
1/18/2005				436					-9.17
1/25/2005	2102	758	3835	5718		-4.97	-3.76	-9.98	-10.94
2/1/2005	321		142			-2.6		-6.44	
2/8/2005	5397	1400	612	446		-19.03	-9.75	-17.92	-20.7
2/15/2005	16000	3822	5140	10223		-9.62	-9.28	-15.48	-15.46
2/22/2005	2644	923	2045	2603		-10.93	-7.6	-12.9	-13.61
3/1/2005	596	1414	343	751		-5.59	-6.38	-12.2	-9.37
3/15/2005	1024	1700	10100	8293		-7.94	-3.61	-9.3	-8.88
3/22/2005	2184	1762	5677	8573		-5.39	-6.83	-11.58	-11.45
3/29/2005		340	953	1092			-6.54	-9.71	-9.33
4/5/2005		439	2172	2136			-1.61	-8.07	-8.29
4/19/2005		168	920	248			-3.48	-7.51	-4.59
4/26/2005	1710	1183	2019	1682		-7.34	-7.33	-11.22	-8.84
5/3/2005	2271	682	6241	8213		-8.7	-4.03	-12.22	-10.33
5/10/2005			2337	2423				-10.7	-8.63
6/14/2005				568					-6.76
8/9/2005			233	201				-6.04	-1.67
9/13/2005	1080					-3.58			
9/20/2005			586	435				-6.86	-6.65
10/12/2005	4175			635		-7.23			-8.18
10/18/2005			330	1854				-9.7	-10.63
10/26/2005			302	302				-5.16	-8.32

11/8/2005		320	444	268		-6.77	-10.28	-9.98
11/22/2005		278	500	1745		-2.88	-8.73	-8.21
11/29/2005		1305	6688	10495		-6.48	-12.48	-11.74
12/6/2005	188		138	632	-12.87		-11.44	-15.3
12/13/2005		723	6125	6180		-6.31	-10.6	-10.05
12/20/2005		936	2959	7029		-6.43	-14.27	-11.17
12/27/2005	6564	7360	13519	13830	-5.54	-11.44	-14.06	-13.65
1/3/2006				413				-11.77
1/10/2006		428	2741	3100		-7.27	-11.36	-12.37
1/17/2006			1518	2859			-8.18	-9.41
1/24/2006			635	947			-9.99	-9.75
1/31/2006				153				-4.4
2/14/2006	1317	351	1818	1153	-8.66	-9.75	-11.53	-16.08
2/22/2006	8112	2559	5690	8503	-12.13	-5.07	-13.1	-9.47
2/28/2006	1206	1820	4447	6730	-7.25	-3.92	-13.57	-10.4
3/6/2006	2386	2618	2734	3016	-7.22	-9.66	-12.19	-12.81
3/14/2006	4933	1700	3630	3777	-7.88	-7.56	-11.31	-12.65
3/21/2006	4633	469	5446	4515	-7.25	-3.92	-16.82	-10.4
3/29/2006	1813	3251	9499	7488	-6.31	-6.17	-14.54	-12.91
4/4/2006	6879	1585	4764	4553	-8.32	-8.36	-11.05	-10.84
4/11/2006	3064	303	3682	6052	-9.04	-3.76	-9.49	-8.89
4/18/2006	441		894	1140	-4.71		-6.99	-6.65
5/17/2006	1393	1969	1747	2375	-9.36	-8.12	-12.11	-13.48
6/13/2006				289				-7.01
7/18/2006	180	425	571		1.45	-3.01	0.41	
9/26/2006			835	785			-17.88	-13.62
10/3/2006		1092		1814		-6.88		-9.17
10/10/2006	235		445		-4.21		-9.17	
10/17/2006			1242				-8.82	
10/31/2006				175				-4.82
11/7/2006		956	1150	2529		-3.92	-8.24	-8.73
11/21/2006	172	163	296	1203	-4.65	-4.43	-13.4	-11.73
12/5/2006	991	2364	2663	3401	-7.92	-8.57	-13.81	-13.52
12/13/2006	1103		1480	985	-5.28		-10.43	-8.03
12/19/2006		654	3271			-8.58	-13.25	
12/26/2006	147	516	213	2772	-4.28	-7.46	-10.52	-12.59
1/3/2007	473	350	1798	2666	-4.5	-4.04	-7.76	-7.44

1/9/2007	178		480		-4.19		-10.29	
1/16/2007		337				-8.83		
1/23/2007	495	879	400		-9.18	-7.32	-14.18	
2/6/2007	1575	984	5154	7418	-6.4	-5.34	-12.47	-10.94
2/15/2007	1448		295	176	-10.04		-7.93	-8.05
2/21/2007	3116	1954	4381	9033	-6.59	-7.3	-11.12	-10.47
2/27/2007		817	1054	797		-8.51	-10.98	-16.36
3/13/2007	524				-4.29			
3/23/2007	241	325	4095	3057	-4.61	-5.08	-7.63	-8.95
3/27/2007			946				-7.63	
4/10/2007		342	1529	1135		-7.11	-10.4	-9.89
4/17/2007	2204	1012	2728	3215	-10.62	-11.12	-12.11	-13.25
5/1/2007			352	833			-7.67	1.7
9/18/2007	1373	973	1031	1030	-4.14	-5.03	-10.54	-9.32
10/2/2007			979	234			-9.21	-11.03
10/9/2007	360	471	325	779	-5.05	-4.29	-6.4	-8.54
10/16/2007		423		405		-2.53		-4.89
10/22/2007			386	671			-11.63	-11.2
11/6/2007		197	1505	715		-4.06	-10.24	-7.81
11/26/2007	2668				-13.95			
12/4/2007	16000	459	5218	3953	-5.52	-4.6	-12.83	-11.18
12/11/2007		306	1189	983		-10.04	-11.89	-12.65
12/18/2007	1821	230	4827	4896	-8.3	-7.88	-14.03	-15.34
12/24/2007			156	176			-10.28	-18.81
12/31/2007			12186	11998			-11.24	-11.76
1/2/2008	13473	5198			-6.95	-6.24		
1/8/2008		297	364	845		-4.07	-12.72	-10.47
1/15/2008		1936		345		-8.59		-8.46
1/22/2008	13014	4929	5019	9945	-9.61	-9.87	-15.06	-16.88
1/29/2008		1452	2449	6110		-4.47	-14.79	-12.38
2/19/2008	3221	2355	9128	10589	-4.45	-5.6	-9.09	-9.57
3/11/2008	252	558	1180	738	-6.18	-7.8	-8.33	-7.33
3/25/2008	188		1553		-3.69		-14.15	
4/1/2008		177				-5.92		
4/22/2008				171				-7.92
4/29/2008				135				-3.74
5/20/2008	3544	196	1840	2384	-7.22	-4.38	-12.05	-9.78

5/27/2008				758				-8.77
7/8/2008	195				-6.25			
9/9/2008			250	2244			-2.8	-7.34
9/23/2008			242				-1.51	
9/30/2008		179	1625			-3.06	-9.2	
10/14/2008		238				-0.83		
10/28/2008		435	5429	9190		-3.01	-10.07	-9.14
11/4/2008	325	164	1213	1501	-3.89	-6.77	-10.73	-9.17
11/25/2008	3858	1713	1327	693	-16.55	-20.35	-22.68	-20.47
12/9/2008	4094	1010	2418	1661	-10.56	-7.29	-11.63	-11.57
12/16/2008	1752	339	2706	2559	-11.5	-6.68	-14.75	-6.39
12/24/2008	2525	585	4716	4805	-6.82	-6.5	-11.25	-11.97
12/30/2008			298	1091			-10.73	-9.34
1/20/2009	1046	2764	9042	10967	-7.19	-7.37	-11.87	-13.27
2/3/2009	9985	1751	3192	3207	-7.61	-9.22	-14.16	-14.73
2/12/2009	4618	3617	3731	5126	-8.37	-9.82	-14.63	-18.02
2/17/2009		595	2574	6210		-11.55	-19.07	-20.44
2/24/2009	950	747		3185	-4.37	-6.14		-9.5
3/3/2009		971	2229	4943		-5.77	-9.38	-9.54
3/17/2009	1165	910	1808	3679	-6.19	-5.51	-9.59	-9.93
4/7/2009	716	753	3369	3498	-4.31	-7.42	-9.78	-12.2
4/14/2009			406	301			-8.37	-9.63
4/28/2009		151	2775	6335		-12.17	-17.44	-15.51
5/26/2009			175				-6.32	
6/2/2009			1705	2824			-13.75	-11.45
6/9/2009			357				-8.91	
6/16/2009			141				-5.95	
8/18/2009			497	336			-0.85	-5.15
9/8/2009		198				-3.82		
9/29/2009	3541				-3.95			
10/6/2009		754	1339	664		-7.52	-17.02	-16.85
10/13/2009		2698	12309	11289		-4.32	-7.2	-9.38
11/10/2009			395	504			-10.92	-9.46
11/17/2009				584				-7.59
11/24/2009	328			199	-8.44			-9.77
12/1/2009	2439	293	1838		-13.47	-7.66	-18.18	
12/8/2009	6668	2587	9170	11108	-6.77	-6.55	-10.61	-11.79

12/15/2009	293	277	1832	2728	-6.89	-3.73	-10.85	-10.21
12/22/2009		273	321	641		-8.28	-13.58	-12.44
12/29/2009			674				-15.01	
1/5/2010		154				-3.22		
1/12/2010	7046	4226	4218	3804	-8.07	-8.49	-13.12	-12.94
1/20/2010	7054	5218	-1000	3249	-10.12	-10.38	-14.7	-15.05
1/26/2010	494	753			-13.08	-12.59		
2/2/2010	5272	2095	5088	3687	-9.22	-7.82	-13.74	-13.13
2/9/2010	2763			189	-13.9			-17.96
2/16/2010	532	236	3007	1508	-7.93	-3.24	-10.59	-10.77
2/23/2010	3976	4179	6955	8043	-8.31	-7.62	-14.58	-13.38
3/2/2010	1694	1177	3398	3660	-8.63	-8.93	-11.17	-11.73
3/9/2010		395	2290	3268		-5.94	-12.67	-12.28
3/23/2010			3495	621			-9.86	-7.02
3/30/2010	2117	1757		6270	-5.05	-5.78		-11.99
4/6/2010	2406	1332	2761	4135	-6.64	-7.94	-12.77	-12.25
4/13/2010		1115	128			-10.62	-10.93	
4/20/2010	1428	518	3088	3129	-7.29	-6.14	-11.78	-13.77
4/27/2010		197	3370	1762		-1.37	-9.07	-9.39
5/4/2010		236	517	1848		-4.41	-11.34	-11.1
5/11/2010			873	1509			-15.71	-12.73
5/24/2010			233	3014			-3.97	-8.55
9/28/2010	424		1130	5090	-5.34		-10.22	-13.41
10/5/2010	672	422	388	464	-4.71	-8.49	-9.66	-9.39
10/12/2010		202	336	406		-4.51	-4.49	-4.9
10/19/2010	352	597	1853	7957	-2.96	-1.7	-5.61	-6.53
10/26/2010	209	129	1683	975	-2.75	-6.57	-12.17	-10.27
11/2/2010		782	2471	2312		-4.8	-10.38	-9.95
11/9/2010				298				-5.61
11/16/2010	484	1952	3267	16000	-6.09	-9.36	-11.21	-12.58
11/23/2010		357	2539	3270		-4.1	-13.16	-14.18
11/30/2010	1602	1122	1873	3346	-13.32	-8.61	-14.15	-15.46
12/7/2010				567				-8.64
12/14/2010	16000	3354	16000	14080	-9.66	-11.89	-16.89	-14.04
12/19/2010				2312				-16.98
12/21/2010	10153	1530	3481	2881	-13.37	-17.94	-24.31	-21.18
12/28/2010	2202	5558	16000	9416	-10.95	-11.56	-19.27	-19.08

1/11/2011				619				-17.21
1/25/2011	286	539	1109	1505	-4.07	-5.93	-9.81	-11.4
2/15/2011	6371	5391	4616	7796	-7.58	-8.95	-11.33	-11.15
2/22/2011	5194	638	1907	2543	-8.69	-6.7	-13.56	-11.55
3/1/2011	482		3951	4420	-4.14		-10.6	-10.01
3/8/2011				216				-8.74
3/15/2011	7981	4577	5171	10532	-9.39	-14.83	-14.23	-11.57
3/22/2011	2589	2748	3526	5441	-6.56	-5.13	-12.96	-12.47
4/5/2011	292	167	1855	1631	-7.17	-4.55	-13.69	-15.36
4/19/2011			337	2001			-7.55	-9.94
5/3/2011	154		852		-3.48		-7.03	
5/10/2011	619	635	1965	2891	-4.26	-5.78	-11.57	-10.68
5/17/2011	610	265	1459	3079	-5.46	-4.09	-9.46	-10.34
5/24/2011			1299	1091			-10.51	-9.59
5/31/2011		529	1425	3403		-4.96	-12.55	-12.49
6/28/2011				5301				-14.71
7/26/2011			230				-7.15	
9/6/2011				2508				-8.97
9/13/2011			219				-2.36	
10/4/2011	3149	1213	7023	5375	-4.97	-6.18	-9.78	-11.54
11/1/2011	1476	1183	2243	1390	-6.26	-6.67	-8.97	-9.95
11/8/2011			1434	542			-19.16	-14.74
11/15/2011		637	768	736		-8.56	-17.27	-18.31
11/8/2011		437				-7.89		
11/15/2011	1514				-7.69			

A3. Extreme Drip Logger Events

A3. 1Extreme Drip Logger Event 1

Table A2.1 Temperature and precipitation at Giant Forest.

	Temperature		Precipitation
Date	**°C**		**mm**
12/14/2010	6.7		0.0
12/15/2010	0.0		2.5
12/16/2010	-1.7		0.0
12/17/2010	0.6		68.6
12/18/2010	1.1		177.8
12/19/2010	1.1		144.8
12/20/2010	-1.7		33.0
Average	**0.9**	**Total**	**426.7**

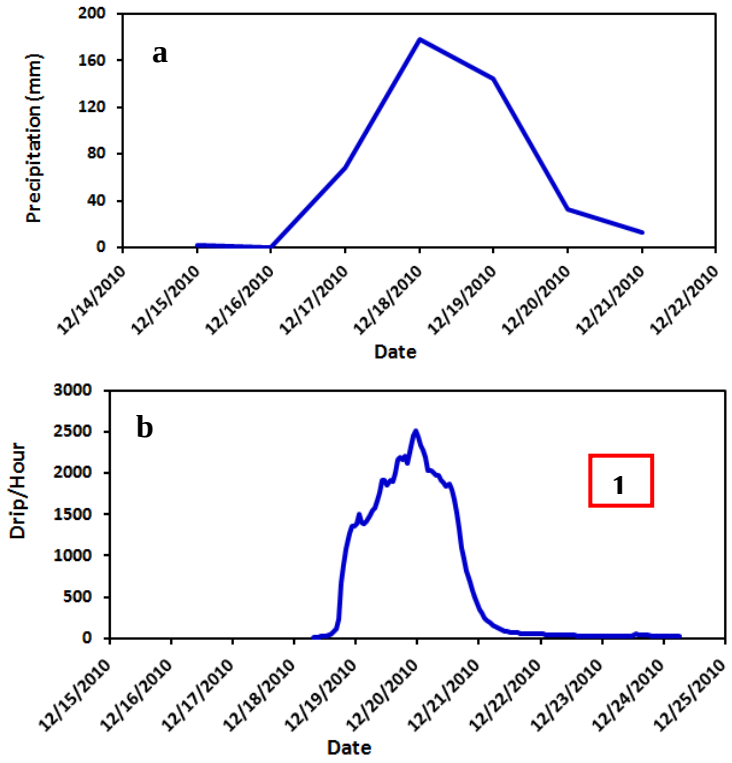

Figure A2. Giant Forest CDEC precipitation data shows the peak amount occurs on 12/18/2010 (177.8 mm) (http://cdec.water.ca.gov (Table A2.1; Fig. A2a), **b.** Driptych drip logger data shows the first extreme event 1) drips/hour started to increase December 18, 2010 and continued to increase until the peak December 19, at 23:16 before decreasing (Table A2.1a; Fig. A2b).

Table A.2.1a. Drip logger drips/hour for the first extreme event peaking December 19, 2010.

Date	Drip/hour	Date	Drip/hour	Date	Drip/hour	Date	Drip/hour
12/17/2010 23:16	11	12/19/2010 17:16	2189	12/21/2010 11:16	80	12/23/2010 5:16	28
12/18/2010 0:16	11	12/19/2010 18:16	2156	12/21/2010 12:16	76	12/23/2010 6:16	29
12/18/2010 1:16	12	12/19/2010 19:16	2206	12/21/2010 13:16	70	12/23/2010 7:16	27
12/18/2010 2:16	11	12/19/2010 20:16	2121	12/21/2010 14:16	66	12/23/2010 8:16	28
12/18/2010 3:16	12	12/19/2010 21:16	2324	12/21/2010 15:16	62	12/23/2010 9:16	27
12/18/2010 4:16	12	12/19/2010 22:16	2454	12/21/2010 16:16	59	12/23/2010 10:16	27
12/18/2010 5:16	12	12/19/2010 23:16	2506	12/21/2010 17:16	57	12/23/2010 11:16	29
12/18/2010 6:16	13	12/20/2010 0:16	2446	12/21/2010 18:16	56	12/23/2010 12:16	39
12/18/2010 7:16	14	12/20/2010 1:16	2337	12/21/2010 19:16	54	12/23/2010 13:16	48
12/18/2010 8:16	14	12/20/2010 2:16	2279	12/21/2010 20:16	53	12/23/2010 14:16	46
12/18/2010 9:16	15	12/20/2010 3:16	2191	12/21/2010 21:16	50	12/23/2010 15:16	41
12/18/2010 10:16	18	12/20/2010 4:16	2023	12/21/2010 22:16	49	12/23/2010 16:16	38
12/18/2010 11:16	19	12/20/2010 5:16	2033	12/21/2010 23:16	49	12/23/2010 17:16	35
12/18/2010 12:16	27	12/20/2010 6:16	1995	12/22/2010 0:16	48	12/23/2010 18:16	33
12/18/2010 13:16	34	12/20/2010 7:16	1968	12/22/2010 1:16	47	12/23/2010 19:16	31
12/18/2010 14:16	56	12/20/2010 8:16	1966	12/22/2010 2:16	46	12/23/2010 20:16	29
12/18/2010 15:16	79	12/20/2010 9:16	1919	12/22/2010 3:16	44	12/23/2010 21:16	30
12/18/2010 16:16	110	12/20/2010 10:16	1887	12/22/2010 4:16	42	12/23/2010 22:16	30
12/18/2010 17:16	224	12/20/2010 11:16	1846	12/22/2010 5:16	41	12/23/2010 23:16	28
12/18/2010 18:16	670	12/20/2010 12:16	1874	12/22/2010 6:16	41	12/24/2010 0:16	26
12/18/2010 19:16	883	12/20/2010 13:16	1797	12/22/2010 7:16	39	12/24/2010 1:16	25
12/18/2010 20:16	1079	12/20/2010 14:16	1673	12/22/2010 8:16	36	12/24/2010 2:16	25
12/18/2010 21:16	1275	12/20/2010 15:16	1515	12/22/2010 9:16	35	12/24/2010 3:16	24
12/18/2010 22:16	1363	12/20/2010 16:16	1322	12/22/2010 10:16	34	12/24/2010 4:16	24
12/18/2010 23:16	1356	12/20/2010 17:16	1097	12/22/2010 11:16	33	12/24/2010 5:16	23
12/19/2010 0:16	1380	12/20/2010 18:16	958	12/22/2010 12:16	33	12/24/2010 6:16	18
12/19/2010 1:16	1507	12/20/2010 19:16	809	12/22/2010 13:16	33	12/24/2010 7:16	19
12/19/2010 2:16	1395	12/20/2010 20:16	682	12/22/2010 14:16	32	12/24/2010 8:16	20
12/19/2010 3:16	1393	12/20/2010 21:16	582	12/22/2010 15:16	31	12/24/2010 9:16	20
12/19/2010 4:16	1419	12/20/2010 22:16	499	12/22/2010 16:16	29	12/24/2010 10:16	19
12/19/2010 5:16	1488	12/20/2010 23:16	426	12/22/2010 17:16	29	12/24/2010 11:16	20
12/19/2010 6:16	1545	12/21/2010 0:16	353	12/22/2010 18:16	29	12/24/2010 12:16	19
12/19/2010 7:16	1579	12/21/2010 1:16	304	12/22/2010 19:16	29	12/24/2010 13:16	20
12/19/2010 8:16	1658	12/21/2010 2:16	241	12/22/2010 20:16	29	12/24/2010 14:16	19
12/19/2010 9:16	1769	12/21/2010 3:16	208	12/22/2010 21:16	30	12/24/2010 15:16	20
12/19/2010 10:16	1915	12/21/2010 4:16	193	12/22/2010 22:16	30	12/24/2010 16:16	19
12/19/2010 11:16	1912	12/21/2010 5:16	158	12/22/2010 23:16	30	12/24/2010 17:16	19
12/19/2010 12:16	1860	12/21/2010 6:16	135	12/23/2010 0:16	31	12/24/2010 18:16	19
12/19/2010 13:16	1919	12/21/2010 7:16	124	12/23/2010 1:16	30	12/24/2010 19:16	18
12/19/2010 14:16	1905	12/21/2010 8:16	114	12/23/2010 2:16	30	12/24/2010 20:16	18
12/19/2010 15:16	1996	12/21/2010 9:16	94	12/23/2010 3:16	30		
12/19/2010 16:16	2159	12/21/2010 10:16	83	12/23/2010 4:16	27		

During the first recorded extreme drip logger event 1) 12/19/2010, the NADP precipitation collection week, 12/14/2010 to 12/21/2010, showed the average temperature above the cave was 0.9 °C and the total daily CDEC precipitation data recorded was 426.7 mm (Table A2.1; Fig. A2a). The precipitation begins to increase with 68.6 mm on 12/17/2010, peaks at 177.8 mm on

12/18/2010, decreases slightly to 144.8 mm on 12/19/2010 then decreases to 33 mm on 12/20/2010 (Table A2.1; Fig. A2a). The drip logger data for that week shows an average drip rate of ~11 drips/hour prior to the beginning of the extreme event which starts to increase 12/18/2010 at 6:16 pm to 13 drips/hour and continues to increase rapidly to 1507 drips/hour 12/19/2010 at 01:16, hovers around there for a few hours, then finally increases on 12/19/2010 at 08:16 from 1658 drips/hour to its peak at 2506 drips/hour on 12/19/2010 at 23:16 where it then decreases relatively slowly to 1887 drips/hour on 12/20/2010 at 10:16, then rapidly to a slightly higher new drip average of ~17 drips/hour (Table A2.1a; Fig.A2b).

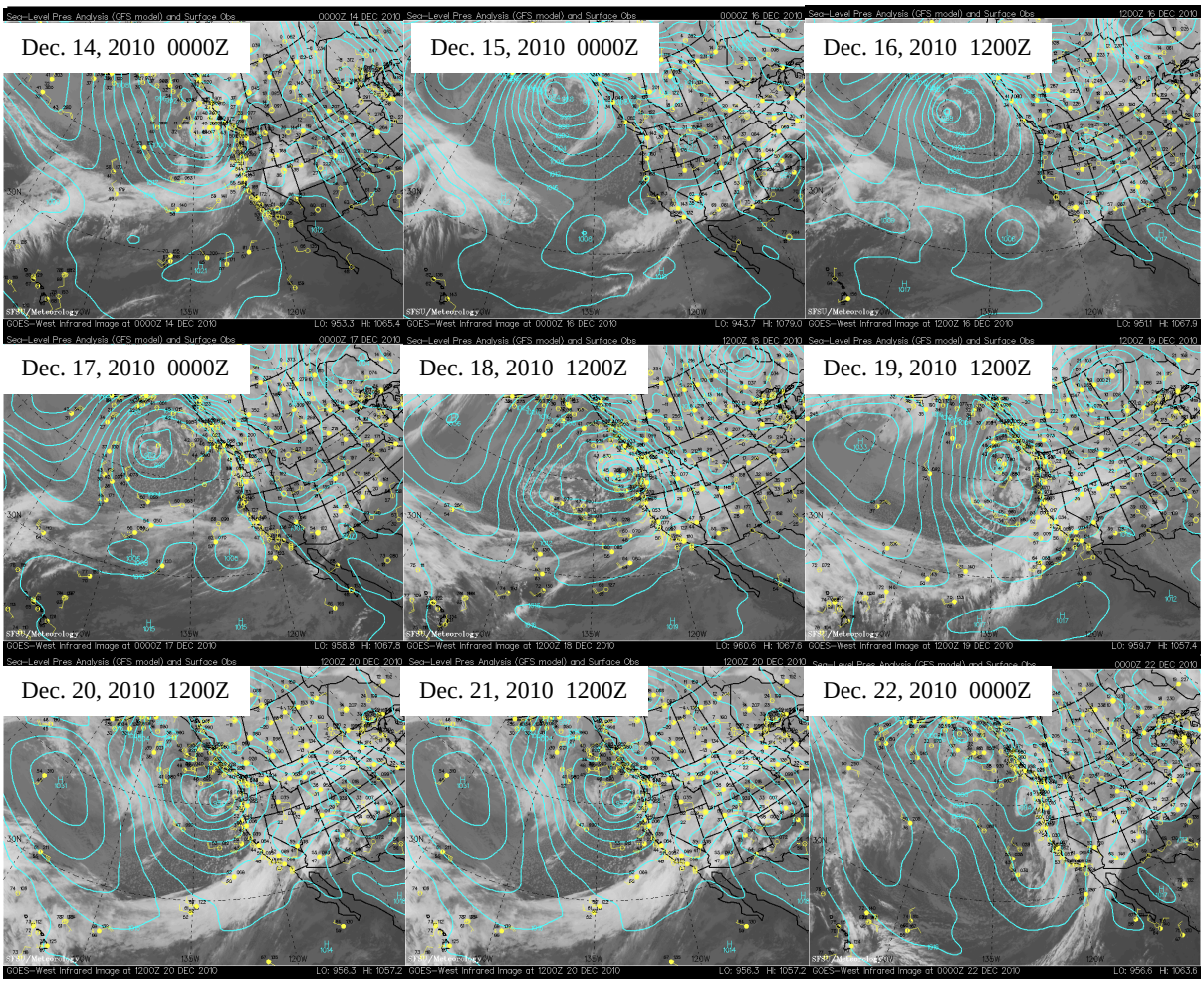

Figure A3. GOES West sea-level pressure analysis (GFS model) and surface observation infrared images from December 14 to December 21, 2010 for the first December extreme drip logger rate increase (http://virga.sfsu.edu/crws/archive/sathts_pac_arch.html)

The GOES West sea-level pressure analysis and surface observation infrared satellite images reveal large amounts of moisture over the Pacific, transported to the California coast, particularly thickening on 12/19/2010 and tapering off on 12/21/2010 (Fig. A3).

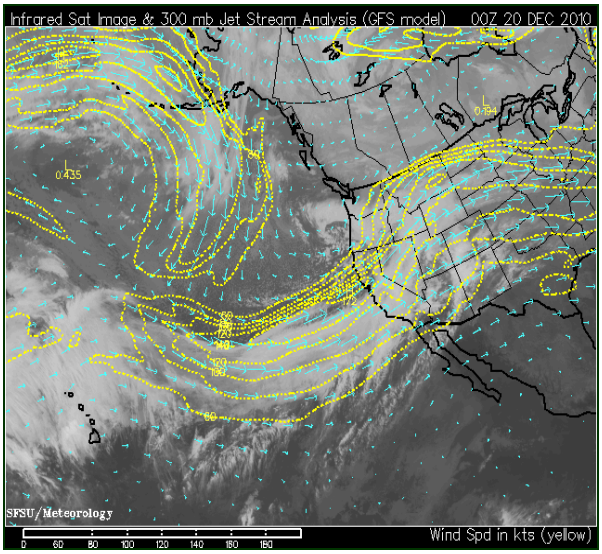

Figure A4. San Francisco State University (SFSU)/ Meteorology infrared satellite image and 300 mb jet stream map (http://virga.sfsu.edu/crws/archive/sathts_pac_arch.html).

The infrared satellite image and 300 mb jet stream map indicates the jet stream is meridional descending sharply from north to south near the Gulf of Alaska and then turning sharply transporting moisture into the California coastline (Fig. A4).

A3.2 Extreme Drip Logger Event 2

Table A2.2. Temperature and precipitation at Giant Forest.

	Temperature		Precipitation
Date	°C		mm
12/28/2010	2.8		20.3
12/29/2010	-2.8		68.6
12/30/2010	-9.4		5.1
12/31/2010	-8.3		7.6
1/1/2011	-2.8		2.5
1/2/2011	-1.7		0.0
1/3/2011	-3.9		7.6
Average	**-3.5**	**Total**	**119.4**

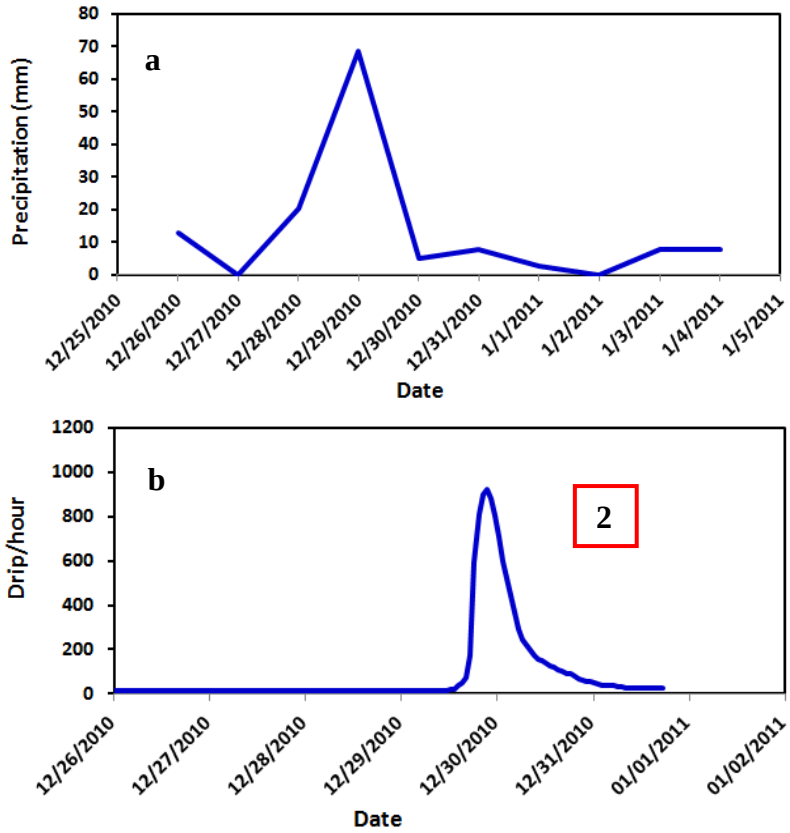

Figure A5. a. Giant Forest CDEC precipitation data shows the peak amount occurs on 12/29/2010 of 68.6 mm (Table A2.2;Fig. A5a), **b.** Driptych drip logger data shows the second extreme event (2) drips/hour started to increase December 29, 2010 about 12:16 h and continued to increase until the peak, late December 29, at 21:16 before decreasing over the next day (Table A2.2a; Fig. A5b).

Table A2.2a. Drip loogger drips/hour for the second extreme event peaking December 29, 2010.

Date	Drip/hour	Date	Drip/hour	Date	Drip/hour	Date	Drip/hour
12/28/2010 21:16	17	12/29/2010 19:16	813	12/30/2010 17:16	93	12/31/2010 15:16	23
12/28/2010 22:16	17	12/29/2010 20:16	900	12/30/2010 18:16	88	12/31/2010 16:16	23
12/28/2010 23:16	17	12/29/2010 21:16	922	12/30/2010 19:16	79	12/31/2010 17:16	23
12/29/2010 0:16	17	12/29/2010 22:16	883	12/30/2010 20:16	67	12/31/2010 18:16	22
12/29/2010 1:16	17	12/29/2010 23:16	804	12/30/2010 21:16	64	12/31/2010 19:16	22
12/29/2010 2:16	16	12/30/2010 0:16	712	12/30/2010 22:16	57	12/31/2010 20:16	23
12/29/2010 3:16	17	12/30/2010 1:16	596	12/30/2010 23:16	53	12/31/2010 21:16	22
12/29/2010 4:16	17	12/30/2010 2:16	524	12/31/2010 0:16	49	12/31/2010 22:16	23
12/29/2010 5:16	17	12/30/2010 3:16	446	12/31/2010 1:16	43	12/31/2010 23:16	22
12/29/2010 6:16	16	12/30/2010 4:16	366	12/31/2010 2:16	40	1/1/2011 0:16	22
12/29/2010 7:16	17	12/30/2010 5:16	290	12/31/2010 3:16	38	1/1/2011 1:16	22
12/29/2010 8:16	16	12/30/2010 6:16	245	12/31/2010 4:16	38	1/1/2011 2:16	21
12/29/2010 9:16	16	12/30/2010 7:16	218	12/31/2010 5:16	35	1/1/2011 3:16	21
12/29/2010 10:16	16	12/30/2010 8:16	197	12/31/2010 6:16	34	1/1/2011 4:16	22
12/29/2010 11:16	16	12/30/2010 9:16	173	12/31/2010 7:16	32	1/1/2011 5:16	21
12/29/2010 12:16	18	12/30/2010 10:16	153	12/31/2010 8:16	27	1/1/2011 6:16	21
12/29/2010 13:16	21	12/30/2010 11:16	151	12/31/2010 9:16	26	1/1/2011 7:16	21
12/29/2010 14:16	38	12/30/2010 12:16	139	12/31/2010 10:16	26	1/1/2011 8:16	21
12/29/2010 15:16	48	12/30/2010 13:16	126	12/31/2010 11:16	25	1/1/2011 9:16	20
12/29/2010 16:16	76	12/30/2010 14:16	119	12/31/2010 12:16	24	1/1/2011 10:16	20
12/29/2010 17:16	173	12/30/2010 15:16	108	12/31/2010 13:16	24	1/1/2011 11:16	20
12/29/2010 18:16	593	12/30/2010 16:16	100	12/31/2010 14:16	24		

A close up view of the drip logger data shows an average drip rate of ~17 drips/hour prior to the beginning of the extreme event which starts to increase 12/29/2010 at 13:16 pm to 21 drips/hour and continues to increase rapidly to the peak rate at 922 drips/hour 12/29/2010 at 21:16, then decreases continuously to a new average of ~20 drips/hour by ~1/1/2011(Table A2.2a; Fig. A5b). During the second recorded extreme drip logger event 2) 12/29/2010, NADP collection week 12/28/2010 to 1/4/2011, the average temperature above the cave was -3.5 °C and the total daily CDEC precipitation data recorded was 119.4 mm (Table A2.2).

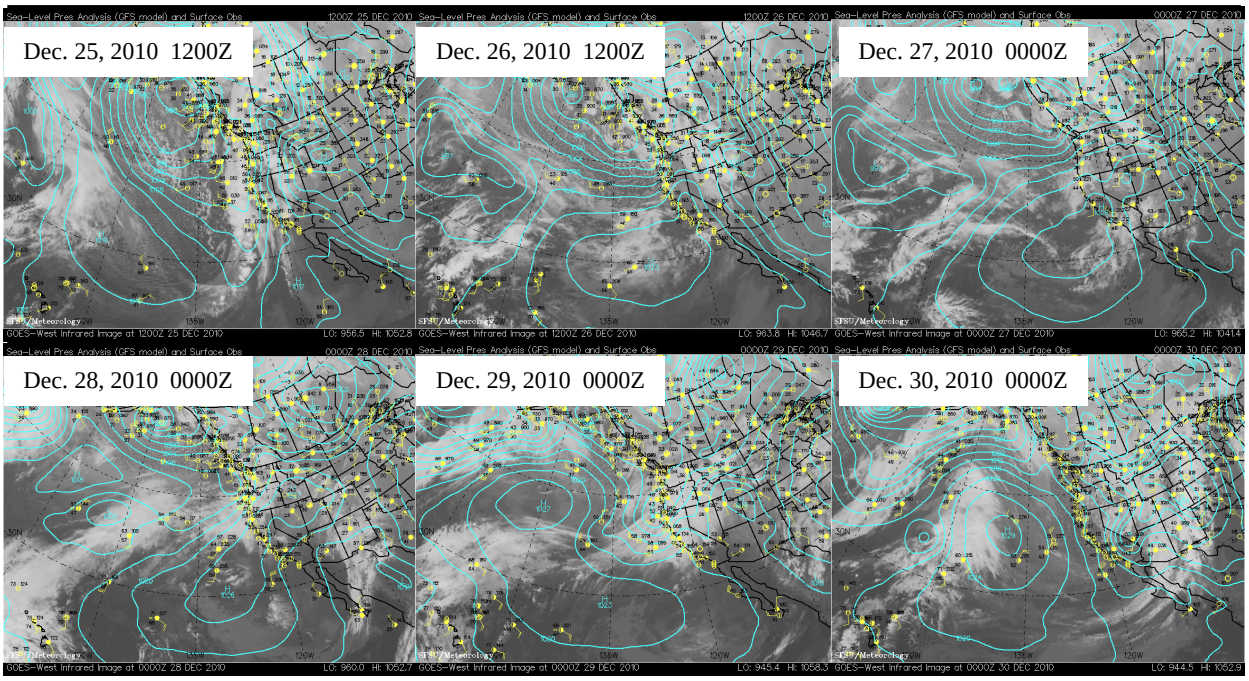

Figure A6. GOES West sea-level pressure analysis (GFS model) and surface observation infrared images from December 25 to December 30, 2010 for the second December extreme drip logger rate increase (12/29/2010) (http://virga.sfsu.edu/crws/archive/saths_pac_arch.html).

The GOES West sea-level pressure analysis and surface observation infrared satellite images indicate the greatest amount of moisture delivered to the Crystal Cave/Giant Forest site appears to be on the 12/29/2010. The satellite images show a high pressure system west of California contributing to moisture being transported to the study site from the higher and mid-latitudes (Fig. A6).

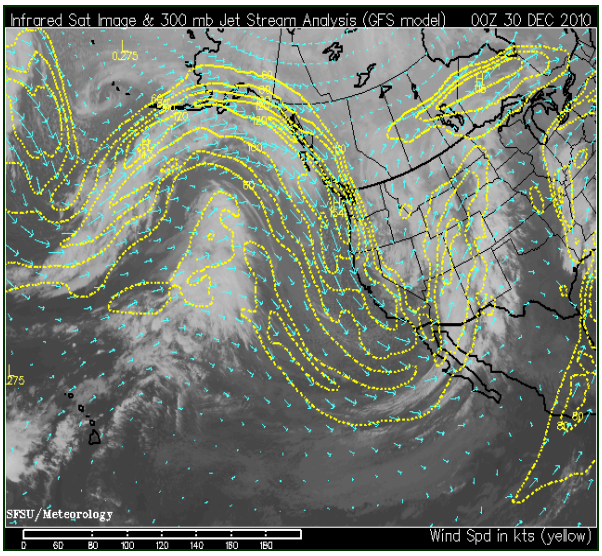

Figure A7. San Francisco State University (SFSU)/ Meteorology infrared satellite image and 300 mb jet stream map (http://virga.sfsu.edu/crws/archive/sathts_pac_arch.html).

The infrared satellite image and 300 mb jet stream map indicates the jet stream is meridional descending sharply from north to south over the California coastline before turning to the east over Baja, CA (Fig. A7).

A3.3 Extreme Drip Logger Event 3

Table A2.3. Temperature and precipitation at Giant Forest.

	Temperature		Precipitation
Date	°C		mm
3/1/2011	2.8		0
3/2/2011	2.8		0
3/3/2011	1.1		0.0
3/4/2011	3.3		10.9
3/5/2011	5.6		0.3
3/6/2011	3.9		0.0
3/7/2011	-1.1		0.0
3/8/2011	-0.6		14.2
Average	**2.2**	**Total**	**25.4**

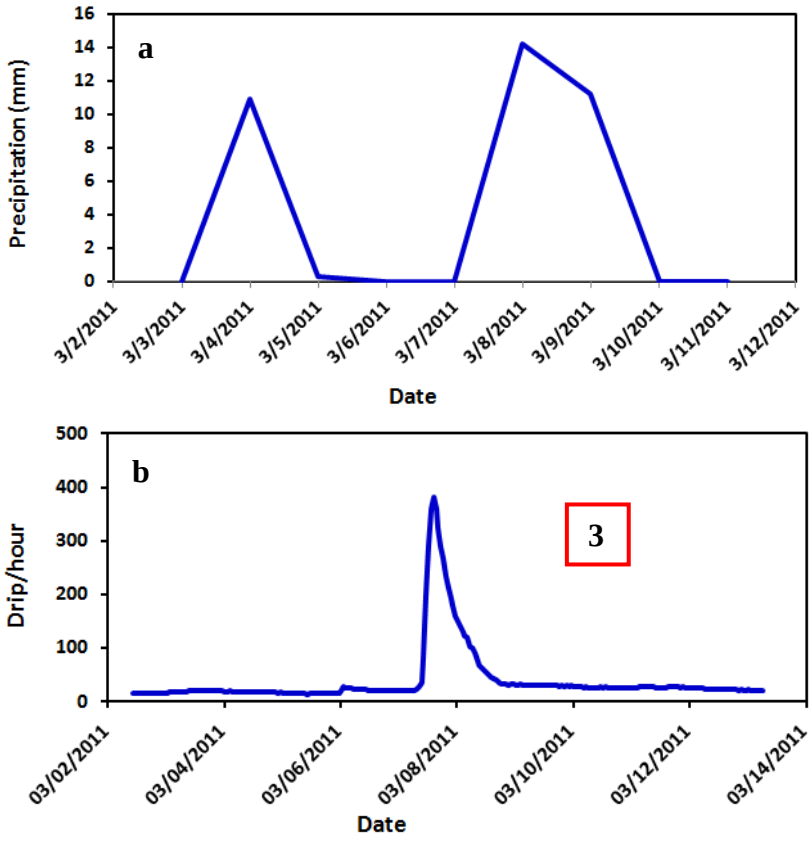

Figure A8. **a**. Giant Forest CDEC precipitation data shows peak amount occurs on 3/4/2011 of 10.9 mm and another on 3/8/2011 of 14.2 mm (Table A2.3; Fig. A8a), **b.** Driptych drip logger data shows the drips/hour of the third extreme event 3) started to increase March 7, 2011 (Table A2.3a; Fig. A8b).

Table A2.3a. Drip loogger drips/hour for the third extreme event peaking March 7, 2011.

Date	Drip/hour	Date	Drip/hour	Date	Drip/hour	Date	Drip/hour
3/5/2011 22:16	16	3/7/2011 1:16	20	3/8/2011 4:16	120	3/9/2011 7:16	30
3/5/2011 23:16	16	3/7/2011 2:16	20	3/8/2011 5:16	102	3/9/2011 8:16	31
3/6/2011 0:16	22	3/7/2011 3:16	20	3/8/2011 6:16	100	3/9/2011 9:16	30
3/6/2011 1:16	27	3/7/2011 4:16	20	3/8/2011 7:16	89	3/9/2011 10:16	31
3/6/2011 2:16	26	3/7/2011 5:16	21	3/8/2011 8:16	76	3/9/2011 11:16	30
3/6/2011 3:16	25	3/7/2011 6:16	20	3/8/2011 9:16	68	3/9/2011 12:16	31
3/6/2011 4:16	25	3/7/2011 7:16	22	3/8/2011 10:16	63	3/9/2011 13:16	30
3/6/2011 5:16	23	3/7/2011 8:16	27	3/8/2011 11:16	58	3/9/2011 14:16	31
3/6/2011 6:16	24	3/7/2011 9:16	35	3/8/2011 12:16	53	3/9/2011 15:16	30
3/6/2011 7:16	23	3/7/2011 10:16	81	3/8/2011 13:16	48	3/9/2011 16:16	30
3/6/2011 8:16	22	3/7/2011 11:16	198	3/8/2011 14:16	46	3/9/2011 17:16	30
3/6/2011 9:16	23	3/7/2011 12:16	293	3/8/2011 15:16	42	3/9/2011 18:16	29
3/6/2011 10:16	22	3/7/2011 13:16	360	3/8/2011 16:16	40	3/9/2011 19:16	30
3/6/2011 11:16	21	3/7/2011 14:16	382	3/8/2011 17:16	36	3/9/2011 20:16	29
3/6/2011 12:16	21	3/7/2011 15:16	358	3/8/2011 18:16	34	3/9/2011 21:16	30
3/6/2011 13:16	20	3/7/2011 16:16	325	3/8/2011 19:16	33	3/9/2011 22:16	29
3/6/2011 14:16	21	3/7/2011 17:16	289	3/8/2011 20:16	32	3/9/2011 23:16	30
3/6/2011 15:16	20	3/7/2011 18:16	267	3/8/2011 21:16	31	3/10/2011 0:16	29
3/6/2011 16:16	21	3/7/2011 19:16	235	3/8/2011 22:16	32	3/10/2011 1:16	28
3/6/2011 17:16	20	3/7/2011 20:16	211	3/8/2011 23:16	32	3/10/2011 2:16	28
3/6/2011 18:16	20	3/7/2011 21:16	192	3/9/2011 0:16	30	3/10/2011 3:16	27
3/6/2011 19:16	21	3/7/2011 22:16	179	3/9/2011 1:16	31	3/10/2011 4:16	26
3/6/2011 20:16	20	3/7/2011 23:16	160	3/9/2011 2:16	32	3/10/2011 5:16	27
3/6/2011 21:16	20	3/8/2011 0:16	151	3/9/2011 3:16	31	3/10/2011 6:16	26
3/6/2011 22:16	20	3/8/2011 1:16	141	3/9/2011 4:16	31	3/10/2011 7:16	25
3/6/2011 23:16	21	3/8/2011 2:16	131	3/9/2011 5:16	31	3/10/2011 8:16	25
3/7/2011 0:16	20	3/8/2011 3:16	123	3/9/2011 6:16	30		

A close up zoomed in view of the drip logger data for that week shows an average drip rate of ~20 drips/hour prior at the beginning of the extreme event which starts to increase 3/7/2011 ~8:16 h to 27 drips/hour and continues to increase rapidly to the peak rate at 382 drips/hour 3/7/2011 14:16 h, then decreases rapidly to a new average of ~25 drips/hour by 3/10/2011 (Table A2.3a; Fig. A8b).

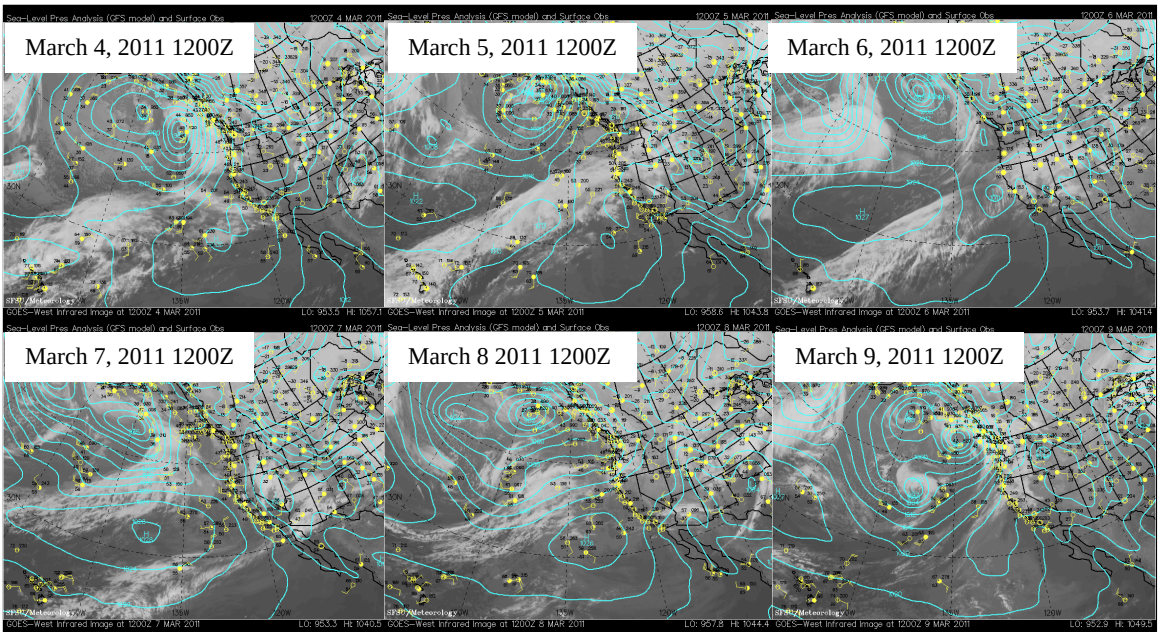

Figure A9. GOES West sea-level pressure analysis (GFS model) and surface observation infrared images from March 4 to March 9, 2011 for the third extreme drip logger rate increase (http://virga.sfsu.edu/crws/archive/sathts_pac_arch.html).

The GOES West sea-level pressure analysis and surface observation infrared satellite images indicate that the greatest amount of moisture delivered to the Crystal Cave/Giant Forest site appears to be on 3/5/2011 and 3/6/2011 (Fig. A9). This is consistent with the other two large events in which it took one to two days for the precipitation to be registered by the data logger in the cave (Table A2.3a). On 3/6/2011, the satellite images show a low pressure system just west of California and another low in the Gulf of Alaska, while on 3/7/2011, the low shifts to a location over the SWUS and the strengthening high becomes conducive for contributing to moisture being transported to the study site from the mid-latitudes (Fig A9).

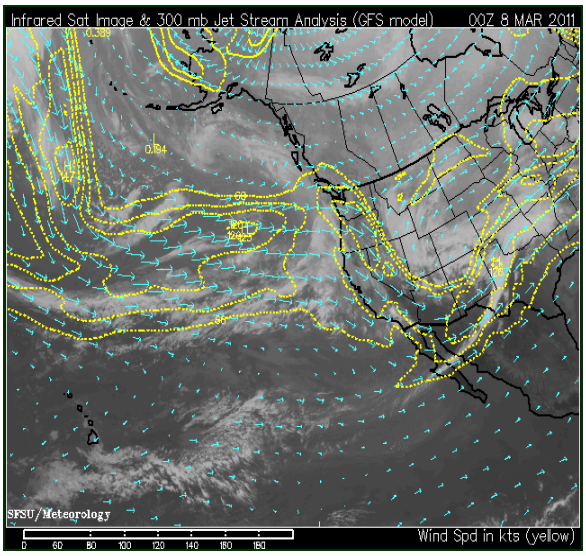

Figure A10. San Francisco State University (SFSU)/ Meteorology infrared satellite image and 300 mb jet stream map (http://virga.sfsu.edu/crws/archive/sathts_pac_arch.html).

The infrared satellite image and 300 mb jet stream map indicates the jet stream is more zonal across the Pacific basin, from north to south over the California coastline (Fig. A10) before turning to the east over Baja, CA.

Table A2.4. Temperature and precipitation at Giant Forest.

	Temperature		Precipitation
Date	°C		mm
12/21/2010	-1.1		12.7
12/22/2010	0.0		27.9
12/23/2010	-0.6		2.5
12/24/2010	5.0		5.1
12/25/2010	6.7		2.5
12/26/2010	-2.8		12.7
12/27/2010	0.0		0.0
Average	**1.3**	**Total**	**83.8**

Analysis of the most negative $\delta^{18}O$ weekly precipitation value (Table A1) indicates the total precipitation was 83.8 mm and the average temperature for the week was 1.3 ^{0}C.

A4. Crystal Cave in Sequoia National Park, CA, CRC-3 stalagmite $\delta^{13}C$ and Mg/Ca, Sr/Ca, and Ba/Ca results.

Table A3. Crystal Cave in Sequoia National Park, CA, CRC-3 stalagmite $\delta^{13}C$ and Mg/Ca, Sr/Ca, and Ba/Ca results.

Distance from top (mm)	Age (Yr AD)	$\delta^{13}C$ (‰ V-PDB)	Mg/Ca (mmol/mol)	Sr/Ca (umol/mol)	Ba/Ca (umol/mol)
0.05	2007.70	-7.43		73.36	19.95
0.10	2007.00	-7.48	2.02	71.01	6.51
0.15	2006.30	-7.64	2.12	72.43	11.78
0.20	2005.60	-7.58	1.80	65.88	6.73
0.25	2004.90	-7.35	2.03	70.91	11.97
0.30	2004.20	-8.02	1.85	68.10	6.60
0.35	2003.50	-7.85	2.25	64.90	10.07
0.40	2002.80	-7.66	1.98	69.27	9.78
0.45	2002.10	-7.44	2.01	64.76	28.53
0.50	2001.40	-7.44	2.01	67.67	8.37
0.55	2000.70	-7.08	1.94	58.27	6.37
0.60	1999.90	-7.13	1.83	62.48	8.10
0.65	1999.20	-6.81	1.88	60.19	6.29
0.70	1998.50	-6.66	1.78	62.54	7.42
0.75	1997.80	-6.49	1.90	59.69	26.68
0.80	1997.10	-6.44	1.77	57.15	8.68
0.85	1996.40	-6.29	1.86	60.85	9.68
0.90	1995.70	-6.36	1.72	70.08	6.71
0.95	1995.00	-6.65	1.75	60.07	5.91
1.00	1994.20	-6.78	1.78	62.63	7.66
1.05	1993.50	-7.12	1.77	61.87	12.96
1.10	1992.80	-7.18		64.80	9.73
1.15	1992.00	-7.92	1.70	69.40	11.99
1.20	1991.20	-8.20	1.72	71.61	11.18
1.25	1990.50	-7.47	1.41	76.23	9.22
1.30	1989.70	-7.92	1.81	65.24	8.22
1.35	1988.90	-7.48	1.47	78.23	15.10
1.40	1988.10	-7.22	1.51	83.09	10.17
1.45	1987.30	-6.71	1.52	75.41	12.15
1.50	1986.50	-6.94	1.59	80.48	9.44

1.55	1985.67	-6.43			
1.60	1984.80	-6.77	1.94	75.83	8.48
1.65	1983.97	-7.10			
1.70	1983.10	-7.23	1.67	71.34	8.44
1.75	1982.20	-6.37	1.47	84.00	8.65
1.80	1981.30	-5.97	1.54	85.38	10.64
1.85	1980.40	-5.88	1.70	82.09	8.84
1.90	1979.50	-6.13	1.77	82.69	9.14
1.95	1978.50	-5.85	2.40	88.12	10.06
2.00	1977.60	-6.09	1.72	83.30	8.86
2.05	1976.59	-6.08			
2.10	1975.60	-6.46	2.38	82.11	10.30
2.20	1973.50	-5.84	2.37	98.03	12.48
2.30	1971.40	-5.91			
2.40	1969.30	-5.33	1.92	89.17	11.24
2.50	1967.10	-5.32	2.33	92.49	10.49
2.60	1964.80	-5.49	2.01	86.49	11.07
2.70	1962.50	-5.84	2.06	88.49	10.38
2.80	1960.10	-6.06	1.90	86.49	11.37
2.90	1957.80	-6.46	2.30	87.93	10.48
3.00	1955.40	-6.51	1.90	87.44	11.99
3.10	1952.90	-6.62	2.00	89.59	9.79
3.20	1950.50	-6.49	1.75	82.48	10.64
3.30	1948.00	-7.04	2.47	83.34	9.72
3.40	1945.60	-6.73	1.63	80.93	10.52
3.50	1943.10	-7.11	1.66	80.62	10.38
3.60	1940.60	-7.60	1.76	84.93	15.98
3.70	1938.20	-7.81	1.63	81.73	9.09
3.80	1935.70	-7.52	1.17	82.03	9.23
3.90	1933.30	-7.44	1.35	84.62	9.67
4.00	1930.80	-7.20	1.26	82.47	10.36
4.10	1928.40	-6.44	1.64	77.18	8.90
4.20	1926.10	-6.64	1.45	77.14	7.46
4.30	1923.70	-6.14	1.59	80.12	10.70
4.40	1921.40	-6.35	1.34	74.21	7.48
4.50	1919.20	-6.87	1.63	71.10	8.01
4.60	1916.90	-7.13	1.39	78.72	7.40
4.70	1914.70	-7.18	1.68	79.81	9.38
4.80	1912.50	-6.49	1.48	79.63	7.95
4.90	1910.40	-6.17	1.79	85.21	9.69

5.00	1908.30	-6.10	1.80	82.62	8.75
5.10	1906.20	-5.58	1.83	85.18	10.58
5.20	1904.20	-6.42	1.78	90.79	19.52
5.30	1902.30	-6.31	1.74	87.38	11.35
5.40	1900.35	-6.60			
5.50	1898.50	-6.02	1.88	91.29	12.10
5.60	1896.70	-6.74	1.79	87.56	15.22
5.70	1894.90	-7.45			
5.80	1893.20	-7.73	1.33	88.49	11.50
5.90	1891.50	-7.77	1.45	97.65	12.18
6.00	1889.90	-7.60	1.26	97.37	11.96
6.10	1888.40	-7.31	1.44	93.74	11.00
6.20	1886.90	-7.54	1.33	90.23	10.68
6.30	1885.50	-7.51	1.51	88.60	10.76
6.40	1884.10	-7.26	1.33	85.18	10.03
6.50	1882.80	-8.03	1.58	83.98	9.80
6.60	1881.50	-7.81	1.24	81.77	10.84
6.70	1880.20	-8.70	1.66	88.46	10.41
6.80	1879.00	-8.78	1.12	80.59	9.29
6.90	1877.80	-8.97	1.39	82.59	10.05
7.00	1876.60	-8.86	1.10	83.71	10.33
7.10	1875.50	-8.42	1.29	86.87	10.33
7.20	1874.40	-8.08	1.14	80.15	9.27
7.30	1873.30	-7.79	1.52	83.61	10.14
7.40	1872.20	-7.92	1.14	81.27	9.40
7.50	1871.20	-7.96	1.52	76.72	9.43
7.60	1870.10	-7.85	1.14	76.39	10.47
7.70	1869.10	-7.89	1.52	77.58	10.00
7.80	1868.00	-8.13	1.27	75.30	9.89
7.90	1867.00	-8.18	1.58	75.29	9.73
8.00	1865.90	-7.86	1.25	74.10	9.32
8.10	1864.90	-8.01	1.50	76.23	9.95
8.20	1863.80	-8.38	1.23	75.46	9.93
8.30	1862.80	-8.18	1.48	75.66	9.97
8.40	1861.70	-8.35	1.29	74.41	9.85
8.50	1860.60	-8.31	1.40	75.04	9.23
8.60	1859.50	-8.32	1.32	74.11	9.83
8.70	1858.40	-8.23	1.94	78.06	9.73
8.80	1857.40	-8.11	1.27	70.60	9.26
8.90	1856.30	-8.25	1.76	75.48	10.43

9.00	1855.20	-7.99	1.38	77.82	9.52
9.10	1854.10	-7.78	1.61	85.01	11.27
9.20	1853.00	-7.64	1.41	78.98	9.80
9.30	1851.80	-7.60	1.73	81.32	10.37
9.40	1850.70	-7.60	2.13	77.96	9.57
9.50	1849.60	-7.38	2.29	83.51	11.53
9.60	1848.50	-7.60	1.42	74.69	8.79
9.70	1847.40	-7.50	1.61	80.90	10.15
9.80	1846.30	-7.55	1.54	60.94	7.40
9.90	1845.17	-7.41			
10.00	1844.10	-7.59	1.58	67.66	8.55
10.10	1842.90	-7.46	1.83	78.38	11.76
10.20	1841.80	-7.29	1.61	78.70	10.24
10.30	1840.70	-6.55	1.84	83.80	12.27
10.40	1839.60	-6.60	1.54	79.28	10.44
10.50	1838.50	-6.82	1.58	79.76	10.96
10.60	1837.40	-6.95	1.45	76.04	9.59
10.70	1836.30	-6.68	1.75	82.94	13.08
10.80	1835.20	-6.43	1.40	77.79	9.40
10.90	1834.10	-6.71	1.63	80.67	11.74
11.00	1833.00	-6.70	1.33	80.10	10.15
11.10	1831.90	-6.65	1.66	86.53	9.22
11.20	1830.80	-7.11	1.34	83.59	10.24
11.30	1829.70	-7.02	1.82	82.49	8.96
11.40	1828.60	-7.34	1.44	81.73	10.42
11.50	1827.50	-7.21	1.85	90.79	11.07
11.60	1826.50	-7.37	1.39	81.44	10.38
11.70	1825.40	-7.64		87.81	29.48
11.80	1824.30	-7.55	1.41	81.92	10.67
11.90	1823.20	-7.55	1.67	86.96	10.26
12.00	1822.20	-7.48	1.70	82.12	11.17
12.10	1821.10	-7.58	1.50	85.22	10.13
12.20	1820.00	-7.38	1.59	86.92	14.18
12.30	1819.00	-7.02	1.67	86.21	9.39
12.40	1817.90	-7.10	1.53	82.16	10.58
12.50	1816.90	-6.66	1.69	89.00	9.34
12.60	1815.90	-6.63	1.54	79.90	9.93
12.70	1814.80	-6.64	1.75	82.20	8.46
12.80	1813.80	-6.75	1.57	82.77	10.18
12.90	1812.80	-6.57	1.97	81.68	9.84

13.00	1811.70	-6.56	1.73	76.97	10.15
13.10	1810.70	-6.17	1.72	79.13	10.04
13.20	1809.70	-6.13	1.87	82.90	10.89
13.30	1808.70	-6.02	1.88	78.74	9.74
13.40	1807.70	-6.03	2.12	70.54	8.79
13.50	1806.70	-6.12	1.86	82.19	10.23
13.60	1805.70	-6.07	1.77	82.32	9.52
13.70	1804.70	-6.46	1.85	80.73	10.52
13.80	1803.70	-6.37	1.76	85.56	10.78
13.90	1802.70	-6.57	1.93	85.99	12.46
14.00	1801.70	-6.85	1.69	89.30	11.47
14.10	1800.80	-6.26	1.86	89.44	12.01
14.20	1799.80	-6.35	1.66	83.24	10.69
14.30	1798.80	-5.86	1.70	84.18	11.22
14.40	1797.80	-5.88	1.61	91.62	10.66
14.50	1796.90	-5.93	1.83	89.08	11.34
14.60	1795.90	-6.11	1.62	83.79	10.07
14.70	1795.00	-6.29	1.72	93.24	29.31
14.80	1794.00	-6.44	1.63	87.76	10.86
14.90	1793.00	-5.59	1.88	92.57	12.04
15.00	1792.10	-5.55	1.75	79.89	9.79
15.10	1791.10	-6.07	1.90	88.73	13.48
15.20	1790.20	-6.42	1.64	90.00	11.85
15.30	1789.20	-6.57	1.68	79.57	13.78
15.40	1788.30	-6.68	1.53	96.15	11.72
15.50	1787.30	-6.94	1.63	106.34	14.77
15.60	1786.40	-7.20	1.44	93.64	11.06
15.70	1785.40	-7.27	1.54	93.87	14.39
15.80	1784.40	-7.61	1.39	87.45	11.18
15.90	1783.50	-7.67	1.56	89.85	12.31
16.00	1782.50	-7.49	1.53	91.76	11.69
16.10	1781.60	-6.86	2.11	96.96	16.27
16.20	1780.60	-5.80	1.92	90.54	11.82
16.30	1779.60	-5.56	2.23	88.97	13.42
16.40	1778.70	-6.40	1.89	85.48	10.69
16.50	1777.70	-6.97	2.12	86.37	12.84
16.60	1776.70	-6.44	1.59	74.62	9.04
16.70	1775.80	-7.82	1.82	77.85	9.74
16.80	1774.80	-8.52	1.60	74.61	9.15
16.90	1773.80	-8.13	1.72	71.30	8.77

17.00	1772.80	-8.29	1.69	70.86	8.75
17.10	1771.90	-6.63	2.10	78.24	11.97
17.20	1770.90	-6.38	2.03	87.75	11.99
17.30	1769.90	-5.74	2.09	81.56	11.65
17.40	1768.90	-5.41	2.13	86.62	11.06
17.50	1768.00	-5.45	2.16	83.11	10.87
17.60	1767.00	-5.93	2.14	83.10	9.71
17.70	1766.00	-5.30	2.30	84.12	11.41
17.80	1765.00	-5.24	2.10	80.07	9.26
17.90	1764.10	-4.65	2.23	80.52	10.92
18.00	1763.10	-4.84	2.14	81.25	9.74
18.10	1762.10	-4.70	2.37	83.54	12.52
18.20	1761.10	-5.33	2.13	85.31	10.96
18.30	1760.10	-4.45	2.28	81.08	9.39
18.40	1759.20	-4.85	1.93	84.30	10.09
18.50	1758.20	-5.22	1.94	78.37	9.43
18.60	1757.20	-5.24	1.85	84.46	10.69
18.70	1756.20	-5.12	2.21	94.03	12.15
18.80	1755.30	-4.87	1.93	90.11	10.24
18.90	1754.30	-4.41	2.35	92.97	14.32
19.00	1753.30	-4.25	2.14	92.04	11.83
19.10	1752.30	-3.98	2.32	95.46	11.82
19.20	1751.40	-4.27	2.20	91.91	11.13
19.30	1750.40	-4.71	2.37	94.93	11.89
19.40	1749.40	-5.31	1.91	90.81	11.23
19.50	1748.40	-5.44	2.14	92.80	11.71
19.60	1747.50	-5.47	1.79	87.54	10.99
19.70	1746.50	-5.80	2.09	92.58	11.43
19.80	1745.50	-6.09	1.74	84.24	10.29
19.90	1744.50	-5.93	2.19	85.75	10.35
20.00	1743.60	-6.11	1.85	90.83	12.09
20.10	1742.60		2.03	90.44	11.72
20.20	1741.60	-5.68	2.50	91.12	11.01
20.30	1740.60	-5.31	1.98	87.15	8.63
20.40	1739.70	-5.71	1.85	86.29	10.90
20.50	1738.70	-5.66	2.00	88.63	9.83
20.60	1737.70	-6.24	1.72	93.04	11.49
20.70	1736.70	-5.80	1.67	95.19	9.91
20.80	1735.80	-6.83	1.51	96.29	12.02
20.90	1734.80	-7.39	1.80	94.84	11.01

21.00	1733.80	-8.59	1.52	94.81	12.05
21.10	1732.80	-7.38	1.57	95.25	10.22
21.20	1731.90	-7.88	2.17	94.07	11.64
21.30	1730.90	-7.80	2.36	97.36	11.07
21.40	1729.90	-7.67	1.46	95.31	12.31
21.50	1728.90	-7.58	1.79	99.91	21.50
21.60	1727.90	-7.75	1.47	90.51	11.45
21.70	1727.00	-6.88	1.83	95.28	13.16
21.80	1726.00	-6.70	1.52	91.02	11.88
21.90	1725.00	-6.26	1.62	89.33	8.92
22.00	1724.00	-6.36	1.74	84.57	11.41
22.10	1723.00	-6.57	1.58	88.72	8.23
22.20	1722.00	-6.39	1.98	83.13	11.86
22.30	1721.10		1.69	84.84	8.41
22.40	1720.10	-6.99	1.90	83.17	9.25
22.50	1719.10	-6.11	1.84	87.86	10.81
22.60	1718.10		1.75	94.80	8.91
22.70	1717.14	-6.22			
22.80	1716.20	-5.94	1.74	86.37	10.45
22.90	1715.20	-6.33	1.91	83.46	16.89
23.00	1714.20	-6.00	1.64	78.96	9.38
23.10	1713.27	-6.37			
23.20	1712.31		1.59	88.95	12.19
23.30	1711.36	-6.64			
23.40	1710.42	-6.67	1.69	79.11	9.50
23.50	1709.48	-6.34			
23.60	1708.56	-6.29	1.50	81.65	8.81
23.70	1707.64	-6.26			
23.80	1706.73	-6.16	1.67	76.97	9.35
23.90	1705.83	-6.03			
24.00	1704.94	-5.94	1.92	79.88	10.15
24.10	1704.06	-5.48	1.83	84.20	9.98
24.20	1703.19	-5.33	1.77	94.06	11.34
24.30	1702.33	-5.35	1.84	86.44	9.95
24.40	1701.48	-5.50	1.94	87.46	9.93
24.50	1700.64	-5.16	2.13	81.86	9.94
24.60	1699.80	-5.01	2.29	75.67	10.24
24.70	1698.98	-4.87	2.41	79.91	10.38
24.80	1698.16	-5.04	2.04	86.22	10.17
24.90	1697.35				

25.00	1696.55	-5.18	2.39	69.83	8.06
25.10	1695.75	-5.39	2.18	84.53	13.38
25.20	1694.95	-5.51	1.83	83.53	10.18
25.30	1694.16	-5.47	1.81	91.81	11.44
25.40	1693.38	-5.71	2.17	73.20	10.03
25.50	1692.60	-5.70	2.00		14.27
25.60	1691.82	-6.05	1.77	82.35	10.56
25.70	1691.05		1.66	85.68	11.00
25.80	1690.27	-6.18	1.96	76.14	9.39
25.90	1689.50	-5.74	1.73	81.70	9.82
26.00	1688.74	-5.79	1.58	83.62	9.71
26.10	1687.97	-5.58	1.84	82.14	11.67
26.20	1687.20	-5.87	1.79	82.75	9.68
26.30	1686.43	-5.59	1.84	73.20	8.87
26.40	1685.67	-5.59	1.54	72.58	7.92
26.50	1684.90	-5.70	1.70	75.98	11.59
26.60	1684.13	-6.02	1.58	76.15	8.70
26.70	1683.36	-5.98	1.78	75.80	9.96
26.80	1682.59	-6.17	1.65	78.28	8.49
26.90	1681.82	-5.93	1.65	72.16	10.05
27.00	1681.05	-6.25	1.65	81.75	10.20
27.10	1680.27	-6.38	1.95	80.16	11.46
27.20	1679.49	-6.13	1.69	80.03	9.86
27.30	1678.71	-6.14	1.80	78.49	12.66
27.40	1677.93	-6.22	1.49	59.90	6.46
27.50	1677.15	-5.87	1.77	82.49	10.31
27.60	1676.36	-5.98	1.68	80.96	10.07
27.70	1675.56	-6.04	1.70	81.24	10.03
27.80	1674.77	-6.19	1.47	81.27	9.18
27.90	1673.97	-6.03	1.84	95.87	12.61
28.00	1673.16	-6.12	1.73	76.80	10.47
28.10	1672.35	-5.79	1.75	82.16	9.79
28.20	1671.53	-6.11	1.77	74.80	9.14
28.30	1670.71	-5.89	1.69	66.96	8.93
28.40	1669.89	-6.07	2.49	69.35	8.33
28.50	1669.06	-5.92	1.83	71.72	9.35
28.60	1668.22	-5.91	1.60	67.33	7.44
28.70	1667.38	-5.49	1.69	68.81	8.02
28.80	1666.53	-5.88	1.61	70.44	8.88
28.90	1665.68	-5.85	1.59	69.47	7.79

29.00	1664.82	-6.09	1.55	67.05	10.28
29.10	1663.95	-6.23	1.86	68.35	12.99
29.20	1663.08	-6.24	1.62	74.73	10.34
29.30	1662.20	-6.49	1.60	76.45	9.78
29.40	1661.31	-7.10			
29.50	1660.42	-6.82	1.64	71.28	9.50
29.60	1659.52	-6.49	1.89	82.49	10.26
29.70	1658.61	-5.80	1.94	76.82	11.88
29.80	1657.70	-6.04	1.98	65.43	8.63
29.90	1656.78	-6.07	1.80	79.84	11.69
30.00	1655.85	-5.97	1.63	76.85	8.11
30.10	1654.91	-5.90	1.53	78.18	10.26
30.20	1653.97	-6.01	1.57	77.48	9.02
30.30	1653.02	-6.02	1.67	77.91	12.26
30.40	1652.06	-6.52	1.54	72.46	8.45
30.50	1651.10	-6.65	1.60	71.75	12.48
30.60	1650.14	-6.83	1.64	62.99	7.78
30.70	1649.17	-6.91	1.60	74.01	13.16
30.80	1648.19	-7.05	1.50	75.38	8.89
30.90	1647.22	-7.02	1.60	73.47	13.81
31.00	1646.24	-6.81	1.52	72.22	8.81
31.10	1645.26	-6.55	1.69	75.11	11.38
31.20	1644.27	-6.45	1.92	63.17	9.88
31.30	1643.29	-6.45	1.79	75.12	11.77
31.40	1642.31	-6.54	1.66	70.80	8.91
31.50	1641.33	-6.69	1.67	69.62	9.50
31.60	1640.35	-6.88	1.59	69.31	8.95
31.70	1639.37	-6.58	1.64	71.85	11.77
31.80	1638.39	-6.57	1.58	68.90	8.46
31.90	1637.42	-6.59	1.61	78.74	12.81
32.00	1636.45	-6.75	1.50	73.48	8.34
32.10	1635.48	-7.02			
32.20	1634.52	-7.12	1.47	73.49	9.28
32.30	1633.56	-7.25	2.12	72.88	35.58
32.40	1632.60	-7.18	1.54	74.45	9.32
32.50	1631.65	-7.10	1.63	72.98	9.78
32.60	1630.70	-7.10	1.46	70.41	9.16
32.70	1629.75	-6.73	2.18	83.52	14.85
32.80	1628.81	-6.95	1.38	70.27	7.48
32.90	1627.86	-6.88	1.55	74.07	9.23

33.00	1626.92	-6.32	1.79	65.00	8.51
33.10	1625.98	-6.18	1.60	73.72	9.91
33.20	1625.04	-5.74	1.47	77.94	9.06
33.30	1624.10	-6.07	1.83	74.83	9.98
33.40	1623.16	-6.19	1.61	83.88	9.54
33.50	1622.22	-6.75	1.66	72.53	9.13
33.60	1621.29	-6.82	1.59	72.51	10.33
33.70	1620.35	-6.43	1.59	75.29	9.44
33.80	1619.41	-6.00	1.80	63.95	9.28
33.90	1618.47	-5.87	1.70	77.24	9.98
34.00	1617.52	-6.02	2.05	56.48	6.40
34.10	1616.58	-5.89	1.63	77.26	10.26
34.20	1615.64	-5.85	1.75	78.82	9.53
34.30	1614.69	-5.81	1.72	77.77	10.33
34.40	1613.74	-5.63	1.53	75.70	9.10
34.50	1612.79	-6.01	1.69	77.69	9.93
34.60	1611.85	-5.92	2.46	46.35	8.27
34.70	1610.90	-6.10	1.92	79.44	10.40
34.80	1609.95	-5.45	1.63	73.59	9.51
34.90	1609.00	-5.26	1.93	73.58	10.02
35.00	1608.05	-5.24	1.61	71.45	9.56
35.10	1607.10	-5.80	2.65	71.08	9.85
35.20	1606.15	-6.29	1.81	74.17	8.25
35.30	1605.20	-6.00			
35.40	1604.25	-5.89	1.69	73.80	7.22
35.50	1603.31	-6.00	1.59	72.05	8.09
35.60	1602.36	-6.01	1.71	76.14	8.81
35.70	1601.42	-5.95	1.52	71.26	9.28
35.80	1600.48	-6.13	1.52	76.08	7.74
35.90	1599.54	-6.20	1.50	78.76	9.37
36.00	1598.60	-6.38	1.46	74.44	7.50
36.10	1597.66	-6.47	1.40	73.37	6.62
36.20	1596.73	-6.59	1.57	64.02	7.74
36.30	1595.80	-6.85	1.52	73.12	7.43
36.40	1594.87	-6.79	1.42	73.35	9.72
36.50	1593.94	-6.59		72.69	11.31
36.60	1593.01	-6.32	1.37	75.64	8.44
36.70	1592.08	-6.69	1.56	71.08	6.38
36.80	1591.15	-6.48	1.47	76.52	10.65
36.90	1590.23	-6.81	1.56	78.73	8.01

37.00	1589.31	-7.00	1.47	73.84	10.01
37.10	1588.38	-7.27	1.63	80.97	12.06
37.20	1587.46	-6.99	1.71	70.42	7.85
37.30	1586.53	-6.48	1.59	75.18	8.91
37.40	1585.61	-6.95	1.53	76.03	7.35
37.50	1584.69	-6.28	1.79	74.39	10.12
37.60	1583.76	-6.57	1.53	72.63	6.52
37.70	1582.84	-6.81	1.80	75.81	11.44
37.80	1581.92	-6.62	1.57	74.28	7.05
37.90	1580.99	-6.57	1.57	73.34	8.57
38.00	1580.06	-7.02	1.52	64.41	10.19
38.10	1579.14	-7.49	1.52	71.28	9.78
38.20	1578.21	-7.40	1.37	76.61	10.39
38.30	1577.28	-7.02	2.06	79.33	32.41
38.40	1576.35	-7.18	1.34	75.02	9.45
38.50	1575.42	-6.85	1.50	73.24	10.87
38.60	1574.48	-6.78	1.51	70.10	9.62
38.70	1573.55	-6.91		73.54	9.57
38.80	1572.62	-7.12	1.53	70.48	10.03
38.90	1571.69			68.57	9.45
39.00	1570.75	-6.95	1.55	70.18	11.34
39.10	1569.82	-6.95	1.82	66.89	10.08
39.20	1568.88	-6.97	1.51	69.78	10.17
39.30	1567.95	-6.98	2.02	74.64	15.16
39.40	1567.01	-6.97	1.66	92.94	8.17
39.50	1566.07	-6.58	1.58	71.36	8.99
39.60	1565.14	-6.69	1.90	58.57	8.61
39.70	1564.20	-6.58	1.71	70.70	8.72
39.80	1563.27	-6.73	1.95	69.23	9.66
39.90	1562.33	-6.96	1.87	68.95	9.24
40.00	1561.40	-7.69	1.69	73.20	13.23
40.10	1560.46	-7.78	1.54	74.15	7.57
40.20	1559.53	-7.59	2.34	78.05	37.58
40.30	1558.59	-6.95	1.69	72.06	7.49
40.40	1557.66	-5.99	1.81	70.71	13.33
40.50	1556.72	-6.63	1.78	68.62	6.78
40.60	1555.79	-6.85	1.64	71.81	12.77
40.70	1554.85	-6.87	1.65	71.06	7.71
40.80	1553.91	-6.99	1.54	71.31	10.18
40.90	1552.97	-6.68	1.71	71.36	7.06

41.00	1552.04	-7.00	1.64	71.16	9.10
41.10	1551.10	-6.01	1.97	73.82	11.55
41.20	1550.16	-6.65	1.88	70.97	9.99
41.30	1549.21	-5.79	1.88	69.44	8.85
41.40	1548.27	-6.33	1.81	76.75	13.17
41.50	1547.33	-6.22			
41.60	1546.38	-6.48	1.72	66.54	12.76
41.70	1545.43	-6.35	1.86	65.84	8.83
41.80	1544.48	-6.80	1.71	65.55	16.37
41.90	1543.53	-6.74	1.82	64.14	8.27
42.00	1542.58	-7.03	1.82	65.36	23.96
42.10	1541.62	-6.93	1.63	64.35	8.26
42.20	1540.66	-7.37	1.57	63.25	10.57
42.30	1539.70	-7.43	1.54	61.92	7.58
42.40	1538.74	-6.94	1.71	63.97	12.29
42.50	1537.78	-6.48	2.29	66.85	11.57
42.60	1536.81	-6.45	1.65	67.88	10.15
42.70	1535.84	-6.00	1.73	65.09	7.91
42.80	1534.87	-6.03	1.67	64.68	8.13
42.90	1533.89	-5.81	1.74	70.83	8.77
43.00	1532.92	-5.77	1.74	63.84	10.21
43.10	1531.94	-5.63	1.63	69.17	4.56
43.20	1530.96	-6.27	1.68	75.28	10.57
43.30	1529.98	-6.52	1.60	69.57	5.85
43.40	1528.99	-6.60	1.63	67.41	12.51
43.50	1528.00	-6.53	1.59	71.66	4.62
43.60	1527.01	-6.61	1.96	70.62	9.63
43.70	1526.02	-6.47	1.51	67.13	5.31
43.80	1525.03	-6.61	1.57	68.58	13.86
43.90	1524.03	-6.64	1.61	69.74	9.16
44.00	1523.03	-6.66	1.64	69.29	9.29
44.10	1522.03	-6.76	1.69	71.67	9.73
44.20	1521.02	-6.43	1.57	69.22	9.20
44.30	1520.02	-6.43	1.62	71.63	9.41
44.40	1519.01	-6.75	1.57	68.94	9.26
44.50	1518.00	-6.72	1.56	72.26	9.75
44.60	1516.99	-7.01	1.46	72.21	8.50
44.70	1515.98	-6.83	1.56	75.21	10.61
44.80	1514.96	-6.75			
44.90	1513.95	-6.49	1.61	74.87	10.42

45.00	1512.93	-6.37	1.65	74.78	12.14
45.10	1511.91	-6.20	1.72	73.49	10.30
45.20	1510.89	-6.44	1.79	72.70	11.00
45.30	1509.87	-6.45	1.78	83.04	11.50
45.40	1508.85	-6.52	1.51	74.83	6.49
45.50	1507.83	-6.45	1.76	75.30	17.47
45.60	1506.81	-6.44	1.55	72.71	6.92
45.70	1505.80	-6.32	1.72	77.68	9.99
45.80	1504.78	-6.42	1.66	74.18	8.46
45.90	1503.76	-6.48	1.73	72.60	9.47
46.00	1502.74	-6.55	2.68	76.28	7.20
46.10	1501.72	-6.60	1.62	75.63	9.65
46.20	1500.70	-6.55	1.53	81.15	9.81
46.30	1499.68	-6.50	1.69	78.85	11.20
46.40	1498.67	-6.09	1.70	79.96	7.89
46.50	1497.65	-5.78	2.41	86.78	13.91
46.60	1496.63	-5.40	1.86	86.91	9.08
46.70	1495.62	-5.52	1.84	84.73	11.84
46.80	1494.60	-6.15	1.65	82.79	8.60
46.90	1493.58	-6.55	1.71	77.00	10.78
47.00	1492.57	-6.83	1.61	74.77	7.89
47.10	1491.55		1.66	76.58	32.86
47.20	1490.53	-7.42	1.56	74.88	9.57
47.30	1489.52	-7.16	1.54	81.24	9.74
47.40	1488.50	-7.63	1.60	70.35	9.62
47.50	1487.48	-7.25	1.59	75.05	10.30
47.60	1486.46	-7.15	1.52	72.51	8.71
47.70	1485.44	-6.60	1.78	77.67	10.48
47.80	1484.43	-6.64	1.58	71.85	10.48
47.90	1483.40	-6.55	1.74	71.97	9.23
48.00	1482.38	-6.99	1.53	83.18	11.01
48.10	1481.36	-6.99	2.40	84.74	11.50
48.20	1480.34	-7.06	1.59	78.67	10.39
48.30	1479.32	-7.05	2.07	79.99	12.19
48.40	1478.29	-7.30	1.68	72.32	9.57
48.50	1477.27	-7.13	1.82	74.05	10.24
48.60	1476.25	-7.12	1.67	72.54	10.19
48.70	1475.23	-6.97	1.95	82.88	12.80
48.80	1474.21	-7.03	1.70	73.34	9.77
48.90	1473.19	-6.90	1.76	77.48	8.55

49.00	1472.18	-6.95	1.63	74.96	9.44
49.10	1471.17	-6.73	1.94	76.15	13.43
49.20	1470.16	-6.70	1.70	73.48	10.86
49.30	1469.15	-6.44	1.82	80.86	11.94
49.40	1468.15	-6.27	1.68	77.44	10.16
49.50	1467.15	-6.33	1.82	81.70	11.38
49.60	1466.15	-6.51	1.65	83.50	12.36
49.70	1465.16	-6.30	1.61	83.24	10.94
49.80	1464.18	-6.61	2.59	82.02	11.86
49.90	1463.20	-6.16	1.69	82.31	10.64
50.00	1462.22	-6.18	1.67	81.21	9.53
50.10	1461.25	-5.99	1.83	88.33	15.96
50.20	1460.29	-6.18	1.70	66.53	8.15
50.30	1459.33	-6.31	1.52	80.73	9.19
50.40	1458.38	-6.40	1.51	80.84	8.85
50.50	1457.43	-6.10	1.71	80.49	12.43
50.60	1456.48	-5.90	1.96	74.19	10.58
50.70	1455.53	-5.67	1.74	78.11	9.72
50.80	1454.59	-5.67	1.69	73.93	8.75
50.90	1453.65	-5.80	1.86	87.42	11.80
51.00	1452.71	-5.45	1.83	81.24	9.00
51.10	1451.76	-5.02	1.81	83.23	10.57
51.20	1450.82	-5.46	1.89	79.26	9.14
51.30	1449.88	-5.47	2.05	80.47	10.91
51.40	1448.93	-5.81	1.93	67.28	8.57
51.50	1447.98	-6.81	1.78	73.36	12.68
51.60	1447.03	-6.75	1.74	63.34	7.70
51.70	1446.08	-6.35	1.76	76.08	10.09
51.80	1445.12	-6.03	1.92	72.81	9.92
51.90	1444.16	-6.50	1.75	76.13	10.44
52.00	1443.19	-6.80	1.66	76.00	9.09
52.10	1442.21	-6.70	1.93	76.91	11.96
52.20	1441.23	-6.97	1.73	69.01	9.84
52.30	1440.24	-7.01	1.71	79.08	9.39
52.40	1439.25	-6.75	1.76	70.14	9.27
52.50	1438.25	-6.46	1.77	80.70	10.47
52.60	1437.25	-6.80	1.80	75.42	9.85
52.70	1436.24	-5.95	1.97	85.07	12.53
52.80	1435.22	-6.02	2.02	87.86	12.04
52.90	1434.20	-5.78			

53.00	1433.17	-5.83	1.89	81.23	9.69
53.10	1432.13	-6.02	1.93	75.66	8.10
53.20	1431.09	-6.11	2.21	84.40	11.38
53.30	1430.04	-6.03	1.83	75.34	7.67
53.40	1428.99	-6.20	2.22	79.92	9.35
53.50	1427.92	-6.68	2.35	80.38	8.97
53.60	1426.86	-6.71	1.89	76.13	8.16
53.70	1425.78	-6.77	1.93	72.52	16.45
53.80	1424.70	-6.66	1.90	83.58	9.33
53.90	1423.62	-6.42	1.78	71.22	7.31
54.00	1422.52	-6.69	1.90	75.88	9.33
54.10	1421.43	-6.61	1.80	72.85	7.02
54.20	1420.32	-6.47	1.74	74.39	11.08
54.30	1419.21	-6.70	1.78	78.14	7.91
54.40	1418.09	-6.25	1.58	79.65	10.05
54.50	1416.97	-6.59	1.82	71.24	7.38
54.60	1415.84	-6.57	1.67	69.36	8.94
54.70	1414.71	-7.04	1.83	71.15	7.26
54.80	1413.57	-6.62	1.81	75.05	9.33
54.90	1412.43	-7.17	1.94	72.31	7.58
55.00	1411.29	-6.76	1.72	73.69	9.12
55.10	1410.14	-6.93	2.01	78.75	10.29
55.20	1408.99	-6.56	1.76	74.39	9.94
55.30	1407.83	-6.69	1.86	78.85	11.58
55.40	1406.67	-6.32	1.70	79.18	9.05
55.50	1405.51	-6.36	1.76	79.87	11.01
55.60	1404.35	-6.12	1.84	80.28	12.29
55.70	1403.18	-6.20	2.20	91.09	10.80
55.80	1402.01	-6.20	1.66	85.66	9.37
55.90	1400.85	-6.75	2.12	86.43	14.34
56.00	1399.68	-7.09	1.85	73.08	12.86
56.10	1398.50	-7.49	1.62	76.40	9.84
56.20	1397.33	-7.10	1.83	79.90	9.49
56.30	1396.16	-7.27	1.83	70.34	10.21
56.40	1394.98	-7.12	1.77	74.74	7.95
56.50	1393.80	-7.15	1.74	74.82	10.13
56.60	1392.62	-6.98	1.65	76.43	9.65
56.70	1391.44	-6.89	1.77	69.79	9.37
56.80	1390.26	-6.74	1.67	79.72	9.99
56.90	1389.07	-6.95	2.08	74.88	12.85

57.00	1387.88	-7.00	2.07	76.99	16.19
57.10	1386.69	-7.20	2.06	67.74	9.70
57.20	1385.49	-7.06	2.35	82.55	12.41
57.30	1384.29	-7.29	1.82	76.17	9.94
57.40	1383.08	-7.14	2.09	77.41	10.74
57.50	1381.87	-7.07	1.73	74.73	8.90
57.60	1380.66	-7.10	1.95	72.60	7.73
57.70	1379.44	-7.35	1.81	74.45	8.48
57.80	1378.22	-7.12	1.98	73.26	7.71
57.90	1376.99	-7.24	1.76	71.32	8.19
58.00	1375.75	-7.09	1.95	79.61	9.40
58.10	1374.51	-7.04	2.29	71.06	8.15
58.20	1373.27	-6.66	2.04	75.26	11.73
58.30	1372.02	-6.76	2.10	72.67	9.01
58.40	1370.77	-6.31	1.97	76.83	10.24
58.50	1369.51	-6.23	2.61	73.18	9.47
58.60	1368.25	-5.90	2.05	74.48	17.98
58.70	1366.99	-6.01	1.95	73.19	9.07
58.80	1365.72	-5.95	1.73	76.76	8.58
58.90	1364.46	-6.21	2.13	79.96	10.95
59.00	1363.19	-6.04	1.96	72.40	10.75
59.10	1361.92	-6.42	1.79	75.72	8.37
59.20	1360.66	-6.23	1.88	77.80	9.64
59.30	1359.39	-6.59	1.74	76.82	8.97
59.40	1358.13	-6.22	2.19	83.30	13.69
59.50	1356.86	-6.39	1.83	78.16	9.52
59.60	1355.60	-6.52			
59.70	1354.34	-6.30	1.76	78.48	9.37
59.80	1353.09	-6.42	1.69	80.86	9.47
59.90	1351.84	-6.53	1.67	75.51	9.02
60.00	1350.59	-6.48	2.13	73.58	9.54
60.10	1349.35	-6.34	1.86	83.42	14.06
60.20	1348.11	-6.63	1.69	74.83	9.59
60.30	1346.88	-6.44	1.73	76.13	9.64
60.40	1345.65	-6.56	1.63	77.33	8.17
60.50	1344.43	-6.46	1.79	74.86	9.14
60.60	1343.21	-6.34	1.88	75.28	9.64
60.70	1341.99	-6.28	1.68	75.40	11.14
60.80	1340.78	-6.35	1.67	72.57	7.29
60.90	1339.57	-6.04	2.28	76.51	11.52

61.00	1338.36	-6.02	1.76	76.66	9.14
61.10	1337.15	-6.16	1.77	71.28	9.05
61.20	1335.95	-5.98	1.80	72.20	9.22
61.30	1334.75	-5.89	2.07	57.76	7.73
61.40	1333.55	-5.86		63.13	8.83
61.50	1332.35	-5.92		58.17	7.65
61.60	1331.16	-6.05	2.29	66.25	9.87
61.70	1329.96	-5.78	2.80	82.20	12.13
61.80	1328.77	-5.81	1.85	75.98	10.12
61.90	1327.58	-5.88	1.75	77.03	9.15
62.00	1326.38	-5.88			
62.10	1325.19	-6.09			
62.20	1324.00	-6.07	1.94	77.03	17.30
62.30	1322.81	-5.83			
62.40	1321.62	-5.86	1.78	69.66	8.36
62.50	1320.43	-6.10			
62.60	1319.24	-6.18	1.91	77.08	9.89
62.70	1318.05	-6.26			
62.80	1316.86	-6.40	2.06	78.60	10.40
62.90	1315.67	-6.41			
63.00	1314.48	-6.43	2.29	76.49	11.39
63.10	1313.29	-6.14	1.85	78.50	10.55
63.20	1312.11	-6.27	2.00	77.39	10.74
63.30	1310.92	-6.00	2.20	73.14	9.97
63.40	1309.74	-5.23	1.95	62.90	8.60
63.50	1308.55	-5.22	1.86	71.24	8.44
63.60	1307.37	-4.85	2.56	86.57	12.17
63.70	1306.18	-4.97	1.88	81.72	10.06
63.80	1305.00	-4.96	2.53	79.03	18.79
63.90	1303.82	-4.88	1.84	82.88	10.00
64.00	1302.64	-4.98	1.98	75.38	9.60
64.10	1301.46	-4.71	2.08	77.39	11.45
64.20	1300.28	-4.68	1.83	75.61	9.04
64.30	1299.10	-4.93			
64.40	1297.92	-5.21	1.87	71.15	10.89
64.50	1296.75	-5.44	1.86	66.09	8.46
64.60	1295.57	-5.68	1.75	74.07	10.33
64.70	1294.39	-5.59	1.59	77.91	9.14
64.80	1293.21	-5.72	1.72	67.65	8.08
64.90	1292.04	-5.71	1.47	72.19	8.62

65.00	1290.86	-5.76	1.49	65.57	7.10
65.10	1289.68	-5.83	1.55	76.17	9.57
65.20	1288.50	-6.00	1.70	76.18	8.65
65.30	1287.32	-5.99	1.70	75.53	9.98
65.40	1286.13	-5.38	2.16	71.74	10.08
65.50	1284.95	-5.11	1.75	76.65	10.32
65.60	1283.76	-5.06	1.97	77.02	8.99
65.70	1282.57	-4.99	1.77	82.42	10.36
65.80	1281.39	-5.12	2.04	81.28	9.93
65.90	1280.19	-5.06	1.62	80.15	9.70
66.00	1279.00	-4.98	1.84	79.12	9.01
66.10	1277.80	-5.08	1.70	84.28	10.73
66.20	1276.60	-5.19			
66.30	1275.40	-5.55	1.60	81.80	10.38
66.40	1274.19	-6.09			1.38
66.50	1272.98	-5.86	1.46	86.28	10.36
66.60	1271.76	-6.22			1.88
66.70	1270.54	-6.15	1.32	80.82	9.68
66.80	1269.31	-6.41			
66.90	1268.08	-6.46			
67.00	1266.83	-5.86			3.32
67.10	1265.58	-5.84	1.61	83.49	11.32
67.20	1264.32	-5.65	1.68	80.71	10.29
67.30	1263.05	-5.32	1.71	82.67	10.78
67.40	1261.77	-4.95	1.83	86.24	10.42
67.50	1260.48	-5.09	1.80	79.68	10.57
67.60	1259.18	-5.37	1.88	86.49	10.87
67.70	1257.87	-5.73	1.70	79.85	10.38
67.80	1256.54	-5.62	1.96	87.39	10.93
67.90	1255.20	-5.66	1.77	82.08	10.87
68.00	1253.85	-5.79	2.30	84.24	26.44
68.10	1252.49	-6.05	1.68	83.94	11.13
68.20	1251.11	-5.72	1.98	88.48	11.38
68.30	1249.72	-5.84	1.68	60.22	7.99
68.40	1248.33	-5.55	1.81	82.83	10.16
68.50	1246.92	-5.69	1.92	78.63	10.25
68.60	1245.51	-5.82	1.85	81.17	9.88
68.70	1244.10	-5.61	2.01	79.23	10.39
68.80	1242.68	-5.63	1.74	86.58	10.45
68.90	1241.26	-5.71	1.75	82.25	10.79

69.00	1239.84	-5.56	2.62	78.42	10.55
69.10	1238.43	-5.62	1.61	80.32	10.04
69.20	1237.01	-5.78	1.85	80.34	12.09
69.30	1235.60	-5.64	1.42	68.17	8.68
69.40	1234.20	-5.94	1.72	79.06	9.02
69.50	1232.80	-5.90	1.67	77.07	10.27
69.60	1231.42	-5.92	1.93	76.64	9.92
69.70	1230.04	-5.61	1.70	76.55	9.94
69.80	1228.68	-5.62	2.29	89.19	12.69
69.90	1227.33	-5.47	1.83	82.41	10.93
70.00	1226.00	-5.45	2.07	84.30	11.06
70.10	1224.68	-4.91	1.82	79.31	10.57
70.20	1223.38	-5.42	2.15	87.39	11.43
70.30	1222.09	-5.23	1.74	80.72	10.33
70.40	1220.82	-5.43	2.15	88.89	24.86
70.50	1219.57	-5.76	1.72	71.64	9.41
70.60	1218.32	-5.83	2.31	81.54	10.83
70.70	1217.09	-5.81	1.77	79.66	10.79
70.80	1215.86	-5.77	2.18	86.32	11.66
70.90	1214.65	-5.58	1.76	79.74	10.68
71.00	1213.45	-5.63	1.86	83.69	10.12
71.10	1212.25	-5.52	1.89	83.32	11.50
71.20	1211.06	-5.49	1.74	78.57	9.35
71.30	1209.87	-5.63	1.70	84.60	10.77
71.40	1208.69	-5.68	1.76	87.42	9.78
71.50	1207.52	-5.52	1.99	76.89	11.08
71.60	1206.35	-5.83	1.71	81.72	8.71
71.70	1205.18	-5.74	1.56	78.31	9.65
71.80	1204.01	-6.09	1.59	75.63	7.96
71.90	1202.84	-5.97	1.63	78.68	17.70
72.00	1201.67	-5.99	1.69	69.62	8.23
72.10	1200.50	-5.77	1.77	78.50	10.19
72.20	1199.33	-5.57	1.60	77.05	9.25
72.30	1198.16	-5.45	1.54	78.54	9.47
72.40	1196.99	-5.25	1.82	79.74	10.78
72.50	1195.82	-5.15	1.58	82.46	9.78
72.60	1194.64	-5.46	2.09	78.01	14.14
72.70	1193.47	-5.23	1.75	81.16	10.53
72.80	1192.30	-5.33	1.60	79.50	9.28
72.90	1191.13	-5.37	1.55	80.83	9.83

73.00	1189.96	-5.52	1.56	81.31	10.19
73.10	1188.79	-5.76	1.43	80.45	9.67
73.20	1187.62	-5.78	1.69	87.83	10.69
73.30	1186.45	-5.55	1.49	84.39	10.07
73.40	1185.28	-5.37	1.40	85.66	10.16
73.50	1184.12	-5.06	1.52	80.71	10.76
73.60	1182.96	-5.06	1.50	84.74	10.01
73.70	1181.80	-5.01	1.51	87.16	10.38
73.80	1180.65	-5.09	1.59	86.45	10.66
73.90	1179.49	-5.48	1.56	84.00	10.19
74.00	1178.34	-5.80	1.62	76.38	9.98
74.10	1177.20	-5.75	1.54	78.80	9.63
74.20	1176.06	-5.54	1.59	75.43	9.37
74.30	1174.92	-5.54	1.59	73.35	10.12
74.40	1173.78	-5.32	1.51	73.09	8.62
74.50	1172.65	-4.97	1.66	77.24	9.80
74.60	1171.52	-4.94	1.65	74.74	9.16
74.70	1170.39	-4.81	1.74	78.45	10.06
74.80	1169.26	-4.93	1.63	76.25	9.77
74.90	1168.14	-4.97	1.62	78.32	9.63
75.00	1167.02	-5.58	2.02	76.72	9.16
75.10	1165.90	-5.53	1.55	77.29	9.82
75.20	1164.78	-5.89	1.53	75.91	9.23
75.30	1163.67	-5.95	1.71	72.56	10.25
75.40	1162.55	-6.07	2.62	71.09	9.28
75.50	1161.44	-6.40	1.58	73.75	9.80
75.60	1160.33	-6.17	1.74	71.17	9.18
75.70	1159.21	-6.03	1.75	75.55	12.22
75.80	1158.10	-5.50	1.69	73.12	10.16
75.90	1156.99	-5.22	1.79	78.55	10.12
76.00	1155.88	-5.43	2.03	77.55	10.16
76.10	1154.77	-4.58	1.93	75.94	11.12
76.20	1153.66	-4.61	1.87	76.67	10.21
76.30	1152.55	-4.60	2.18	62.58	9.31
76.40	1151.44	-4.89	1.75	76.99	9.54
76.50	1150.34	-4.50	1.76	74.00	9.87
76.60	1149.23	-5.24	1.89	74.12	10.02
76.70	1148.13	-5.54	1.65	72.55	10.06
76.80	1147.03	-5.98	1.67	74.14	9.72
76.90	1145.94	-5.56	1.66	72.79	9.73

77.00	1144.85	-5.36	1.66	74.73	9.64
77.10	1143.76	-5.24	2.21	62.17	9.26
77.20	1142.68	-5.26	1.69	79.98	10.69
77.30	1141.60	-5.35		82.94	12.90
77.40	1140.53	-5.97	1.57	84.08	11.22
77.50	1139.46	-5.85	1.62	85.09	11.58
77.60	1138.40	-6.20	1.47	81.99	10.55
77.70	1137.35	-5.82	1.64	82.46	11.05
77.80	1136.30	-6.12	1.56	78.63	10.03
77.90	1135.26	-6.44	1.52	78.59	9.72
78.00	1134.23	-6.08	1.73	74.81	9.93
78.10	1133.20	-6.50	1.75	68.67	8.48
78.20	1132.19	-5.88	1.80	74.42	10.60
78.30	1131.18	-6.52	1.81	66.58	8.01
78.40	1130.17	-5.94	1.80	76.85	10.08
78.50	1129.17	-6.26	1.66	73.75	9.18
78.60	1128.18	-6.02	1.91	70.36	13.84
78.70	1127.18	-5.89	1.78	75.40	9.31
78.80	1126.19	-6.18	1.76	71.84	9.47
78.90	1125.20	-5.89	1.81	71.40	8.89
79.00	1124.21	-5.60	1.88	70.08	9.40
79.10	1123.22	-5.47	1.90	77.24	9.14
79.20	1122.23	-4.27	1.93	80.44	10.56
79.30	1121.23	-5.26	2.03	76.35	10.27
79.40	1120.24	-4.93	1.82	79.64	10.29
79.50	1119.24	-5.42	1.95	79.19	9.86
79.60	1118.23	-4.89	1.83	85.59	11.18
79.70	1117.22	-5.01	1.91	85.59	10.38
79.80	1116.20	-5.09	1.75	87.54	11.71
79.90	1115.17	-5.45	1.72	86.09	10.68
80.00	1114.14	-5.39	1.67	90.74	11.80
80.10	1113.10	-5.67	1.60	88.53	11.45
80.20	1112.05	-5.75	1.59	91.14	12.63
80.30	1110.99	-5.53	1.81	87.44	12.07
80.40	1109.92	-5.30	1.65	90.60	38.69
80.50	1108.85	-4.81	1.58	83.63	10.60
80.60	1107.77	-5.04	1.65	87.74	11.39
80.70	1106.68	-5.63	1.58	88.21	11.40
80.80	1105.59	-5.36	1.64	85.63	11.91
80.90	1104.50	-5.79	1.49	87.55	10.82

81.00	1103.40	-5.80	1.56	86.36	17.10
81.10	1102.30	-5.73	1.57	85.87	11.83
81.20	1101.19	-5.70	1.54	85.71	12.34
81.30	1100.09	-5.55	1.64	81.08	11.06
81.40	1098.98	-5.30	1.68	87.71	12.88
81.50	1097.87	-5.12	1.52	85.49	11.18
81.60	1096.76	-5.11	1.56	82.82	11.45
81.70	1095.66	-5.24	1.42	84.05	10.14
81.80	1094.55	-5.50	2.35	78.19	10.60
81.90	1093.45	-5.60	1.50	80.91	9.99
82.00	1092.34	-5.95	1.82	77.43	10.42
82.10	1091.24	-5.61	1.77	64.20	8.20
82.20	1090.15	-6.24	1.52	72.47	9.78
82.30	1089.06	-6.33	1.64	79.24	9.85
82.40	1087.96	-6.83	1.57	78.57	9.85
82.50	1086.88	-6.81	1.52	70.59	8.53
82.60	1085.79	-6.19	1.55	75.42	11.28
82.70	1084.71	-6.69	1.55	73.91	9.17
82.80	1083.62	-6.50	1.60	76.47	9.50
82.90	1082.54	-6.74			
83.00	1081.47	-6.47	1.47	77.40	10.00
83.10	1080.39	-7.15	1.52	70.40	8.64
83.20	1079.32	-6.32	1.59	74.83	13.12
83.30	1078.24	-6.31	1.68	74.36	9.09
83.40	1077.17	-6.25	1.65	76.14	9.84
83.50	1076.10	-5.97	1.64	75.47	8.62
83.60	1075.03	-5.89	1.93	78.13	11.49
83.70	1073.96	-5.82	1.81	76.53	9.94
83.80	1072.89	-5.90	1.72	80.74	10.08
83.90	1071.83	-5.86	1.81	76.05	10.26
84.00	1070.76	-5.81	1.77	84.04	13.95
84.10	1069.69	-5.53	1.91	78.53	10.79
84.20	1068.63	-5.59	1.79	75.85	15.49
84.30	1067.56	-5.23	1.87	79.36	11.20
84.40	1066.49	-5.66	1.87	77.91	9.34
84.50	1065.43	-5.24	1.87	79.07	11.03
84.60	1064.36	-5.36	1.75	73.54	7.37
84.70	1063.30	-5.07	1.94	81.79	11.29
84.80	1062.23	-5.41	1.93	76.93	8.79
84.90	1061.16	-5.10	2.08	71.50	9.40

85.00	1060.10	-5.44	2.06	89.44	9.57
85.10	1059.03	-5.40	1.79	84.45	10.78
85.20	1057.96	-5.54	1.81	80.26	10.69
85.30	1056.89	-5.36	1.65	81.92	10.20
85.40	1055.82	-5.92	1.74	77.62	11.39
85.50	1054.75	-5.83	1.79	72.44	8.98
85.60	1053.68	-5.83	1.83	78.58	11.43
85.70	1052.60	-5.76		78.01	10.53
85.80	1051.53	-5.80	1.95	70.18	10.01
85.90	1050.45	-5.81	1.71	76.43	12.09
86.00	1049.37	-5.76	2.04	72.69	10.84
86.10	1048.29	-5.58	1.73	76.70	8.84
86.20	1047.21	-5.57	1.85	74.01	11.16
86.30	1046.13	-5.58	1.72	78.56	8.80
86.40	1045.05	-5.60	1.66	75.42	8.68
86.50	1043.96	-5.52	1.84	76.72	9.10
86.60	1042.88	-5.37	1.74	75.92	8.90
86.70	1041.79	-5.56	1.76	81.89	9.88
86.80	1040.70	-5.55	1.75	81.13	11.19
86.90	1039.62	-5.23	1.72	81.53	9.48
87.00	1038.53	-5.68	1.70	79.97	9.32
87.10	1037.44	-5.30	1.94	78.49	10.54
87.20	1036.35	-5.43	1.67	82.69	7.31
87.30	1035.26	-5.52	1.93	62.23	7.43
87.40	1034.17	-5.75	1.69	85.47	8.07
87.50	1033.09	-5.72	1.42	82.76	9.85
87.60	1032.00	-5.58	1.53	86.55	6.59
87.70	1030.91	-5.54	1.66	84.13	10.03
87.80	1029.83	-5.63	1.60	77.92	6.01
87.90	1028.74	-5.46	1.73	79.54	11.39
88.00	1027.66	-5.22	1.73	78.14	8.13
88.10	1026.58	-5.08	1.98	68.57	8.71
88.20	1025.50	-4.75	2.51	83.36	9.62
88.30	1024.42	-4.78	1.82	81.41	9.35
88.40	1023.34	-4.91	1.91	80.50	9.20
88.50	1022.26	-4.60	2.00	78.39	9.81
88.60	1021.18	-4.75	1.99	78.72	9.29
88.70	1020.11	-5.01			
88.80	1019.03	-4.68	2.00	80.27	11.40
88.90	1017.96	-4.54	1.83	78.45	9.21

89.00	1016.89	-4.81	1.96	79.91	10.66
89.10	1015.82	-4.37	2.15	77.14	10.61
89.20	1014.75	-4.65	2.01	78.32	9.72
89.30	1013.68	-4.58	1.97	87.27	10.20
89.40	1012.61	-4.58	1.98	80.36	13.32
89.50	1011.54	-4.64	1.82	80.59	9.10
89.60	1010.48	-5.09	1.86	82.58	10.24
89.70	1009.42	-4.84	1.95	68.90	7.56
89.80	1008.35	-5.22	1.81	77.26	9.63
89.90	1007.29	-5.05	1.82	83.43	9.38
90.00	1006.23	-5.48	1.89	77.38	11.06
90.10	1005.17	-5.30	1.79	80.77	10.73
90.20	1004.11	-5.53	2.15	80.78	13.34
90.30	1003.05	-5.32	1.78	80.50	9.48
90.40	1002.00	-5.54	2.07	79.44	12.58
90.50	1000.94	-5.49	1.71	80.25	9.75
90.60	999.88	-5.81	1.86	77.49	10.88
90.70	998.83	-5.73	1.81	76.96	10.11
90.80	997.77	-6.00	1.76	79.09	11.88
90.90	996.71	-5.86	1.69	75.89	9.65
91.00	995.66	-6.14	1.65	75.76	9.48
91.10	994.60	-6.06	1.75	72.63	9.42
91.20	993.54	-6.33	1.63	72.91	9.62
91.30	992.49	-6.47	1.76	70.79	9.81
91.40	991.43	-6.73	1.69	73.96	10.09
91.50	990.37	-6.54	1.77	70.44	9.91
91.60	989.31	-6.69	1.88	77.82	10.99
91.70	988.25	-6.33	1.91	73.61	11.96
91.80	987.19	-6.44	1.71	74.39	10.01
91.90	986.12	-6.23	1.80	68.08	9.22
92.00	985.06	-6.45	1.69	72.28	9.35
92.10	983.99	-6.44	1.94	75.82	11.74
92.20	982.92	-6.46	1.64	76.36	10.35
92.30	981.86	-6.50	1.72	76.10	10.54
92.40	980.79	-6.53	1.65	77.74	10.48
92.50	979.71	-6.43	1.83	77.23	11.53
92.60	978.64	-6.65	1.77	79.26	10.35
92.70	977.57	-6.23	1.68	78.87	10.33
92.80	976.50	-6.49	1.84	76.05	10.32
92.90	975.43	-6.49	1.96	64.94	7.92

93.00	974.35	-6.47			
93.10	973.28	-6.48		77.99	9.97
93.20	972.21	-6.78	1.70	80.13	11.37
93.30	971.14	-6.52		82.87	10.07
93.40	970.07	-6.80	1.65	79.26	10.44
93.50	969.00	-6.44	1.73	83.61	17.10
93.60	967.93		1.66	82.79	10.84
93.70	966.87	-6.74	1.94	86.65	11.48
93.80	965.80	-6.67	1.61	81.73	10.65
93.90	964.74		1.73	84.65	10.63
94.00	963.68	-6.67	1.59	83.75	10.29
94.10	962.62	-6.52	1.82	83.25	11.27
94.20	961.57	-6.52	1.78	84.31	11.73
94.30	960.51	-6.72	1.78	79.73	10.68
94.40	959.46	-6.68			
94.50	958.41	-6.58	1.81	85.19	11.24
94.60	957.35	-6.50	1.61	75.07	11.36
94.70	956.30	-6.42	1.84	79.64	11.14
94.80	955.25	-6.79			
94.90	954.20	-6.50	1.67	89.36	11.71
95.00	953.15	-6.83			
95.10	952.09	-6.65	1.68	88.29	11.70
95.20	951.04	-6.94	1.64	83.63	11.24
95.30	949.98	-6.92	1.68	80.83	10.53
95.40	948.93	-7.10	2.47	77.36	10.28
95.50	947.87	-6.76	1.65	69.52	10.52
95.60	946.80	-6.85	1.57	83.90	12.49
95.70	945.74	-7.00	1.66	79.93	10.91
95.80	944.67	-7.09	1.54	81.21	10.61
95.90	943.60	-6.99	1.76	82.24	12.78
96.00	942.52	-6.90	1.50	86.06	13.17
96.10	941.44	-6.86	1.62	86.64	11.19
96.20	940.36	-6.77	1.61	85.45	12.64
96.30	939.28		1.96	81.82	12.44
96.40	938.19	-6.68	1.56	85.52	11.41
96.50	937.10	-6.69	2.26	92.23	15.50
96.60	936.00	-6.75	1.60	85.44	12.10
96.70	934.91	-6.56	1.96	83.91	12.60
96.80	933.81	-6.73	1.57	86.60	11.73
96.90	932.72	-6.33	1.77	86.37	11.62

97.00	931.62	-6.35	1.66	86.33	11.68
97.10	930.53	-6.31	1.69	80.66	10.55
97.20	929.43	-6.43	1.61	89.74	12.05
97.30	928.33	-6.43	1.83	87.41	13.74
97.40	927.24	-6.48	1.69	88.65	12.35
97.50	926.15	-6.32	1.99	89.72	11.89
97.60	925.06	-6.61	1.53	82.68	10.87
97.70	923.97	-6.70	1.78	78.72	11.08
97.80	922.89	-6.69	1.67	77.08	12.54
97.90	921.81	-6.89	1.62	77.89	10.61
98.00	920.73	-6.84	1.80	80.62	11.77
98.10	919.66	-6.39	1.61	82.51	10.81
98.20	918.59	-6.48	1.54	85.99	13.01
98.30	917.52	-5.78	2.05	74.93	13.25
98.40	916.46	-5.98	1.60	84.23	11.03
98.50	915.40	-6.11	2.04	77.36	9.93
98.60	914.34	-6.18	1.97	88.05	13.08
98.70	913.28	-6.41	2.29	97.98	16.01
98.80	912.22	-5.80	1.72	84.53	11.80
98.90	911.17	-6.66	1.83	82.90	11.91
99.00	910.11	-6.77	1.65	81.00	10.73
99.10	909.06	-7.00	2.19	70.25	10.47
99.20	908.00	-6.82	1.74	87.34	12.28
99.30	906.94	-7.02		79.20	11.53
99.40	905.88	-7.23	1.63	72.44	12.18
99.50	904.82	-6.84	1.75	84.11	11.61
99.60	903.76	-6.95	1.55	82.78	11.37
99.70	902.69	-7.02	1.77	80.83	11.55
99.80	901.62	-7.42	1.58	76.64	10.55
99.90	900.54	-7.22	1.71	76.73	10.80
100.00	899.47	-7.34	1.61	76.62	11.02
100.10	898.38	-7.20	1.74	80.40	11.34
100.20	897.29	-6.60	1.73	83.18	13.17
100.30	896.20	-6.90	1.80	88.59	11.15
100.40	895.11	-6.70	1.58	84.55	10.18
100.50	894.01	-6.73	1.96	86.99	11.59
100.60	892.91	-6.41	1.58	88.08	26.72
100.70	891.81	-6.21	1.87	84.44	12.30
100.80	890.70	-5.81	1.54	82.75	10.57
100.90	889.60	-6.57	1.67	80.07	10.31

101.00	888.49	-6.59	1.69	80.63	10.70
101.10	887.38	-6.72	1.42	82.55	8.06
101.20	886.28	-6.67	1.76	80.28	9.53
101.30	885.17	-6.64	1.50	82.04	7.72
101.40	884.07	-6.65	1.75	85.67	8.83
101.50	882.96	-6.03	1.85	85.40	9.02
101.60	881.86	-6.02	1.77	84.50	8.47
101.70	880.76	-5.84	1.96	87.43	9.13
101.80	879.67	-6.09	1.98	80.73	9.66
101.90	878.57	-6.19	2.12	79.60	9.08
102.00	877.48	-5.92	1.71	79.60	8.03
102.10	876.40	-5.95	2.09	88.72	12.66
102.20	875.32	-6.05	1.89	91.10	13.53
102.30	874.24	-6.08	1.97	79.88	11.02
102.40	873.17	-6.30	1.65	87.96	13.60
102.50	872.09	-6.47	1.54	85.42	10.96
102.60	871.03	-6.64	1.59	83.79	11.54
102.70	869.96	-6.69	1.55	85.47	10.89
102.80	868.90	-6.76	1.23	80.07	9.76
102.90	867.83	-7.01	1.37	80.64	11.28
103.00	866.77	-6.87	1.29	79.21	10.36
103.10	865.71	-7.12	1.49	81.19	11.59
103.20	864.65	-7.17	1.49	76.42	11.89
103.30	863.60	-7.43	1.63	80.62	12.32
103.40	862.54	-7.94	1.33	72.87	9.43
103.50	861.48	-7.70	1.93	76.26	12.53
103.60	860.42	-7.83	1.45	74.23	10.59
103.70	859.36	-7.47	1.59	78.91	12.42
103.80	858.30	-7.47	1.50	79.29	10.68
103.90	857.24	-7.13	1.70	74.40	10.62
104.00	856.18	-6.85	1.51	83.62	10.91
104.10	855.12	-6.44	1.47	88.44	10.76
104.20	854.05	-6.57	1.60	88.28	10.88
104.30	852.99	-6.61			
104.40	851.92	-5.85	1.69	78.18	11.52

A5. NADP weekly archived precipitation sample amounts, corresponding $\delta^{18}O$ values, and CDEC corresponding average weekly temperature from 2001 to 2011.

Table A4. NADP weekly archived precipitation sample amounts, corresponding $\delta^{18}O$ values, and CDEC corresponding average temperature from 2001 to 2011.

Date On	Date Off	Ppt (mm)	$\delta^{2}H$	$\delta^{18}O$	Temp °C
1/2/2001	1/9/2001	5.1	-135.65	-18.03	7.54
1/9/2001	1/16/2001	97.8	-123.31	-17	-1.11
1/23/2001	1/30/2001	61.2	-89.71	-13.36	-2.11
2/6/2001	2/13/2001	115.3	-72.78	-11.56	-4
2/13/2001	2/20/2001	46.5	-95.02	-13.87	-2.11
2/20/2001	2/27/2001	58.9	-143.69	-18.88	-1.67
2/27/2001	3/6/2001	24.9	-105.07	-13.85	-0.33
3/6/2001	3/13/2001	11.4	-82.98	-11.78	1
3/20/2001	3/27/2001	5.8	-21.86	-4.59	7.14
4/3/2001	4/10/2001	91.2			-5
4/17/2001	4/24/2001	69.1	-85.79	-12.34	2.69
7/3/2001	7/10/2001	8.4	-23.06	-3.6	16.67
10/23/2001	10/30/2001	6.6	-108.55	-13.44	13.26
10/30/2001	11/6/2001	30.5	-100.06	-13.9	8.89
11/6/2001	11/13/2001	26.2	-48.19	-7.66	7.08
11/20/2001	11/27/2001	93.2	-65.19	-9.76	0.32
11/27/2001	12/4/2001	121.7	-72.52	-11.1	-2.22
12/4/2001	12/11/2001	9.4	-69.46	-10.79	0.4
12/11/2001	12/18/2001	23.9	-94.67	-13.48	-0.56
12/18/2001	12/26/2001	44.5	-82.03	-12.37	0.56
12/26/2001	1/2/2002	114.3	-113.55	-15.18	4.35
1/2/2002	1/8/2002	25.4	-74.81	-11.19	5.56
1/22/2002	1/29/2002	69.6	-124.7	-16.69	-4.07
1/29/2002	2/5/2002	6.4	-70.53	-10.8	-1.25
2/12/2002	2/19/2002	33.8	-100.85	-15.49	3.8
3/5/2002	3/12/2002	85.9	-73.04	-10.65	2.64
3/12/2002	3/19/2002	20.6	-87	-12.73	-3.61
3/19/2002	3/26/2002	48.3	-65.1	-9.88	3.06
4/16/2002	4/23/2002	12.4	-44.92	-7.84	2.71

4/23/2002	4/30/2002	19.1	-42.46	-7.38	3.67
4/30/2002	5/7/2002	7.6	-60.5	-9.06	6.35
5/14/2002	5/21/2002	47.2	-54.87	-8.73	-0.28
10/1/2002	10/8/2002	22.9			6.56
11/5/2002	11/12/2002	270.8	-59.56	-9.06	7.67
12/10/2002	12/17/2002	99.1	-55.56	-9.3	2.64
12/17/2002	12/23/2002	9.6	-60.07	-10.15	-3.97
12/23/2002	12/31/2002	127.3	-82.45	-12.44	-1.11
1/7/2003	1/14/2003	8.5			5.32
2/10/2003	2/19/2003	92.2	-141.39	-18.99	1.88
2/19/2003	2/25/2003	9.9	-96.32	-13.4	2.15
2/25/2003	3/4/2003	51.6	-88.68	-12.72	-1.78
3/11/2003	3/18/2003	99.8	-61.76	-9.7	3.19
3/31/2003	4/8/2003	47	-61.68	-9.97	-0.19
4/8/2003	4/15/2003	63.8	-69.92	-10.98	5.08
4/15/2003	4/22/2003	30.5	-62.25	-9.74	0.21
4/22/2003	4/29/2003	22.1	-57.69	-9.15	0.49
4/29/2003	5/6/2003	58.7	-85.7	-12.45	1.53
5/6/2003	5/13/2003	29.7	-59.8	-9.52	3.89
5/13/2003	5/20/2003	2.8	-76.48	-10.6	11.11
7/22/2003	7/29/2003	9.1	3.02	0.88	20.56
7/29/2003	8/5/2003	80.3	-32.7	-5.12	18.15
10/28/2003	11/5/2003	18.5	-78.1	-12.48	3.06
11/5/2003	11/12/2003	43.2	-73.77	-11.5	2.38
11/12/2003	11/18/2003	22.1	-150.5	-20.63	2.22
12/16/2003	12/23/2003	15.2			6.32
1/20/2004	1/27/2004	1.8			1.3
1/27/2004	2/3/2004	35.8	-92.24	-13	0
2/10/2004	2/17/2004	8.1	-81.91	-11.5	3.33
2/17/2004	2/24/2004	46	-108.48	-15.11	0.37
2/24/2004	3/2/2004	109.2	-80.01	-11.84	-2.36
3/23/2004	3/30/2004	14.5	-101.32	-13.26	7.22
4/13/2004	4/20/2004	5.1	-56.16	-8.75	2
9/14/2004	9/21/2004	1.8			11.04
10/12/2004	10/19/2004	55.6	-53.94	-8.75	10.14
10/19/2004	10/26/2004	54.6	-56.68	-9.7	1.94
10/26/2004	11/2/2004	41.9			-0.83

11/2/2004	11/9/2004	24.6	-95.6	-14.06	4.56
11/9/2004	11/16/2004	4.3			2.89
11/16/2004	11/23/2004	1.7			2.64
11/23/2004	11/30/2004	34.3	-71.38	-10.26	2.96
11/30/2004	12/7/2004	34.3			-1.53
12/7/2004	12/14/2004	8.4	-107.32	-15.06	9.54
12/21/2004	12/28/2004	15.2	-165.03	-21.83	2.85
12/28/2004	1/4/2005	68.8	-87.77	-13.19	-2.71
1/4/2005	1/11/2005	217.7	-76.82	-11.58	-2.11
1/25/2005	2/1/2005	56.5	-64.71	-9.98	0.9
2/1/2005	2/8/2005	1.8	-36.32	-6.44	1.74
2/8/2005	2/15/2005	8.6	-134.68	-17.92	2.41
2/15/2005	2/22/2005	56.4	-111.33	-15.48	1.6
2/22/2005	3/1/2005	28.7	-90.93	-12.9	0.56
3/1/2005	3/8/2005	5.1	-87.89	-12.2	2.22
3/15/2005	3/22/2005	151.6	-59.59	-9.3	1.25
3/22/2005	3/29/2005	83.6	-81.3	-11.58	0.07
3/29/2005	4/5/2005	13.2	-60.63	-9.71	3.68
4/5/2005	4/12/2005	30	-51.9	-8.07	4.81
4/19/2005	4/26/2005	12.2	-43.99	-7.51	3.75
4/26/2005	5/3/2005	29.7	-73.13	-11.22	4.58
5/3/2005	5/10/2005	91.2	-83.62	-12.22	3.41
5/10/2005	5/17/2005	34	-76.77	-10.7	5.46
8/9/2005	8/16/2005	4.3	-41.44	-6.04	18.25
9/6/2005	9/13/2005	2			10.56
9/20/2005	9/27/2005	8.9	-45.37	-6.86	12.36
10/18/2005	10/26/2005	5.8	-63.83	-9.7	10.14
10/26/2005	11/1/2005	4.6	-31.92	-5.16	8.7
11/1/2005	11/8/2005	1.5			8.25
11/8/2005	11/15/2005	6.9	-67.53	-10.28	8.7
11/22/2005	11/29/2005	8.9	-60.49	-8.73	4.44
11/29/2005	12/6/2005	98.5	-86.13	-12.48	1
12/6/2005	12/13/2005	3.8	-84.28	-11.44	4.86
12/13/2005	12/20/2005	90.2	-64.5	-10.6	4.44
12/20/2005	12/27/2005	41.9	-99.25	-14.27	7.08
12/27/2005	1/3/2006	199.4	-98.21	-14.06	4.63
1/10/2006	1/17/2006	41.9	-71.24	-11.36	2.64

1/17/2006	1/24/2006	22.6	-46.21	-8.18	1.02
1/24/2006	1/31/2006	9.4	-64.82	-9.99	1.94
2/14/2006	2/21/2006	31.8	-65.83	-11.53	-3.43
2/21/2006	2/28/2006	78	-92.25	-13.1	3.57
2/28/2006	3/7/2006	69.1	-93.79	-13.57	-1.11
3/7/2006	3/14/2006	50	-78.07	-12.19	-4.65
3/14/2006	3/21/2006	57.9	-77.53	-11.31	-4.22
3/21/2006	3/28/2006	79.5	-125.9	-16.82	2.5
3/28/2006	4/4/2006	144.3	-105.23	-14.54	0.49
4/4/2006	4/11/2006	70.4	-70.52	-11.05	0.9
4/11/2006	4/17/2006	54.2	-63.02	-9.49	3.26
4/17/2006	4/25/2006	14	-41.82	-6.99	5.22
5/16/2006	5/23/2006	24.9	-88.2	-12.11	12.99
7/18/2006	7/25/2006	11.4	-10.48	0.41	22.78
9/26/2006	10/3/2006	12.2	-134.1	-17.88	15.4
10/10/2006	10/17/2006	7.1	-59.68	-9.17	7.22
10/17/2006	10/24/2006	18.5	-59.4	-8.82	9.13
11/7/2006	11/14/2006	16.9	-56.27	-8.24	7.22
11/21/2006	11/28/2006	4.1	-94.74	-13.4	-0.83
12/5/2006	12/12/2006	41.1	-95.55	-13.81	5.76
12/12/2006	12/19/2006	22.1	-61.87	-10.43	1.27
12/19/2006	12/27/2006	48.2	-89.54	-13.25	5
12/27/2006	1/2/2007	5.1	-85.11	-10.52	3.06
1/2/2007	1/9/2007	24.4	-51.36	-7.76	9.31
1/9/2007	1/16/2007	6.9	-55	-10.29	-1.43
1/23/2007	1/30/2007	5.8	-100.25	-14.18	4.6
2/6/2007	2/13/2007	75.9	-84.84	-12.47	3.25
2/13/2007	2/20/2007	4.8	-60.87	-7.93	2.71
2/20/2007	2/27/2007	96.3	-72.03	-11.12	-1.11
2/27/2007	3/6/2007	16.3	-70.85	-10.98	5.14
3/20/2007	3/27/2007	59.2	-75.7	-7.63	3.96
3/27/2007	4/3/2007	13.5	-61.98	-7.63	4.79
4/10/2007	4/17/2007	23.4	-74.01	-10.4	2.86
4/17/2007	4/24/2007	40.1	-91.5	-12.11	0.83
5/1/2007	5/8/2007	4.1	-50.16	-7.67	5.08
9/18/2007	9/25/2007	14.2	-69.77	-10.54	11.67
10/2/2007	10/9/2007	14.4	-54.47	-9.21	9.91

10/9/2007	10/16/2007	3.8	-40.09	-6.4	7.38
10/23/2007	10/30/2007	13.7	-79.74	-11.63	13.75
11/6/2007	11/13/2007	21.6	-71.9	-10.24	9.03
12/4/2007	12/11/2007	87.6	-90.57	-12.83	1.74
12/11/2007	12/18/2007	18	-80.26	-11.89	-0.21
12/18/2007	12/24/2007	71.1	-98.53	-14.03	0.63
12/24/2007	12/31/2007	5.1	-64.77	-10.28	-0.28
12/31/2007	1/8/2008	188	-74.63	-11.24	1.11
1/8/2008	1/15/2008	5.1	-92.02	-12.72	4.31
1/22/2008	1/29/2008	71.1	-106.49	-15.06	-2.15
1/29/2008	2/5/2008	77.7	-111.08	-14.79	-3.75
2/19/2008	2/26/2008	147.8	-61.71	-9.09	0.63
3/11/2008	3/18/2008	18	-55.5	-8.33	1.67
3/25/2008	4/1/2008	22.9	-105.14	-14.15	2.99
5/20/2008	5/27/2008	26.2	-88.1	-12.05	4.58
7/8/2008	7/15/2008	2.3			20.87
9/9/2008	9/16/2008	4.6	-20.08	-2.8	17.38
9/23/2008	9/30/2008	5.3	-5.3	-1.51	17.43
9/30/2008	10/7/2008	22.9	-53.56	-9.2	12.5
10/28/2008	11/4/2008	79.8	-60.28	-10.07	8.47
11/4/2008	11/12/2008	19.8	-63.94	-10.73	5.4
11/25/2008	12/2/2008	19.1	-171.06	-22.68	8.49
12/9/2008	12/16/2008	57.4	-73.76	-11.63	1.39
12/16/2008	12/23/2008	34.3	-109.51	-14.75	-2.64
12/23/2008	12/30/2008	69.5	-78.89	-11.25	-0.28
12/30/2008	1/6/2009	4.8	-81.14	-10.73	2.99
1/20/2009	1/27/2009	127.8	-83.86	-11.87	2.15
2/3/2009	2/10/2009	85.1	-98.54	-14.16	4
2/10/2009	2/17/2009	87.4	-99.38	-14.63	0.66
2/17/2009	2/24/2009	38.1	-138.98	-19.07	0.66
3/3/2009	3/10/2009	34.3	-56.28	-9.38	-2.69
3/17/2009	3/24/2009	28.2	-65.5	-9.59	3.06
4/7/2009	4/14/2009	50.3	-64.54	-9.78	1.43
4/14/2009	4/21/2009	5.8	-43.7	-8.37	6.18
4/28/2009	5/5/2009	38.4	-122.26	-17.44	6.98
5/26/2009	6/2/2009	2.3	-42.84	-6.32	6.98
6/2/2009	6/9/2009	25.1	-90.66	-13.75	6.98

6/9/2009	6/16/2009	5.1	-57.19	-8.91	7.78
6/16/2009	6/23/2009	2.8	-36.92	-5.95	12.29
8/18/2009	8/25/2009	9.4	-10	-0.85	18.82
9/8/2009	9/15/2009	2.3			16.18
10/6/2009	10/13/2009	18	-123.34	-17.02	7.15
10/13/2009	10/20/2009	196.9	-49.52	-7.2	9.29
11/10/2009	11/17/2009	7.6	-69.38	-10.92	5.21
11/24/2009	12/1/2009	4.3			6.75
12/1/2009	12/8/2009	53.1	-134.06	-18.18	-0.14
12/8/2009	12/15/2009	156.7	-62.94	-10.61	-1.74
12/15/2009	12/22/2009	34.3	-71.41	-10.85	4.24
12/22/2009	12/29/2009	7.6	-92.6	-13.58	-0.21
12/29/2009	1/5/2010	11.2	-104.37	-15.01	3.75
1/12/2010	1/19/2010	64	-84.43	-13.12	1.88
1/19/2010	1/26/2010	162.8	-99.89	-14.7	-2.62
2/2/2010	2/9/2010	84.1	-95.99	-13.74	-1.25
2/9/2010	2/16/2010	4.1			3.13
2/16/2010	2/23/2010	58.9	-71.18	-10.59	1.74
2/23/2010	3/2/2010	102.6	-102.75	-14.58	1.11
3/2/2010	3/9/2010	69.3	-60.88	-11.17	-1.74
3/9/2010	3/16/2010	38.6	-81.56	-12.67	0.35
3/23/2010	4/6/2010	131.1	-64.96	-9.86	-1.94
4/6/2010	4/13/2010	68.8	-85.44	-12.77	1.75
4/13/2010	4/20/2010	1.5	-72.4	-10.93	5
4/20/2010	4/27/2010	67.6	-86.06	-11.78	3.68
4/27/2010	5/4/2010	57.9	-52.85	-9.07	3.13
5/4/2010	5/11/2010	9.4	-74.7	-11.34	4.38
5/11/2010	5/18/2010	12.4	-96.77	-15.71	5.56
5/18/2010	5/24/2010	3			2.99
5/24/2010	6/1/2010	5.1	-20.2	-3.97	6.74
9/28/2010	10/5/2010	17.3	-70.18	-10.22	15
10/5/2010	10/12/2010	6.4	-54.8	-9.66	9.51
10/12/2010	10/19/2010	5.1	-31.32	-4.49	13.54
10/19/2010	10/26/2010	26.9	-41.07	-5.61	6.11
10/26/2010	11/2/2010	25.7	-82.9	-12.17	6.94
11/2/2010	11/10/2010	36.6	-72.2	-10.38	7.15
11/10/2010	11/16/2010	2			4.79

11/16/2010	11/23/2010	93	-73.02	-11.21	1.67
11/23/2010	11/30/2010	50.8	-80.01	-13.16	-2.43
11/30/2010	12/7/2010	28.2	-99.28	-14.15	5.69
12/14/2010	12/21/2010	498.9	-109.3	-16.89	0.63
12/21/2010	12/28/2010	44.7	-172.61	-24.31	1.25
12/28/2010	1/4/2011	154.7	-150.03	-19.27	-3.47
1/25/2011	2/1/2011	21.3	-68	-9.81	3.61
2/15/2011	2/22/2011	115.3	-66.82	-11.33	-3.33
2/22/2011	3/1/2011	141	-90.63	-13.56	-3.75
3/1/2011	3/8/2011	46.7			2.22
3/15/2011	3/22/2011	76.2	-100.5	-14.23	-0.42
3/22/2011	3/29/2011	51.9	-90.28	-12.96	-1.04
4/5/2011	4/12/2011	47.5	-98.36	-13.69	0
4/12/2011	4/19/2011	2.3			4.51
4/19/2011	4/26/2011	5.6	-53.59	-7.55	3.68
5/3/2011	5/10/2011	13.7	-46.49	-7.03	8.19
5/10/2011	5/17/2011	38.1	-80.02	-11.57	4.24
5/17/2011	5/24/2011	26.2	-66.83	-9.46	3.82
5/24/2011	5/31/2011	22.1	-71.21	-10.51	5.35
5/31/2011	6/7/2011	21.6	-91.44	-12.55	4.86
7/26/2011	8/2/2011	3.6	-59.47	-7.15	18.75
9/13/2011	9/20/2011	3	-14.82	-2.36	15.21
10/4/2011	10/11/2011	113	-66.87	-9.78	4.68
11/1/2011	11/8/2011	40.9	-57.47	-8.97	1.18
11/8/2011	11/15/2011	20.3	-145.34	-19.16	4.03
11/15/2011	11/22/2011	13.2	-130.92	-17.27	2.85

A6. Results of Climate Indices Combinations with Daily Precipitation Amount (> 100 mm/day) in Western US

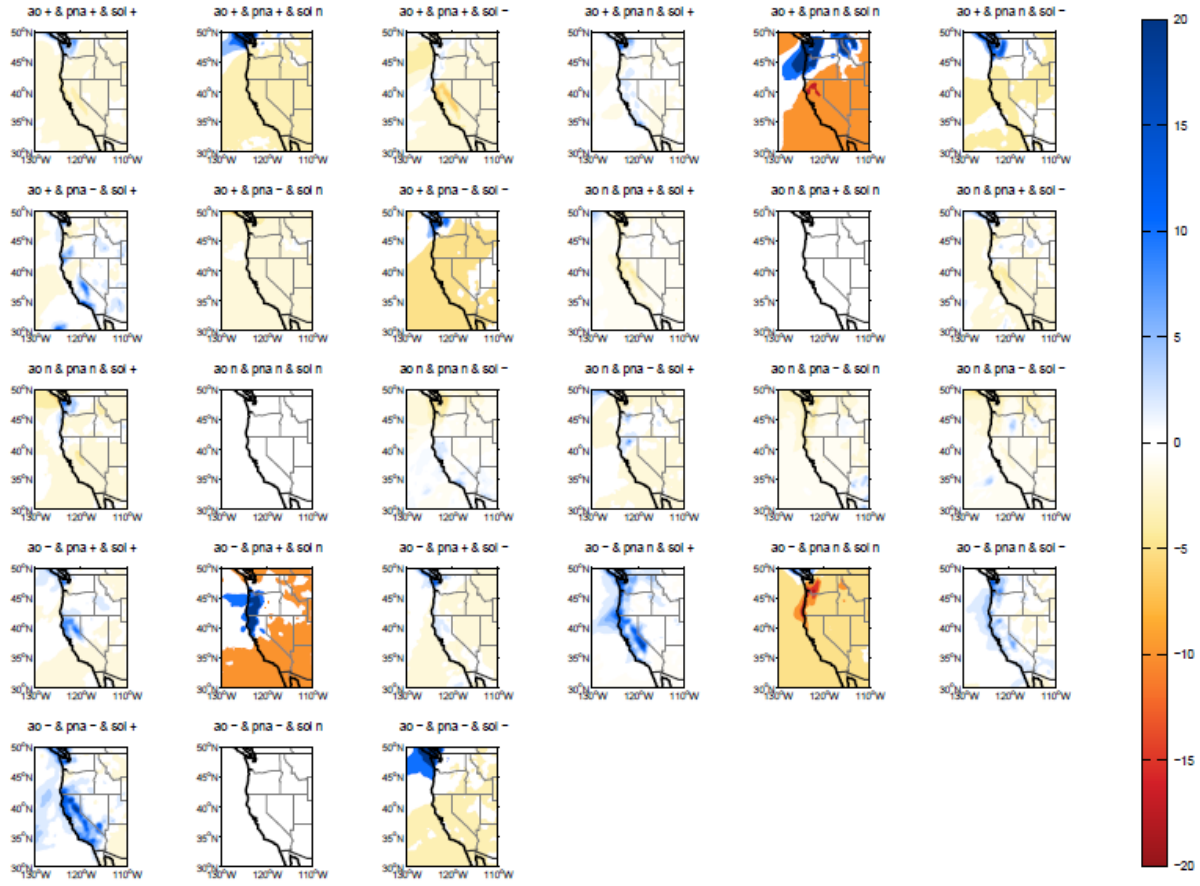

Figure A11a. Shading represents anomalous daily precipitation >100mm/day over the western U.S. during the combination of the **AO, PNA, and SOI** from *2001 to 2011*.

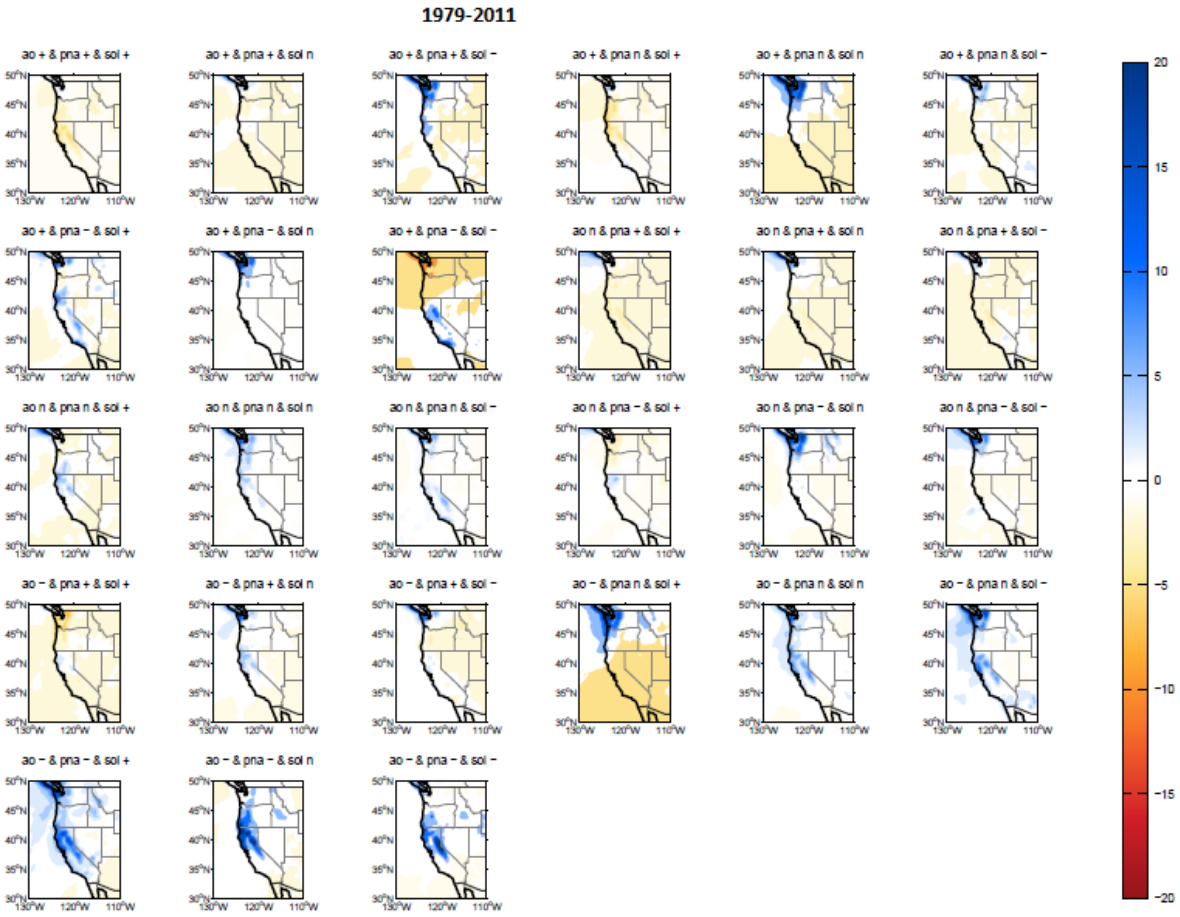

Figure A11b. Shading represents anomalous daily precipitation >100mm/day over the western U.S. during the combination of the **AO, PNA, and SOI** from *1979 to 2011*.

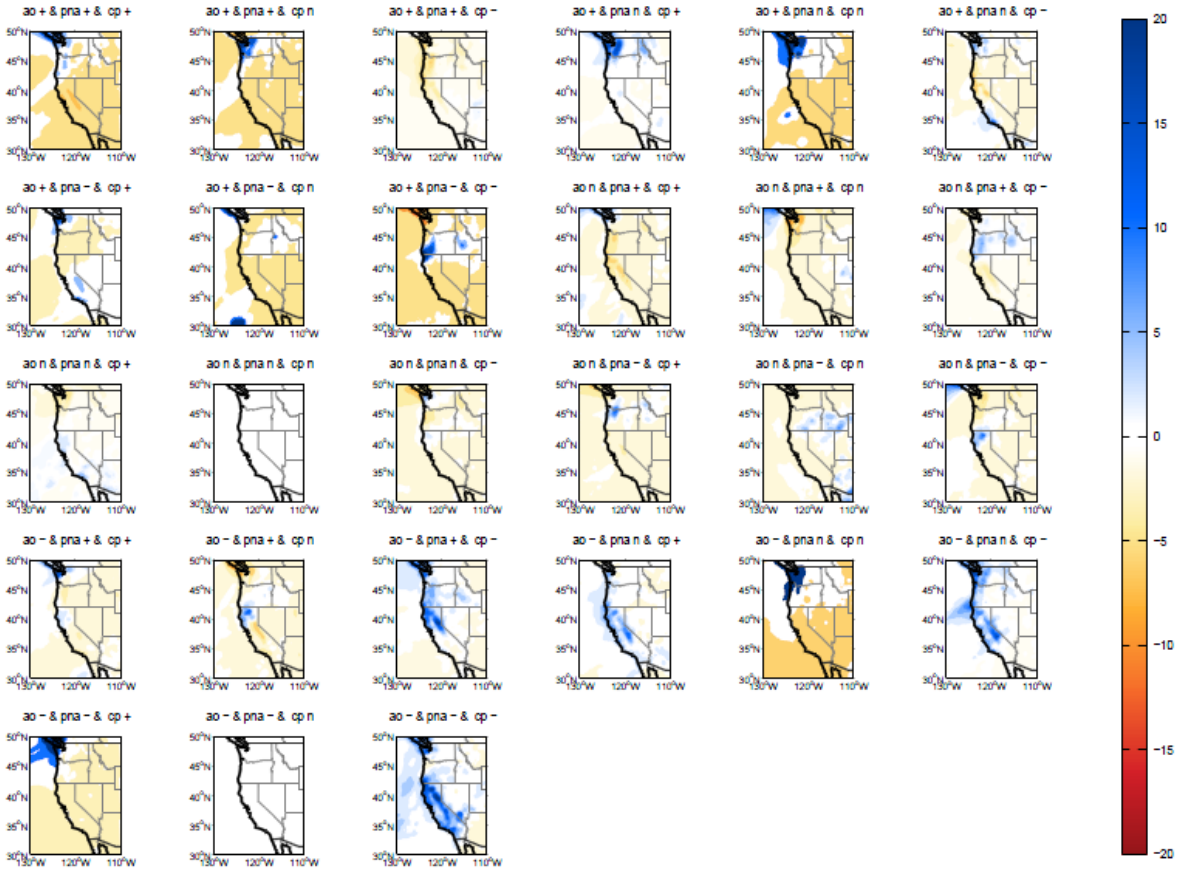

Figure A11c. Shading represents anomalous precipitation >100mm/day over the western U.S. during the combination of the **AO, PNA, and CP** from 2001 to 2011.

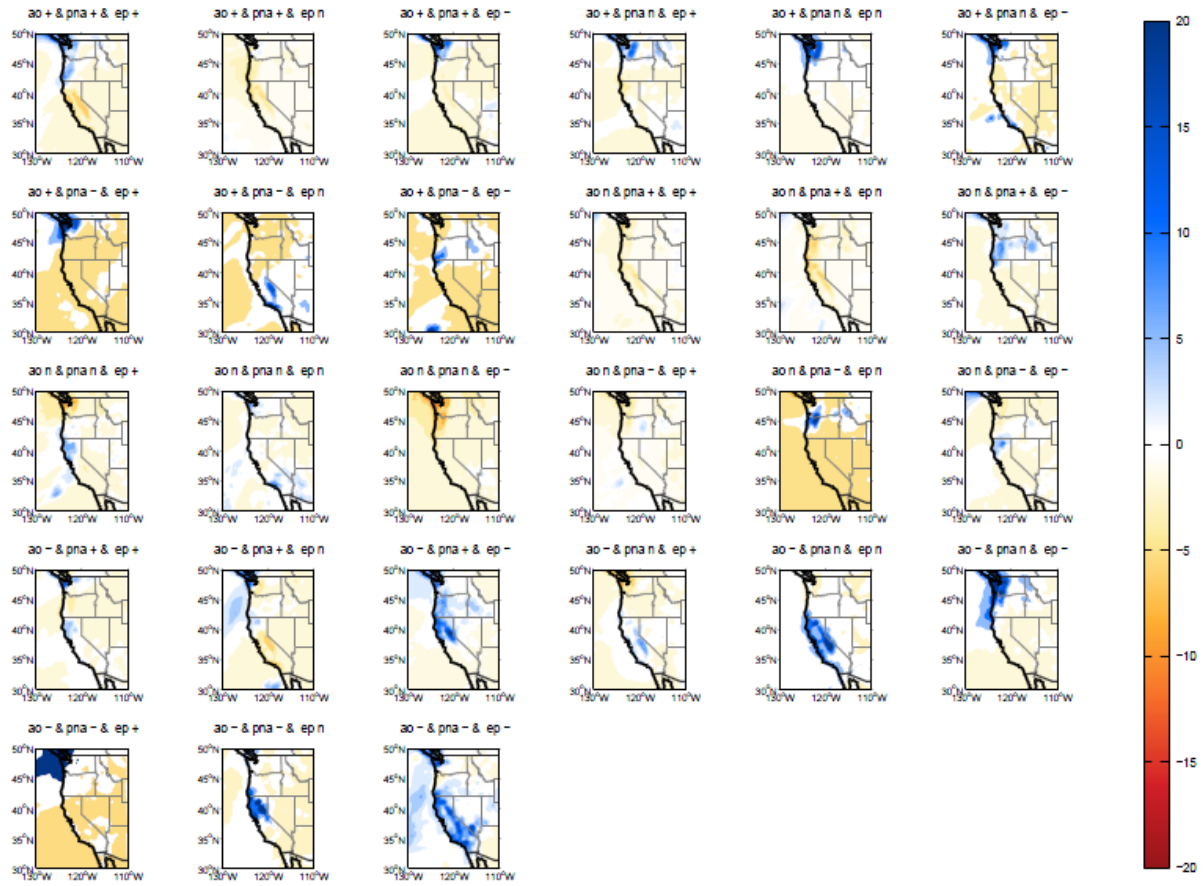

Figure A11d. Shading represents anomalous precipitation >100mm/day over the western U.S. during the combination of the **AO, PNA, and EP** from 2001 to 2011.

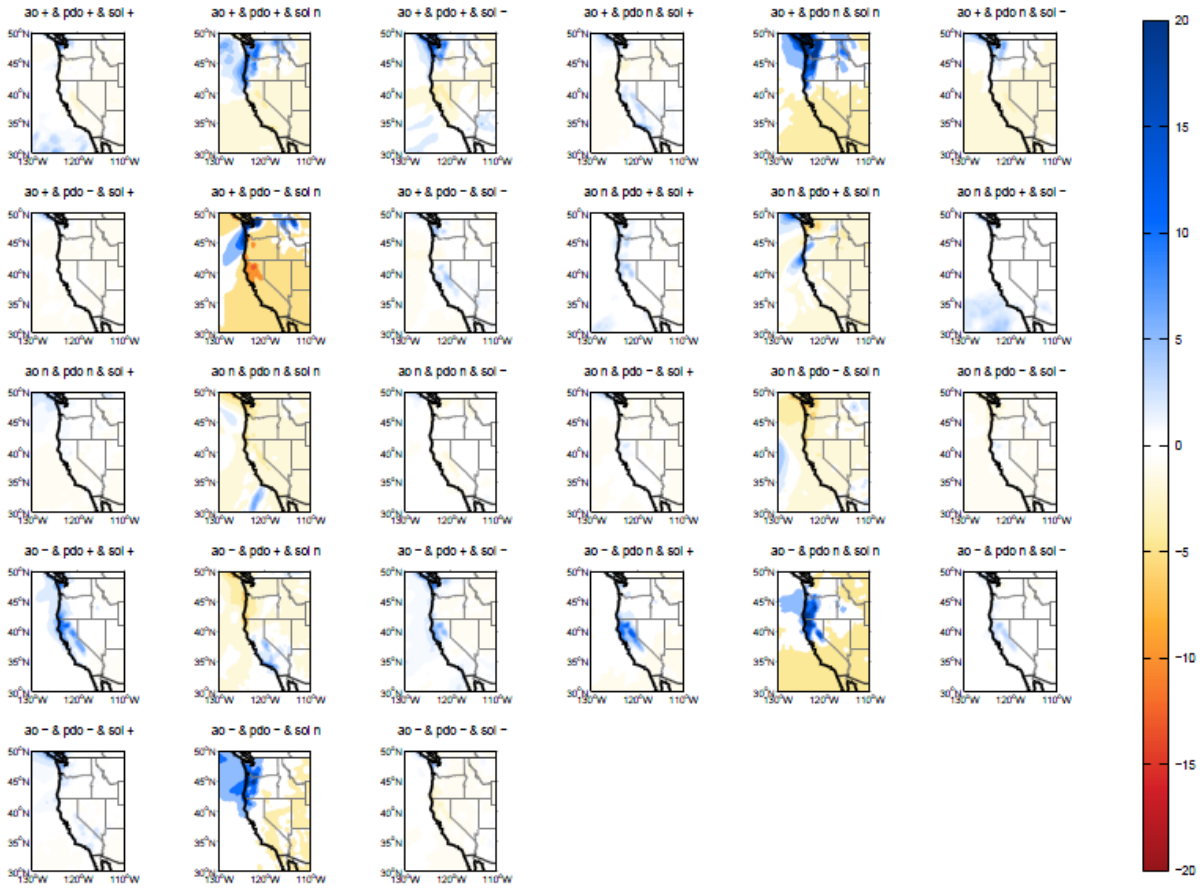

Figure A11e. Shading represents anomalous precipitation >100mm/day over the western U.S. during the combination of the **AO, PDO, and SOI** from 2001 to 2011.

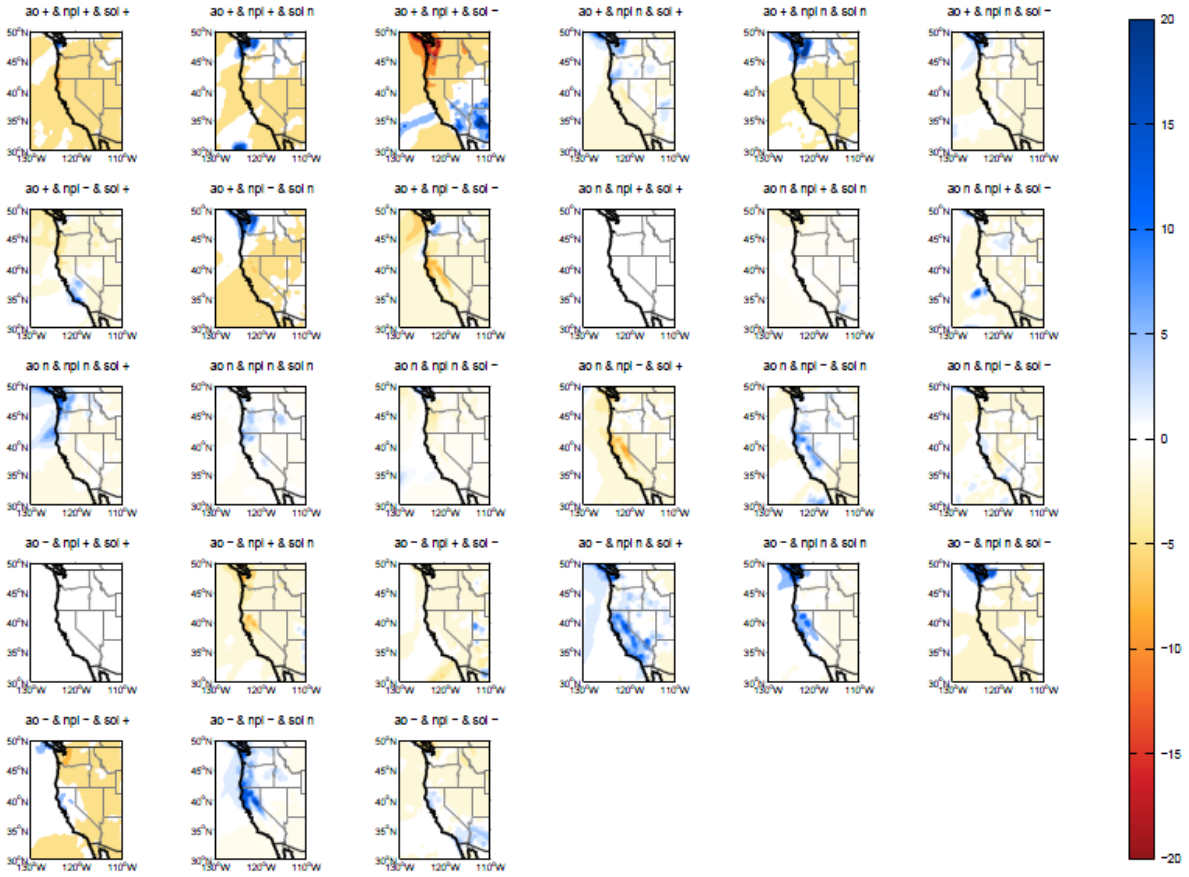

Figure A11f. Shading represents anomalous precipitation >100mm/day over the western U.S. during the combination of the **AO, NPI, and SOI** from 2001 to 2011.

A7. References

Baker, A., Smith, C. L., Jex, C., Fairchild, I. J., Genty, D., Fuller, L., 2008. Annually Laminated Speleothems: a Review. *International Journal of Speleology.* 37, 193-206.

Genty, D., Baker, A., Barnes, W., 1997. Comparison of annual luminescent and visible laminae in stalagmites. *Comptes Rendus De L Academie Des Sciences Serie Ii Fascicule a-Sciences De La Terre Et Des Planetes.* 325, 193-200.

Nešić, M., Marković, M., Trajković, R., Pavlović, D., Ilić, M., Mitić, V., Stankov-Jovanović, V., 2010. Total content of organic acids in plants from fire affected forest. *Biol.Nyssana*. 1, 65-69.

Swetnam, T. W., Baisan, C. H., Caprio, A. C., Brown, P. M., Touchan, R., Anderson, R. S., Hallett, D. J., 2009. Multi-millennial fire history of the giant forest, Sequoia National Park, California, *USA. Fire Ecology.* 5, 120-150.